Rapid access to functional oil-filled nanocapsules through nanoprecipitation

Luxiao Chai

N°d'ordre NNT : 2019LYSEI047

THESE de DOCTORAT DE L'UNIVERSITE DE LYON

opérée au sein de

L'Institut National des Sciences Appliquées de Lyon

Ecole Doctorale N° ED34

Matériaux de Lyon

Spécialité/ discipline de doctorat : Matériaux

Soutenue publiquement le 15/07/2019, par :

Luxiao CHAI

Rapid access to functional oil-filled nanocapsules through nanoprecipitation

---

Le jury composé de :

MARGAILLAN, André	Professeur (Université de Toulon)	Président
BERNARD, Julien	Chargé de recherche CNRS (INSA Lyon)	Examinateur
FLEURY, Etienne	Professeur (INSA Lyon)	Directeur de thèse
NOUVEL, Cécile	Professeur (ENSIC)	Rapporteur
HALILA, Sami	Chargé de recherche CNRS (CERMAV)	Rapporteur

Département FEDORA – INSA Lyon - Ecoles Doctorales – Quinquennal 2016-2020

SIGLE	ECOLE DOCTORALE	NOM ET COORDONNEES DU RESPONSABLE
CHIMIE	**CHIMIE DE LYON** **http://www.edchimie-lyon.fr** Sec. : Renée EL MELHEM Bât. Blaise PASCAL, 3e étage **secretariat@edchimie-lyon.fr** INSA : R. GOURDON	M. Stéphane DANIELE Institut de recherches sur la catalyse et l'environnement de Lyon IRCELYON-UMR 5256 Équipe CDFA 2 Avenue Albert EINSTEIN 69 626 Villeurbanne CEDEX **directeur@edchimie-lyon.fr**
E.E.A.	**ÉLECTRONIQUE, ÉLECTROTECHNIQUE, AUTOMATIQUE** **http://edeea.ec-lyon.fr** Sec. : M.C. HAVGOUDOUKIAN **ecole-doctorale.eea@ec-lyon.fr**	M. Gérard SCORLETTI École Centrale de Lyon 36 Avenue Guy DE COLLONGUE 69 134 Écully Tél : 04.72.18.60.97 Fax 04.78.43.37.17 **gerard.scorletti@ec-lyon.fr**
E2M2	**ÉVOLUTION, ÉCOSYSTÈME, MICROBIOLOGIE, MODÉLISATION** **http://e2m2.universite-lyon.fr** Sec. : Sylvie ROBERJOT Bât. Atrium, UCB Lyon 1 Tél : 04.72.44.83.62 INSA : H. CHARLES **secretariat.e2m2@univ-lyon1.fr**	M. Philippe NORMAND UMR 5557 Lab. d'Ecologie Microbienne Université Claude Bernard Lyon 1 Bâtiment Mendel 43, boulevard du 11 Novembre 1918 69 622 Villeurbanne CEDEX **philippe.normand@univ-lyon1.fr**
EDISS	**INTERDISCIPLINAIRE SCIENCES-SANTÉ** **http://www.ediss-lyon.fr** Sec. : Sylvie ROBERJOT Bât. Atrium, UCB Lyon 1 Tél : 04.72.44.83.62 INSA : M. LAGARDE **secretariat.ediss@univ-lyon1.fr**	Mme Emmanuelle CANET-SOULAS INSERM U1060, CarMeN lab, Univ. Lyon 1 Bâtiment IMBL 11 Avenue Jean CAPELLE INSA de Lyon 69 621 Villeurbanne Tél : 04.72.68.49.09 Fax : 04.72.68.49.16 **emmanuelle.canet@univ-lyon1.fr**
INFOMATHS	**INFORMATIQUE ET MATHÉMATIQUES** **http://edinfomaths.universite-lyon.fr** Sec. : Renée EL MELHEM Bât. Blaise PASCAL, 3e étage Tél : 04.72.43.80.46 **infomaths@univ-lyon1.fr**	M. Luca ZAMBONI Bât. Braconnier 43 Boulevard du 11 novembre 1918 69 622 Villeurbanne CEDEX Tél : 04.26.23.45.52 **zamboni@maths.univ-lyon1.fr**
Matériaux	**MATÉRIAUX DE LYON** **http://ed34.universite-lyon.fr** Sec. : Stéphanie CAUVIN Tél : 04.72.43.71.70 Bât. Direction **ed.materiaux@insa-lyon.fr**	M. Jean-Yves BUFFIÈRE INSA de Lyon MATEIS - Bât. Saint-Exupéry 7 Avenue Jean CAPELLE 69 621 Villeurbanne CEDEX Tél : 04.72.43.71.70 Fax : 04.72.43.85.28 **jean-yves.buffiere@insa-lyon.fr**
MEGA	**MÉCANIQUE, ÉNERGÉTIQUE, GÉNIE CIVIL, ACOUSTIQUE** **http://edmega.universite-lyon.fr** Sec. : Stéphanie CAUVIN Tél : 04.72.43.71.70 Bât. Direction **mega@insa-lyon.fr**	M. Jocelyn BONJOUR INSA de Lyon Laboratoire CETHIL Bâtiment Sadi-Carnot 9, rue de la Physique 69 621 Villeurbanne CEDEX **jocelyn.bonjour@insa-lyon.fr**
ScSo	**ScSo*** **http://ed483.univ-lyon2.fr** Sec. : Véronique GUICHARD INSA : J.Y. TOUSSAINT Tél : 04.78.69.72.76 **veronique.cervantes@univ-lyon2.fr**	M. Christian MONTES Université Lyon 2 86 Rue Pasteur 69 365 Lyon CEDEX 07 **christian.montes@univ-lyon2.fr**

*ScSo : Histoire, Géographie, Aménagement, Urbanisme, Archéologie, Science politique, Sociologie, Anthropologie

Résumé

Ce projet de thèse avait pour objectif l'élaboration de glyconanocapsules à coeur huileux par nanoprecipitation à partir de polymers biocompatibles et biodégradables. Dans ce but, nous avons tout d'abord élaboré une série de glycopolymères à base de poly(alcool vinylique) (PVA) par copolymérisation radicalaire de type RAFT suivie d'une réaction d'alcoolyse sélective. En parallèle, nous avons synthétisé une seconde famille de glycopolymères en hydrolysant partiellement des chaînes de poly(2-ethyl-2-oxazoline) (PEOX) et d'autre part, en réalisant une réaction d'amination réductrice entre les amines secondaires obtenues (PEOX-*co*-PEI) et le lactose. S'appuyant sur les diagrammes de phase des systèmes ternaires eau/acetone/huile et eau/acetone/polymère, nous avons ensuite identifié les conditions de basculement de solvent (dans les domains Ouzo et SFME) permettant simultanément la formation de nanogouttelettes d'huile et l'adsorption de chaînes polymère à l'interface, conditions essentielles à l'obtention de nanocapsules à coeur huileux. Afin d'assurer leur pérennité en milieu aqueux, l'écorce de ces nano-objets a été réticulée chimiquement et/ou physiquement, dans le cas des nanocapsules à base de PVA par ajout de Na_2SO_4 (salting out). Enfin, moyennant l'ajout de réactifs et de principes actifs dans les phases aqueuse et organique respectivement, ce procédé de basculement en une étape a permis de construire des glyconanocapsules contenant des molécules de principe actif dissoutes dans le coeur huileux et possédant une membrane polymère réticulée dégradable en conditions réductrices Enfin, Il a été démontré que ces glyconanocapsules sont capables de libérer un principe actif encapsulé en réponse à un stimulus et d'interagir avec certaines lectines.

Mots clés: poly(alcool vinylique); poly(2-ethyl-2-oxazoline); glycopolymère; nanoprécipitation; glyconanocapsules; encapsulation.

Abstract

In this PhD work, we designed a series of precisely-defined water-soluble PVA-based glycopolymer chains with tunable compositions using RAFT copolymerization and selective alcoholysis reactions. In a second approach, we prepared a library of poly(2-ethyl-2-oxazoline)-based glycopolymers by partial acidic hydrolysis and reductive amination reactions with sugar residues.

Relying on the establishment of phase diagrams for water/acetone/oil and water/acetone/polymer ternary systems (commercial PVA, PVA or polyoxazoline-based glycopolymers), we identified the conditions of solvent shifting (in the Ouzo and /or the SFME domains) for which oil-filled nanocapsules can be constructed in one step thanks to spontaneous emulsification of the oil and concomitant adsorption of the polymer chains at the interface. Stabilization of the nanocapsules in water was typically achieved by covalent cross-linking of the shell or, in the case of PVA-based materials, by addition of Na_2SO_4 (salting out). This straightforward nanoprecipitation process was further effortlessly implemented to confer redox-sensitivity to the polymer shell (to trigger the release of actives), decorate the nanocapsules with diverse molecules of interest and to entrap hydrophobic actives within the oily core. Release of the drugs and bioactivity of the nanocapsules were demonstrated.

Keywords: poly(vinyl alcohol); poly(2-ethyl-2-oxazoline); glycopolymer; nanoprecipitation; glyconanocapsules; encapsulation.

Acknowledgement

This PhD project is funded by the China Scholarship Council (CSC). Thanks CSC gave me the opportunity to work and study in INSA.

First, I must show my sincere gratitude to my supervisors, Pr. Etienne Fleury and Dr. Julien Bernard, to give me this opportunity to lead this PhD project. Your kind guidance, constant encouragement, patience and comprehensive always gave me energy to persist on research. No matter what work I will do in the future, my four years with you are my treasure.

My colleagues and my friends Xibo and Biao, thank you teaching me a lot in research and always concerned me like big brothers. Hope you two everything goes well.

Thanks to my so many kind friends and colleagues from China and in France. I like Lyon and IMP so much because all of you. Our four years together will be unforgettable to me.

Extraordinary thanks to Mr. Song Hongbing for your public sharing on economic and cultural story, which spent more than a hundred weekends with me. The way of your analysis and argumentation has benefited me a lot in thinking. I am always be your fan.

Great thanks to my family, whenever and wherever, love you.

Finally, special thanks to myself for my insistence in life and work during these four years. Here I want to express my sincere respect for all the researchers.

Abbreviations

AIBN	2,2-azobisisobutyronitrile
ATRP	atom transfer radical polymerization
ROP	ring-open polymerization
$CDCl_3$	deuterated chloroform
CD_2Cl_2	deuterated dichloroform
CRP	controlled radical polymerization
CTA	chain transfer agent
RAFT	reversible addition-fragmentation chain transfer
D_2O	deuterium oxide
DCC	N, N'-dicyclohexylcarbodiimide
***d*-DMSO**	deuterated dimethyl sulfoxide
DLS	dynamic light scattering
DNA	deoxyribonucleic acid
DMF	dimethylformamide
DMSO	dimethyl sulfoxide
E. Coli	*Escherichia coli*
ESI-MS	electrospray ionization mass spectrometry
SEC	size-exclusion chromatography
M	monomer
I	initiator
M_W	molecular mass averages of the weight
Mn	molecular mass averages of the number
NaOH	sodium hydroxide
K_2CO_3	potassium carbonate
HCl	hydrochloric acid
NMR	nuclear magnetic resonance
PEG	polyethylene glycol
PS	polystyrene
ROMP	ring-open metathesis polymerization

TEM	transmission electron microscopy
THF	tetrahydrofuran
HD	hexadecane
CROP	cationic ring opening polymerization
FDA	U.S. Food and Drug Administration
DP	degree of polymerization
MADIX	macromolecular design by interchange of xanthate
MeOH	methanol
EtOH	ethanol
D_z/d_z/d_{DLS}	z-average diameter
d_{TEM}	TEM diameter by image processing
IPDI	isophorone diisocyanate
SFME	surfactant-free microemulsion
Na_2SO_4	sodium sulfate
ConA	*Concanavalin A*
DTT	dithiothreitol
CPT	camptothecin
LCST	low critical solution temperature

Table of Contents

General Introduction

General Introduction

Saccharides and saccharide-functionalized (macro)molecules, i.e. glycolipids, glycoproteins or polysaccharides, are essential components of living organisms. This family of highly abundant (macro)molecules not only play a major role in a myriad of biological processes but also constitute ubiquitous structural materials in nature (insect and crustacean shells, vegetal cell walls, energy storage…). Since the pioneering studies on saccharides by Emil Fischer[1] in the late nineteenth century, intense synthetic efforts have notably been paid to develop methodologies affording the large-scale production of precisely-defined carbohydrate-containing polymers or glycopolymers. These glycomaterials are indeed appealing candidates to mimic the function and the activity of natural glycoconjugates and gain further insight into biological systems.[2]

Considering that biocompatible and biodegradable glycopolymers are promising macromolecular tools for numerous biological and pharmaceutical applications, the initial objectives of this PhD work are to design original well-defined water-soluble glycopolymer chains relying either on poly(vinyl alcohol) or poly(*N*-2-ethyl-2-oxazoline) backbones and the incorporation of pendant sugar moieties via RAFT or cationic ring opening polymerizations followed by post-functionalization methods. In a second step, we will aim at exploiting these series of building blocks in order to build bioactive drug-loaded shell-functionalized glyconanocarriers using the nanoprecipitation technique in the Ouzo and Surfactant-Free MicroEmulsion domains.

This manuscript is divided into five chapters.

The first chapter (***Chapter 1***) will aim at describing the main chemical and physical routes to build up glyconanocapsules and at presenting the

significance of glycopolymers in encapsulation applications.

In the ***Chapter 2***, we will describe the first synthesis of PVA-based glycopolymers by combining RAFT polymerization of vinyl esters and selective alcoholysis of chloroacetate pendant groups. Properties of resulting PVA-based glycopolymers will be further characterized and discussed.

In the ***Chapter 3***, we will investigate the generation of PVA-based nanocapsules and glyconanocapsules through nanoprecipitation in OUZO and SFME domains. With respect to the potential bioapplications of PVA-based nancapsules, methods allowing for stabilizing the polymer shell in water with a minimal amount of chemical cross-linker will be investigated. The bioactivity and the loading/release capacities of these nanocapsules will be explored in the final part.

The ***Chapter 4*** will describe the synthesis of poly(2-oxazoline)-based glycopolymers containing lactose by acid hydrolysis followed by reductive amination and the preparation of the corresponding glyconanocapsules via nanoprecipitation in OUZO and SFME domains. Shell functionalization, more precisely PEGylation, loading of the nanocapsules core with actives and pH-responsiveness of the resulting nanocarriers will be subsequently investigated.

The final part (***Chapter 5***) will provide details on experiment protocols, including the used materials, the characterization methods, the polymerization procedures, the generation and the functionalization of nanocapsules by solvent shifting.

1. K. Freudenberg, *Advances in Carbohydrate Chemistry*, **1967**, 21, 1-38.

2. Y. Miura, *J. Polym. Sci. A: polymer chemistry*, **2007**, 45, 5031-5036.

Chapter 1

Preparation of Glyconanocapsules

Chapter 1 Preparation of Glyconanocapsules

1.1 Introduction

Polymer capsules are core-shell colloidal systems displaying an empty cavity or a liquid (oil, water or solvent) or solid core surrounded by a polymer membrane (**Scheme 1.1**).[1,2,3] This family of colloids are of particular interest in order to protect (bio)molecules from degradation, to mask a taste or a scent, to limit the vaporization of volatiles, to control the release of active principles as a function of time and to promote targeted delivery. The applications of polymer capsules are numerous including food, tobacco, paper, textiles, care products, pharmaceutics, catalysis, self-healing… The wall materials can be chosen among natural polymers, polysaccharides (alginate, chitosan, starch, cellulosic gum arabic…) or proteins, biodegradable polyesters (such poly-ε-caprolactone, polylactide, polylactide-co-glycolide), polypeptides, urea or melamine-formaldehyde, polyurethane, polyurea or polyamide and so on. Actives can be dispersed and/or dissolved in the core in solid, liquid or gas form and their release can be triggered by different stimuli such as temperature, pH, light or mechanical stress.

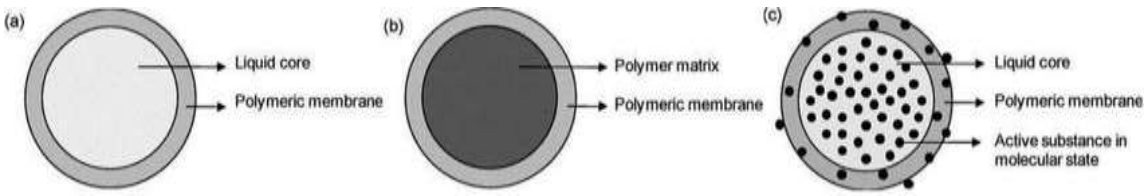

Scheme 1.1: Different polymer capsular structures with (a) liquid core, (b) polymer matrix and (c) active substance encapsulation.

Depending on the desired applications, polymer capsules with dimensions ranging from tens of nanometers to several hundreds of micrometers can be designed. Routes to microcapsules have been established for decades relying on various physical methods, such as spray drying, centrifugal extrusion, air-suspension coating and solvent evaporation, or chemical methods such as

coacervation or interfacial polymerizations. In contrast, the generation of polymeric nanocapsules -which are promising candidates for biomedical applications owing to their subcellular size- appears to be less trivial.[4] Classical methods include self-organization of amphiphilic block copolymers into polymersomes, emulsification techniques or template-assisted approaches such as layer-by-layer techniques and so on, see **Scheme 1.2**.

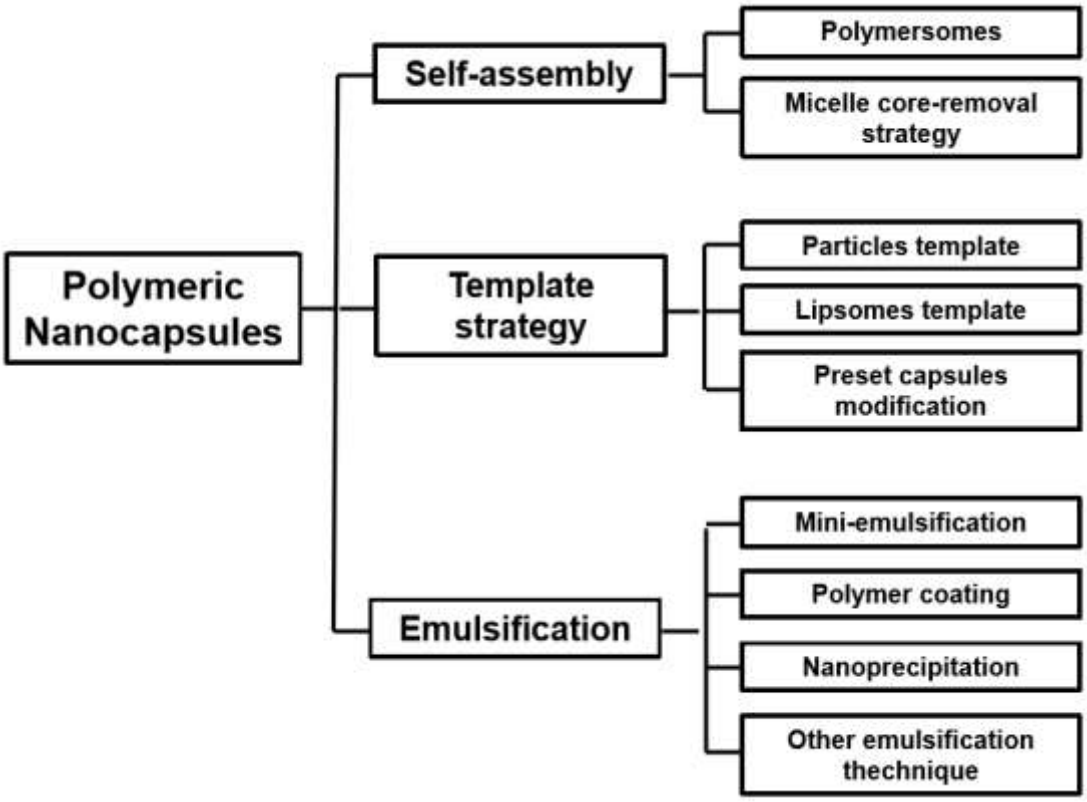

Scheme 1.2: Routes to polymeric nanocapsules

1.2 Access to glyconanocapsules preparation

Because carbohydrate residues are playing a key role in a myriad of biological processes, i.e. immune defense, cellular communication, signal transduction, a lot of attention has been recently paid to the development of synthetic methods relying on different polymerization techniques (ROMP, ATRP, RAFT…) and affording the preparation of precisely-defined glycopolymers with different architectures and glycomaterials thereof.[5,6] The fabrication of nanocarriers and

in particular, nanocapsule made of or decorated with carbohydrates are also raising increasing interest for biomedical applications, see **Scheme 1.3**, as the presence of the sugar residues provide nanocapsules with targeting properties through specific interactions with complementary binding sites, stealth properties and/or controlled release.

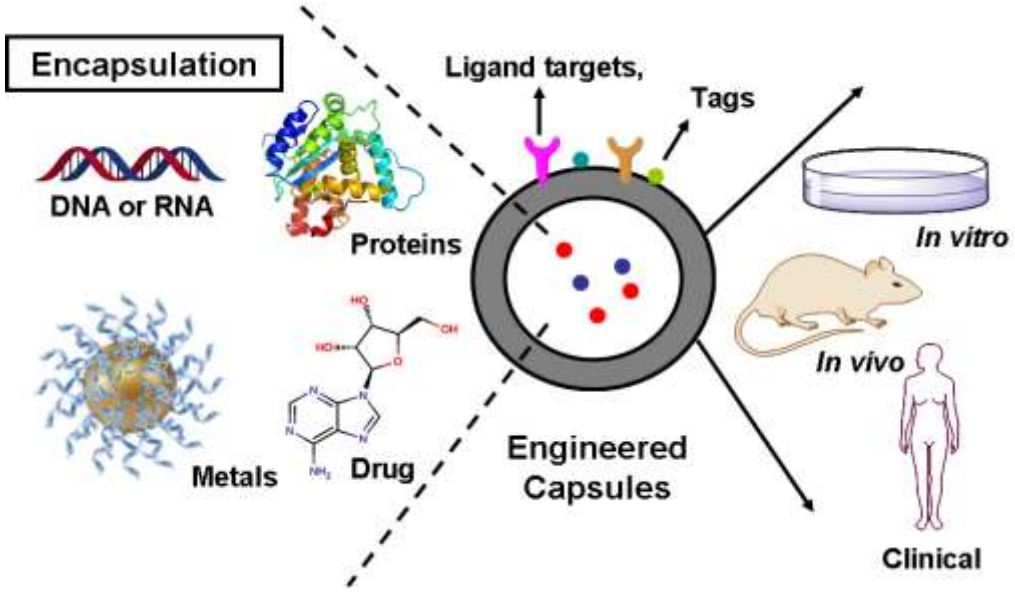

Scheme 1.3: Engineered glyconanocapsules for biomedical applications.

1.2.1 Self-assembly strategy

The self-assembly of amphiphilic block copolymers or graft copolymers in a selective solvent is presently the technique of choice to generate vesicular systems. In the next section, we will report on the routes to polymersomes from glycosylated block copolymers and on the synthesis of hollow glyconanoparticles by combination of amphiphilic copolymer self-assembly or selective core removal.

1.2.1.1 Polymersomes

Polymersomes are hollow particles made of bilayers of amphiphilic copolymers. They possess comparable structures as liposomes but are significantly more stable. Polymersomes are generally built in water from block copolymers with hydrophilic segment weight fraction less than 35% and molar masses typically ranging from 2-20 $kg.mol^{-1}$. Depending on the nature of the amphiphilic copolymers and/or the use of one or several amphiphilic copolymers, the polymersomes possess polymer membranes with different internal organization (see **Scheme 1.4**)[7].

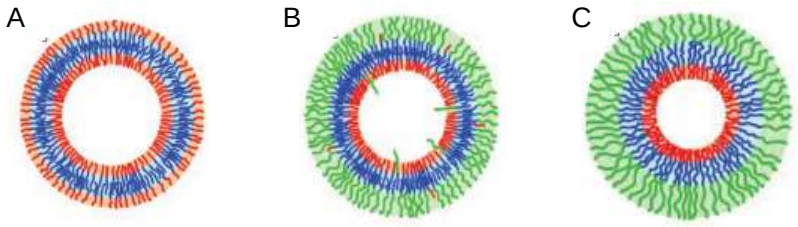

Scheme 1.4: Different polymersome morphologies from the self-assembly of copolymer (A) AB diblock, (B) binary mixture of AB and BC diblocks, and (C) ABC triblock.

Amphiphilic vinyl block glycopolymers by sequential polymerizations

The large majority of glycopolymersomes (or glycovesicles) constructed by self-assembly of amphiphilic copolymers rely on precisely-defined block copolymers generated by controlled radical polymerization techniques (ATRP, RAFT…).
In 1999, Fu-Mian Li and coworkers reported the preparation of glycopolymer-based vesicles from the self-assembly of amphiphilic block copolymers (**Table 1.1**, **entry 1**)[8,9,10]. A series of precisely-defined amphiphilic block copolymers, namely polystyrene-*b*-poly[(2-*β*-D-glucopyranosyloxy)ethyl acrylate] (PS-*b*-PGEA) with different length and composition (PS_{55}-*b*-$PGEA_9$, Mn=8300 g/mol, *Đ*=1.24; PS_{77}-*b*-$PGEA_6$, Mn=12000 g/mol, *Đ*=1.27; PS_{88}-*b*-$PGEA_4$, Mn=9700 g/mol, *Đ*=1.18; and PS_{101}-*b*-$PGEA_7$, Mn=13000 g/mol, *Đ*=1.28) were

synthesized by sequential ATRP polymerizations. Spontaneous self-assembly of these block copolymers was performed by first dissolving them in organic solvent (DMF, THF, dioxane or their mixtures) to give a final copolymer concentration ~ 1.0 wt%. After stirring at room temperature for 24h, 5-20 wt% of water was added very slowly followed by dialysis to remove the organic solvent. Different morphologies were obtained depending on the nature of the solvents. In the case of PS_{55}-*b*-$PGEA_9$, spheres were generated in pure DMF wherease rods were observed in a DMF/dioxane mixtures (70/30 wt%). Vesicles of 70-250 nm in size could be formed when increasing to 80 wt% or 100 wt% of dioxane in DMF/dioxane mixture (**Figure 1.1**).

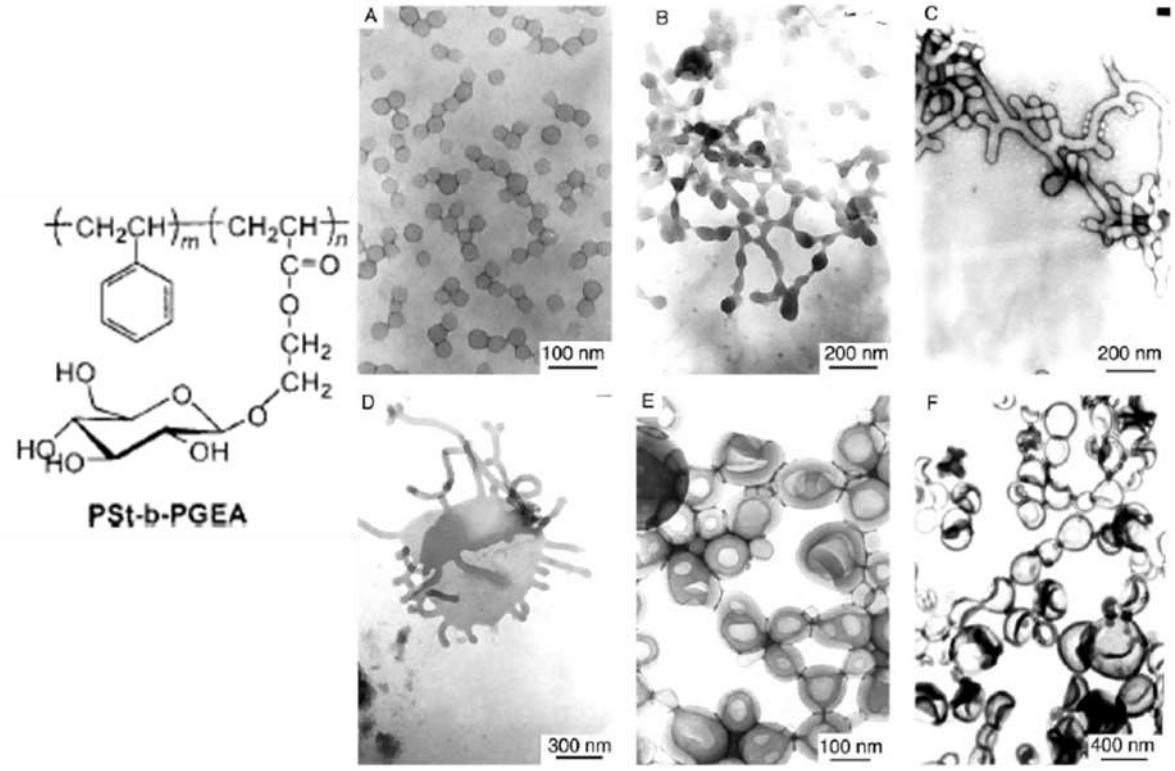

Figure 1.1: Various self-assembled morphologies of PS55-b-PGEA9 from spheres to vesicles with content of dioxane (wt. %): (A) 0, (B) 10, (C) 30, (D) 50, (E) 80, (F) 100.

In 2004, the group of Chaikof synthesized a library of [poly(*L*-alanine)-*b*-poly(2-acryloyloxyethyllactoside)-*b*-poly(*L*-alanine)] block copolymers ($A_xG_yA_x$, where x and y refer to the degrees of polymerization of the poly(*L*-alanine) and poly(2-acryloyloxyethyllactoside) blocks respectively) by combining ATRP and Ring

Open Polymerization (ROP) techniques (**Table 1.1, entry 2**)[11,12]. Different morphologies, spheres, vesicles, worms and large aggregates, were obtained through direct dissolution of the glycopolymer-polypeptide triblock copolymers, $A_9G_{52}A_9$ and $A_{22}G_{52}A_{22}$ in aqueous solution by tuning polymer concentrations (2.5-10 mg/mL) and pH (2 or 6.7).

In 2008, Chang-Ming Dong and coworkers synthesized two series of 4-arm star-shaped amphiphilic block copolymers SPCL-*b*-PGAMA and SPCL-*b*-PLAMA via ROP of *ε*-caprolactone (*ε*-CL) using pentaerythritol as initiator, conversion of the PCL chain ends into ATRP initiators and subsequent chain-extension by ATRP polymerization of gluconamidoethylmethacrylate (GAMA) or lactobionamidoethylmethacrylate (LAMA)[13,14]. Various morphologies were observed after self-assembly of the block copolymers in aqueous solution. Copolymers with short hydrophobic PCL blocks (e.g. $SPCL_{15}$-*b*-$PLAMA_7$) generated spherical micelles and worm-like aggregates while polymer stars with long hydrophobic blocks, *i.e.* $SPCL_{50}$-*b*-$PGAMA_5$ and $SPCL_{75}$-*b*-$PLAMA_{11}$, yielded vesicles with hydrodynamic diameters of 250 nm and 432 nm, respectively (**Table 1.1**, **entry 3** and **4**). Using a similar synthetic approach, the same group prepared star-shaped block copolymers PAMAM-*b*-PCL-*b*-PGAMA from PAMAM dendrimers (with 12 hydroxyl terminal groups) by sequential ROP of *ε*-CL and ATRP of GAMA[15]. Self-assembly of PAMAM-*b*-PCL_{28}-*b*-$PGAMA_3$, PAMAM-*b*-PCL_{28}-*b*-$PGAMA_9$ and PAMAM-*b*-PCL_{28}-*b*-$PGAMA_{28}$ in water generated sugar-decorated vesicles with hydrodynamic diameters around 100, 150 and 300 nm, respectively (**Table 1.1**, **entry 5**). Thanks to the hydrophobic character of the PAMAM and PCL blocks, PAMAM-*b*-PCL_{28}-*b*-$PGAMA_{28}$ based vesicles were loaded with nimodipine (hydrophobic drug, loading efficiency ~ 74%). Moreover, the resulting nanoparticles were stable for 14 days at 37°C or 50 days at 4°C making them promising materials for drug delivery purposes.

In order to improve the biodegradability of the PCL-based polymers, the same

group also threaded *α*-cyclodextrin rings (*α*-CDs) onto PCL backbones to generate a macroinitiator (PPR) and finally synthesized triblock glycopolymers PGAMA-PPR-PGAMA by direct ATRP of GAMA monomer.[16] Depending on the weight fraction of PGAMA segments (f_{PGAMA}), the self-assembly of the copolymers gave rise to diverse morphologies in water. $PGAMA_{15}$-PPR_{20}-$PGAMA_{15}$ (f_{PGAMA}=65.0%, $M_{n,NMR}$=39 kDa, *Đ*=1.34) generated spherical micellar aggregates with an average diameter of 121 ± 12 nm whereas polymersomes with an average diameter 81±4 nm were obtained for $PGAMA_4$-PPR_{20}-$PGAMA_4$ (f_{PGAMA}=35.8%, $M_{n,NMR}$=33 kDa, *Đ*=1.43) (**Table 1.1**, **entry 6**). The specific binding of PGAMA-PPR-PGAMA with Con A led to the formation of large aggregates ~ 1.81 ± 0.6 μm in size.

In 2008, G. Pasparakis and C. Alexander aimed at designing artificial eukaryotic cells in order to control the transport of molecules at biointerfaces (**Table 1.1**, **entry 7**). To do so, the authors first prepared glycosylated synthetic vesicles from ATRP or RAFT-made poly(2-glucosyloxyethyl methacrylate)-*block*-poly((diethyleneglycol methacrylate) block polymers $PGEMA_{10}$-*b*-$PDEGMA_{50}$ (Mn=11.2 kDa, *Đ*=1.34) and $PGEMA_{28}$-*b*-$PDEGMA_{36}$ (Mn=15.2 kDa, *Đ*=1.11).[17] Whereas unimers were exclusively observed below 15°C, the formation of vesicles was observed upon heating. At 20°C, glycovesicles with hydrodynamic diameters of 251 and 500 nm were built from $PGEMA_{10}$-*b*-$PDEGMA_{50}$ respectively. Further increase of the temperature (37°C) resulted in the construction of the glycovesicles (180 and 300 nm) owing to the thermo-responsive character of the PDEGMA block. The authors further demonstrated that the glucose-decorated vesicles bind more efficiently to FITC ConA than linear PGEMA and that the dimensions of the glycovesicles have a significant influence on the lectin/glycovesicles interactions. Finally, the authors highlighted the capacity of the glycovesicles to interact with *E coli* strains expressing FimH adhesins and to deliver molecules in the cytoplasm of the bacteria.

In 2011, the groups of Borsali and Muller reported the preparation of dye-free fluorescent glycovesicles from direct self-assembly of π-conjugated galactose-based amphiphilic block copolymers in water (**Table 1.1**, **entry 8**)[18]. To design the suitable block copolymers, *α*-propargyl-functionalized poly(3-*O*-methacryloyl-D-galactopyranose) (PMAGP, Mn=24.4 kg/mol, DP_n=97, *Đ*=1.06) was grown by ATRP from an initiator bearing an alkyne moiety and a poly(3-hexylthiophene) block (Mn=4250 g/mol, DP_n=25, *Đ*=1.06) displaying a terminal azide unit (P3HT) was synthesized using Grignard metathesis polymerization. P3HT-*b*-PMAGP block copolymer was finally obtained by "CuAAC click chemistry". Aggregation behavior of the block copolymer in water was investigated starting from a 1.0 wt.% P3HT-*b*-PMAGP solution in THF, a water-miscible organic medium in which the block copolymer chains are molecularly dissolved. The self-assembly was then triggered by slow addition of THF/Water mixture followed by a rapid addition of water to finally reach a 98/2 wt/wt water/THF composition. After evaporation of THF and filtration, the aggregation behavior of P3HT-*b*-PMAGP diblock was studied by dynamic light scattering (DLS) revealing the presence of particles with a hydrodynamic radius R_h~89 nm. The radius of gyration determined by static light scattering was 83 nm suggesting the formation of vesicular nanostructures (R_g/R_h close to 1 ~ 0.93). The preparation of P3HT-*b*-PMAGP-based vesicles was further assessed by AFM and TEM microscopy techniques (**Figure 1.2**). Photophysical properties of P3HT-*b*-PMAGP were strongly impacted by the nature of solvent. Owing to the aggregation of the π-conjugated P3HT blocks, the introduction of water in the block copolymer organic solution (THF) resulted in a strong shift of the absorption peak maximum (442 nm → 483 nm) and in the presence of an additional band at 550 nm whereas emission bands observed at 580 and 630 nm in pure THF were accompanied with another weak band at 470 nm after addition of water (95/5 wt/wt water/THF). In pure water, photoexcitation of the glycovesicles at 365 nm induced an emission maximum at 470 nm.

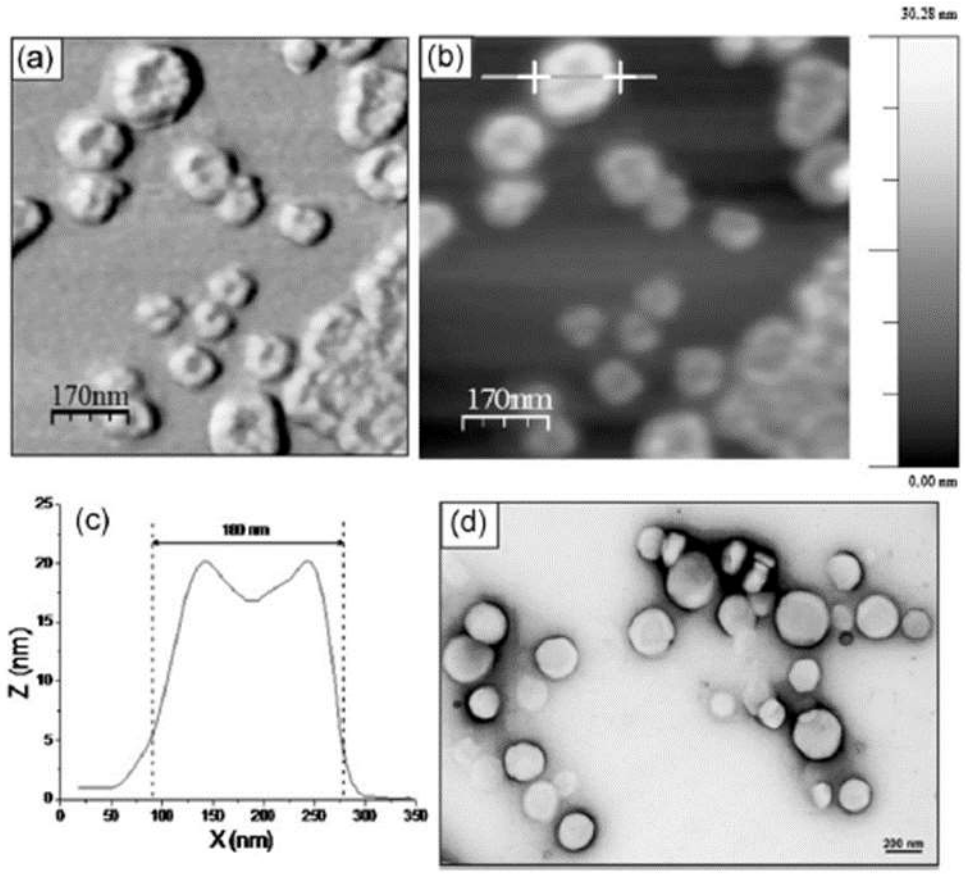

Figure 1.2: (a) AFM phase and (b) topographic images (intermittent contact mode) of P3HT-*b*-PMAGP vesicles; (c) Topographic cross-section profile corresponding to the horizontal blue line on the AFM topographic image (b); (d) TEM image of vesicles after negatively staining the sample with uranyl acetate.

In 2012, Albertin and co-workers reported the synthesis of poly(NAM)-*b*-poly(NAGlc)-*b*-poly(NAM) triblock copolymers through RAFT polymerization of N-acryloylmorpholine (NAM) and subsequent chain extension with *N*-*β*-D-glucopyranosylacrylamide (NAGlc).[19] At 9/91 water/THF v/v %, a triblock copolymer with a molar mass of 24 kg.mol^{-1} and *Đ*=1.06 and a molar fraction around 0.14 for the central PNAGlc block was shown to self-organize into vesicles with an average hydrodynamic diameter of 380 nm (**Table 1.1**, **entry 9**).

In 2012, a photo-responsive amphiphilic block glycopolymer,

poly(pyrenylmethyl methacrylate)-*b*-poly(3-*O*-4-vinylbenzoyl-D-glucopyranose) (PPy_{29}-*b*-PBG_{32}, *M*n=21200 g/mol, *Đ*=1.46), was synthesized by S. Menon and S. Das via ATRP (**Scheme 1.5**).[20] The self-assembly of PPy_{29}-*b*-PBG_{32} was triggered by addition of water to a polymer solution in DMF (1 mg/ml) resulting in the preparation of vesicular structures with a hydrodynamic diameter of 473 nm and a PDI ~0.094 by DLS (**Table 1.1**, **entry 10**). The glycovesicles were dissociated upon exposition of the dispersion to UV light (λ=340 nm) owing to the conversion of PPy block into PMA block by photo-solvolysis reaction (resulting in a substantial increase of the overall hydrophilicity of the polymer).

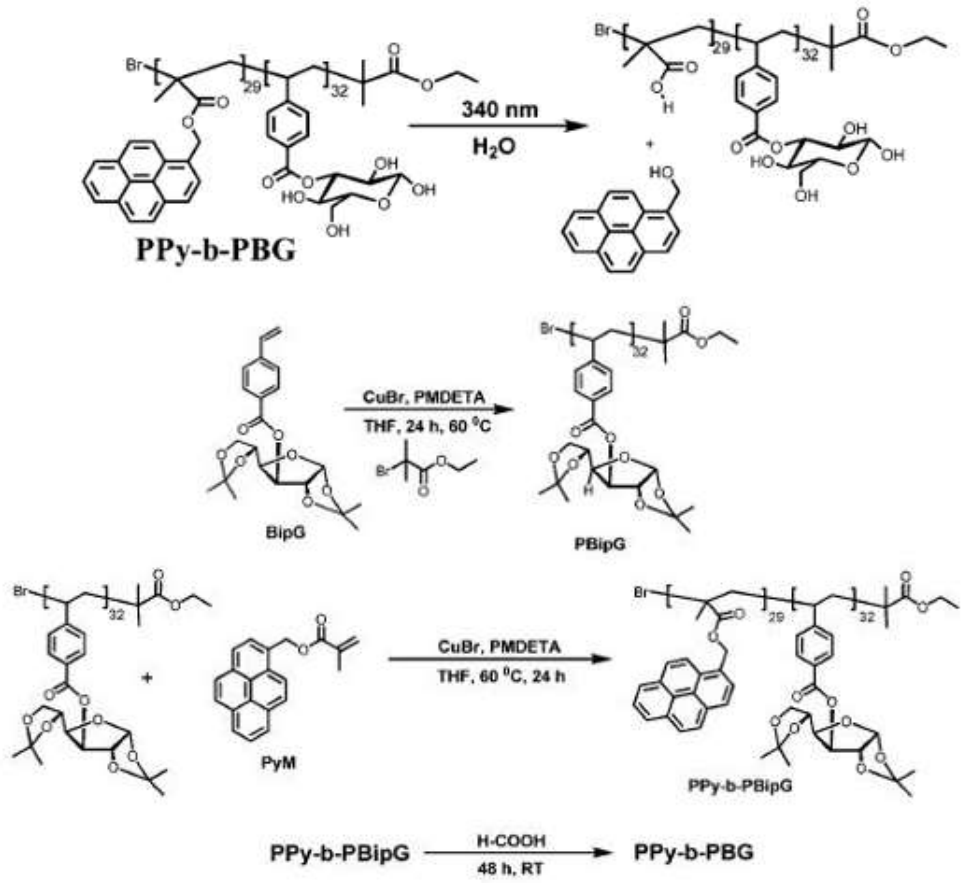

Scheme 1.5: Synthesis of PPy-*b*-PBG light-sensitive block copolymers by ATRP and light-induced modification of the glycopolymer.

One year later, photo-responsive glycovesicles with a hydrodynamic diameter of 366 nm (DLS) were built by the same group from poly(spiropyran methacrylate)-*block*-poly(3-*O*-4-vinylbenzoyl-D-glucopyranose) amphiphilic

diblock copolymer (PSP_8-*b*-PBG_{32}, $M_{n,NMR}$=16600 g/mol), see **Table 1.1**, **entry 11** and **Scheme 1.6**.[21] Exposing the vesicles to UV light (at λ=360 nm for 2 h) led to the destruction of the vesicular morphology and the formation of tiny aggregates (48 nm by DLS). A second irradiation of the solution at 560 nm promoted the regeneration of vesicles together with micelles. These photo-responsive vesicles were further shown to promote controlled release of payload (hydrophobic dyes, *e.g.* Coumarin 7) and re-encapsulation。

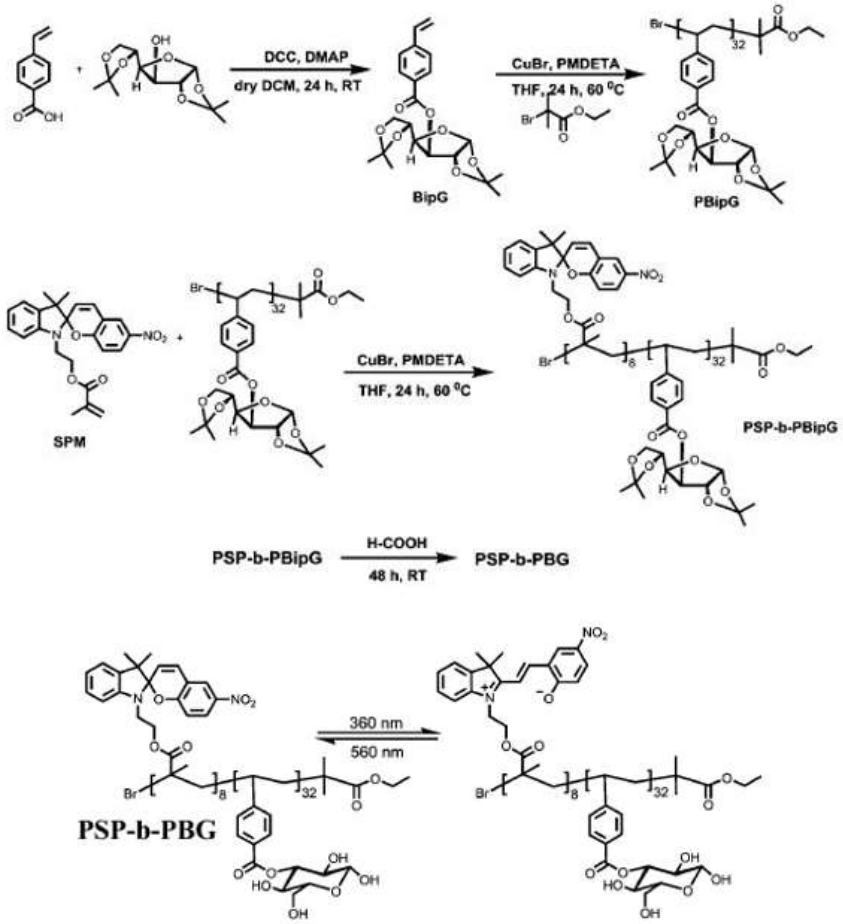

Scheme 1.6: Synthesis of PSP-*b*-PBG glycopolymer by using ATRP and light-induced isomerization of glycopolymer.

In 2012, Jiang and coworkers exploited the RAFT polymerization to synthesize a temperature-responsive phenylboronic acid (BA) ended poly(N-isopropylacrylamide) (BA-PNIPAM, Mw=7000 g/mol, *Đ*=1.10, LCST≈32°C) via RAFT polymerization, as well as two glycopolymers with *N*-linked pendant

galactose or glucose residues (PGal, Mn=14 kg/mol, *Đ*=1.18, PGlc, Mw=14 kg/mol, *Đ*=1.20).[22] After mixing of BA-PNIPAM and PGal or PGlc under alkaline conditions (pH 9), boron oxygen cyclic ester bonds were formed between BA and sugars, resulting in “graft-like” PV-*Gal* and PV-*Glc* complexes. Due to the temperature-sensitive character of the PNIPAAM block (~32°C), the PV-*Gal* and PV-*Glc* (PV/Gx, 2/1) were shown to self-assemble at 33°C, leading to uniform sugar covered vesicles with R_h of 62 nm and 68 nm, respectively (**Table 1.1**, **entry 12**).

In 2014, Poly(styrene)-*block*-poly(4-vinylbenzyl 2,3,4,6-tetra-*O*-acetyl-*α*-D-mannopyranoside) (PS_x-*b*-$PManAc_y$, x=75, y=7, 9, 19 and 25, *Đ*≤1.10) were produced by Jiang’s group via sequential RAFT polymerizations mediated by S-ethyl-S′-(α,α′-dimethyl-α″-acetic acid) trithiocarbonate.[23] Self-assembly of the block copolymers was triggered in THF by quantitatively deprotecting the acetylated glycopolymer block using tetrabutylammonium hydroxide. Upon addition of TBAOH in water, the solution (at 2 mg/ml) immediately turned milky. In agreement with these macroscopic observations, PS_{75}-*b*-$PManAc_{25}$ unimers detected before deprotection (R_h=3 nm) disappeared in favor of large aggregates of PS_{75}-*b*-$PMan_{25}$ (R_h=43 nm, *Đ*=0.08). DLS/SLS and cryo-TEM analyses confirmed the formation of vesicles in THF with a middle layer of glycopolymer and inner and outer layers of PS for PS_{75}-*b*-$PMan_{25}$ and PS_{75}-*b*-$PMan_{19}$ (R_h=25 nm, *Đ*=0.07) whereas sub-30 nm micelles with glycopolymer cores were obtained with copolymers exhibiting shorter glycopolymer blocks. Reduction of chloroauric acid was further performed (without addition of reducing agent) to grow sub-5nm gold nanoparticles within the shell of the glycovesicles which acted then as green nanoreactors. The authors finally investigated the influence of water on the self-assembly of the diblocks. Addition of water (up to 27 wt.%) in a dispersion of vesicles in THF induced a reshuffling of the diblock chains resulting in an inversion of morphology from glyco-inside to glyco-outside organizations. Interestingly, glyco-inside vesicular structures in

THF were transformed in glyco-outside micelles in water (PS_{75}-*b*-$PMan_{25}$, R_h=11 nm, PDI=0.08; PS_{75}-*b*-$PMan_{19}$, R_h=12 nm, PDI=0.07) whereas glyco-inside micellar structures changed to glyco-outside vesicles (PS_{75}-*b*-$PMan_9$, R_h=60 nm, PDI=0.35; PS_{75}-*b*-$PMan_7$, R_h=102 nm, PDI=0.15). (**Figure 1.3**, **Table 1.1**, **entry 13**).

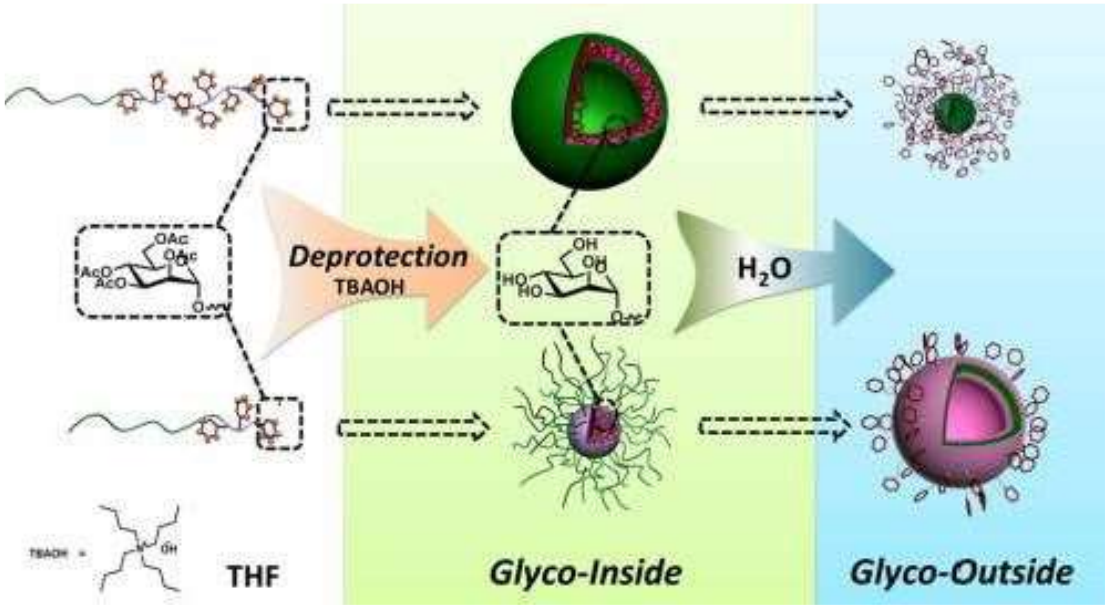

Figure 1.3: Deprotection-triggered self-assembly and structure translation process of PS-*b*-PMan copolymers.

Using a similar synthetic approach (sequential polymerization of styrene and vinyl benzyl glycomonomers), the same group synthesized block copolymers having benzoyl or acetyl lactose pendant groups, PS-*b*-PLacBz and PS-*b*-PLacAc. A library of protected diblocks was designed: ***SbB*$_{15}$** (PS_{115}-*b*-$PLacBz_{15}$, Mn=15.7 kg/mol, *Đ*=1.21), ***SbA*$_{13}$** (PS_{115}-*b*-$PLacAc_{13}$, Mn=16.3 kg/mol, *Đ*=1.21), ***SbA*$_7$** (PS_{115}-*b*-$PLacAc_7$, Mn=14 kg/mol, *Đ*=1.19) and ***SbB*$_5$** (PS_{115}-*b*-$PLacBz_5$, Mn=13.1 kg/mol, *Đ*=1.21).[24] The addition of TBAOH resulted in the generation of assemblies with different dimensions and morphologies as a function of the kinetics of deacetylation/debenzoylation. For SbA_{13}, the deprotection led to the preparation of vesicles with R_h≈24 nm. In contrast, the removal of Bz protecting groups in SbB_{15} was significantly slower resulting in the formation of vesicles with R_h≈58 nm. Similarly, the rapid deprotection of SbA_7 gave rise to micelles

with R_h≈14 nm whereas slow debenzoylation of SbB_5 afforded vesicles with R_h≈14 nm (**Table 1.1**, **entry 14**).

In 2018, the same group designed triblock glycopolymers P-Acm-n via RAFT polymerizations and post-polymerization modification (P: PEG; Acm: acetyl protected sugar block with m, the degree of polymerization (DP); n: DP of PS block)[25], Four different copolymers were synthesized: P-Ac50-36 (Mn=42.2 kDa, *Đ*=1.26), P-Ac100-60 (Mn=59.1 kDa, *Đ*=1.38), P-Ac100-140 (Mn=96.3 kDa, *Đ*=1.24), and P-Ac100-350 (Mn=88.6 kDa, *Đ*=1.40). The self-assembly of **P-Acm-n** was induced by briefly adding water to the copolymers solution (in THF) and dialysing against water. Glycovesicles with hydrodynamic radius of 61 nm, 128 nm, 65 nm and 100 nm were obtained from P-Ac50-36, P-Ac100-60, P-Ac100-140, and P-Ac100-350 respectively (**Table 1.1**, **entry 15**). Addition of NaOH into vesicles aqueous solution had a major impact on the morphology of the self-assemblies leading to the creation of bigger vesicles and micelles. This morphological transition was mainly induced by carbohydrate-carbohydrate interactions (CCI). Next, Ca^{2}+ was added in the deprotection process. As a result, P-Ac50-36 vesicles and P-Ac100-140 vesicles evolved to micelles whereas PAc100-60 and P-Ac100-350 vesicles reshaped into lamella sheets and micelles, respectively. This may be caused by the modification of the H/L ratio (DP ratio of hydrophilic to hydrophobic blocks) and the CCI for the different copolymers., the morphological transitions were assigned to the drastic change of H/L ratio after deprotection for P-Ac50-36 and P-Ac100-140 and to CCI for PAc100-60 and P-Ac100-350. In order to work under physiological conditions, the authors also investigated enzyme-catalyzed deprotection of the sugar residues using lipase type I (from wheat germ) in water at neutral pH. Similar to the NaOH treatment, lipase-catalyzed deacetylation of the block copolymer (P-Ac50-36) initiated a vesicle-to-micelle transition. On this basis, ovalbumin-loaded P-Ac50-36-based glycovesicles were shown to release 90% of the cargo after 70 h in the presence of the lipase. When ovalbumin (OVA)-

encapsulated glycovesicles were internalized by dendritic cells (DCs), lipases from lysosomes induced the presentation of the antigen to T cells (**Scheme 1.7**).

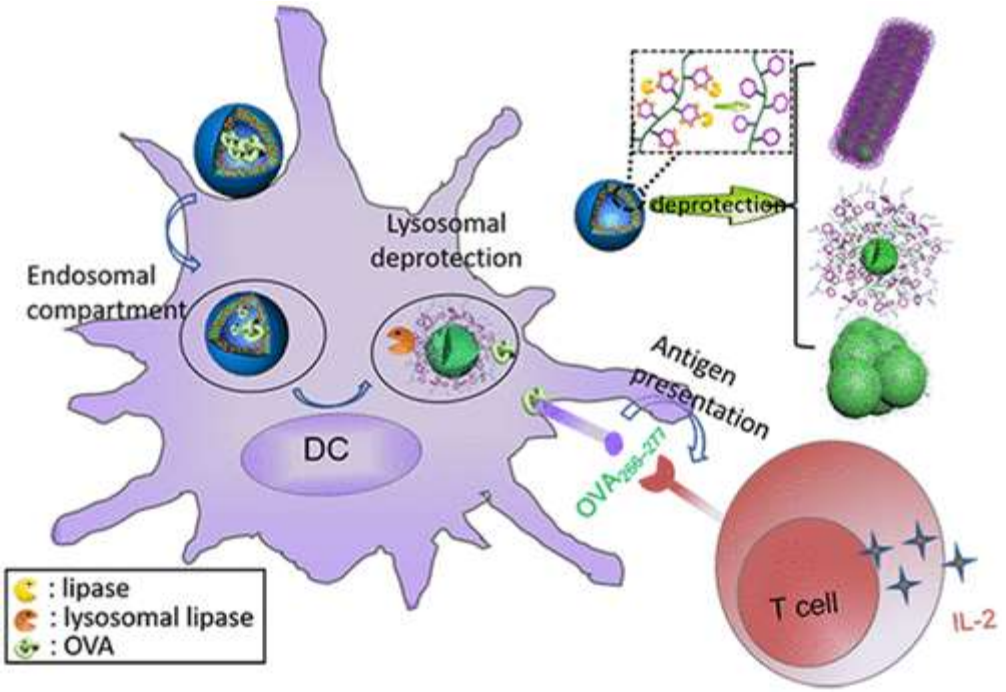

Scheme 1.7: The deprotection-triggered self-assembly to glycovesicles and cellular uptake efficiency of free OVA, OVAloaded Glyco-vesicle, OVA/Glyco-vesicle mixture and OVA/Glyco-micelle mixture after 24 h incubation

In 2015, Tongfei Shi and coworkers synthesized star-shaped poly(*ε*-caprolactone)-*block*-poly(2-aminoethyl methacrylate)-*block*-poly(gluconamidoethylmethacrylate) (SPCL–PAMA–PGAMA) glycopolymers by combining ROP of *ε*-caprolactone monomer using pentaerythritol initiator and two-step RAFT polymerization of AMA and GAMA using four arms star shaped SPCL-CTP (via esterification of SPCL-OH with 4-cyano-4-(phenylcarbonothioylthio) pentanoic acid) as macro-RAFT agents (**Table 1.1**, **entry 16**)[26]. The resulting glycopolymer $SPCL_{27}$-$PAMA_{10}$-$PGAMA_{11}$ (Mn=31.4 kg/mol, *Đ*=1.13) self-assembled into vesicles in PBS with an average diameter of 59 nm. Water-soluble CdTe QDs of 2.8-4.0 nm decorated with carboxylic acid groups were coupled with the amine groups of the glycopolymer vesicles giving birth to Gly@QDs vesicles (80 nM QDs) with hydrodynamic diameters around

72 nm from DLS. The Gly@QDs vesicles could bind Con A without alteration of their luminescent properties. After internalization through an endocytosis pathway, Gly@QDs vesicles (emitting in the green) were easily observed in Hep G2 cells, demonstrating their potential interest for targeted drug delivery and imaging purposes.

In 2017, Y. Xiao, H. Sui and J. Du prepared glycovesicles from poly(ethylene oxide)-*block*-poly[(7-(2-methacryloyloxyethoxy)-4-methylcoumarin)-*stat*-2 (diethylamino)ethyl methacrylate-stat-(*α*-D-glucopyranosyl)ethyl methacrylate] [PEO_{43}-*b*-P-(CMA_8-*stat*-DEA_{80}-*stat*-$GEMA_{12}$) synthesized via ATRP from PEG macroinitiator (Mn=9.7 kg/mol, *Đ*=1.17).[27] Self-assembly of the copolymer in THF/H_2O (1:3, v/v) starting from a solution at of 2.0 mg/mL in THF resulted in the formation of glycovesicles with a hydrodynamic diameter of 362 nm by DLS analysis after elimination of THF by dialysis (**Figure 1.4**, **Table 1.1**, **entry 17**). FITC-Con A (75 µg/mL) was then bound to the glycovesicles (without inducing the formation of vesicle-vesicle aggregates) with a loading efficiency of 34 %. FITC-Con A-coated nanoparticles were then photo-cross-linked owing to the presence of coumarin moieties within the shell (photodimerization at 365 nm for 5 seconds, degree of cross-linking around 50%). Both the structure and the size of the glycopolymersomes were maintained after cross-linking. Addition of free glucose to these sugar sponges resulted in the cleavage of Con A-polymer shell interactions (physical cross-links) and a significant increase of the vesicle size (from 390 to 701 nm upon addition of 1.5 mg/mL glucose). The sugar sponge presented low cytotoxicity against normal liver L02 cells and an excellent antidiabetic activity was observed for 2 days after injection to type I diabetic KM mice without using insulin or other hypoglycemic drugs.

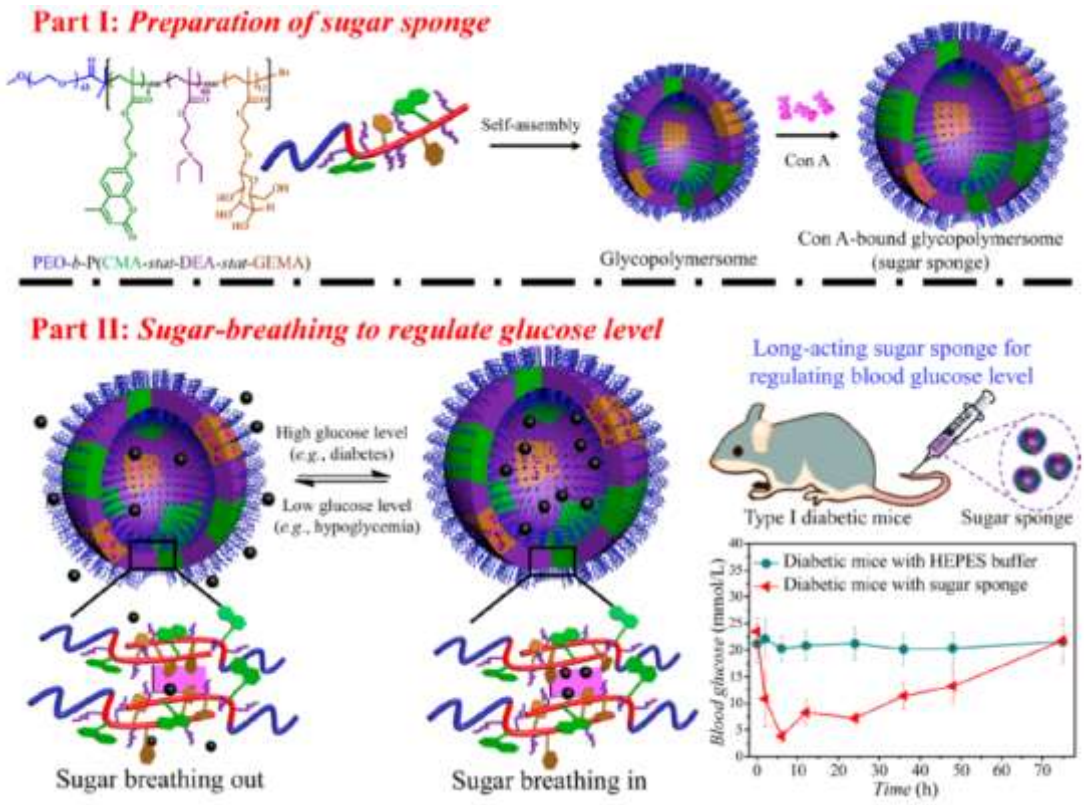

Figure 1.4: Preparation of sugar sponge and its blood glucose regulation behavior via sugar breathing.

In 2018, the group of Stenzel reported on curcumin-triggered morphological transitions in block copolymer self-assemblies.[28] Poly(1-*O*-methacryloyl-*β*-D-fructopyranose)-*b*-poly(methyl methacrylate) (Poly(1-*O*-MAFru)$_{36}$-*b*-PMMA$_{192}$) was synthesized by sequential RAFT polymerizations of 1-*O*-MAFru and MMA and deprotection of the fructose motifs. The block copolymer was dissolved in THF at a concentration of 2 mg/mL in the presence (or not) of curcumin (at 0.37 or 0.75 mg/mL) followed by injection of water and dialysis. In the absence of the drug, the self-organization of the block copolymer in water led to rod-like micelles as highlighted by TEM and SAXS analyses. Interestingly, the addition of curcumin to poly(1-*O*-MAFru)$_{36}$-*b*-PMMA$_{192}$ induced a morphology transition from rod-like micelles (no drug) to big vesicles of 179 nm or small vesicles of 134 nm when the concentration of curcumin was 0.37 and 0.75 mg/ml in solution depending on the amount of drug located in the shell (**Figure 1.5**, **Table**

1.1, **entry 18**). SANS measurements highlighted that the addition of curcumin and its interactions with the fructose-functionalized blocks provokes a significant dehydration of the glycopolymer shell which affects the process of association of the diblock in aqueous medium but also the final cell uptake of the resulting nano-objects (owing to fructose units mobility restrictions which alter their recognition by MCF-7 cell receptors).

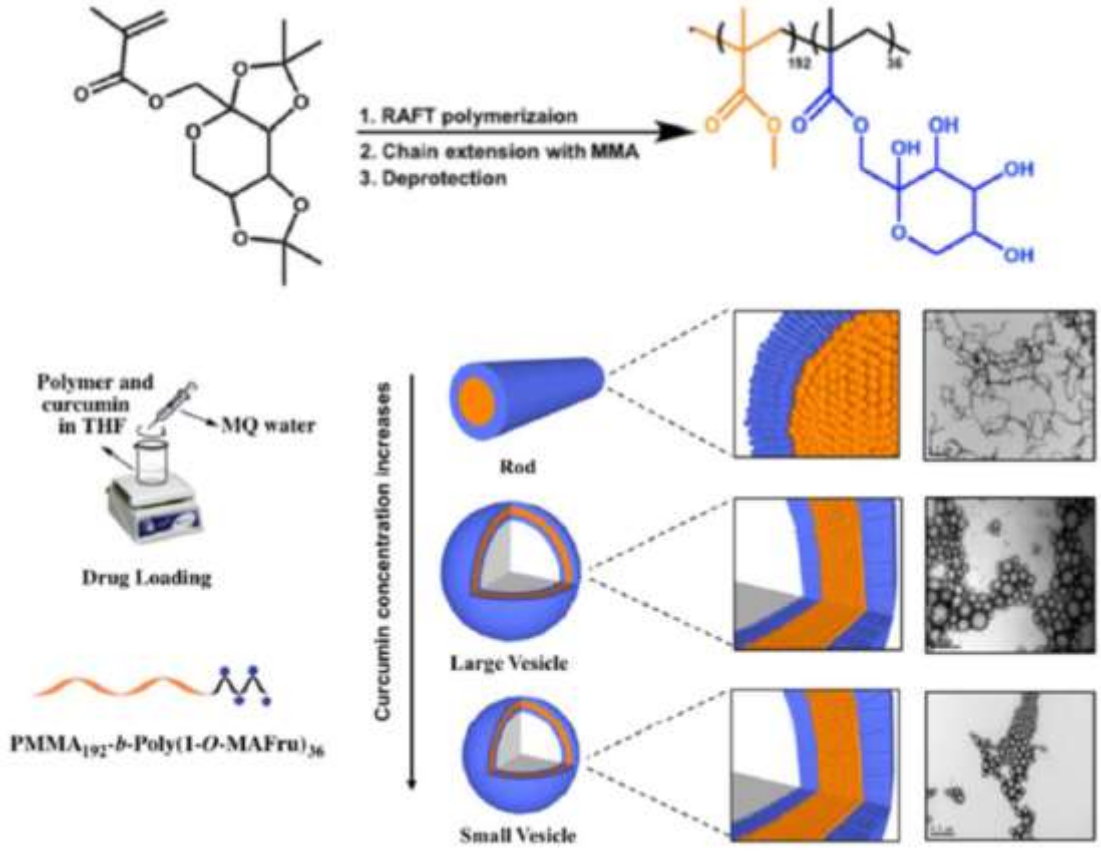

Figure 1.5: (Top) Synthesis of Poly(1-*O*-MAFru)$_{36}$-*b*-PMMA$_{192}$ and (bottom) various morphologies formed by self-assembly of Poly(1-*O*-MAFru)$_{36}$-*b*-PMMA$_{192}$ (2 mg/ml) in the presence of different amount of curcumin: 0 mg/mL, 0.37 mg/mL and 0.75 mg/mL by TEM. Scale bar = 500 nm

In 2018, J. Quan et al. designed a series of novel thermo-responsive double hydrophilic block glycopolymers (TDHBGs)[29]. The desired poly(di(ethyleneglycol)methyl ether methacrylate)-*block*-poly(6-*O*-vinyladipoyl-D-galactose) (PDEGMA-*b*-POVNG) was synthesized by sequential RAFT

.

polymerizations of DEGMA and OVNG using cyanomethyl methyl(4-pyridyl)carbamodithioate (CMPCD) as chain transfer agent (**Figure 1.6**, **Table 1.1**, **entry 19**). By tuning the initial molar fraction of OVNG (OVNG+DEGMA), a series of glycopolymers (TDHBG-1, f_{OVNG}=11.0%, Mn=5.54×10^4 g/mol; TDHBG-2, f_{OVNG}=12.2%, Mn=5.70×10^4 g/mol; TDHBG-3, f_{OVNG}=14.6%, Mn=5.91×10^4 g/mol) with different LCSTs (35.5, 31.4 and 30.3 °C respectively) were obtained. At T=25°C, self-assembly of TDHBG-1 in water (at 0.20 mg/mL) gave birth to spherical hollow particles with an average radius of about 30 nm (micelle-1) whereas other morphologies (worm-like, ellipsoids…) were obtained upon decrease of polymer concentration C=0.02 mg/mL or increase of temperature (45°C). Similar self-assembly behavior in aqueous medium was highlighted with TDHBG-2 and TDHBG-3 copolymers.

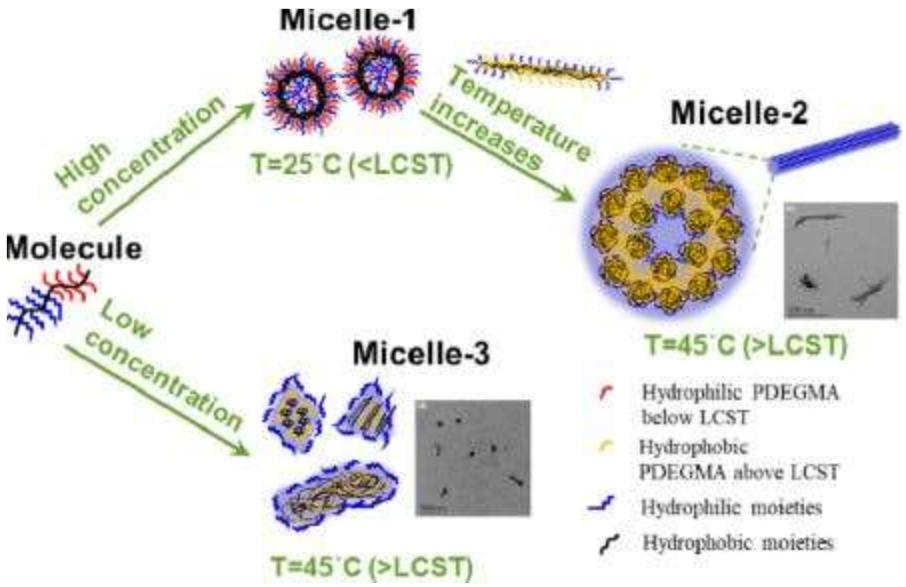

Figure 1.6: Morphologies transition of TDHBG-1 under various temperature and polymer concentration in aqueous solution.

Under the impetus of Hawkett, Pan, Charleux and Armes[30,31,32], Polymerization-induced self-assembly (PISA) has recently emerged as a method of choice for both controlling polymer chain growth and the organization of the resulting block

copolymers into diverse morphologies (i.e. nanospheres, worm-like micelles, or vesicles, see **Scheme 1.8**).[33] PISA can be performed under dispersion or emulsion polymerization conditions in aqueous or organic media at very high solid content (up to 40-50 % w/w) making it of great interest for industrial applications. In spite of the potential applications of glyconanoparticles in the biomedical field, examples of PISA processes involving glycopolymer blocks are still scarce.

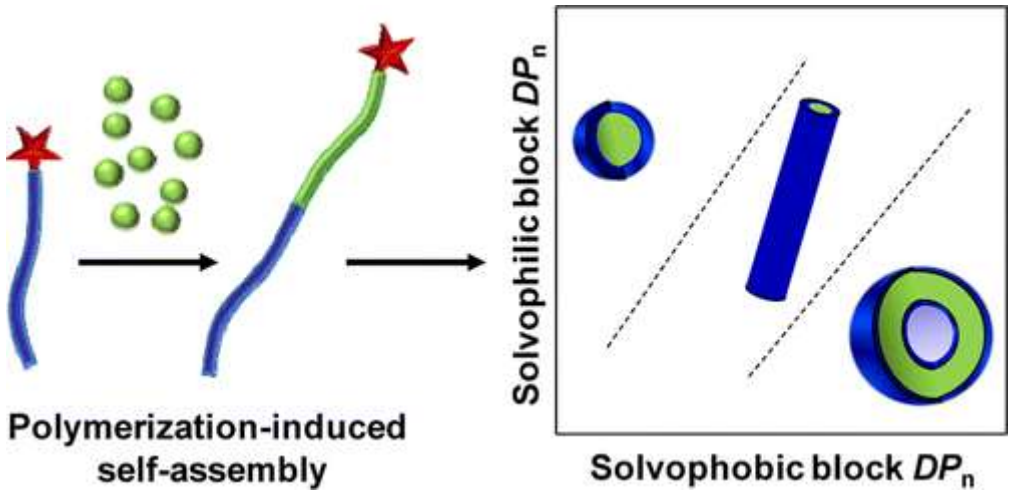

Scheme 1.8: Principle of Polymerization-Induced Self-Assembly (PISA).

In 2013, Armes and coworkers reported the preparation of biocompatible galactose-functionalized diblock copolymer nano-objects by “PISA” in aqueous solution.[32] With that aim, RAFT polymerization was initially employed to produce two homopolymers of a galactose-functionalized methacrylic monomer ($PGalSMA_{34}$, Mn=16.3 kg/mol, $Đ$=1.13) and of glycerol monomethacrylate ($PGMA_{51}$, Mn=16.2 kg/mol, $Đ$=1.15). The resulting, $PGalSMA_{34}$ and $PGMA_{51}$, were further used together as macroCTAs at 1:9 molar ratio to mediate the polymerization of 2-hydroxypropyl methacrylate (HPMA). Depending on the length of the PHPMA block and the copolymer concentration in the aqueous solution, spherical nanoparticles, worm-like micelles, or vesicles were generated. Interestingly, glycovesicles were obtained when the degree of polymerization of PHPMA was 270 (1:9 $PGalSMA_{34}$ + $PGMA_{51}$)-$PHPMA_{270}$) and

the solids content ranged from 10 to 20% wt. (**Figure 1.7**, **Table 1.1**, **entry 20**). Based on turbidimetric lectin binding tests, Armes and co-workers further established that the galactose-functionalized nano-objects were able to interact with galectins *in vitro* and that fluorophore-loaded vesicles (rhodamine B octadecyl ester) were quickly internalized by HDF cells where the dye was intracellularly released.

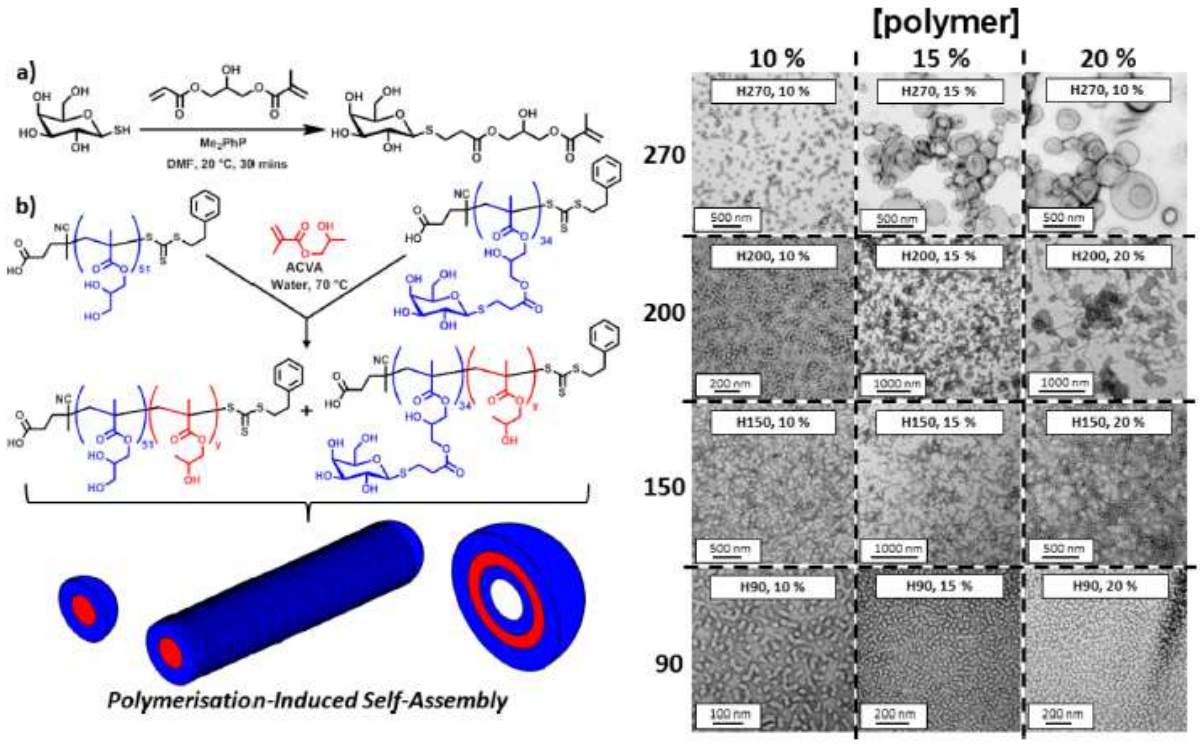

Figure 1.7: (Left) design of various nano-objects via block copolymer self-assembly via PISA; (Right) representative TEM images of the nanoparticles made of (1:9 $PGalSMA_{34}$+$PGMA_{51}$)-$PHPMA_x$.

In 2018, the group of Six prepared dextran-based graft copolymers by photo-PISA (**Scheme 1.9**).[34] Hydroxyl groups of dextran chains (Mn=32 kg/mol, *Đ* =1.4) were first partially reacted with photosensitive 4-(propylthiocarbonothioylthio)-4-cyanopentanoic acid (TTC) in DMSO (2.5 TTC per 100 sugar units and approximatively 5 TTC groups per dextran chain) to prevent precipitation of the resulting macroCTA chains (DexTTC) in aqueous medium after derivatization. Aqueous dispersion polymerization of 2-hydroxypropyl methacrylate was further undertaken under UV irradiation (365

nm) in the presence of DexTTC. By tuning the irradiation time (10 and 60 min) and the solids content (5 and 20 wt%), a series of Dex-g^{5}-PHPMA$_y$ copolymers (5 being the average number of PHPMA grafts per dextran chain and *y,* the number-average degree of polymerization of each graft) with various PHPMA graft length and different morphologies were obtained (**Figure 1.8**, **Table 1.1**, **entry 21**). Depending on the length of PHPMA grafts, micelles and worm-like micelles were produced at low solids contents (5 wt%) whereas glycovesicles (R_h~100-110 nm) were observed at high solids content (20 wt%) and high values of y (typically superior to 400).

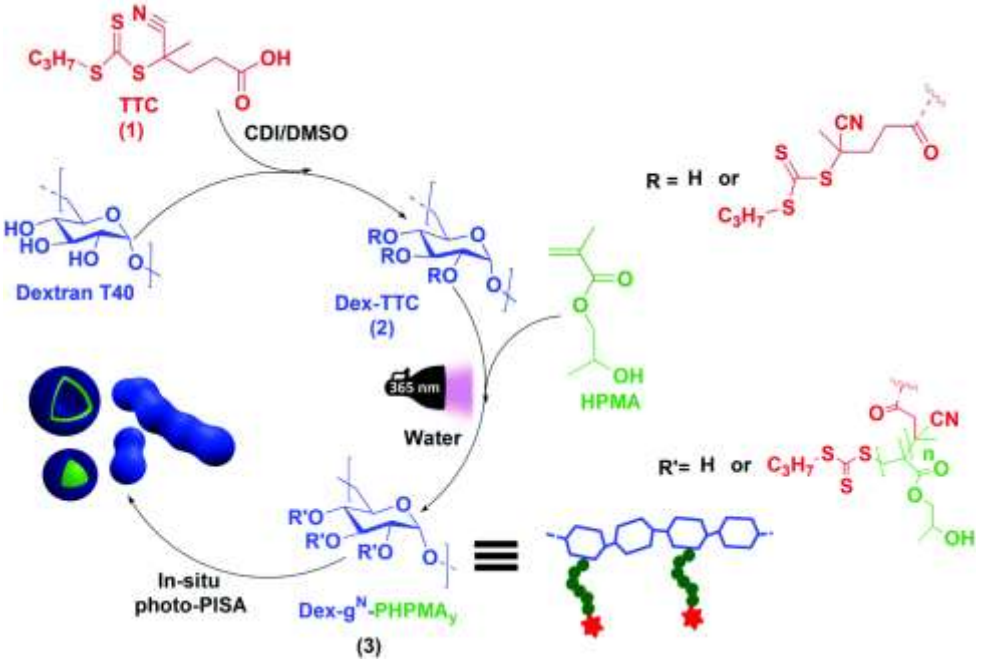

Scheme 1.8: Synthetic pathway to Dex-g^{N}-PHPMA$_y$-based glyco-nanostructures using the aqueous photo-PISA process.

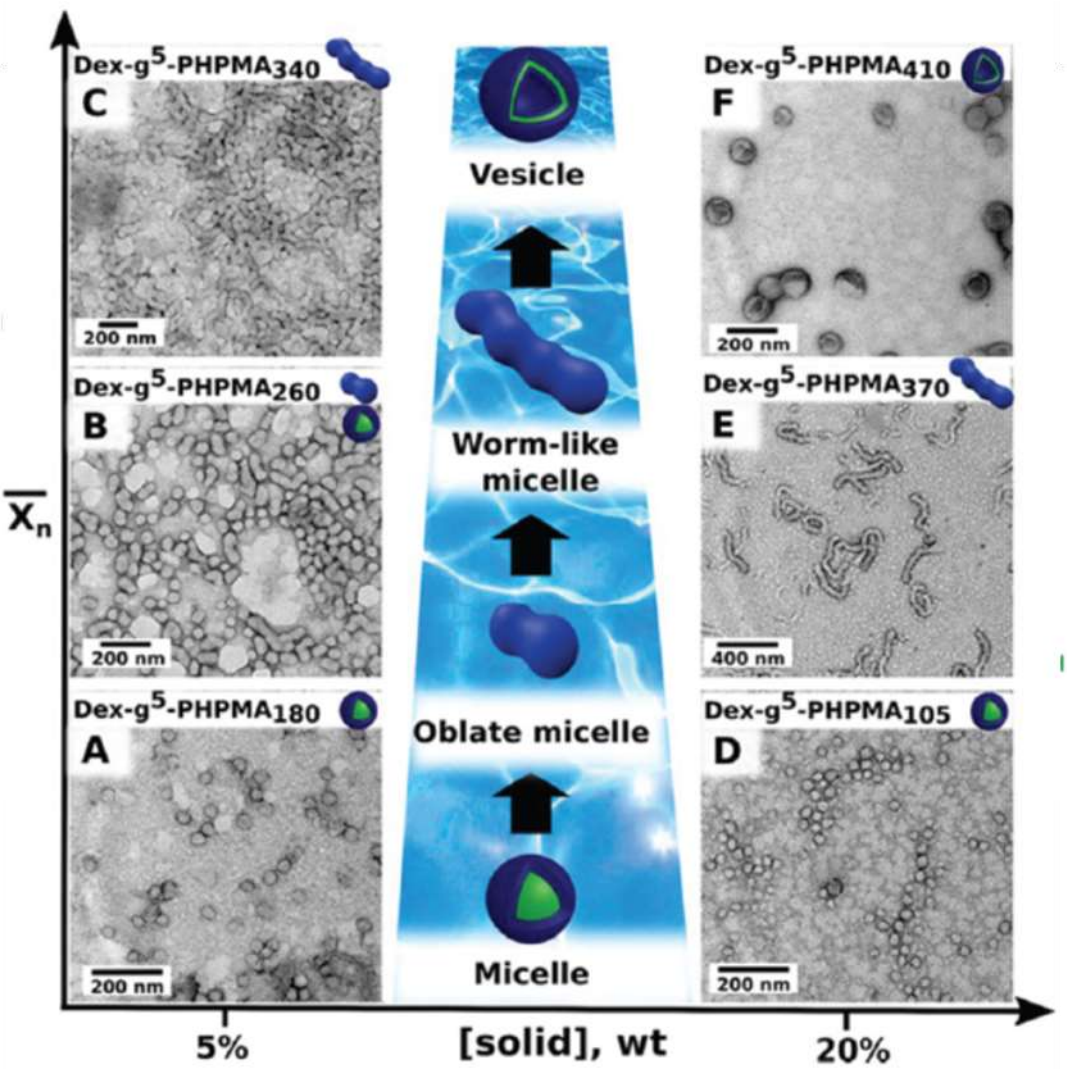

Figure 1.9: TEM images of a series of Dex-g^5-PHPMA$_y$ based glyco-nanostructures prepared by the aqueous photo-PISA. Samples were observed at 1 mg/mL.

Recently, Yan et al. synthesized heptyl-mannose-functionalized nanoparticles with diverse morphologies by PISA (**Scheme 1.10**).[35] P(HMM$_9$-*co*-EMM$_{34}$) macroCTA ($Mn_{,SEC}$=9.2 kg/mol, $Đ$<1.20) was first prepared by RAFT copolymerization of N-[7-(*α*-D-mannopyranosyloxy)heptyl] methacrylamide (HMM) and N-[2-(*α*-D-mannopyranosyloxy)ethyl] methacrylamide (EMM) in the presence of 4-cyano-4-(phenylcarbonothioylthio) pentanoic acid (CPADB) and 4,4′-azobis(4-cyanovaleric acid) (ACPA) at 70°C in D_2O/DMSO (1/1, v/v) using $[EMM]_0+[HMM]_0)/[CPADB]_0$=50. Chain extensions (GMA) were further carried out with glycidyl methacrylate (at 70°C in demineralized water, pH=7) at

different $[GMA]_0/[P(HMM_9\text{-}co\text{-}EMM_{34})]_0/[ACPA]_0$ ratio, (X/1/0.2, X=200, 400, 600 and 800). Targeting PGMA degrees of polymerization between 200 and 600 afforded the generation of spherical 100 nm-nanoparticles (X=200 or 400, at 5 or 10 wt% solids content) (**Table 1.1**, **entry 22**) or polydisperse worm-like structures (X=600 at 5% wt solids content). Vesicles of 840 nm in size were finally prepared when the degree of polymerization of PGMA block was 800 (at 5% w/w solids content). Owing to the capability of heptyl *α*-D-mannose motifs to establish strong interactions with FimH adhesin, a virulence factor of *E coli*, the incubation of heptyl-mannose-functionalized glyconanoparticles with Adherent Invasive *Escherichia coli* AIEC LF82 (for 12 h) resulted in agglutination of the bacteria.

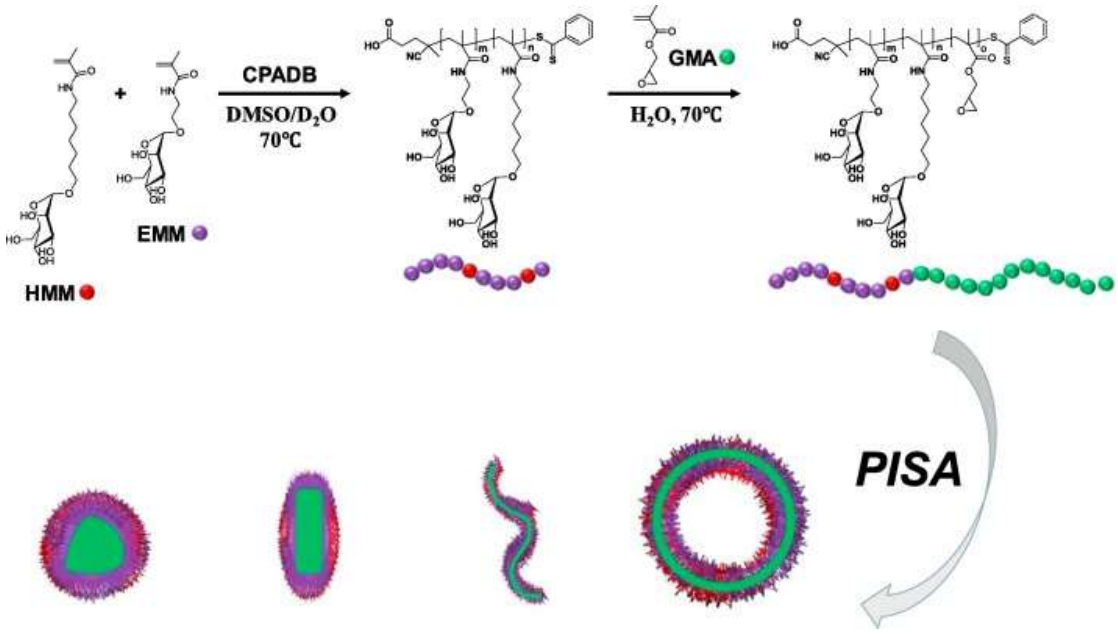

Scheme 1.10: Route to heptyl mannose decorated glyconanoparticles with tunable morphologies using polymerization-induced self assembly.

Table 1.1: Preparation of glyconanocapsules by self-assembly strategy from amphiphilic vinyl block glycopolymers obtained by sequential polymerizations.

Entry	Classification	Polymer	Protocol of self-assembly	Solvent	Size (nm)	Ref.
1	Polymersome	PS-*b*-PGEA	Solvent shifting	Dioxane/DMF	100-400	8-10
2	Polymersome	poly(*L*-alanine)-*b*-poly(2-acryloyloxyethyllactoside)-*b*-poly(*L*-alanine)	CMC	H_2O	250 (R_h)	11-12
3	Polymersome	poly(ε-caprolactone)-*b*-poly(glucobionamidoethyl methacrylate)	Solvent shifting	DMF/H_2O	250	13
4	Polymersome	poly(ε-caprolactone)-*b*-poly(lactobionamidoethyl methacrylate)	Solvent shifting	DMF/H_2O	148	14
5	Polymersome	poly(amido amine)-b-poly(3-caprolactone)-b-poly(D-gluconamidoethyl methacrylate)	Solvent shifting	DMF/H_2O	305	15
6	Polymersome	(poly(*D*-gluconamidoethyl methacrylate)-PCL-poly(*D*-gluconamidoethyl methacrylate)	Solvent shifting	DMF/H_2O	81	16
7	Polymersome	poly(2-glucosyloxyethyl methacrylate)-*block*-poly(diethyleneglycol methacrylate)	T	H_2O	182	17
8	Polymersome	poly(3-hexylthiophene)-*block*-poly(3-O-methacryloyl-D-galactopyranose)	Solvent shifting	THF/H_2O	89	18
9	Polymersome	poly(*N* -acryloylmorpholine)-*b*-poly(*N*-acryloyl-β -D-glucopyranosylamine)-*b*-poly(*N*-acryloylmorpholine)	Solvent shifting	THF/H_2O	380	19
10	Polymersome	poly(pyrenylmethyl methacrylate)-*b*-poly(3-*O*-4-vinylbenzoyl-D-glucopyranose)	Solvent shifting	DMF/H_2O	473	20
11	Polymersome	poly(spiropyran methacrylate)-*block*-poly(3-*O*-4-vinylbenzoyl-D-glucopyranose)	Solvent shifting	DMF/H_2O	366	21
12	Polymersome	poly(N-isopropylacrylamide)-*graft*-polygalactoside	T	H_2O	68 (R_h)	22
13	Polymersome	Poly(styrene)-*block*-poly(ManAc)	De-acetylation	THF/H_2O	42 (R_h)	23

14	polymersome	Poly(styrene)-*block*-poly(lactose)	De-acetylation	THF/H_2O		24
15	Polymersome	Poly(ethylene glycol)-*block*-polystyrene-poly(Acetyl-glucose-4-chloromethylstyrene)	Solvent shifting	THF/H_2O		25
16	polymersome	poly(ε-caprolactone)-*b*-poly(2-aminoethyl methacrylate-*b*-poly(gluconamidoethylmethacrylate)	Solvent shifting	DMSO/H_2O	59	26
17	Polymersome	PEO-*b*-P-(CMA-*stat*-DEA-*stat*-GEMA)	Solvent shifting	THF/H_2O	362 (Rh)	27
18	Polymersome	poly(1-*O*-methacryloyl-*β*-Dfructopyranose)-*b*-poly(methyl methacrylate)	Solvent shifting	THF/H_2O		28
19	Polymersome	poly(di(ethyleneglycol)methyl ether methacrylate)-*block*-poly(6-*O*-vinyladipoyl-D-galactose)	T	H_2O	62 (R_h)	29
20	Polymersome	poly(GalSMA)-*b*-poly(HPMA), poly(GMA)-*b*-poly(HPMA)	PISA	H_2O		32
21	Polymersome	dextran-*graft*-poly(HPMA)	Photo-PISA	H_2O		34
22	Polymersome	P((HMM_9-*co*-EMM_{34})-*b*-GMA_{800})	PISA	H_2O	121	35

CMC: Critical Micelle Concentration. T: Temperature.

Amphiphilic vinyl block glycopolymers by post-modification

In 2006, the group of Schlaad reported the preparation of glycosomes from thiol-ene modification of 1,2-polybutadiene-*block*-polystyrene (PB_{85}-*b*-PS_{351}) block copolymer with 1-thioglucose (**Table 1.2**, **entry 1**)[36] The self-assembly behavior of the resulting amphiphilic copolymer (17 wt.% glucose) was investigated both in THF and water. When the polymer was directly dissolved in THF at a concentration of 0.02 wt.%, large vesicles having a polystyrene corona and a R_h≈250 nm (as determined by DLS) were formed. Addition of water up to 4 wt.% destroyed these assemblies (obtention of a clear solution) and promoted the formation of small micelles or non-aggregated polymer coils (R_h≈15-30 nm as determined by DLS). Further increase of water content to 6 wt.% and above led to the formation of vesicles (R_h≈120 nm) with a glucose corona. These vesicles were shown to remain stable after evaporation of THF. One year later, the same group investigated the thiol-ene modification of 1,2-polybutadiene chains with a degree of polymerization ~ 40 with 1-thioglucose (**Table 1.2**, **entry 2**)[37]. The resulting copolymer (degree of functionalization=55%) self-assembled into unilamellar vesicles with a bilayer membrane of R_h~130 nm through direct dissolution in water. In 2009, Schlaad and coworkers further synthesized glycosylated PB-PEO amphiphilic block copolymers (**Figure 1.9**, **Table 1.2**, **entry 3**) by post-modification of 1,2-polybutadiene-*b*-poly(ethylene oxide) (PB_x-PEO_y) with 2,3,4,6-*tetra*-*O*-acetyl-1-*thio*-*β*-D-glucopyranose through photoaddition (glycopolymer 1, x=65, y=212, number of glucose units=33, *Đ*=1.16; glycopolymer 2, x=68, y=34, number of glucose units=30, *Đ*=1.08).[38] After deacetylation, the two glycopolymers were directly dispersed into pure water (0.025-0.1 wt%), generating large aggregates (R_g = 550 ±20 nm, R_h = 520 ± 20 nm for glycopolymer 1; R_g,= 270± 40 nm, R_h = 280±30 nm for glycopolymer 2). As suggested by the value of $R_{g,0}/R_{h,0}$ close to 1, TEM analysis revealed that the aggregates are vesicles in both systems. Interestingly, 2D-NOESY-NMR and SERS experiments indicated that the thin

membranes of these glycovesicles adopt an asymmetric structure with sugar residues on the outside and PEO blocks on the inside (**Figure 1.9 C**) after 2D-NOESY-NMR and SERS analysis of ~1 wt.% solution of 1 in D_2O.

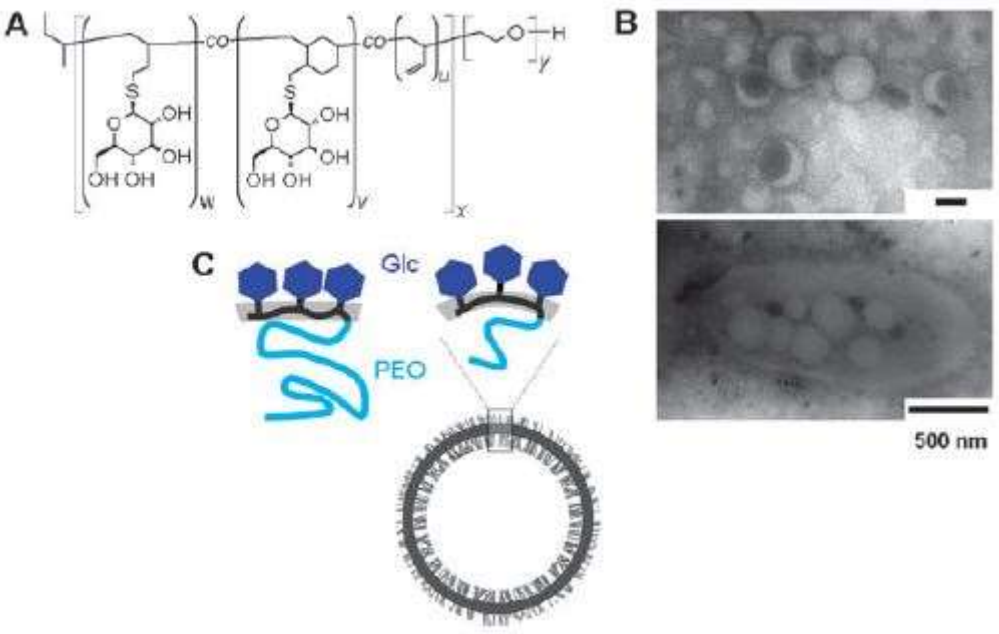

Figure 1.9: (A) Chemical structure of PB-PEO-based glycopolymers 1 (w + v = 0.51, u = 0.06, x = 65, y = 212) and 2 (w + v = 0.44, u = 0.09, x = 68, y = 34); (B) TEM images of collapsed vesicles using 0.2 wt.% glycopolymer 1 in water; (C) Monolayered vesicles constructed with glycopolymer 1 (left) and 2 (right) via spontaneous self-assembly.

In 2008, Schlaad and coworkers prepared a glycopolyamide homopolymer (POxaGlc) by cationic polymerization of 2-(3-butenyl)-2-oxazoline (degree of polymerization ~ 63 and $Đ$=1.13) followed by the “thio-click” photoaddition of an acetylated thio-glucose derivative and the deprotection of the glucose groups (MeONa in methanol/chloroform mixture).[39] The direct dissolution of the homopolymer in water (at a concentration of 0.3 wt.%) generated unilamellar vesicles with a diameter of 60 nm as estimated by TEM and several hundred nanometer long hollow nanofibers (**Table 1.2**, **entry 4**). The authors suggested that the rather hydrophobic poly(N-acyl-ethyleneimine) main chains stand parallel to the interface whereas the sugar motifs are pointing in the aqueous medium.

In 2010, Borsali and coworkers reported vesicular morphologies produced from thermoresponsive maltoheptaose-block-poly(N-isopropylacrylamide) (Mal_7-*b*-$PNIPAM_n$) hybrid copolymer.[40] A series of Mal_7-*b*-$PNIPAM_n$ having different molar masses and volume fractions were synthesized in a few steps. First, maltoheptaose was reacted with propargylamine and subsequent N-acetylated with acetic anhydride to obtain alkyne-functionalized *β*-N-acetylpropargyl maltoheptaosylamide (**1**). The authors subsequently prepared a library of azido-α-functionalized poly(N-isopropylacrylamide)s by ATRP (N_3-PNIPAMn, n=28, 45, 119 and 220, Mn=5700-34900 g/mol, *Đ*=1.19-1.23). Then, **1** was efficiently conjugated to N_3-PNIPAMn via "click" reaction using sodium ascorbate and copper sulfate in water resulting in the formation of the diblock copolymers Mal_7-*b*-$PNIPAM_{28}$, Mal_7-*b*-$PNIPAM_{45}$, Mal_7-*b*-$PNIPAM_{119}$ and Mal_7-*b*-$PNIPAM_{220}$ with cloud point temperatures (T_{cp}) ranging from 73.9 to 39.4°C with the shortest and the longest PNIPAM blocks respectively. N_3-$PNIPAM_{220}$ (Mn=34900 g/mol, *Đ*=1.23, T_{cp}=36.4°C) and Mal_7-*b*-$PNIPAM_{220}$ were dissolved in water (0.2 g/L) at room temperature (below the T_{cp}). Heating aqueous solutions of Mal_7-*b*-$PNIPAM_{220}$ above T_{cp} (47°C) triggered the formation of glycovesicles (R_g=145 nm, R_g/R_h=1.01) whereas N_3-$PNIPAM_{220}$ logically self-assembled into nanoparticles (R_g=122 nm, R_g/R_h=0.67) (**Table 1.2**, **entry 5**).

In 2014, the group of Stenzel described the preparation of poly(*N*-isopropylacryl amide)-*block*-poly(*N*-homocysteine thiolactone acrylamide) (polyNIPAAM-*b*-polyTiaAm) via RAFT polymerization and the modification of the pendent thiolactone groups with various amines (*n*-propylamine, *n*-hexylamine and *n*-dodecylamine, 1 equivalent per thiolactone).[41] The thiol group released after opening of the thiolactone was finally reacted with 2-bromoethyl-2′,3′,4′,6′-tetra-*O*-acetyl-*α*-D-mannopyranoside (initially added in excess to the reaction mixture) to produce a library of amphiphilic glycopolymers after complete deacetylation of the mannose units. After purification by dialysis against water, the polymer was freeze-dried and redissolved in DMF. To promote the

formation of narrowly distributed self-assemblies, water was then slowly added to the polymer solution and the samples were finally dialyzed against water. This procedure afforded the preparation of micelles around 30 nm in size (from *n*-propyl-substituted copolymers), large compound micelles of around 500 nm (*n*-dodecyl-substituted copolymers) or vesicles (*n*-hexyl-substituted copolymers) with diameters around 100-600 nm. These nano-objects were shown to specifically bind Con A lectin (**Scheme 1.11**, **Table 1.2**, **entry 6**).

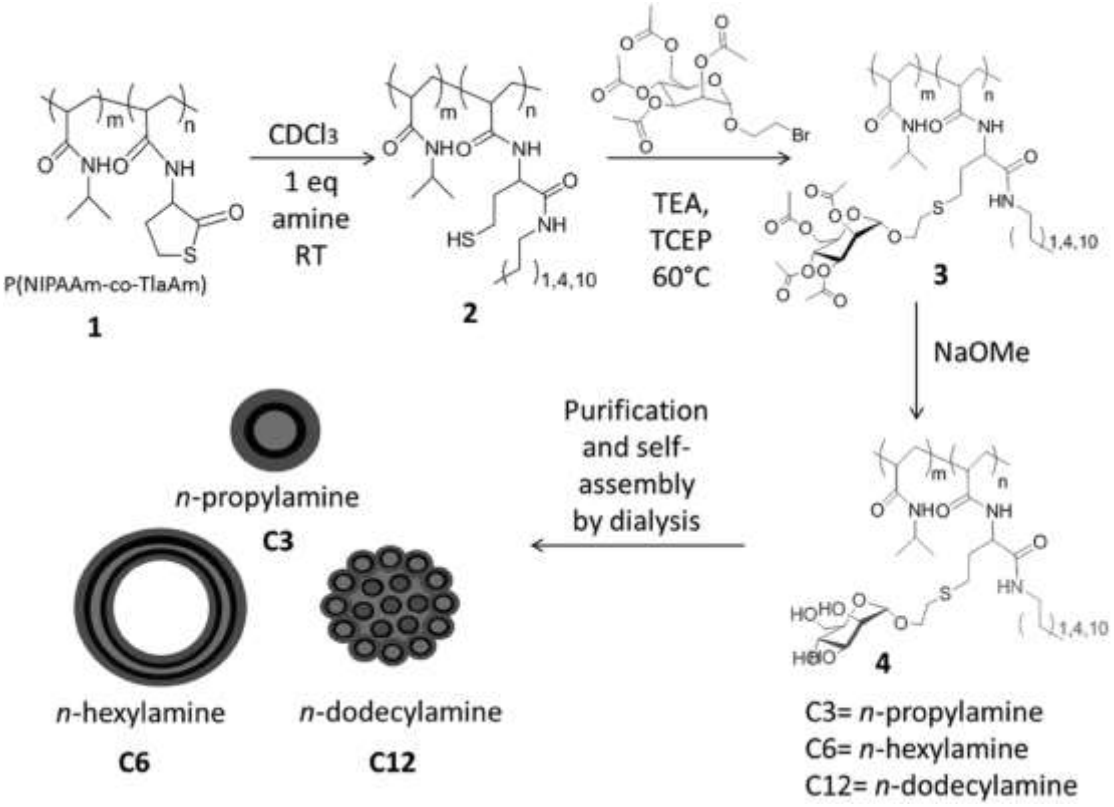

Scheme 1.11: One-pot reaction pathway to glycopolymer-based nanostructures.

Amphiphilic block glycopeptides

Because of their biodegradability, biocompatibility, tunable functionality and stimuli-responsiveness, polypeptide-based block and graft copolymers have been extensively studied for biological applications. Their self-assembly in aqueous solution has been the subject of many recent researches. For instance,

mannose-modified polylysine copolymers have been produced by Wang and coworkers in 2010.[42] First, two poly(*L*-lysine) (DP=32 or 61) were obtained by ring-opening polymerization (ROP) of *ε*-benzyloxycarbonyl-L-lysine N-carboxyanhydride (Z-Lys NCA), followed by the removal of the protective groups. Two amphiphilic copolymers P(M/Lys$_5$-*co*-Lys$_{27}$) and P(M/Lys$_{14}$-*co*-Lys$_{47}$) were then prepared by post-polymerization modification of poly(*L*-lysine) with 2,3,4,6-Tetra-*O*-acetyl-α-D-mannopyranosyl isothiocyanate (AcM-NCS) in DMF and subsequent deacetylation in basic methanol aqueous solution. When dissolved directly in water (0.1 mg/mL) at pH 6.25, random coils were generated from P(M/Lys$_5$-*co*-Lys$_{27}$). At pH>10, vesicles with diameters of 45-80 nm were generated as evidenced by TEM. The wall thickness of the vesicles were 12 nm and 20 nm, respectively. At pH 4, both copolymers formed spherical micelles 10-15 nm in size. Besides, the addition of anionic surfactant SDS into the copolymer solution (0.2 mg/mL) at pH 4 induced a transition from spherical micelles to rod-like micelles (**Figure 1.10**, **Table 1.2**, **entry 7**).

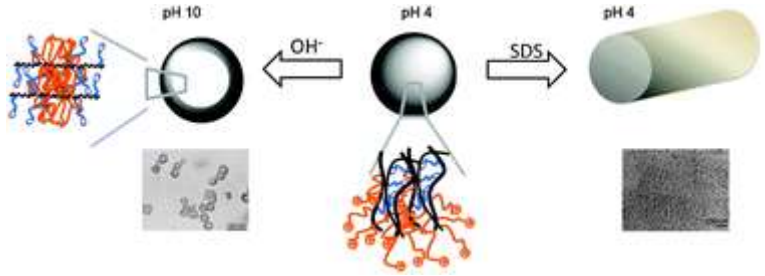

Figure 1.10: Morphological transition of P(M/Lys-*co*-Lys)-based self-assemblies observed in aqueous solution upon pH shifting or addition of SDS: vesicles (pH 10), spherical micelles (pH 4) and rod-like micelles (pH 4, SDS).

In 2012, Lecommandoux, Heise and co-workers reported the preparation of polymersomes from poly(*γ*-benzyl-*L*-glutamate)-*block*-poly(galactosylated propargylglycine) (PBLG-*b*-PGG) amphiphilic glycopolypeptides (**Scheme 1.12**, **Table 1.2**, **entry 8**).[43] Based on sequential ring-open polymerization (ROP) of benzyl-*L*-glutamate and propargylglycine (PG) N-carboxyanhydrides and subsequent glycosylation via Cu(I) azide-alkyne Huisgen 1,3-dipolar

cycloaddition (“click” reaction), $PBLG_{20}$-*b*-PGG_{18} (Mn=11200 g/mol, *Đ*=1.08), $PBLG_{20}$-*b*-PGG_{25} (Mn=11500 g/mol, *Đ*=1.17) and $PBLG_{20}$-*b*-PGG_{32} (Mn=16200 g/mol, *Đ*=1.17) were produced. The copolymers were then dissolved in a solution of DMSO at 10 mg/ml. By controlling the order of injection (DMSO in water or water in DMSO) and the addition speed, the block copolymers were proven to self-assemble into different morphologies. When water was injected into DMSO in a few seconds, mixtures of spherical and wormlike structures were observed whatever the composition of the copolymers. Increasing the addition speed to 2 h didn’t modify the assemblies significantly. When DMSO was injected into water, polymersomes with an average hydrodynamic diameter of less than 100 nm were clearly evidenced for $PBLG_{20}$-*b*-PGG_{18} and $PBLG_{20}$-*b*-PGG_{25}. In contrast, a mixture of spherical micelles and polymersomes was observed for $PBLG_{20}$-*b*-PGG_{32}. Owing to the presence of peripheral galactose units, the vesicles were shown to specifically bind Con A lectin.

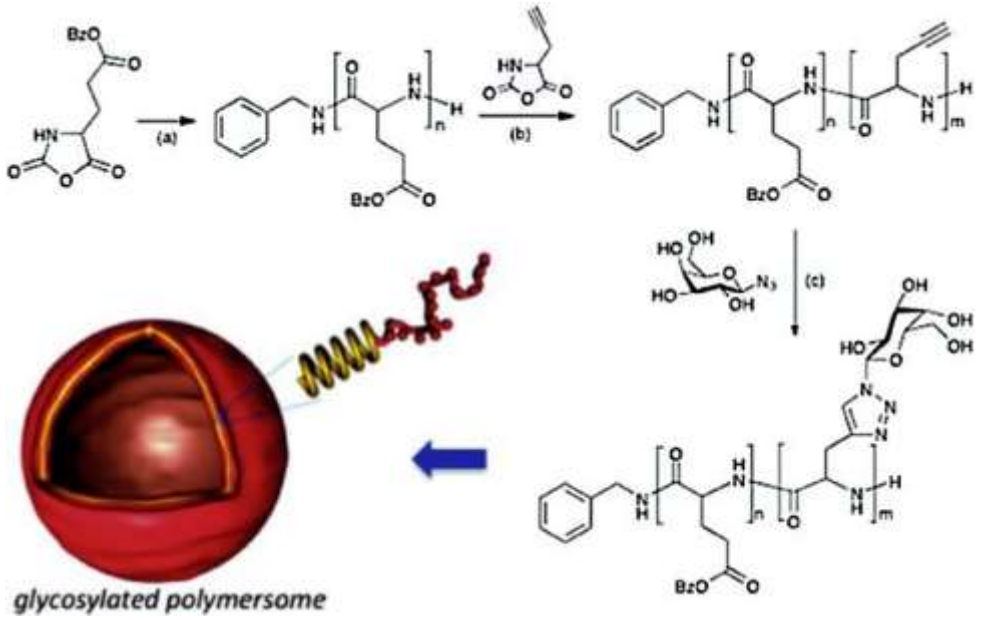

Scheme 1.12: Synthesis of PBLG-*b*-PGG Glycopeptide block copolymers via (a) DMF, benzylamine, 0°C; (b) DMSO, r.t.; (c) Cu $(PPh_3)_3Br$, Et_3N, DMSO, 30°C.

In 2013, the group of Deming prepared two glycosylated amphiphilic diblock copolypeptides. Hydrophilic segments, poly(*α*-gal-C) (DP=65, *Đ*=1.09) and poly(*α*-gal-K) (DP=65, *Đ*=1.07), were first prepared by polymerization of

2,3,4,6-tetra-*O*-acetyl-*α*-D-galactopyranosyl-L-lysine-N-carboxyanhydride (***α*-gal-K NCA**) or 2,3,4,6-tetra-*O*-acetyl-*α*-D-galactopyranosyl-L-cysteine-N-carboxyanhydride (***α*-gal-C NCA**) using (PMe3)4Co as initiator in THF. These blocks were further chain-extended with L-leucine N-carboxyanhydride (**Leu NCA**). After removal of the protecting groups, amphiphilic poly(*α*-D-galactopyranosyl-L-cysteine)$_{65}$-*b*-(leucine)$_{20}$ (**(*α*-gal-C)$_{65}$L$_{20}$**, Mn=30910 g/mol, *Đ*=1.09) and poly(*α*-D-galactopyranosyl-L-lysine)$_{67}$-b-(leucine)$_{20}$ (**(*α*-gal-K)$_{65}$L$_{20}$**, Mn=33130 g/mol, *Đ*=1.07) were obtained.[44] The self-assembly of (*α*-gal-K)$_{65}$L$_{20}$ in water gave rigid sheet-like membranes due to the stiffness of the hydrophilic segments which limited their ability to effectively solubilize and stabilize the assemblies against further aggregation. Self-organization of (*α*-gal-C)$_{65}$L$_{20}$ which displays more flexible hydrophilic segments afforded vesicles with diameters ranging from hundreds of nanometers to a few microns (**Scheme 1.13**, **Table 1.2**, **entry 9**). The vesicles could bind *Ricinus communis* Agglutinin I (RCA$_{120}$) and encapsulate Texas Red labeled dextran.

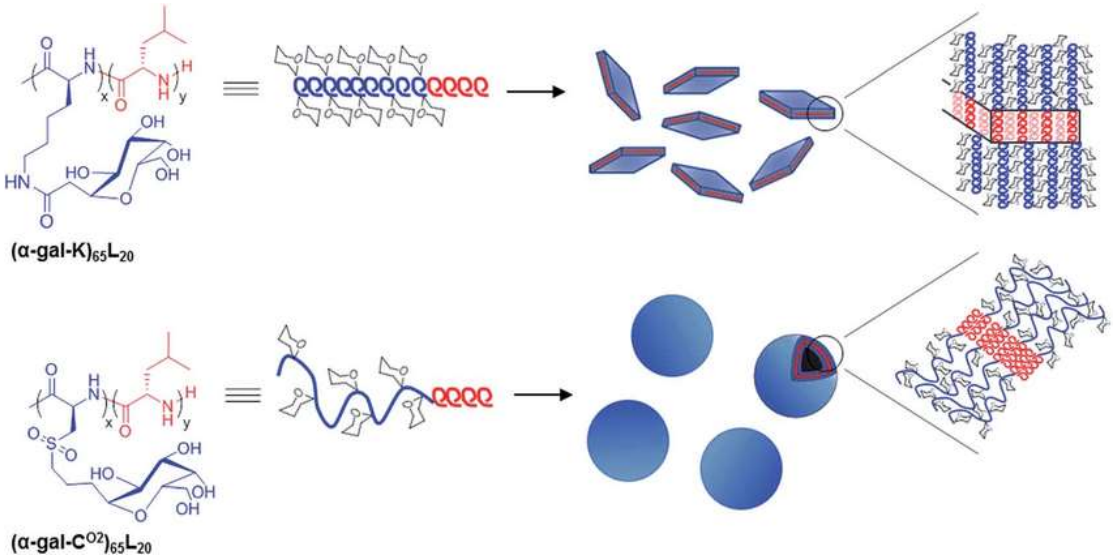

Scheme 1.13: Structure of the amphiphilic glycosylated diblock copolypeptides prepared by Deming and self-assemblies thereof.

In 2013, the group of Jan synthesized amphiphilic poly(L-lysine)-*g*-hexanoyl-*g*-lactobionolactone glycopolypeptide (PLHG) (**Table 1.2**, **entry 10**).[45] In a first

step, poly(N_{α}-(carbobenzyloxy)-L-lysine) (PZLL, DP=192, Mw=50340 g/mol, *Đ*=1.14) was prepared by ROP of N_{α}-(carbobenzyloxy)-L-lysine. After removing the Z group (carboxybenzyl) by using HBr and reacting the amino group with hexanoyl anhydride, PLH were synthesized. Poly(L-lysine)-graft-hexanoyl-lactobionolactone (PLHG) was finally obtained by the direct conjugation of lactobionolactone onto the amino group of PLL with CDI catalysis. From FTIR measurements, the number of amino groups grafted with hexanoic acid and lactobionolactone were calculated to be 72 and 30, respectively. Hence the PLH and PLHG copolypeptides were denoted as K_{192}-*g*-H_{72} and K_{192}-g-H_{72}-*g*-Lac_{30}. PLHG vesicles were either prepared by dialysis or by rehydration and further cross-linked with genipin. For the dialysis method, PLHG was initially dissolved in methanol and dialyzed against PBS (pH 7.4). The resulting hydrodynamic radius of the assemblies was ~ 110 nm and the polydispersity index (PDI) values below 0.3. Upon decrease of the pH to 4.68 (by adding 0.1 M HCl), the hydrodynamic radius of the assemblies increased to 132 nm. For the rehydration method, the sizes of the vesicles were between 97 and 112 nm under neutral conditions.

The preparation of the glycosyl-*N*-carboxyanhydride (NCA) monomer from *ε*-Boc-protected CbzLysOBn and propargyl 1,2-orthoester of per-*O*-acetylated-glucose/mannose was reported by Gupta in the presence of $HAuCl_4$/CH_2Cl_2/4 Å MS powder/rt.[46] ROP of the NCA yielded a series of alkyne-terminated glycopolypeptides nAcGP (n=average chain length of glycopeptide), including 10AcGP (mannose, Mn=5.6 kg/mol, *Đ*=1.07), 20AcGP (galactose, Mn=11.6 kg/mol, *Đ*=1.09), 20AcGP (mannose, Mn=11.6 kg/mol, *Đ*=1.10) and 40AcGP (galactose, Mn=22.1 kg/mol, *Đ*=1.13). In a second vial, azide-terminated PCL was synthesized by ROP of *ε*-caprolactone using an azide functionalized dihydroxy initiator, producing $(PCL_{25})_2$ (Mn=12.4 kg/mol, *Đ*=1.14) and $(PCL_{50})_2$ (Mn=23.0 kg/mol, *Đ*=1.21). Alkyne-terminated GPs were then coupled with azide-terminated PCLs by CuAAC reaction to generate glycopolypeptide-

polycaprolactone [nAcGP-(PCL$_m$)$_2$]. After deprotection of the sugar residues, a panel of amphiphilic nGP-(PCLm)2 copolymers, *i.e.* 10GP-(PCL$_{25}$)$_2$, 20GP-(PCL$_{25}$)$_2$, 20GP-(PCL$_{50}$)$_2$ and 40GP-(PCL$_{50}$)$_2$ were yielded, (**Scheme 1.14**).[47] Self-assembly of these copolymers in water (at 0.5 mg/ml) generated nano-objects evolving from nanorods to sheets and micelles for 10GP-(PCL$_{25}$)$_2$, 20GP-(PCL$_{50}$)$_2$ and 40GP-(PCL$_{50}$)$_2$ respectively. Whereas 20GP-(PCL$_{25}$)$_2$ self-assembled into vesicles with diameter 55 ± 10 nm as determined by TEM (**Table 1.2**, **entry 11**). The mannosylated vesicles were non-cytotoxic and were internalized in MDA-MB-231 breast cancer cells demonstrating their potential for drug delivery applications.

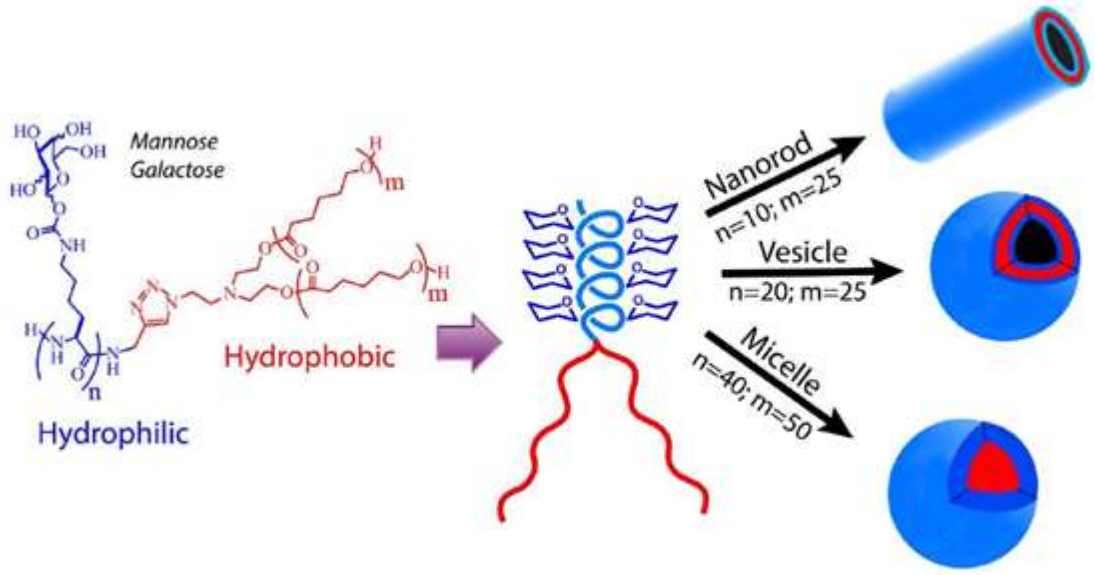

Scheme 1.14: Chemical structure of nGP-(PCLm)2 star copolymers and resulting nanostructures after self-assembly in aqueous solution.

Table 1.2: Preparation of glyconanocapsules by self-assembly strategy from amphiphilic glycopeptide and amphiphilic vinyl block glycopolymers obtained by post-modification.

Entry	Classification	Polymer	Protocol of self-assembly	Solvent	Size (nm)	Ref.
1	Polymersome	1,2-polybutadiene-*block*-polystyrene	CMC	THF or H_2O	50 (R_h)	36
2	Polymersome	1-thioglucose-modified 1,2-polybutadiene	CMC	H_2O	130(R_h)	37
3	Polymersome	glycosylated polybutadiene-*block*-poly(ethylene oxide)	CMC	H_2O	280(R_h)	38
4	Polymersome	glucose-modified polyoxazoline	CMC	H_2O		39
5	Polymersome	Maltoheptaose$_7$-block-poly(N-isopropylacrylamide)$_{220}$	CMC	H_2O	144	40
6	polymersome	Modified poly(N-isopropylacryl amide-*co*-N-homocysteine thiolactone acrylamide)	Solvent shifting	DMF/H_2O	100-600	41
7	polymersome	P(Mannose/Lysine-*co*-Lysine)	CMC	H_2O	45-80	42
8	Polymersome	poly(γ-benzyl-L-glutamate)-*b*-poly(galactosylated propargylglycine)	Solvent shifting	DMSO/H_2O		43
9	Polymersome	poly(α-gal-C^{O2})-*block*-poly(L-leucine)	Solvent shifting	THF/H_2O		44
10	Polymersome	poly(L-lysine)-*g*-hexanoyl-*g*-lactobionolactone	Solvent shifting	Methanol/H_2O	110 (R_h)	45
11	Polymersome	glycopolypeptide-*block*-poly(ε-caprolactone)	Solvent shifting	DMSO/H_2O	55	47

CMC: Critical Micelle Concentration.

Polysaccharidic and synthetic macromolecular blocks

Owing to their large availability in nature, it is desirable to design vesicular systems from oligosaccharides, polysaccharides or derivatives. A pioneering work in this direction has been reported by the group of B. J. Ravoo with vesicles composed of cyclodextrin (CDs) derivatives. Following are the structures of synthetic cyclodextrin derivatives and functional conjugates described in the literature.[48-58]

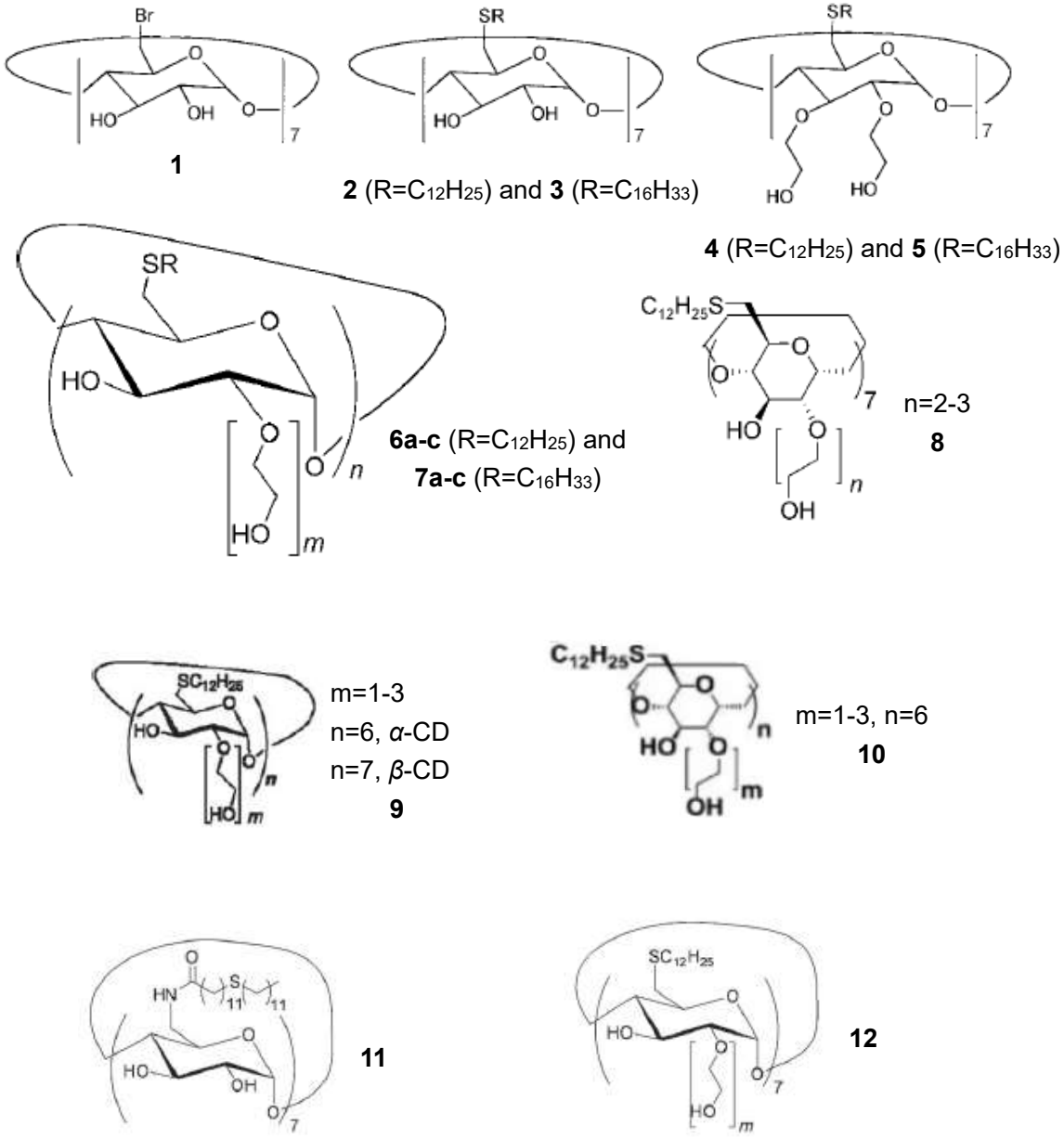

Figure 1.11: Various cyclodextrin derivatives (host molecules) synthesized by the group of Ravoo.

a

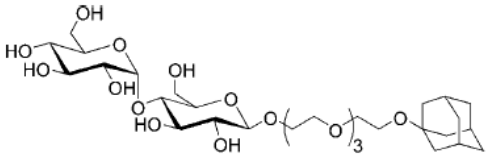

b

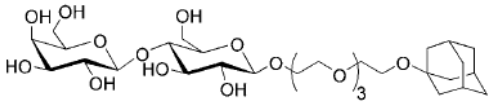

c

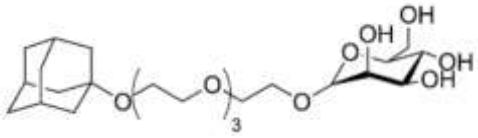

d

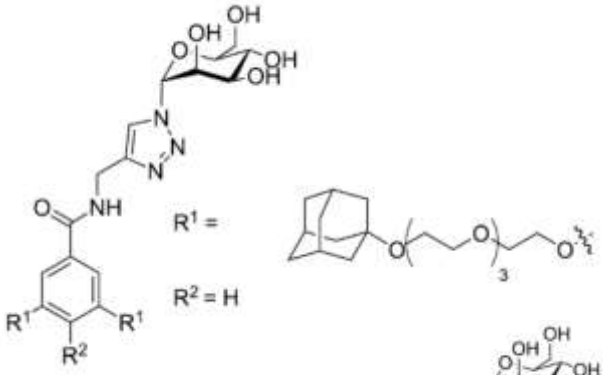

e

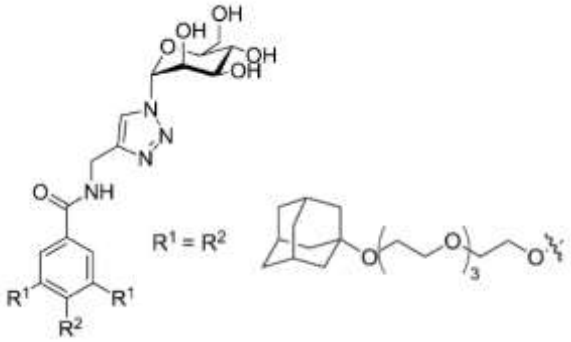

f

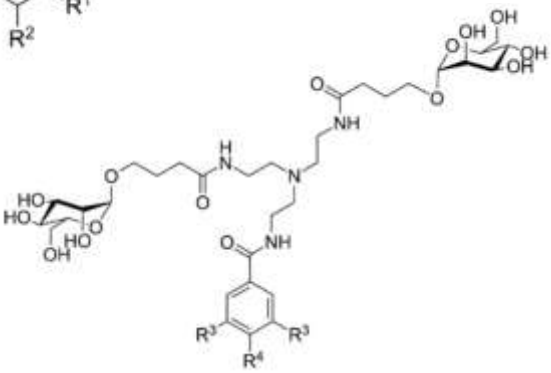

g

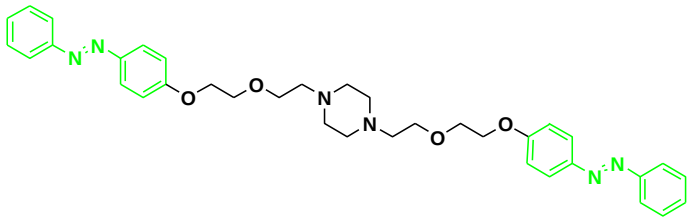

h

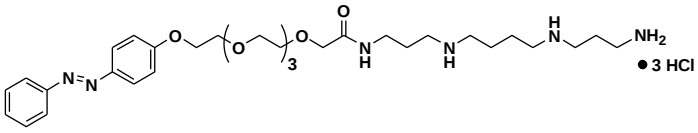

i

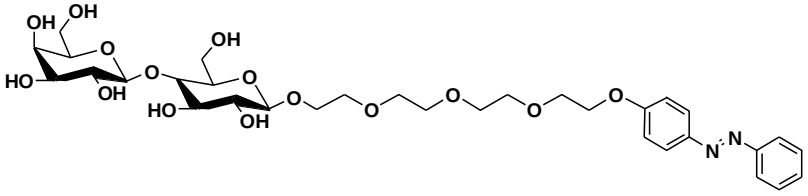

j

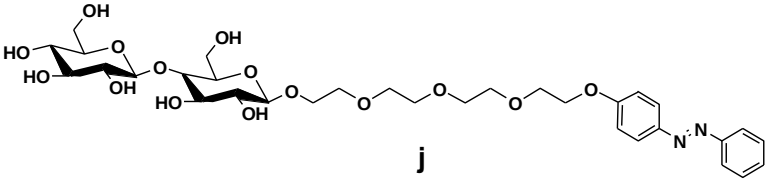

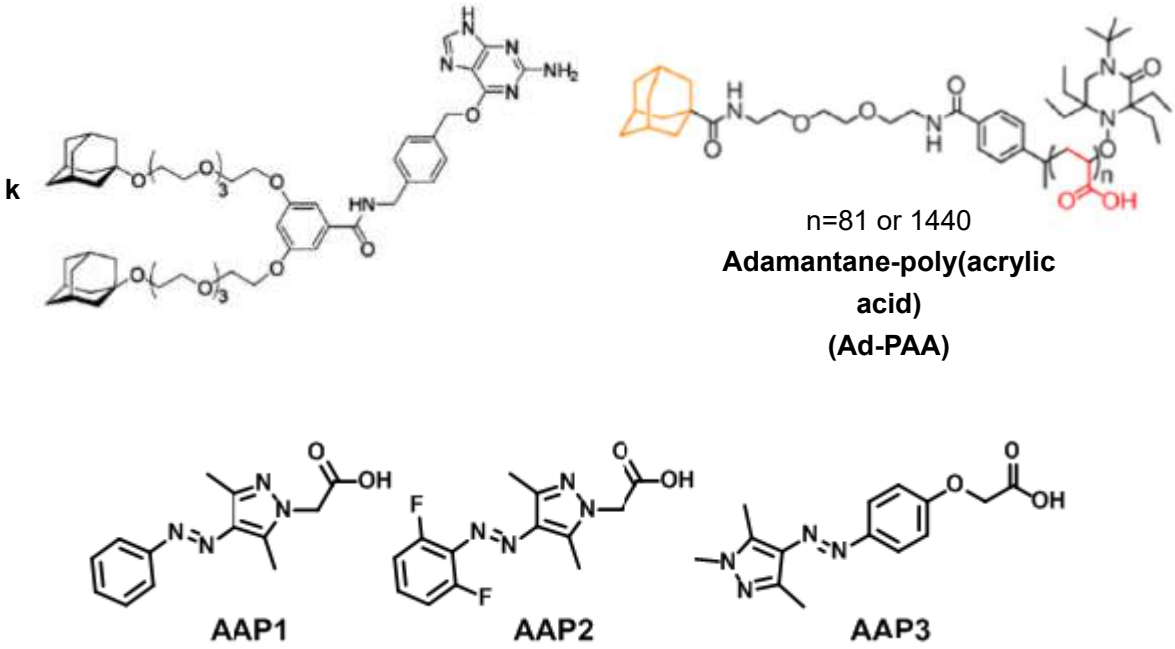

Figure 1.12: Various adamantane and azobenzene conjugates (guest molecules) synthesized by the group of Ravoo.

In 2000, the group of Ravoo reported bilayer vesicles composed of amphiphilic *β*-cyclodextrin (CDs) derivatives.[48] Heptakis(6-bromo-6-deoxy)-*β*-cyclodextrin (**1**) was obtained from *β*-cyclodextrin per-bromination at the C6 position and subsequently reacted with potassium n-dodecylthiolate and n-hexadecylthiolate to yield 6-alkylthioethers (**2, 3**). After hydroxyethylation with an excess of ethylene carbonate at 150°C using K_2CO_3 as base, amphiphilic cyclodextrin derivatives (**4, 5**) were obtained. Cyclodextrins 4 and 5 were readily dispersed in water by sonication at 50°C for 1 h and subsequent heating under stirring until no flocculation was detected. The self-assembly of the modified CDs in aqueous solution resulted in the formation of spherical bilayer vesicles with diameters ranging from 50 to 300 nm as observed by TEM (**Table 1.3**, **entry 1**). In 2005, Ravoo and co-workers further extended the library of amphiphilic CD derivatives by grafting n-dodecyl and n-hexadecyl groups on the primary side of *α*-/*β*-/*γ*-cyclodextrins through 6-S-alkylation and poly(ethylene glycol) on the second side (**6, 7**).[49] With these derivatives in hand,

the authors prepared vesicles with an average diameter of 140-160 nm or 80-100 nm by extrusion or by sonication (**Table 1.3**, **entry 2**). The resulting nonionic bilayer *β*-CDs vesicles presented better affinity for adamantane carboxylate than *α*-CDs vesicles and *γ*-CDs vesicles. Amphiphilic *β*-cyclodextrins vesicles from CD derivative **8** (vesicles made by extrusion, diameter around 100 nm) were further decorated with maltose–adamantane conjugate **a** and lactose–adamantane conjugate **b** through host-guest interactions, resulting complexes which could bond to Con A and peanut agglutinin (PNA), respectively.[50] Vesicles (diameter 100-150 nm) from **8** were also decorated with mannose–adamantane conjugates (guest/host complex 1:1) with one, two or three adamantane units as well as one or two mannose units (guests **c, d, e, f**) to investigate the multivalent interaction with Con A.[51] It was found that the interaction was reduced with the lower surface coverage with mannose. Moreover, aggregates were destroyed by adding competing binders (**Table 1.3**, **entry 3**).

Relying on the trans-azobenzene *α*- or *β*-CD host guest photoswitchable complexation (the cis-azobenzene photoisomer is not suitable for host-guest complexation with the CDs), Ravoo and co-workers further reported a supramolecular system where 100 nm CD-based glycovesicles (**9**), could be reversibly aggregated (up to 1 μm) in the presence of difunctional azobenzene guest molecules upon irradiation at 350 nm (*cis* form, **g**) followed by irradiation at 455 nm (*trans* form) (**Figure 1.13**, **Table 1.3**, **entry 4**).[52] The same group also described the preparation of ternary supramolecular complexes based on same bilayer amphiphilic CD vesicles (**9**), azobenzene-spermine guest molecule **h** and DNA.[53] The surface of the CD vesicles was first decorated with positively charged **h**. Negatively charged DNA was then conjugated to **h** through ionic interactions so that release and capture of DNA could be controlled by light irradiation.

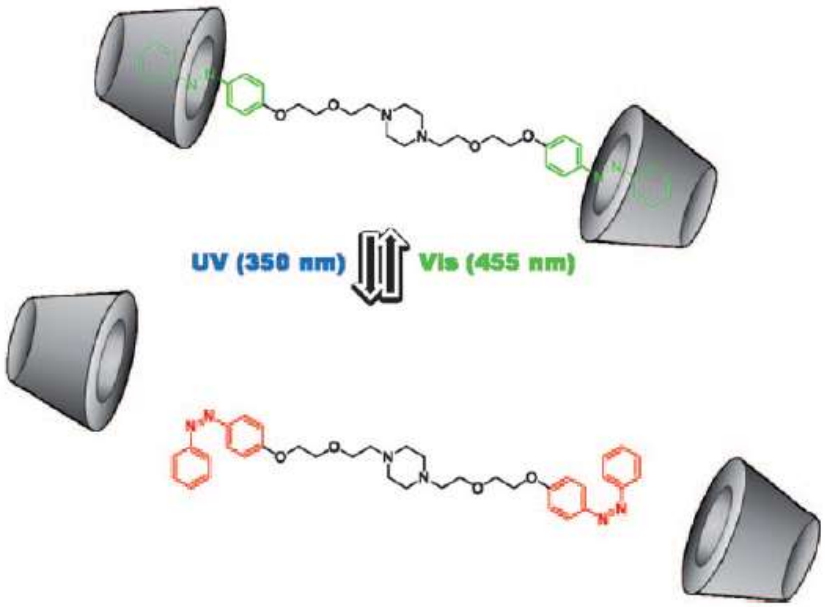

Figure 1.13: Light-responsive inclusion of azobenzene guest molecule in *α*-CD and *β*-CD.

In 2012, another two photo-responsive *α*-CDV (from **10**, diameter less than 100 nm) decorated with photo-responsive *trans*-azobenzene-lactose (*trans*-**i**) and/or *trans*-azobenzene-maltose conjugate (*trans*-**j**) were reported.[54] Multivalent interactions of PNA with lactose **e** and Con A with maltose **j** at the CDV surface led to agglutination of vesicles. Upon UV irradiation of ternary complex of CDV, *trans*-**i**, and PNA at 350 nm, the azobenzene-lactose conjugates detached from the vesicle surface (particle size decreases from 900 nm to about 100 nm). Upon subsequent UV irradiation at 455 nm, CDV, *trans*-**i**, and PNA reassembled (size increasing from 90 nm to 1000 nm). The photoinduced capture and release of lectins in ternary complex is highly efficient, highly selective, and fully reversible (**Table 1.3**, **entry 5**).

In 2016, the group synthesized three water soluble photoswitchable guest molecules **AAP1-3** (Figure 1.12) after introducing a carboxylic acid group and further functionalization of AAP (arylazopyrazole).[55] Irradiation with green light (520 nm) or UV-light (365 nm) enabled to switch between *E*-AAP and *Z*-AAP isomers. Unilamellar bilayered CDVs (from **8**, hydrodynamic diameter 100 nm)

were prepared in aqueous HEPES buffer (20 mM, pH = 7.2). After addition of 10 μM *E*-AAP1, the vesicles showed aggregated state of 2200 nm in size (DLS). Upon 365 nm irradiation, the CDVs aggregates redispersed (one population with R_h=136 nm). This light-induced switching between the aggregated and dispersed state by host-guest interaction was possible over at least five cycles without decreasing efficiency. Compared to *E*-AAP1. The addition of *E*-AAP2 to *β*-CD showed lower binding affinity and *E*-AAP3 showed even no aggregation (**Table 1.3**, **entry 6**).

The group also prepared adamantane functionalized poly(acrylic acid) (**Ad-PAA**, DP=81, Mn=11.1 kDa, *Đ*=1.2, Figure 1.12) by nitroxide-mediated polymerization of *tert*-butyl acrylate, followed by hydrolysis of tert-butyl groups with trifluoroacetic acid. Unilamellar CDV (**8**, R_h=128 nm) were prepared by extrusion in buffer (20 mM HEPES and 0.15 M NaCl) at pH 7.4. Addition of 0.025 mM Ad-PPA solution to 0.1 mM CDV yielded Polymer-Decorated Vesicles (PDV, R_h=142 nm, stable at pH=4-12) by anchoring *via* host-guest recognition. Cross-linking of 50% acrylic acid with 2,2′-(ethylenedioxy)bis(ethyleneamine) in the presence of 1-[3-(dimethylamino)propyl]-3-ethylcarbodiimide hydrochloride (EDCI) generated Polymer-Shelled Vesicles (PSV, R_h=150 nm, stable at pH=6-12). Owing to the steric barrier provided by the cross-linked shell, leakage of sulforhodamine B in PSV was ~8% after 8 h whereas the percentage of leakage reached 14% in the case of PDV.[56] Cross-linking of PDV with cystamine (in the presence of EDCI) afforded the preparation of vesicles ($PSV_{SS,}$ R_h=170 nm) capable to encapsulate a payload and to release cargo under redox trigger (**Table 1.3**, **entry 7**)[57].

Ravoo and coworkers further investigated the specific binding of *β*-CDs vesicles (**11, 12**) with adamantane-functionalized fluorescent SNAP-fusion proteins obtained by ligation of bisadamantane **k** and fluorescent SNAP-fusion proteins using SNAP-tag technology.[58] As demonstrated by surface plasmon resonance

technique (SPR), the adamantane-labelled SNAP-fusion proteins were proven to bind specifically onto CD-coated surfaces.

In 2005, M. Lee and coworkers reported the formation of stable mannose-coated nanovesicles from the self-assembly of mannose-terminated rod-coil molecules synthesized by glycosylation of a *tetra*(p-phenylene) (rod) oligo(ethylene glycol) (coil) conjugate with per-acetylated bromo-D-mannose and subsequent deprotection of the acetyl protecting groups.[59] The hydrodynamic diameter of the vesicles was around 36 nm (as measured by DLS). The resulting vesicles were effectively loaded with a hydrophilic fluorescent dye (calcein) which was shown to be progressively released over a period of 40 h. Thanks to the presence of mannose ligands on their shell, the vesicles established strong interactions with FimH adhesins of bacterial type 1 pili (*E coli*) while retaining thier size and their shape (**Table 1.3**, **entry 8**). Driven by geometrical constraints, rod-coil molecules consisting of di[tetra(*p*-phenylene)] with longer oligo(ethylene oxide) chain tended to form spherical micelles of R_h ~20 nm in aqueous solution. In contrast, derivatives based on a twin-rod segment self-assembled to cylindrical micelles with a uniform diameter of about 20 nm and lengths up to several micrometers, which may be caused by the more tapered shape of individual molecules and strong π-π interactions between aromatic segments (**Figure 1.14**)[60.]

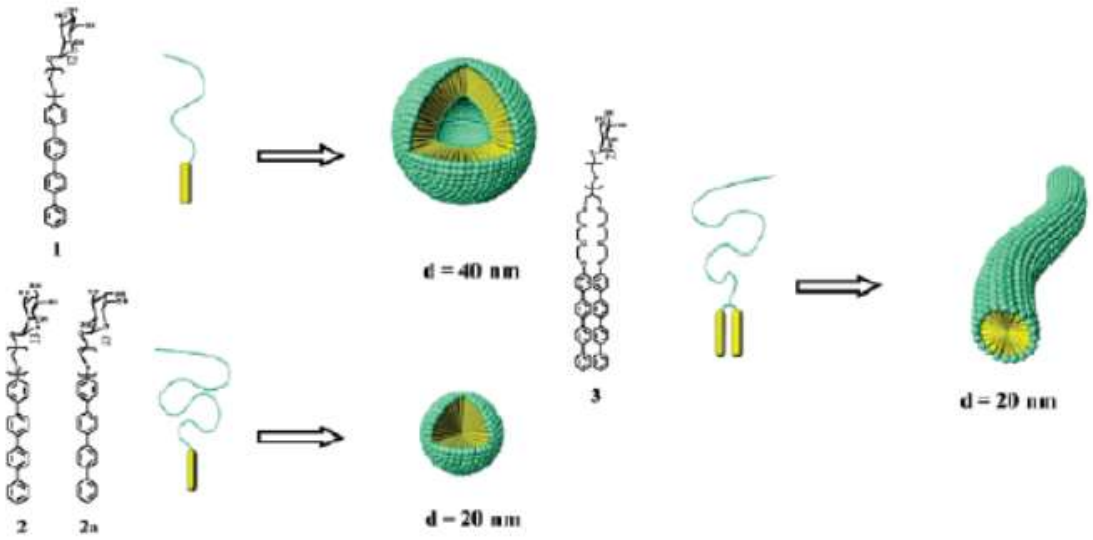

Figure 1.14: Molecular structure of rod-coil compounds **1**-**3** and schematic representation of vesicles and spherical or cylindrical micelles thereof in water.

In 2007, Gnanou and coworkers prepared a series of amphiphilic dextran-*b*-polystyrene diblock copolymers and investigated their self-assembly in water (**Table 1.3**, **entry 9**).[61] Owing to the presence of an aldehyde group in anomeric position, the authors initially end-functionalized the polysaccharide chains (M_n=6.6 kg/mol) with a bromoisobytyramide group through reductive amination with sodium cyanoborohydride ($NaCNBH_3$). After silylation of the hydroxyl groups to ensure facile dissolution of the polymer in common organic solvents, the dextran-based ATRP macroinitiator was engaged in the polymerization of styrene (in toluene) (see **scheme 1.15**). The resulting polymers were finally deprotected under acidic conditions to afford a library of amphiphilic block copolymers, dextran-*b*-PS_n with n= 5 (*Đ*=1.4, ϕ_{PS} = 11% vol), 15 (*Đ*=1.4, ϕ_{PS} = 27% vol), 145 (*Đ*=1.6, ϕ_{PS} =78% vol), 270(*Đ*=1.7, ϕ_{PS} =87% vol) and 775 (*Đ*=1.9, ϕ_{PS} = 95% vol). The authors investigated the influence of the block copolymer composition on the morphology of the self-assemblies.[62] Dextran$_{40}$-*b*-PS_5 generated rod-like micelles after direct dissolution in water. Dextran$_{40}$-*b*-PS_{270} generated vesicles with a hydrodynamic radius around 140 nm in DMSO/THF mixtures (with a DMSO volume fraction ~ 30-45%). In contrast, nanoparticles

(R_h=120 nm) were formed when the content of DMSO was superior to 80%. Dextran$_{40}$-*b*-PS$_{775}$ self-organization in DMSO/THF mixtures (volume fraction of DMSO below 30%) led to the formation of vesicles with a hydrodynamic radius around 110 nm (R_h) whereas, nanoparticles (R_h=65-115 nm) were obtained at high DMSO content (DMSO>80%) (**Table 1.3**, **entry 10**).

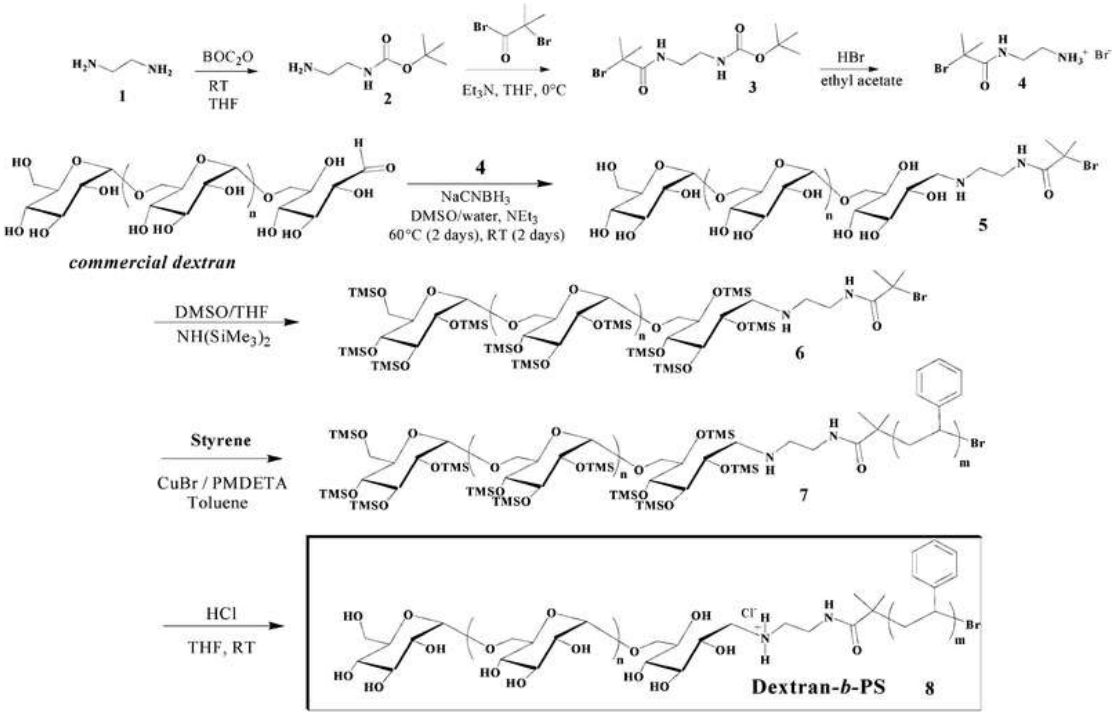

Scheme 1.15: Synthetic strategy to dextran-*b*-PS block copolymer by ATRP.

Lecommandoux and co-workers prepared amphiphilic dextran-*block*-poly(γ-benzyl L-glutamate) (dextran-*b*-PBLG) copolymers through ROP of azido end-functionalized g-benzyl L-glutamate N-carboxylic anhydride (BLGNCA) (DP_n=59) and subsequent coupling with alkyne-terminated dextran (Mn=6.6 kg/mol) by click chemistry[63]. The copolymer self-assembled in DMSO/water into small polymersomes with a hydrodynamic radius 45 nm by solvent shifting process (**Table 1.3**, **entry 11**).

Starch-based vesicles with controlled size were successfully achieved by the group of P. Wang in 2010.[64] Waxy maize starch (Mw=180 kg/mol) was first modified with palmitoyl chloride (PA) and acetic anhydride (AC) leading to a

series of 4 amphiphilic polymers S-PA-AC with various degree of substitution (DS_{PA} ranging from 0.005 to 0.3 and DS_{AC} ranging from 2.78 to 2.51) were finally generated. The self-assembly of the derivatized starch chains was carried out by addition of water into the polymer solution in THF. At low degree of substitution in PA (such as for S-PA-AC1 where DS_{PA}=0.005 and DS_{PA}= 2.78), the formation of spherical micelles of 150 nm (measured by TEM) was favored. Increasing DS_{PA} induced a progressive morphological transition from spherical micelles to vesicles from 200 to 700 nm in size (as typically observed with S-PA-AC with DS_{PA}=0.2 and DS_{AC}=2.58). The size of the vesicles was easily tuned (from 300 to 1000 nm or more) by varying the initial concentration of polymer in THF (2, 5, 8, 10 and 15 mg/mL) (**Table 1.3**, **entry 12**).

In 2012, Sheng and coworkers prepared hollow polymer nanocapsules based on cholesterol-modified dextran (Chol-Dex) and poly($_{D,L}$-lactic acid) (PLA).[65] Chol-Dex (the degree of substitution here defined as the percentage cholesterol content per 100 glucopyranosidic unit was 8.2%) was synthesized by reacting cholesterol 3-hemisuccinyl chloride with dextran (Mw=40 kDa) using triethylamine as catalyst. PLA with molar masses ranging 210 from to 48000 $g.mol^{-1}$ were tested. The self-assembly was performed by co-dialysis of the Chol-Dex/PLA polymer solution (at different Chol-Dex/PLA weight ratio: 3:1, 2:1 and 1:1) in DMSO against water. With the exception of the PLA with the lowest molar mass which promoted the synthesis of nanoparticles of 50-80 nm in size (TEM), nanocapsules were formed whatever the Chol-Dex/PLA ratio (**Figure 1.15**, **Table 1.3**, **entry 13**).

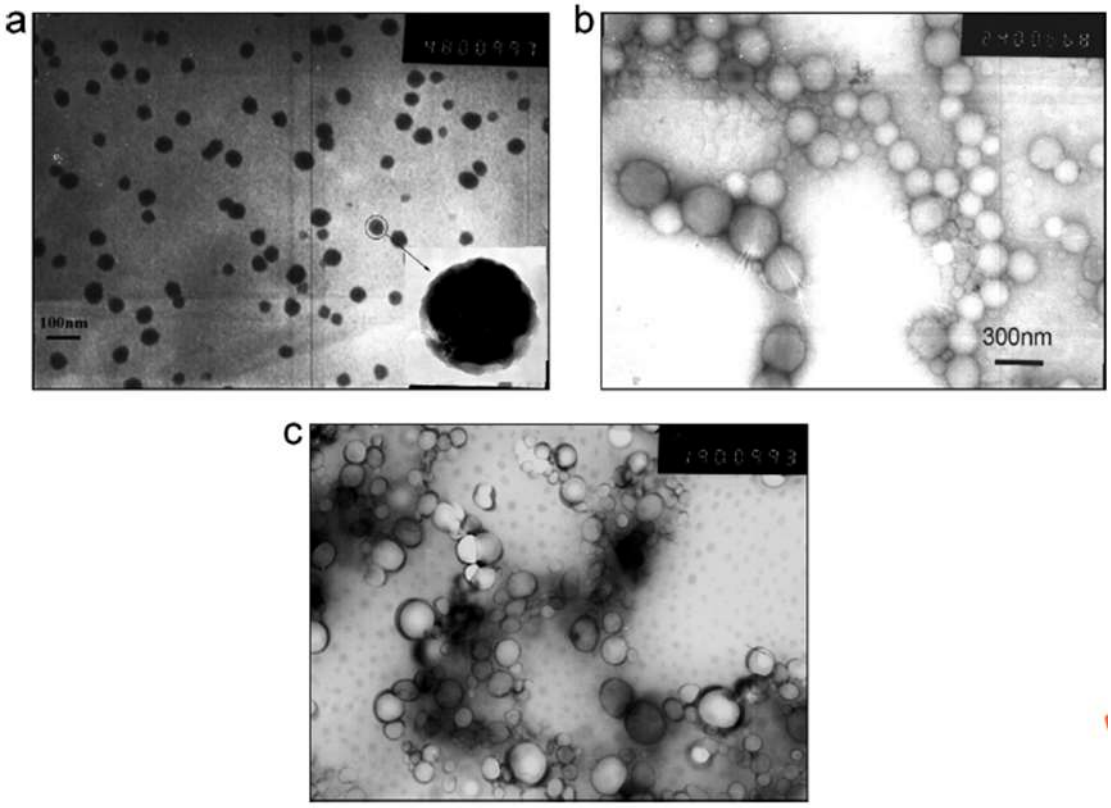

Figure 1.15: TEM micrographs of aggregates prepared from Chol-Dex and PLA oligomers of different molecular weights: (a) 210 Da; (b) 360 Da; and (c) 940 Da.

In 2012, Holger Frauenrath and coworkers reported sugar-decorated carbon nanocapsules with controlled morphology and surface chemistry by combination of precursor amphiphiles self-assembly in water and carbonization of oligo(ethynylene)s at low temperature.[66] First, a glucose-terminated hexa(ethynylene) amphiphile was designed by repetitive sequential bromination and Pd-catalyzed oligo(ethylynene) elongation starting from 4-pentyn-1-yl glucoside and final deacetylation of the glucose residue. The glucose-terminated hexa(ethynylene) gave birth to broadly size distributed multilamellar vesicles with dimensions ranging from 20 to 140 nm and a PDI =1.34 by addition of water to an oligomer solution in methanol/dioxane. After vesicle extrusion (using membranes with 50 or 100 nm pore sizes), dispersions of unilamellar vesicles (TEM) with a hydrodynamic diameter of 76 and 116 nm

(DLS) were obtained (**Table 1.3**, **entry 14**). UV irradiation of the dispersions at 1°C triggered quantitative carbonization of the membrane as evidenced by UV/Vis, solid ^{13}C NMR, XPS and Raman spectroscopy and led to the formation of colloidally stable "irregularly shaped capsules" with a graphite-like amorphous carbon shell and similar dimensions as their precursors (D_h ~ 80 nm and 116 nm) (**Figure 1.16**).

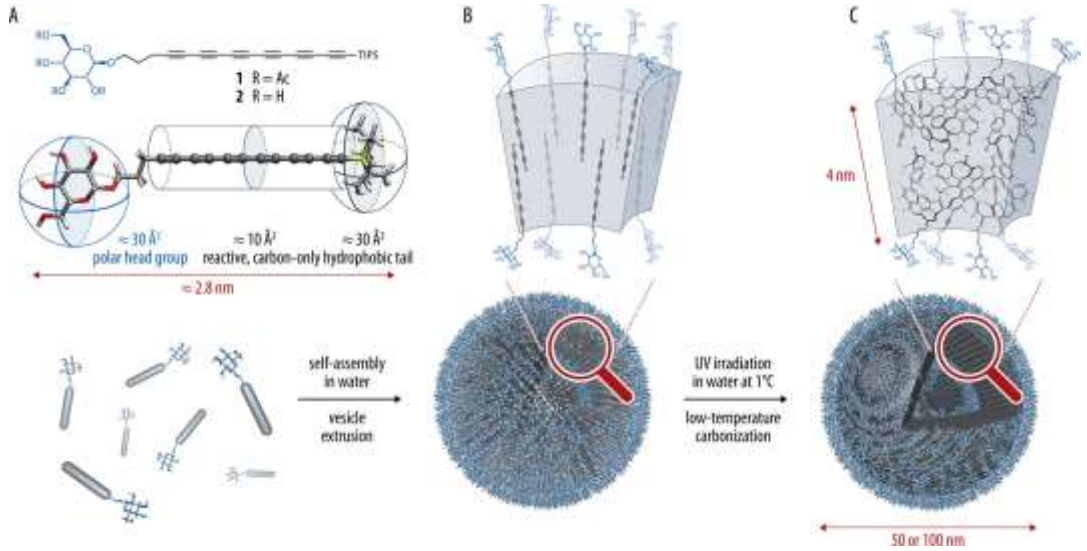

Figure 1.16: Preparation of carbon nanostructures with controlled morphology and surface chemistry through self-assembly and UV irradiation.

In 2015, the group of J-L. Six synthesized a series of amphiphilic polymers with a dextran backbone (Mw=34.8 kg/mol, *Đ*=1.14) and poly(diethylene glycol cholesteryl ether acrylate) (PDEG-CholA) liquid crystal grafts Dex-g^N-PDEGCholA^F (N being the number of PDEGCholA grafts per 100 glucopyranosic units of dextran backbone and F, the weight fraction of PDEGCholA in amphiphilic glycopolymer) (**Scheme 1.16**)[67]. Briefly, after a partial acetylation of dextran OH functions and subsequent grafting of ATRP initiator groups onto the unprotected OH functions with 2-bromoisobutyryl bromide (B^{i}BB), Dex$_{TAc}$Br$_{TBr}$ macroinitiators were synthesized and applied to initiate the ATRP of DEGCholA. The Dex-g^N-PDEGCholA^F were finally obtained after the deprotection of the Dex$_{TAc}$-g-PDEGCholA glycopolymers. Depending

on the variety of $Dex_{TAc}Br_{TBr}$ macroinitiators, several Dex-g^{N}-PDEGCholA^{F} were prepared, including: Dex-g^{24}-PDEGCholA^{90} (Mn=5800 g/mol, *Đ*=1.2), Dex-g^{66}-PDEGCholA^{73} (Mn=6800 g/mol, *Đ*=1.2), Dex-g^{5}-PDEGCholA^{79} (Mn=12600 g/mol, *Đ*=1.2) and Dex-g^{15}-PDEGCholA^{50} (Mn=11000 g/mol, *Đ*=1.3). Vesicular morphologies were generated from these copolymers by solvent shifting procedure in THF/water or DMSO/water, with size ranging between 47-68 nm (DMSO/water procedure) and 47-63 nm (THF/water procedure) (**Table 1.3**, **entry 15**).

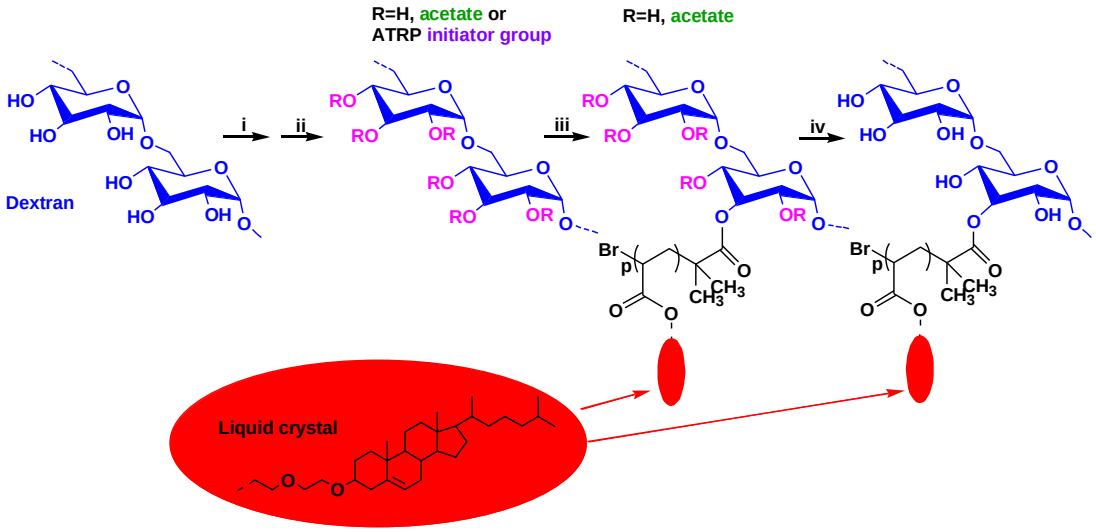

Scheme 1.16: Route to Dex-g^{N}-PDEGCholA^{F} glycopolymers. i) Partial acetylation. ii) Esterification by 2-bromoisobutyryl bromide. iii) ATRP of DEGCholA. iv) Deacetylation.

In 2015, H. Schlaad and coworkers synthesized three double hydrophilic block copolymers, *i.e.* dextran-*block*-poly(ethylene oxide) (Dex-PEO), pullulan-*block*-poly(ethylene oxide) (Pul-PEO), and dextran-*block*- poly(sarcosine) (Dex-PSar) by coupling the terminal aldehyde group of the dextran or pullulan chains (~20000 g.mol^{-1}) with the hydroxy amine chain end of PEO or PSar blocks (~20000 g.mol^{-1}) under acidic conditions (1/1 DMSO/Water mixture at pH=3) (**Table 1.3**, **entry 16**).[68] Self-assembly of Dex-PEO in water was investigated using direct dissolution and electroformation methods at low polymer concentrations (0.1, 0.5,1% and 0.5% respectively). Interestingly, long time was required before observing any aggregation with the dissolution method whereas

small aggregates were instantaneously formed through electroformation. However, after one week, aggregates with a hydrodynamic radius ~ 250 nm (at 0.1 and 0.5%) or higher than 700nm (at 1%) were detected by DLS in the direct dissolution solutions. SLS (ρ=0.93 for 0.5% polymer solution) and cryoSEM analyses confirmed the generation of vesicles from the double hydrophilic Dex-PEO block copolymer (**Figure 1.17**). Higher concentrations of copolymer (10-25 wt%) promoted the formation of polymer vesicles with diameters ranging from 2 to 20 µm with all the double hydrophilic block copolymers.

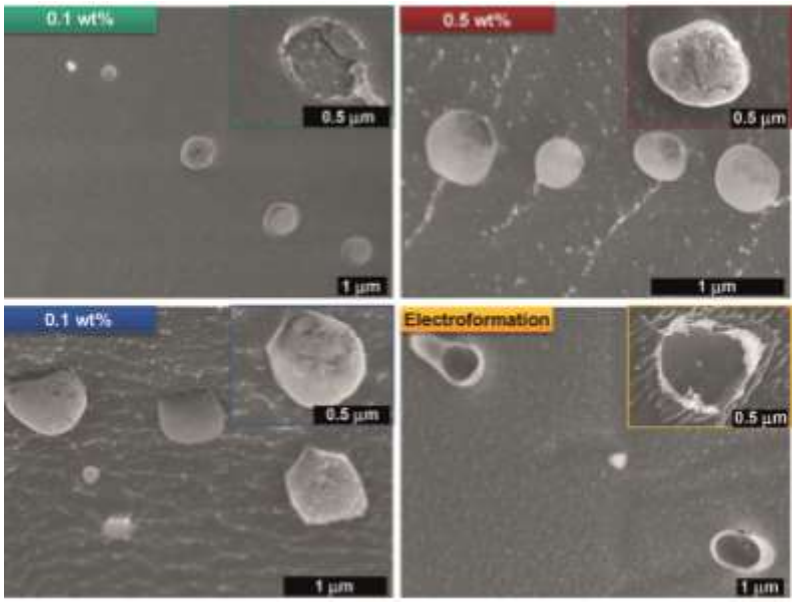

Figure 1.17: Cryogenic scanning electron microscopyofthe direct dissolution and electroformation solutions of Dex-PEO.

In 2017, the group of Schmidt presented the synthesis of two double hydrophilic block copolymers pullulan-*block*-poly(*N*,*N*-dimethylacrylamide) (Pull-*b*-PDMA, Mn=21500 g·mol^{-1}, *Đ*=1.9) and pullulan-*block*-poly(*N*-ethylacrylamide) (Pull-*b*-PEA, Mn=26500 g·mol^{-1}, *Đ*=1.6).[69] The alkyne end-functionalized pullulan (Mn=16000 g·mol^{-1}, *Đ*=1.8) was obtained by controlled depolymerization of commercially available pullulan at 85°C in 0.025 M hydrochloric acid solution and subsequent functionalization in acetate buffer at 50°C via reductive amination. Azido terminated PDMA (Mn=16800 g·mol^{-1}, *Đ*=1.26) and PEA (Mn=13900 g·mol^{-1}, *Đ*=1.37) were accessible via RAFT polymerization using

an azido functionalized trithiocarbonate namely dodecylthiocarbonylthio-2-methylpropanoic acid 3'-azidopropylester as chain transfer agent. The block copolymers were finally obtained by CuAAc coupling of alkyne end-functionalized pullulan chains and azide end-functionalized polyacrylamide blocks (**Scheme 1.17**). The block copolymers self-assembled into vesicular structures in aqueous solution which was prepared by shaking and filtering (0.45 µm syringe filters) of the mixture with different polymer weight percentage. The hydrodynamic radii of Pull-*b*-PDMA vesicles were around 85 and 110 nm at 0.1 wt.% and 1.0 wt.% polymer aqueous solution and, 125 and 180 nm at 0.1 wt.% and 1.0 wt.% for Pull-*b*-PEA vesicles (**Figure 1.18**, **Table 1.3**, **entry 17**).The authors stressed the main role of the difference of hydrophilicity (second virial coefficient A_2= 3.2·10^{-4} mol·cm^3 g^{-2} for pullulan and A_2= 8.0·10^{-4} mol·cm^3 g^{-2} for PDMA~PEA) between the pullulan and the PEA blocks in the successful self-assembly of the double hydrophilic diblocks.

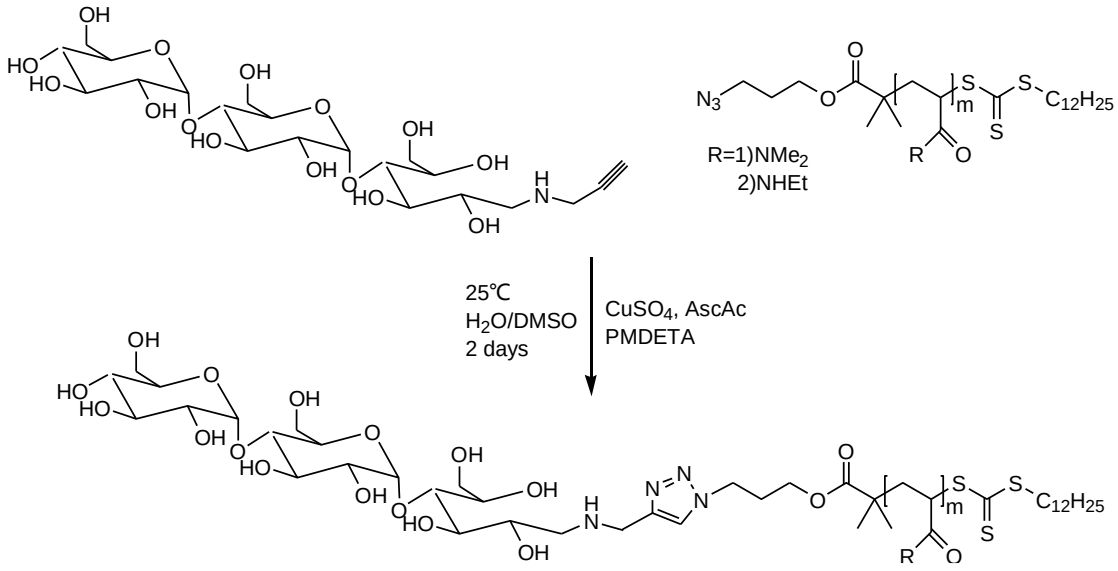

Scheme 1.17: CuAAC conjugation of alkyne-functionalized pullulan chains and azide terminated polyacrylamide.

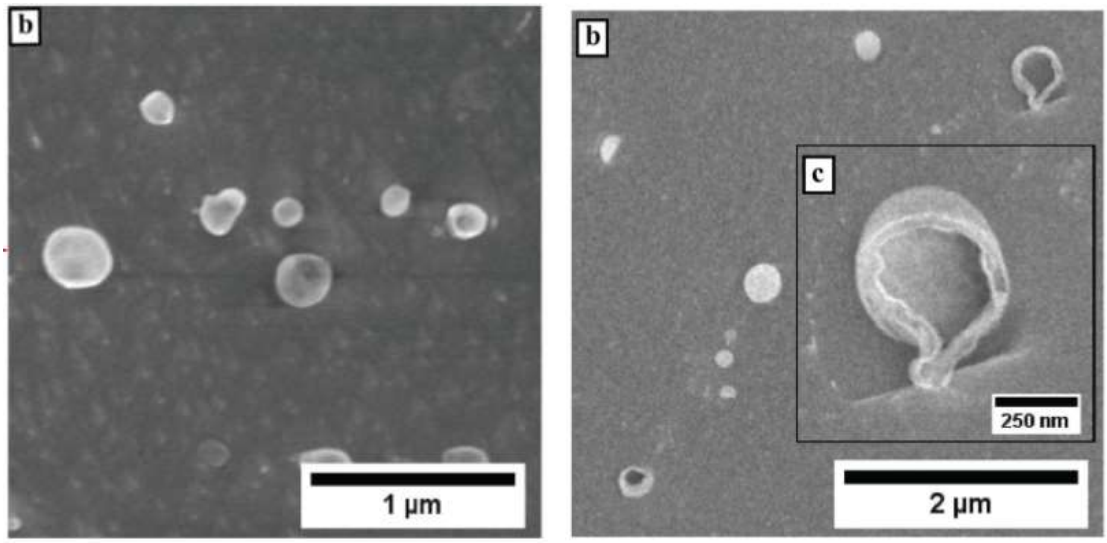

Figure 1.18: Cryo SEM micrograph of self-assembled spherical vesicles at a concentration of 0.5 wt.% in water (left) Pull-*b*-PDMA and (right) Pull-*b*-PEA.

Maltooligosaccharide-*b*-poly(propylene glycol)$_n$ amphiphilic block copolymers (DP_n maltooligosaccharides = 3, 5 or 8 and n=17, 21, 43 or 63) were prepared by Nishimura et al. using CuAAC between azide-functionalized poly(propylene glycol) monobutyl ether and alkyne functionalized maltooligosaccharides.[70] The self-assembly of maltopentaose-*b*-poly(propylene glycol)$_{43}$ in phosphate buffered saline (PBS) resulted in the generation of vesicular structures with a bilayer membrane and an average diameter of around 100–150 nm. Similar morphologies were observed with the other carbohydrate-containing block copolymers. Furthermore, the membrane thickness increased with the degree of polymerization of the oligosaccharide. When the degree of polymerization of the maltooligosaccharides varied from 3 and 63, the membrane thickness increased from 5.0±1.0 nm to 15.5±5.6 nm, respectively (**Figure 1.19**, **Table 1.3**, **entry 18**). The authors showed that the encapsulation of low molar mass molecules such as rhodamine 6G was negligible within the vesicles whereas loading efficiency around 13.9% was attained for FITC-BSA proteins suggesting that the membrane of the vesicles exhibits a molecular weight dependent permeability. To extend the scope of the glycovesicles, other

proteins, horseradish peroxidase, α-chymotrypsin and β-galactosidase, were successfully entrapped within the cavity of the glycovesicles (loading yields of 8.6, 10.7 and 9.8% respectively). The authors finally proved that the resulting systems act as efficient biocatalyst nanoreactors and can be internalized in HeLa cells without restricting their bioactivity.

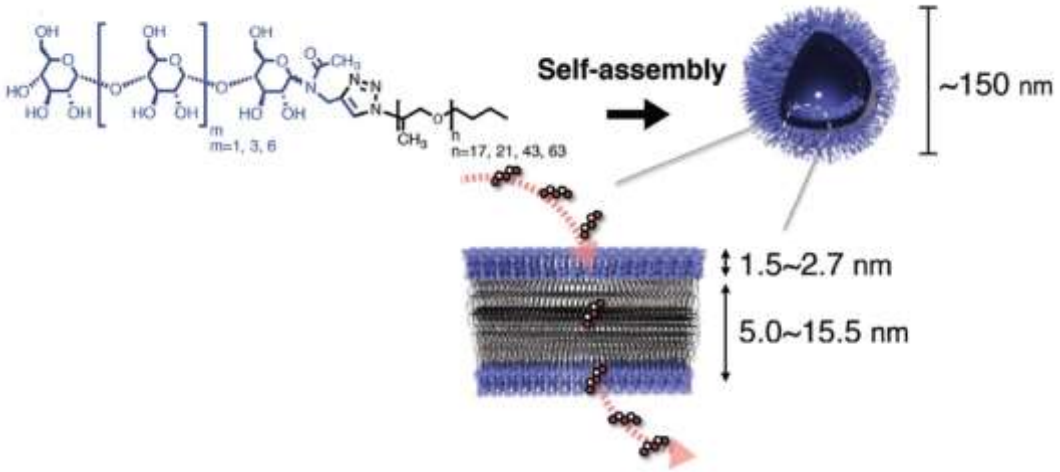

Figure 1.19: Amphiphilic maltooligosaccharide-*b*-PPG and glycovesicles thereof.

Recently, the same group prepared glycovesicles from maltopentaose-*b*-PPG$_{45}$ block copolymer by direct hydration method followed by extrusion.[71] The obtained vesicles were further treated at room temperature for 12 h using 1, 2, 3, 4 and 5 equivalents (eq.) of divinyl sulfone as cross-linker (DVS). In the presence of 1 or 2 eq. of DVS, vesicles were cross-linked through oxo Michael reaction without alteration of the dimensions as compared to the non-treated vesicles (100-150 nm). Higher DVS content resulted in an increase in size (3 eq DVS) or the formation of precipitates (4-5 eq DVS) (**Table 1.3**, **entry 19**).

Glycodendrimers (GDs) are constituted of highly branched “dendrons” emanating from a central multifunctional core unit and carrying many terminal reactive groups on which bioactive saccharides can be conveniently attached.[72] The design of various glycodendrimers for the conception of glycovesicles establishes a chemical platform that mimics natural features in size and shape,

and also allows customized implementation of bioactive epitopes, in structural and topological terms[73]. In 2013, the group of Percec produced the first examples of amphiphilic Janus glycodendrimers containing two identical carbohydrates in their hydrophilic part through an. accelerated modular synthesis. 7 libraries containing 51 amphiphilic Janus glycodendrimers (Janus-GDs) with D-lactose, D-galactose and D-Mannose in their hydrophilic part (**Figure 1.20**, **Table 1.3**, **entry 20**).[74] By injection of THF or ethanol solution of glycodendrimers into water or buffer and programming the concentration from which they were injected (from 0.0625 to 10 mg/mL), these libraries assembled into various morphologies including unilamellar spherical vesicles, polygonal vesicles, tubular vesicles, micelles, with diameters of 42-406 nm by DLS. In addition, these assemblies were stable over time in water and in buffer, exhibited narrow molecular-weight distribution (PDI<0.3), and displayed dimensions that were programmable by the concentration of the solution (from 0.0625 to 2 mg/ml) from which they are injected.

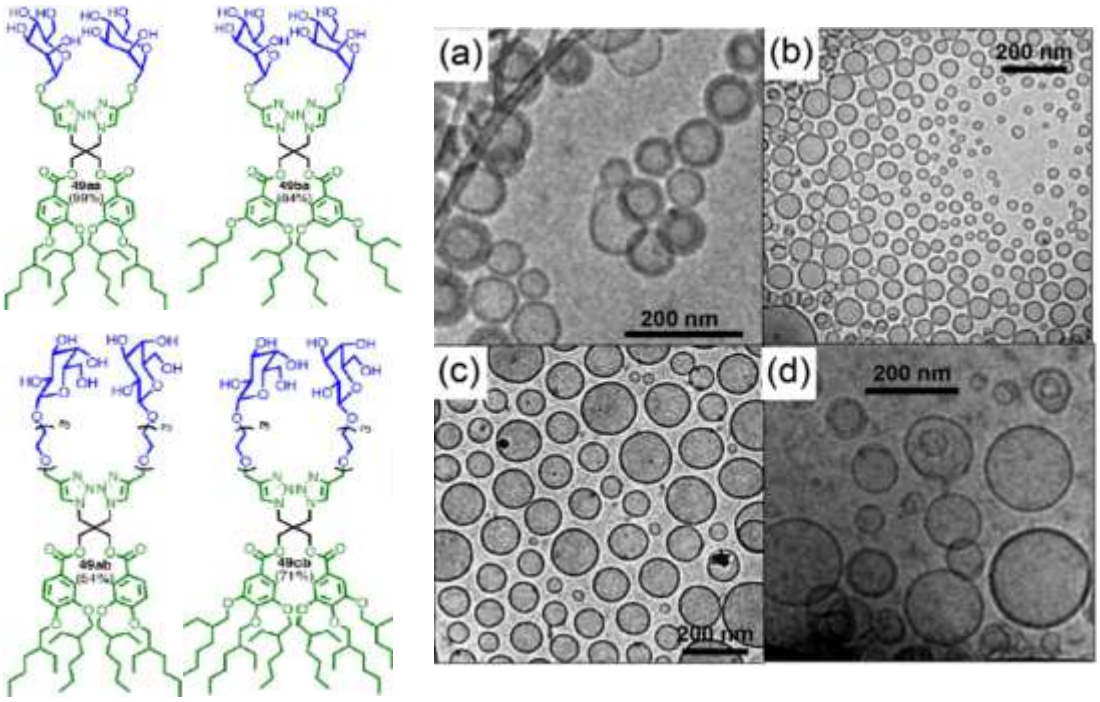

Figure 1.20: (Top) Amphiphilic Janus Glycodendrimers and (bottom) cryo-TEM images from (a) (3,4)2Et8G1-PE-TRZi-Man2 49aa, (b) (3,4)2Et8G1-PE-TRZi-3EOGal2 49ab, (c) (3,5)2Et8G1-PE-TRZi-3EOGal2 49bb, and (d) (3,4,5)2Et8G1-PE-TRZi-3EOGal2 49cb.

In order to gain further knowledge about the design of glycodendrimersomes, the same group subsequently synthesized three new series of amphiphilic Janus glycodendrimers with 3 different topologies and 3 different sugars, i.e. D-mannose, D-galactose, and D-lactose as head groups.[75] The first series contained ten twin-twin carbohydrate Janus GDs, the second one; seven JGDs with a single hydrophobic dendron and a single carbohydrate headgroup, and the third, three twin-mixed triethylene glycol (TEG): carbohydrate GDs. All the Janus compounds self-assembled into soft unilamellar multivalent glycovesicles by simple injection of THF solutions of glycodendrimers into water or buffer. The authors further showed that unilamellar glycodendrimersomes (GDSs) are versatile cell membrane mimetics capable to bind lectins such as homodimeric galectin-1[76] or human adhesion/growth-regulatory lectin galectin-8[77] thanks to the presentation of sugars in their hydrophilic segments.

The same group also prepared amphiphilic Janus GDs with mono- and bivalent and mixed-type D-mannose (Man)-presenting headgroups by an accelerated modular synthetic strategy. Methoxytriethoxy fragments were used as spacers or space-filling chains. Simple injection of THF solution of Janus GDs into 4-(2-hydroxyethyl)-1-piperazineethanesulfonic acid (Hepes) buffer produced, monodisperse multilamellar onion-like glycodendrimersomes (GDSs) due to the presence of the methoxytriethoxy fragments (**Figure 1.21**).[78] At constant concentration in mannose (0-1 mM), the dimensions of the vesicles and the number of bilayers was dictated by the architecture of the dendrons (**Table 1.3**, **entry 21**). Binding of GDSs to Con A was easily tuned by varying the density of sugars, the sequence or the spacer length.

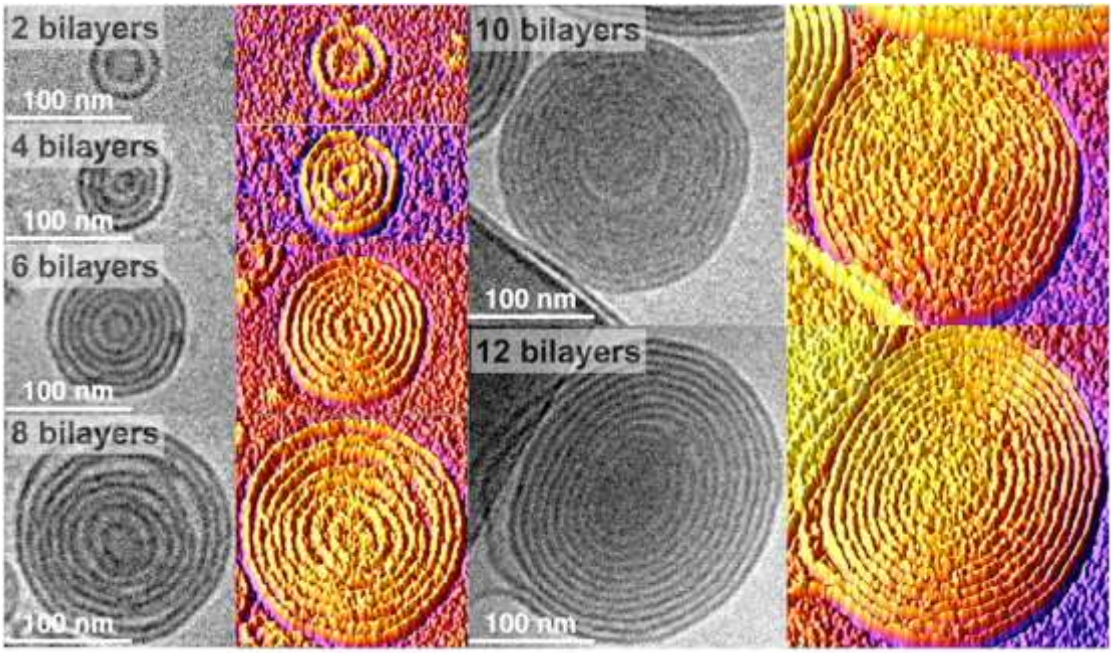

Figure 1.21: Selected cryo-TEM images of onion-like GDSs self-assembled from 0.1 mM Janus GD 5a-Man 3EO (1,2,3,4,5,6,7)-3EOMan(8)-3EO(9) and their 3D intensity-plotting images with different numbers of bilayers and diameters.

In 2016, Percec and coworkers reported the coassembly of GDS and bacterial membrane vesicles (BMVs) into functional cell-like hybrid vesicles.[79] Twin–twin molecules containing twin-hydrophobic and twin-hydrophilic dendrons JD-3 ((3,5)12G1-PE-(3,4,5)-3EO-G1-$(OCH_3)_6$, bilayer thickness ~ 4.5-4.9 nm) were used. An ethanol solution of JD-3 and BMVs was injected into PBS to produce monodispersed hybrid vesicles with dimensions of about 140 nm by DLS (**Scheme 1.18**, **Table 1.3**, **entry 22**). The encapsulated fluorescent dye rhodamine 6G (Rho) (479 Da) diffused out of the vesicles whereas fluorescent dye calcein with higher Mw=622 Da (close in size to the porin diffusion limit) stayed within the hybrid vesicles. These results demonstrated the potential impact of the produced artificial cell-like hybrid assemblies in diverse fields such as targeted drug delivery, vaccines, and other areas of nanomedicine.

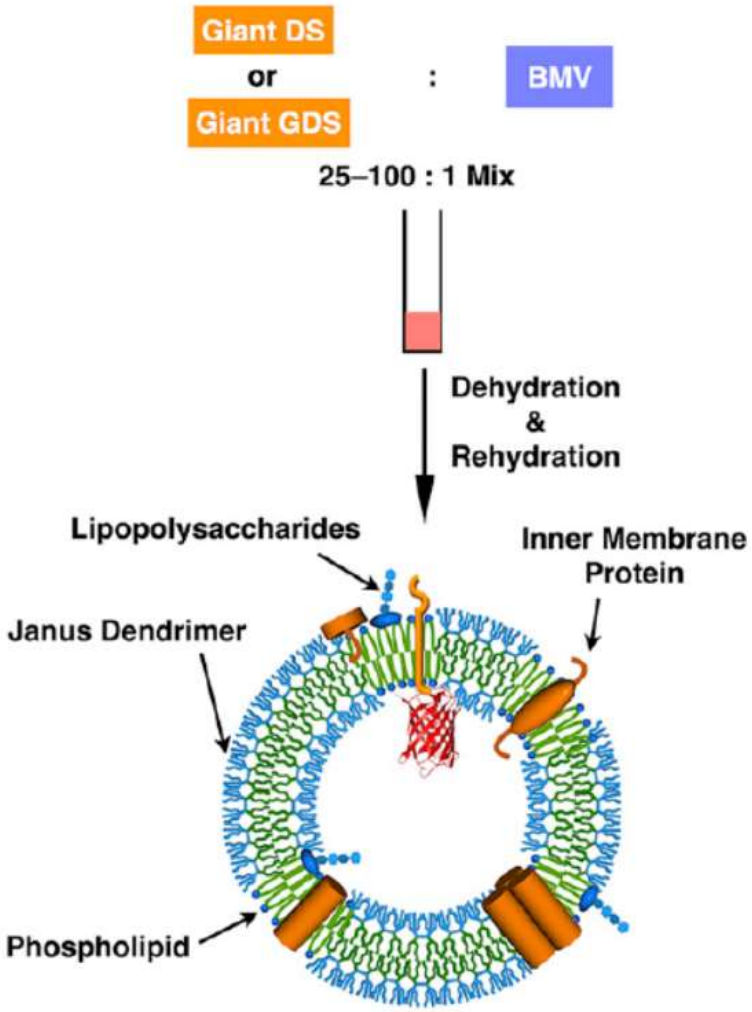

Scheme 1.18: Illustration of the coassembly of hybrid giant vesicles from giant DSs, giant GDSs.

In 2016, E. R. Gillies and coworkers synthesized a library of *α*-galactose-functionalized dendron-lipid hybrids (**Table 1.3**, **entry 23**). The hybrids were built from polyester dendrons (G0-G4) displaying peripheral amine groups and isothiocyanate derivatives of C-linked *α*-Galactose.[80] Conjugation of these molecules afforded a series of amphiphilic glycodendron-lipid hybrids named L-G*X*-Gal with *X* ranging from 0 to 4 (**Figure 1.22**). THF and DMSO were selected as the organic solvent for G0/G1 and G2/G3/G4 hybrids respectively. Upon addition of water, G0-G2 hybrids self-assembled into glycodendrimersomes with diameters around 200-300 nm whereas higher generations of hybrids mainly gave birth to micelles with hydrodynamic diameters ~ 10 nm (DLS)

owing to the increase of the hydrophilic fraction in G2/G3/G4 architectures and increased curvature. Fluorescent Nile red-loaded L-G3-Gal and L-G3-OH assemblies were prepared and incubated with lectin GSL 1-coated agarose beads. The emission of fluorescence observed with L-G3-Gal assemblies certificated the specific binding between α-Gal residues and GSL 1. Importantly, morphologies built from the highest generations of dendrons exhibited enhanced binding to GSL 1.

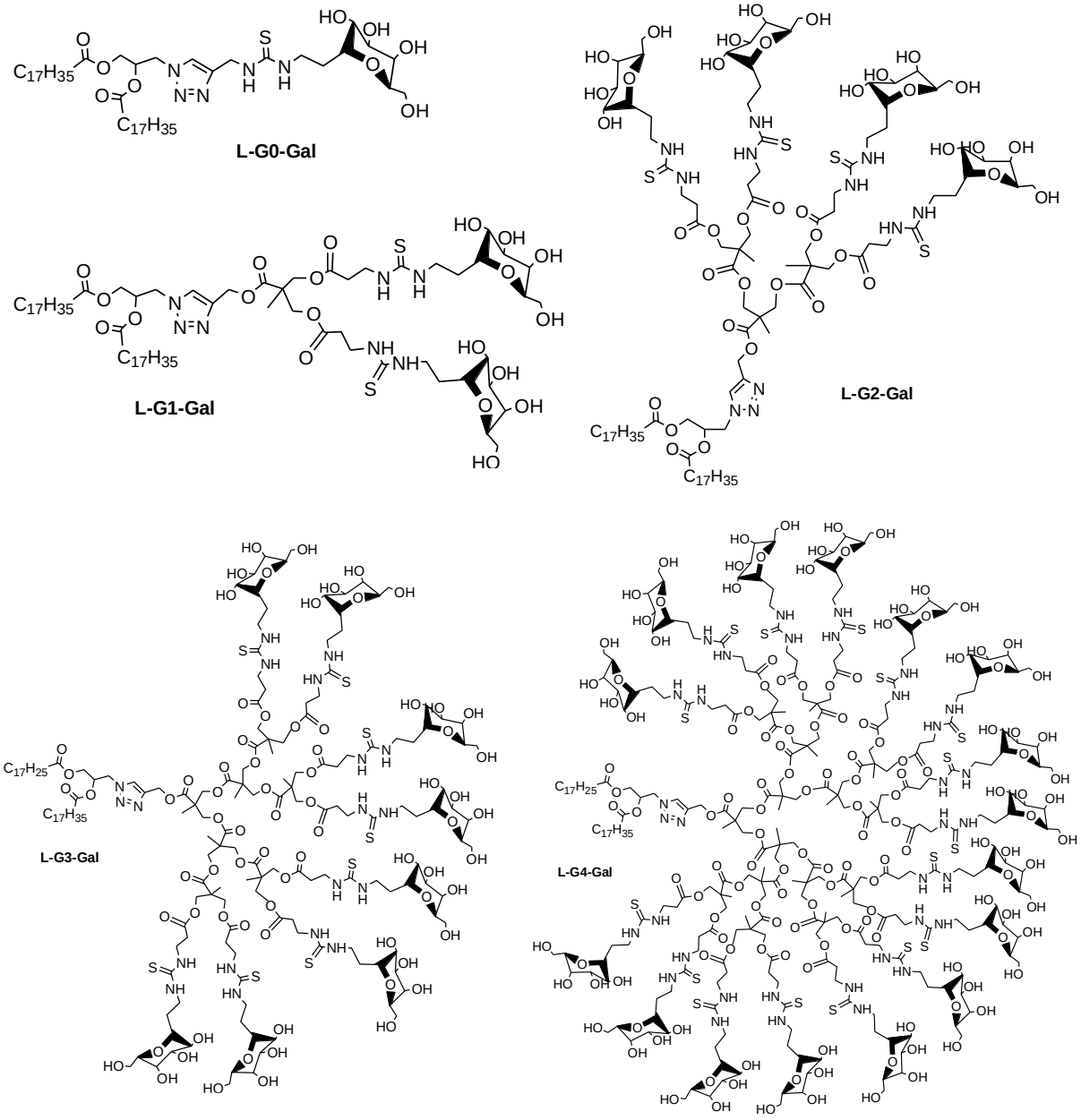

Figure 1.22: Chemical structures of the α-Gal-functionalized dendron-lipid hybrids.

Table 1.3: Preparation of glyconanocapsules by self-assembly strategy from polysaccharidic and synthetic macromolecular blocks.

Entry	Classification	Polymer	Protocol of self-assembly	Solvent	Size (nm)	Ref.
1	Polymersome	heptakis(6-alkylthio)-*β*-clycodextrins	CMC	H_2O	50-300	48
2	Polymersome	6-S-alkylation-cyclodexatrin-PEG	CMC	H_2O	140-160	49
3	Polymersome	heptakis(6-alkylthio)-*β*-clycodextrins	CMC	CMC	100-150	50-51
4	Polymersome	cyclodextrins	CMC	H_2O	100	52-53
5	Polymersome	*trans*-azobenzene-carbohydrate	CMC	H_2O	107	54
6	Polymersome	arylazopyrazole conjugated 6-S-alkylation-cyclodexatrin-PEG	CMC	H_2O	100	55
7	Polymersome	cyclodextrins	CMC	H_2O	150 /170	56-57
8	Polymersome	*α*-D-mannopyranoside conjugated oligo(ethylene oxide)-*block*-tetra(p-phenylene)	CMC	H_2O	40	59-60
9	Polymersome	dextran-*b*-polystyrene	Solvent shifting	DMSO-THF/H_2O		61
10	Polymersome	dextran-*b*-polystyrene	CMC	H_2O	140/110(R_h)	62
11	Polymersome	dextran-*block*-poly(γ-benzyl $_L$-glutamate)	Solvent shifting	DMSO/H_2O	45	63
12	Polymersome	starch-*block*-poly(palmitoyl)-*block*-poly(acetic anhydride)	Solvent shifting	THF/H_2O	200-1000	64
13	Polymersome	cholesterol-dextran/poly($_{D,L}$-lactic acid)	Solvent shifting	DMSO/H_2O		65
14	Polymersome	biofunctional hexaynes	CMC	H_2O	20-140	66
15	Polymersome	dextran-*graft*-poly(diethylene glycol cholesteryl ether acrylate)	Solvent shifting	THF/H_2O DMSO/H_2O	47-63	67
16	Polymersome	dextran-*block*-poly(ethylene oxide) pullulan-*block*-poly(ethylene oxide) dextran-*block*-poly(sarcosine)	CMC	H_2O	250 (R_h)	68

17	Polymersome	pullulan-*b*-poly(*N*,*N*-dimethylacrylamide) pullulan-*b*-poly(*N*-ethylacrylamide)	CMC	H_2O	200-500	69
18	Polymersome	maltooligosaccharide-*b*-poly(propylene glycol)$_n$	CMC	H_2O	100-150	70
19	Polymersome	maltopentaose-b-poly(propylene glycol)$_{45}$	CMC	H_2O	100-150	71
20	Polymersome	(3,4)2Et8G1-PE-TRZi-Man2 49aa	Solvent shifting	THF (or ethanol)/H_2O	42-406	74
21	Polymersome	Janus-GDs	Solvent shifting	THF/H_2O	74-206	78
22	Polymersome	(3,5)12G1-PE-(3,4,5)-3EO-G1-$(OCH_3)_6$	Solvent shifting	THF/H_2O	140	79
23	Polymersome	Janus-GDs	Solvent shifting	THF or DMSO/H_2O	200-300	80

CMC: Critical Micelle Concentration.

1.2.1.2 Micelle core removal strategy

As previously described, amphiphilic copolymers often self-organize into core-shell micelles in aqueous medium. Hollow structures can then be generated after cross-linking of the shell and selective removal of the core. The core elimination can be achieved by enzymatic degradation, hydrolysis, ozonolysis or aminolysis, and so on. In 2005, Zhang and coworkers prepared pyrene end-labeled poly(Ɛ-caprolactone)-*block*-poly[6-*O*-(4-vinylbenzyl)-D-galactose] (Py-PCL_{32}-*b*-$PVBG_{10}$, Mn=7700 g/mol, *Đ*=1.28) by combination of ROP and ATRP polymerization techniques (**Table 1.4**, **entry 1**).[81] After ROP and coupling with bromoisobutyryl bromide, Br-terminated PCL (Mn=5800 g/mol, *Đ*=1.33) was used to initiate the polymerization of VBIG (6-*O*-(4-vinylbenzyl)-1,2:3,4-di-*O*-isopropylidene-D-galactose) by ATRP, yielding protected Py-PCL-*b*-PVBG (Mn=9000 g/mol, *Đ*=1.28). After deprotection of the sugar residues, the amphiphilic Py-PCL-*b*-PVBG chains were self-assembled into spherical micelles via solvent shifting (addition of water in a DMF solution of Py-PCL_{32}-*b*-$PVBG_{10}$ of 1mg/mL). The PVBG shell was then cross-linked by addition of glutaraldehyde in acidic conditions either to the aqueous dispersion of the aggregates (method 1) or to the aggregate solution before dialyzing away the DMF (method 2). As illustrated by TEM pictures given in **Figure 1.23**, method 1 led to the formation of small aggregates and hollow particles (with diameters consistent with those of the objects before degradation) after dialysis against water whereas method 2, afforded shell cross-linked hollow particles with size between 50 and 120 nm owng to efficient PCL core degradation under basic conditions (pH=13).

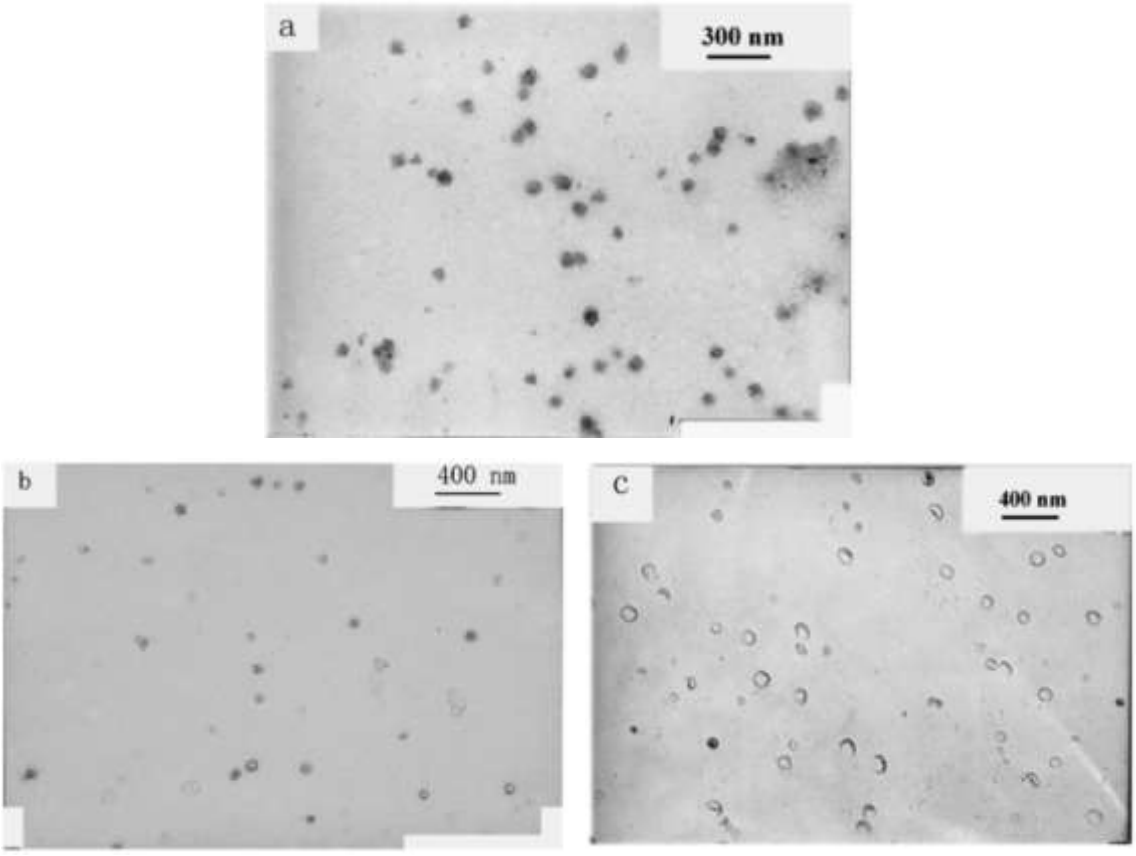

Figure 1.23: TEM micrographs of Py-PCL$_{32}$-*b*-PVBG$_{10}$ aggregates (1 mg/mL) before degradation of the PCL core (a) and after degradation of the PCL core and crosslinking by method 1 (b) or method 2 (c).

In 2009, S. R. S. Ting et.al prepared amphiphilic poly(lactide)-*block*-poly(6-*O*-acryloyl-R-D-galactopyranose) block copolymers (PLA$_x$-*b*-PAGP$_y$, x=170, y= 41 or 216) by i) ROP of dimethyl-1,4-dioxane-2,5-dione in toluene initiated by an hydroxyl-functionalized trithiocarbonate, *i.e.* 2-(benzylsulfanylthiocarbonylsulfanyl) ethanol, and catalyzed by Sn(Oct)$_2$, ii) RAFT polymerization of 1,2:3,4-Di-*O*-isopropylidene-6-*O*-acryloyl-R-D-galactopyranose in α,α,α-trifluorotoluene mediated by the PLA macroCTA and iii) deprotection of the sugar units using formic acid (**Scheme 1.19**, **Table 1.4**, **entry 2**).[82] The resulting amphiphilic block copolymers were shown to self-assemble in water (and methanol) and micelles with a hydrodynamic diameter ~ 280 nm were generated from PLA$_{170}$-*b*-PAGP$_{216}$. Preservation of the trithiocarbonate at the extremity of the block copolymer chains finally allowed

for cross-linking the shell of the particles through RAFT polymerization of hexanediol diacrylate (HDA). After treatment of the PLA core with hexylamine, hollow sugar nanocages were formed as confirmed by TEM analyses.

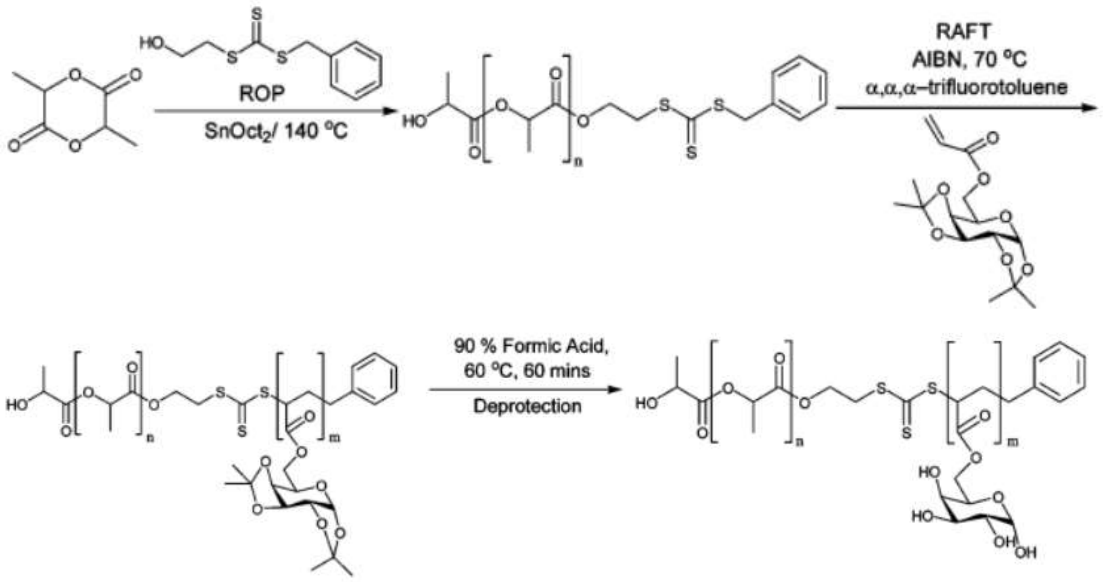

Scheme 1.19: Synthesis of D,L-Polylactide-*block*-poly(6-*O*-acryloyl-R-D-galactopyranose).

In 2015, poly(ethylene glycol)-*b*-poly(*β*-benzyl-L-aspartate) (PEG-*b*-PBLA) block copolymers with varying PEG length were prepared by Yang *et al*. via ROP of *β*-benzyl-L-aspartate N-carboxyanhydride using PEG_{45}-NH_2 or PEG_{114}-NH_2 as an initiator (**Scheme 1.20**)[83]. Deprotection of the PBLA block (in NaOH solution) generated poly(ethylene glycol)-*b*-poly(aspartic acid) (PEG-*b*-PAsp). Glucosamine-containing copolymer PEG_{45}-*b*-P(Asp-*co*-AspGA)$_{90}$ was obtained by amidification of the PAsp block (40% of the carboxylic acid groups coupled with glucosamine). PEG_{114}-*b*-P(Asp-*co*-AspPBA)$_{100}$ was obtained in a similar manner with 3-aminophenylboronic acid (80% of the carboxylic acid groups coupled with APBA). Dropwise addition of phosphate-buffered saline (PBS) solution (pH 7.4) of *α*-cyclodextrin (*α*-CD, 2 $g.L^{-1}$) into PBS solution of PEG_{45}-*b*-P(Asp-*co*-AspGA) (2 $g.L^{-1}$) with *α*-CD/polymer weight ratio 1:1, 1.5:1 and 2:1 resulted in the inclusion of *α*-CD rings onto PEG blocks which in turn triggered the self-assembly of the copolymers into micelles with a hydrodynamic diameter (D_h) of 43.7, 42.3 and 46.7 respectively. Then, a basic aqueous solution of

PEG_{114}-*b*-P(Asp-*co*-AspPBA) (pH 10) was poured into the dispersion to generate *α*-cyclodextrin/PEG_{45}-*b*-P(Asp-*co*-AspGA)/PEG_{114}-*b*-P(Asp-*co*-AspPBA) mixed micelles and promote the cross-linking of the shell by complexation of phenyl boronic acid with glucosamine. Dialysis against PBS 7.4 at 50 °C for 2 days ensured the removal of the *α*-CD rings located within the core of the micelles leading to the fabrication of glucose-responsive polymer vesicles composed of cross-linked PEG_{45}-*b*-P(Asp-*co*-AspGA)/PEG_{114}-*b*-P(Asp-*co*-AspPBA) shell layer and PEG chains as inner and outer coronas. The diameter of the vesicles determined by DLS study was 60 nm (D_h). Vancomycin was finally encapsulated in the vesicles (loading efficiency 48.3%, loading content 38.2%). Owing to the sugar sensitivity of the cycloborate rings ensuring the crosslinking of the vesicles, the cargo was released in a controlled manner upon addition of glucose or fructose in PBS 7.4 at 37°C (**Table 1.4**, **entry 3**).

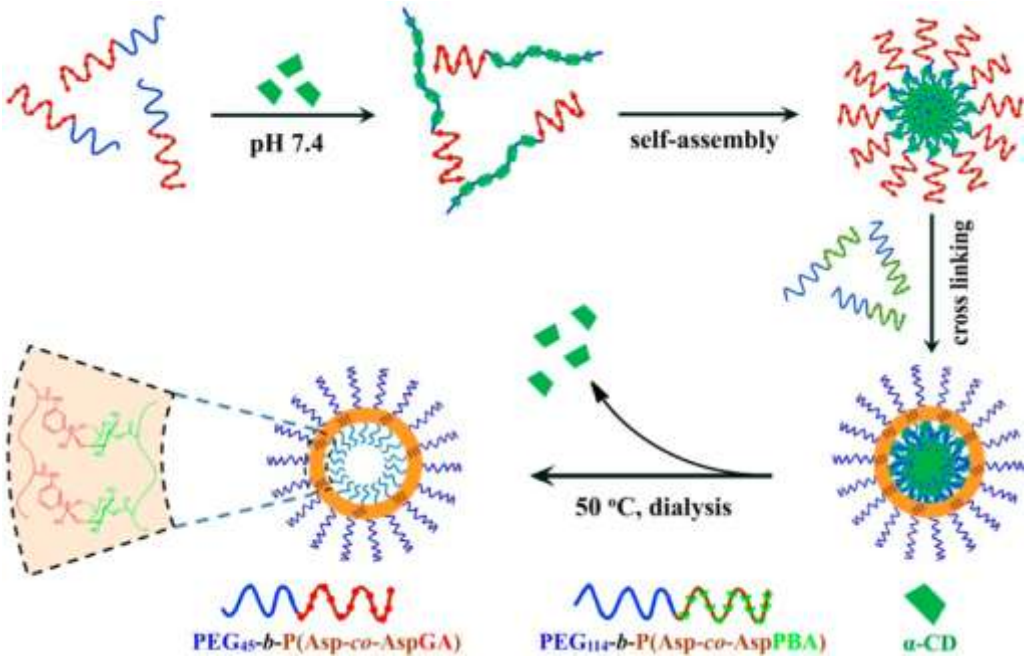

Scheme 1.20: Polymer vesicles by core-removal of α-CD/ PEG-*b*-PAsp micelles.

In 2016, the group of Borsali prepared an azide-functionalized PMMA block (Mn=5100 g/mol, *Đ*=1.24) by ATRP polymerization using an azide-functionalized initiator. An alkyne moiety was anchored at the reducing end of maltoheptaose oligosaccharides. Coupling of the two complementary blocks by

CuAAC afforded the preparation of maltoheptaose-*block*-poly(methyl methacrylate) (MH-*b*-$PMMA_{48}$, Mn=6600 g/mol, *Đ*=1.20) amphiphilic block copolymer.[84] The water/acetone mixture solution (0.78/0.22, w/w) of copolymer (3 mg/mL) was slowly added (0.5 mL h^{-1}) to 3 mL of Milli water and stirred. Acetone was removed to trigger the self-assembly of the copolymers into large compound micelles (LCMs, R_h 70 nm) composed of a PMMA core and a MH shell. Shell-cross-linking with DVS followed by exposition to UV (for 2-48 h) resulted in the construction of hollow glyconanoparticles with R_h 40-65 nm (**Figure 1.24**, **Table 1.4**, **entry 4**).

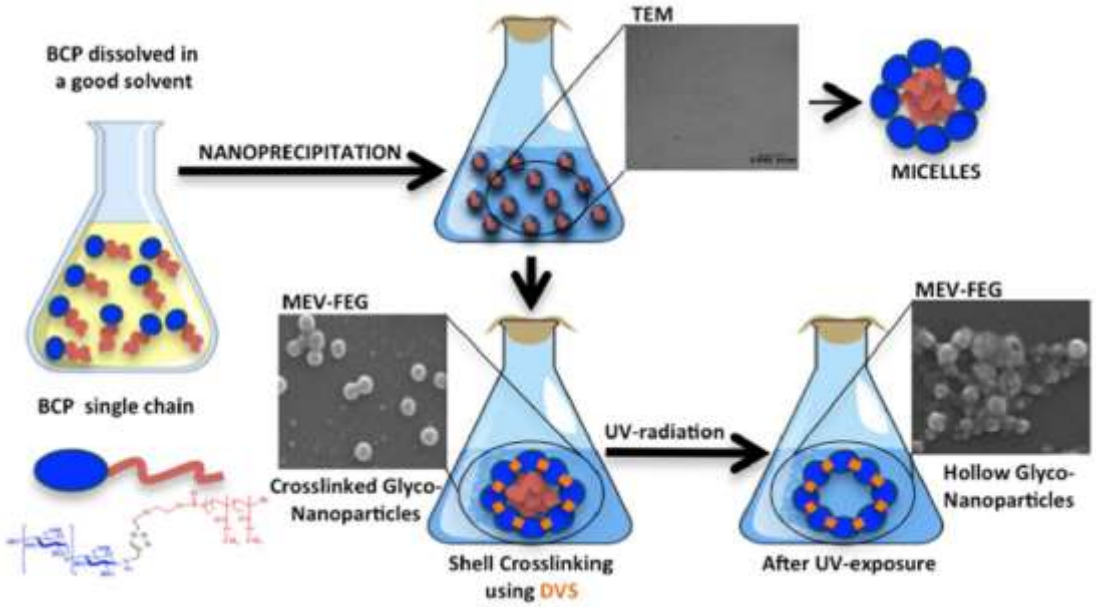

Figure 1.24: The photodegradatiion of non-cross-linked and cross-linked micelles.

Table 1.4: Preparation of glyconanocapsules by micelle core removal strategy.

Entry	Classification	Polymer	Protocol of self-assembly	Solvent	Size (nm)	Ref.
1	Polymersome	poly(ε-caprolactone)-*block*-poly[6-*O*-(4-vinylbenzyl)-D-galactose]	Core-removal	DMF/H_2O	50-120	81
2	Polymersome	poly(lactide)-*block*-poly(6-*O*-acryloyl-R-D-galactopyranose)	Core-removal	H_2O	280	82
3	Polymersome	PEG_{45}-*b*-P(Asp-*co*-AspGA)/PEG_{114}-*b*-P(Asp-*co*-AspPBA)	Core-removal	H_2O	60.3 (R_h)	83
4	Polymersome	maltoheptaose-*block*-poly(methyl methacrylate)	Core-removal	Acetone/H_2O	44 (R_h)	84

1.2.2 Template strategy

The template strategy relies on the deposition of polymer chains on diverse preformed substrates (liposomes, biomacromolecules, silica particles, polymer particles…) to fabricate hollow nanostructures. The layer-by-layer deposition (L-b-L) pioneered by Iler[85] and further developed by Decher[86,87] is the most common technique for the generation of a polymer shell onto diverse templates. Historically, the L-b-L template strategy consists in the sequential adsorption of oppositely charged polyelectrolytes onto a template core which can be further removed to produce monolayered or multilayered hollow capsules. Briefly, the process can be described as follows: (1) a template having a specific surface charge is immersed in a solution which contains an oppositely charged polyelectrolyte and one layer of this polyelectrolyte is adsorbed, (2) After washing to remove the excess of polyelectrolyte, an oppositely charged polyelectrolyte is immersed in the solution and a second layer is adsorbed, (3) Steps 1 and 2 are repeated until the desired multilayered structure is obtained, (4) the core is finally removed to generate a cavity (**Scheme 1.21**).[88] More generally, the deposition of polymer chains brings into play electrostatic, hydrogen bonding, host-guest and hydrophobic interactions or, covalent binding. More importantly, owing to its versatility and tunability, the L-b-L strategy allows for precisely controlling the structure the thickness and the functionalinaty of the layer. As described below, polymer capsules built by L-b-L constitute a vast platform for biomedical applications.

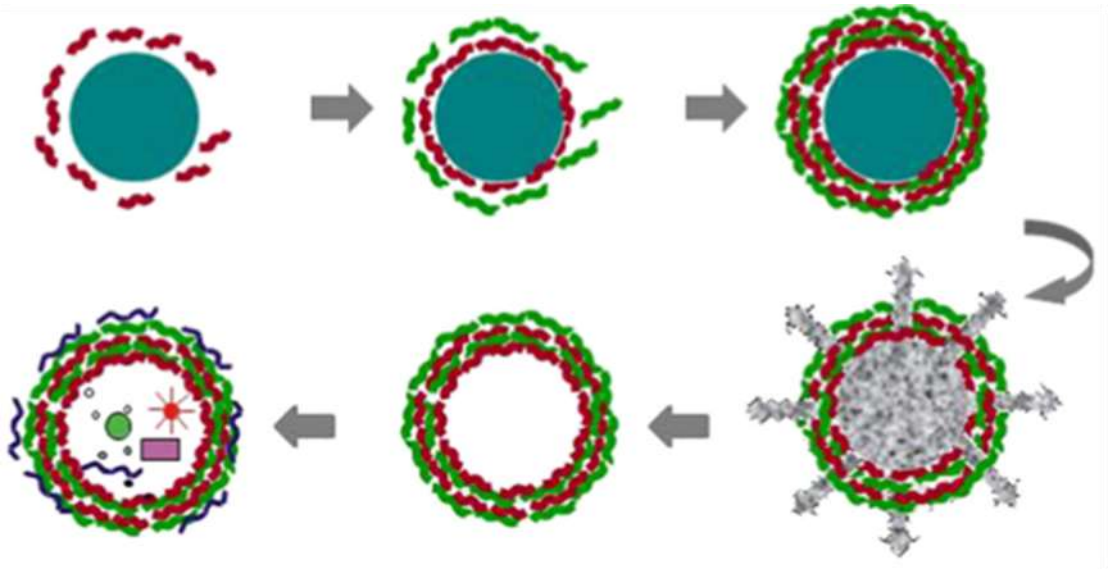

Scheme 1.21: Polymeric capsule fabrication by L-b-L assembly: deposition of the shell on the template; removal of the template core; loading the core with desirable components.

1.2.2.1 Particles as templates

In this part, we will limit our discussion to the construction of nanocapsules based on glycopolymer chains. It is however worth noting that many reports describe the preparation of nanocapsules using template strategies and polysaccharides, oligosaccharides or derivatives (dextran[89,90,91,92], cyclodextrin[93], chitosan[94], pectin[95], hyaluronan[96]…).

In 2006, the group of Lin prepared galactose-carrying nanocapsules using electrostatic L-b-L technique.[97] Biocompatible poly-(vinyl raffinose-*co*-acrylic acid) anionically charged glycopolymers (PRCA) were first synthesized in water via redox copolymerization of 1-*O*-vinyldecanedioyl raffinose generated by enzymatic coupling and acrylic acid for 24h at 20°C using 0.3%Fe^{2+}/0.3%$K_2S_2O_8$/0.3%H_2O_2. With 0, 1, 3, 7, 50 and 100 mol-% of vinyl raffinose ester monomer in the feed, a library of copolymers were obtained containing raffinose ester 0, 0.8, 4.1, 6.2, 47.7 and 100 mol-% (Mn=(0.28-7.27)×10^6 g/mol and *Đ*=1.6-4.2). Crystals of acyclovir, an antiviritic drug, were investigated as templates after grounding and fractionation by sedimentation.

The charged glycopolymer was first adsorbed on acyclovir crystal templates resulting in enhanced water dispersability and a ξ-potential value ~ -31 mV. The coated particles were then immersed to a solution of positively charged poly-(dimethyldiallyl ammonium chloride) to generate the second layer (ξ-potential value ~ +25 mV). Ten layers were finally coated onto the crystalline templates by alternatively adsorbing oppositely charged PRCA and PDDA chains. Crystal templates were removed by treatment with pH 1.4 hydrochloric acid buffer resulting in the formation of hollow nanocapsules with a membrane thickness around 100 nm (**Table 1.5**, **entry 1**).

In 2010, T. Nakahira and coworkers reported the fabrication of glycopolymer hollow particles by combining emulsion polymerization and core-removal methods.[98] Nanoparticles with a diameter of 440 nm were initially synthesized by radical copolymerization of styrene (St) and 2-chloropropionyloxyethyl methacrylate (CPEM) under mini-emulsion conditions. The presence of chloropropionyl groups at the surface of the submicron-sized P(St-CPEM) particles was then exploited to grow glycopolymer grafts by AGET-ATRP of N-2-4-(vinylbenzenesulfonamido)ethyl lactobionamide (VBSAELA) leading to the generation of P (St-CPEM)-*g*-PVBSAELA core–shell particles with a diameter of 755 nm (thickness of the glycopolymer shell around 160 nm). After selective dissolution of P(St-CPEM) core in THF at room temperature, PVBSAELA hollow particles with a diameter of 640 nm were finally obtained (**Figure 1.25**, **Table 1.5**, **entry 2**).

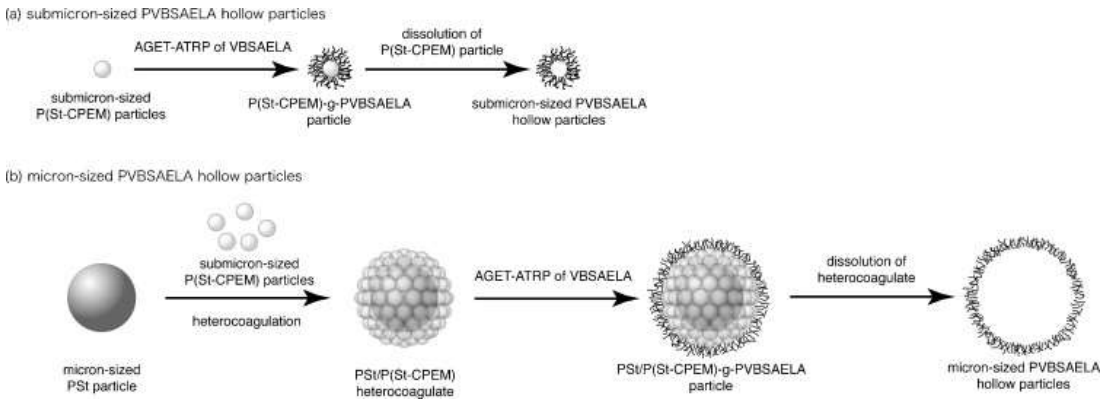

Figure 1.25: Schematic presentation of submicron-sized and micron-sized PVBSAELA hollow capsules by L-b-L.

In 2012, Schatz and co-workers set up a biomimetic self-assembly process to mimick virus morphologies where the genetic material is enclosed within a protein shell.[99] First, positively charged small-interfering RNA (siRNA, 23 base pairs, 14.6 kg/mol) /branched polyethyleneimine PEI (25 kg/mol) complexes were prepared in Hepes buffer solutions (10 mM, pH 7.6) at different nitrogen/phosphate (N/P) ratio. Above N/P=2 (corresponding to the isoelectric point of this system), stable positively charged aggregates were formed (ξ = +30 mV) and the diameter of the polyelectrolyte complexes ranged from 140 nm (N/P=2) to 185 nm (N/P=10). No trace of free PEI was detected after complexation. A solution of negatively charged hyaluronan-*block*-poly(*γ*-benzyl L-glutamate) block copolymer in DMSO (hyaluronan: Mn=5140 g/mol, *Đ*=1.41; PBLG: Mn=5000 g/mol, *Đ*=1.1), simulating the glycoproteins that typically surround the DNA/RNA material in virus systems and capable to self-assemble into vesicular structures in aqueous medium, was mixed with the aqueous solution of polyelectrolyte complexes. To favor interactions between polyelectrolyte complexes and the hyaluronate block (to ensure coating of the aggregates) over direct self-assembly of the block copolymer into vesicles, the water content was limited to 2.5 vol %. After mixing, the surface charge of the nano-objects was moderately negative (ξ = -10 mV) confirming the adsorption of the block copolymers and the steric stabilization of the polyelectrolyte

complexes. The medium was progressively enriched in water (to reach 80 vol % water) “to turn on” the amphiphilic character of the block copolymer and to trigger the formation of a bilayered membrane onto the electrostatic complex of PEI and siRNA (D_h ~ 150 nm, ξ = -33 mV). Interestingly it was shown that copolymer coated polyelectrolyte complexes display a higher gene silencing activity than uncoated complexes (**Figure 1.26**, **Table 1.5**, **entry 3**).

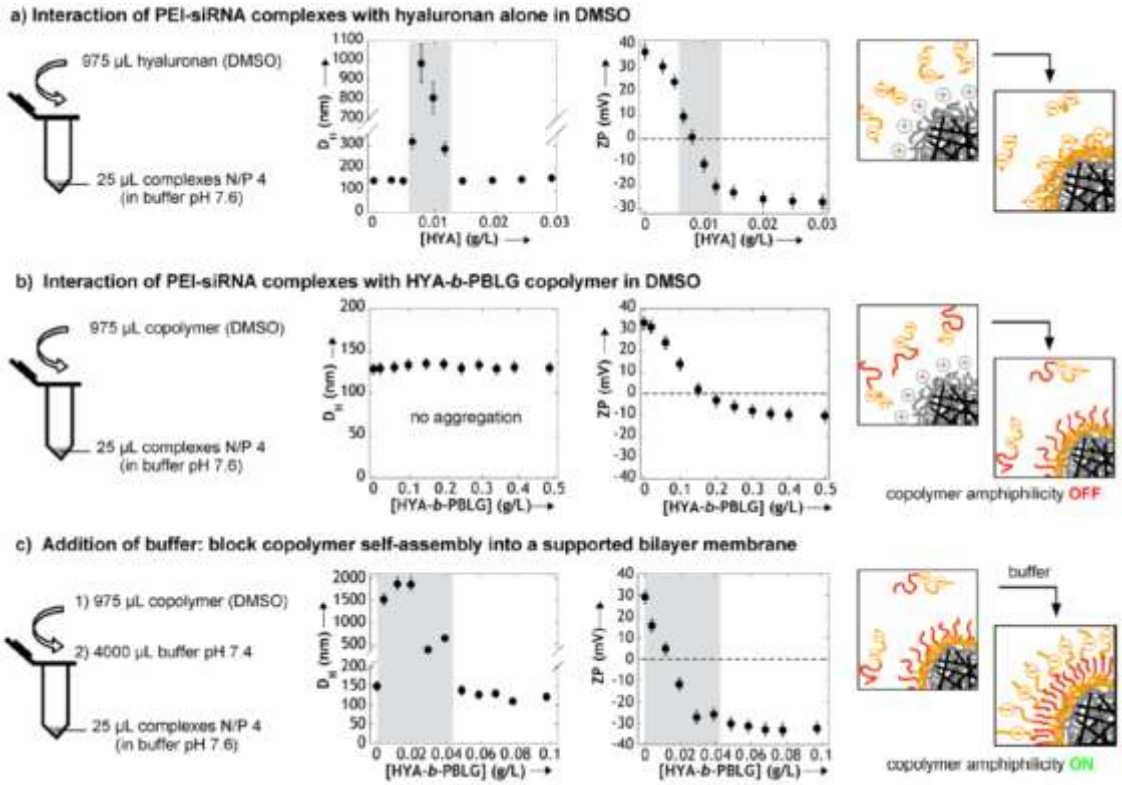

Figure 1.26: (a) Interaction of hyaluronan (HYA) with siRNA−PEI complexes (N/P = 4, CsiRNA = 30 µM) in DMSO/Hepes buffer (97.5/2.5) (v/v). (b and c) Two-step assembly of HYA-b-PBLG copolymer around siRNA−PEI polyelectrolyte complexes. First step (b): Interaction of the copolymer with complexes in DMSO/Hepes buffer (97.5/2.5) (v/v). Second step (c): Addition of Hepes buffer in the medium up to a final DMSO/buffer composition of 20/80 (v/v). The mean hydrodynamic diameter (DH) and zeta potential (ZP) of resulting particles are plotted as a function of the concentration of hyaluronan (a) or copolymer (b and c). The gray area represents the domain of colloidal instability where particles sediment. Importantly, the amphiphilicity of the copolymer is turned OFF and ON when changing from DMSO to buffer.

In 2014, D. Yu's group prepared [CS-NAC/p(GAMA-*r*-AAPBA)] nanocapsules through via L-b-L self-assembly.[100] Negatively charged poly(D-gluconamidoethyl methacrylate-*r*-3-acrylamidophenylboronic acid) [p(GAMA-*r*-AAPBA)] random copolymers were first synthesized by radical copolymerization of GAMA and AAPBA (at 1:1, 2:1 and 4:1 GAMA/AAPBA molar ratio). Positively charged chitosan-N-acetyl-L-cysteine conjugates (CS-NAC) were synthesized through reaction of N-acetyl-L-cysteine and chitosan by amidation in order to promote the formation of disulfide bonds between chains, stabilize the resulting nanocapsules (through cross-linking reactions) and control their degradation. After sequential deposition of positively and negatively charged polymers onto preformed SiO_2-NH_3^+-decorated silica nanoparticles (diameter 110 nm), multilayered nanoparticles with diameters ranging from 253 to 272 nm were built depending on the GAMA content. The polymer shell was cross-linked in the presence of chloramine T (D_h=110 nm) and the silica core was removed by treatment with NH_4F/HF solution (v: m=1:10). Hollow multilayer disulfide cross-linked nanocapsules were finally obtained (D_h=254 nm) (**Scheme 1.22**, **Table 1.5**, **entry 4**). Thanks to the presence of boronic acid groups within the shell, the capsules exhibited glucose sensitivity. Addition of glucose (3 mg/ml in PBS buffer) induced a significant swelling of the capsules from 254 nm to 424 nm whereas the vesicles shrank back to 267 nm after removal of glucose. Insulin was loaded in the capsules with an encapsulation efficiency around 60%. At a glucose concentration of 3 mg/ml, the release of insulin was less than 8% in 24 h at pH = 1.4. This value jumped to 70% (in 24 h) at pH 7.4.

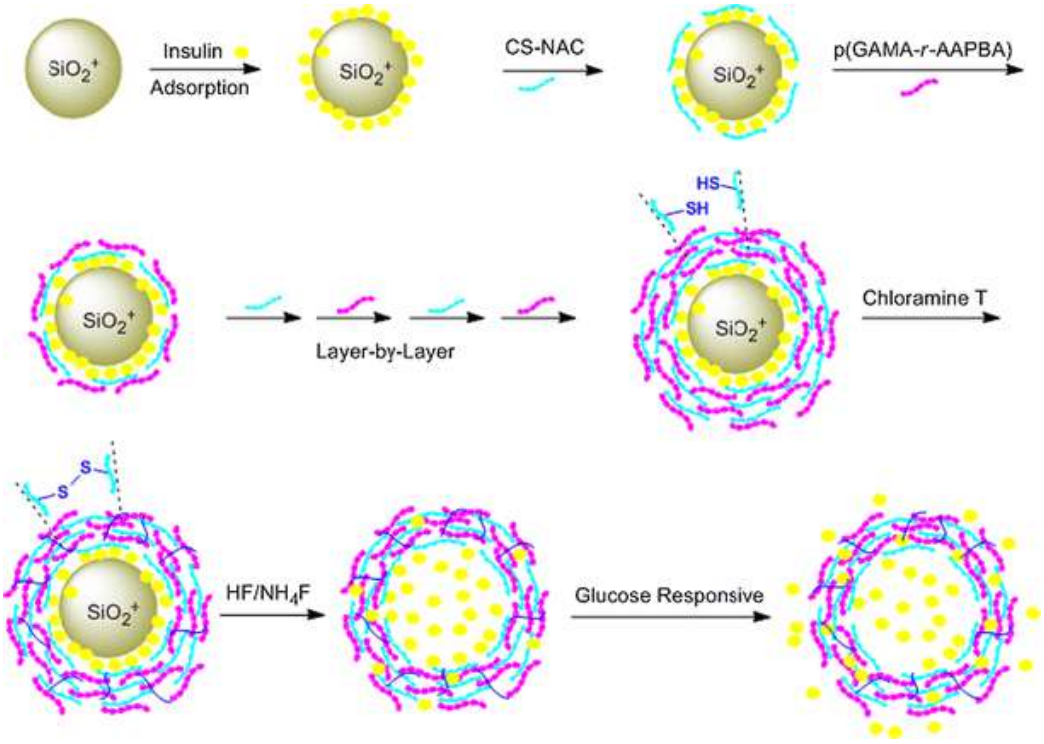

Scheme 1.22: Preparation of glucose-responsive glyconanocapsules by L-b-L strategy.

In 2016, M. Akashi and coworkers prepared glucose-responsive capsules by L-b-L assembly based on amine-modified SiO_2 nanoparticle templates.[101] The shell was composed of ten alternating layers of poly(γ-glutamic acid)-*g*-3-aminophenylboronic acid) and lactobionic acid functionalized chitosan oligosaccharides polyelectrolytes (GC) assembled in pH 5.0 buffer at 2 mg/mL. The SiO_2 template (diameter ~ 195 nm) was removed by redispersion of the core-shell nanoparticles (diameter 235 nm) in NH_4F/HF (8M/2M) resulting in hollow $(γ\text{-PGA-}g\text{-APBA/GC})_5$ capsules (d_{TEM} ~ 240 nm) with glucose sensitivity due to competitive BA/lactobionic acid (LA) and BA/glucose interactions. This last property was finally exploited to design insulin delivery systems (**Scheme 1.23**, **Table 1.5**, **entry 5**).

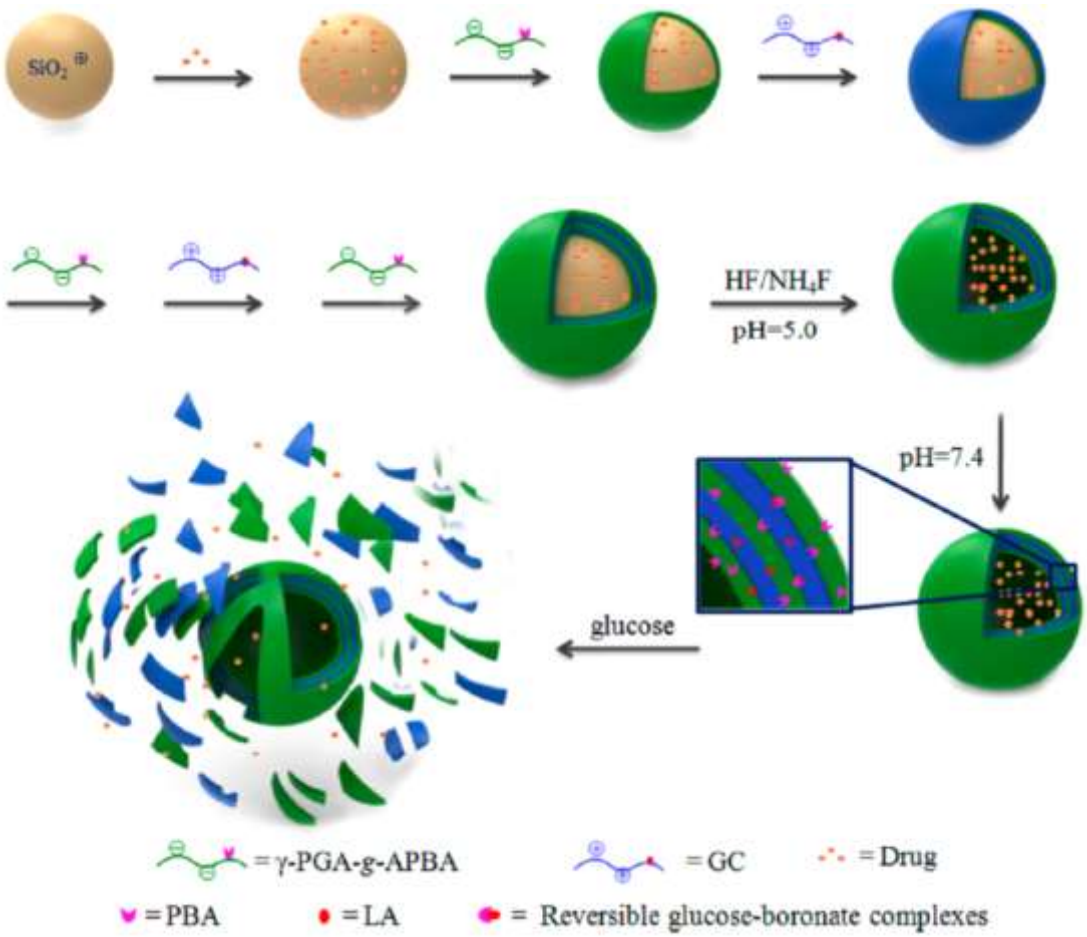

Scheme 1.23: Fabrication, Drug Loading, and Release of Polyelectrolyte Capsules Based on *γ*-PGA-*g*-APBA and GC.

1.2.2.2 Liposomes as templates

Owing to their low toxicity, their biodegradability and their vesicular structure, liposomes have been extensively employed in drug delivery applications. For targeting purposes, significant efforts have been paid to the decoration of liposomes with sugar moieties through supramolecular inclusion of functionalized molecules.[102,103,104,105] On the contrary, little attention has been focused so far on the use of liposomes as templates for the conception of glycocapsules using glycopolymers, electrostatic interactions and L-b-L strategy.

In 2012, Chen and coworkers prepared chitosan-coated and folate-modified–

chitosan-coated liposomes (CCLs and FCCLs) for tumor-targeted drug delivery.[106] Liposomes (161 nm in size) were first prepared using phosphatidylcholine/cholesterol (weight ratio 4:1) by injection method. The folate–chitosan conjugates (FA-CS) were generated by conjugating folate to the amino groups of chitosan (CS) using a carbodiimide-based activating agent. After incubating CS or FA-CS with liposome suspensions under acidic pH (weight ratio of CS or FA–CS to PC=1:8), liposome-templated nanoparticles (CCLs R_h=178.4 nm and FCCLs R_h=182 nm) were fabricated (**Table 1.5**, **entry 6**). The fluorescein encapsulation efficiency attained 91.2, 94.2 and 94.3% for naked liposomes, CCLs and FCCLs respectively. After dialysis in PBS for 24 h, the release was 65.57, 55.22 and 55.76%, respectively. The difference in release rate between liposomes and polymer-coated liposomes was attributed to their different stability and permeability.

In 2013, Klemetsrud et al. reported pectin-coated liposomes and investigated their interactions with mucin.[107] Lipsomes composed of dipalmitoyl phosphatidylcholine (DPPC) and dipalmitoyl trimethylammoniumpropane (DPTAP) were prepared by the film method. Three methoxy modified pectin, LM (Mw 76 kg/mol, degree of esterification 35%), HM (Mw 110 kg/mol, degree of esterification 70%) and AM (Mw 96 kg/mol) were first used for liposomes coating and the resulting nano-objects were then incubated with mucin. The diameters of the resulting capsules varied from 312 to 582 nm depending on the liposome/mucin ratio (weight ratio between 0.02 and 0.1%) (**Table 1.5**, **entry 7**).

In 2015, the group of Ratner reported glycopolymer-augmented liposomes (**Figure 1.27**, **Table 1.5**, **entry 8**).[108] Glycopolymers , poly(ManEMA-*co*-CMA), (90% mol of ManEMA, Mn=24.8 kg.mol^{-1}, *Đ*=1.10) and poly(GalEMA-*co*-CMA) (88% mol of GalEMA, Mn=24.3 kg.mol^{-1}, *Đ*=1.10), were first synthesized by RAFT copolymerization of cholesterol methacrylate and per-*O*-acetylated

galactose/mannose-functionalized methacrylate and further deprotected using sodium methoxide in methanol. A mixture of DSPC/Cholesterol/Rhodamine DHPE 60/25/0.05 or DSPC/Cholesterol/Rhodamine DHPE/ DSPE-mPEG(2000) 60/25/0.05/5 was dissolved in chloroform and evaporated to form a lipid film. The film was subsequently hydrated in glycopolymer aqueous solution to form the glycopolymer augmented liposomes. The glycopolymers were anchored to the liposomes by insertion of the pendent cholesterol groups in the hydrophobic lipid bilayer. Mannose, galactose and PEG-functionalized liposomes showed particle size ranging from 120-170 nm. The produced glycopolymer functionalized vesicles showed specific receptor-mediated uptake for BMDM and RAW264.7 cells.

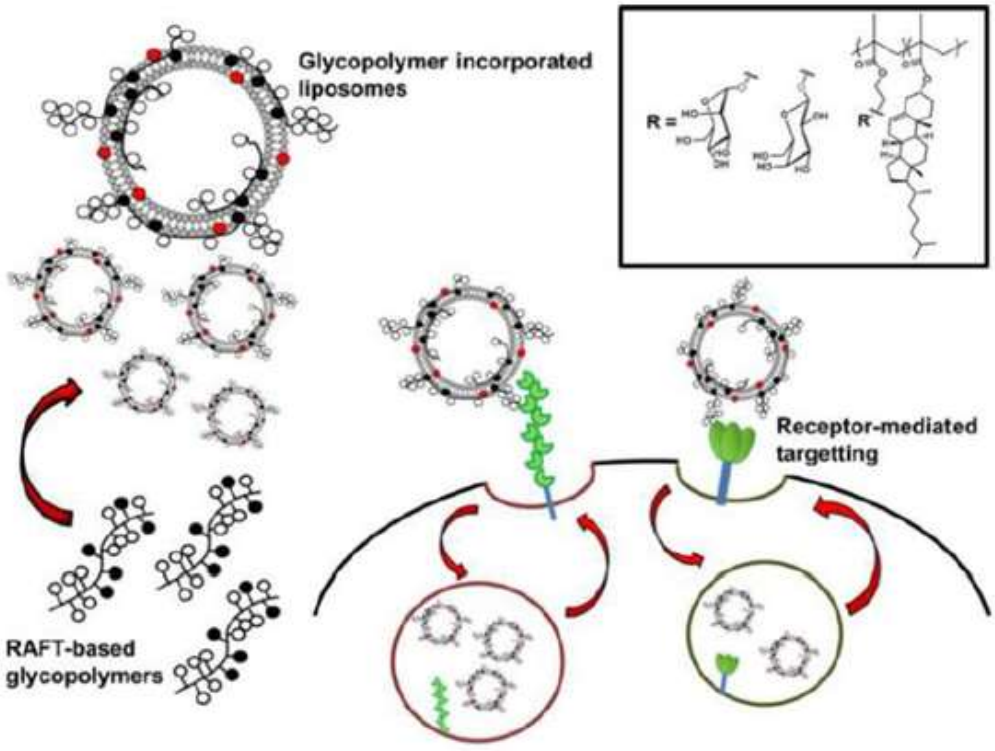

Figure 1.27: Glycopolymer-augmented lipsomes and their in vitro uptake by BMDM and RAW264.7 cells.

The introduction of hydrophobic groups into chitosan chains enhance the membrane integrity and structural rigidity of coated liposomes. In 2007, the group of Bin reported pharmacokinetics of N-palmitoyl chitosan anchored

docetaxel liposomes.[109] N-palmitoyl chitosan (NPC) was synthesized from chitosan (Mw 65 kDa, degree of acetylation 10%) and palmitic anhydride by heating and stirring in acetic acid/methanol mixturing (1/5, v/v). Two docetaxel-loaded lipsomes PDLs (EE=96.1±0.48%, R_h=219 nm) and PEGDLs (EE= 96.4±0.21%, R_h=223 nm) were prepared by the film dispersion method from docetaxel /cholesterol /EPC (mass ratio 1:3:25) and docetaxel /cholesterol /EPC /PEG-DSPE (mass ratio 1:3:25:5). By anchoring NPC on the surface of PDLs via electrostatic attraction and hydrophobic interactions, NDLs capsules (R_h=231 nm) were generated. The release of anti-cancer agent docetaxel in fetal calf serum (FCS) at 37 °C after 24 h was 63±1.98, 59±2.18 and 31±1.52% for PDLs, PEGDLs and NDLs, respectively. The comparatively lower release of docetaxel in the case of NDLs was ascribed to the more stable outer surface of the particles (**Table 1.5**, **entry 9**).

Amphiphilic *N*-octyl-*O*-sulfate chitosan (NOSC) was prepared by octylation of amino group at C-2 position and sulfonylation at C-6 position of chitosan (viscosity average molecular weight 65000 $g.mol^{-1}$, deacetylation degree ~97%) by Ping et al.[110] Based on this, the group of Zhang prepared NOCS modified calcein liposomes (CLs), NOCS modified docetaxel liposomes (DLs) and chitosan modified DLs, named NCLs, NDLs and CDLs, respectively.[111] For NDLs prepared at NOSC/SPC (soybean phosphatidylcholine) weight ratio ranging from 0 to 15%, the docetaxel entrapment efficiency varied from 100 to 85%, while the capsule size increased from 138.1±2.1 to 147.6±1.9 nm. After incubation with 1.5 wt% bovine serum albumin in PBS, the capsule size of CDLs rapidly grew from 400 nm (10 min) to 800 nm (60 min). A similar trend was observed with NDLs. The insertion of NOSC within the membrane of the capsules significantly impacted the release of calcein (30% for NCLs vs 50% for CLs in 50h) (**Table 1.5**, **entry 10**).

In 2015, the group of Lv synthesized *N*-Octyl-*N*-Arginine-Chitosan (OACS)

coated Cyclosporine A (CsA) liposomes (CL), named OACS-CL, by rotary-film evaporation method.[112] The amphiphilic *N*-Octyl-*N*-Arginine-Chitosan (OACS) was obtained by reaction of L-arginine with *N*-octyl CS at room temperature (**Scheme 1.24**).[113] The capsule size increased from 58 to 110 nm by increasing the DS of arginine (0-20%) and octyl (0-30%). However, these derivatizations had barely no impact on the encapsulation efficiency (EE, 95-98%) and on the drug loading efficiency (DL, 8-9%) of CsA (**Table 1.5**, **entry 11**). Note though that the presence of the polymer coating had an influence on the kinetics of CsA release in FaSSGF medium at pH 1.2 (19% of released CsA in 4h in the case of CL *vs* 11% for OACS-CL). This might be caused by the protonating of amino group and guanidine group of OACS at so low pH condition. In the case of in vivo study to gavage rats with CsA at a dose of 15 mg/kg, the OACS-CL showed enhanced CsA absorption when comparing with commercial preparation of microemulsions (Tianke) and CsA suspensions after 3 or 4h of administration.

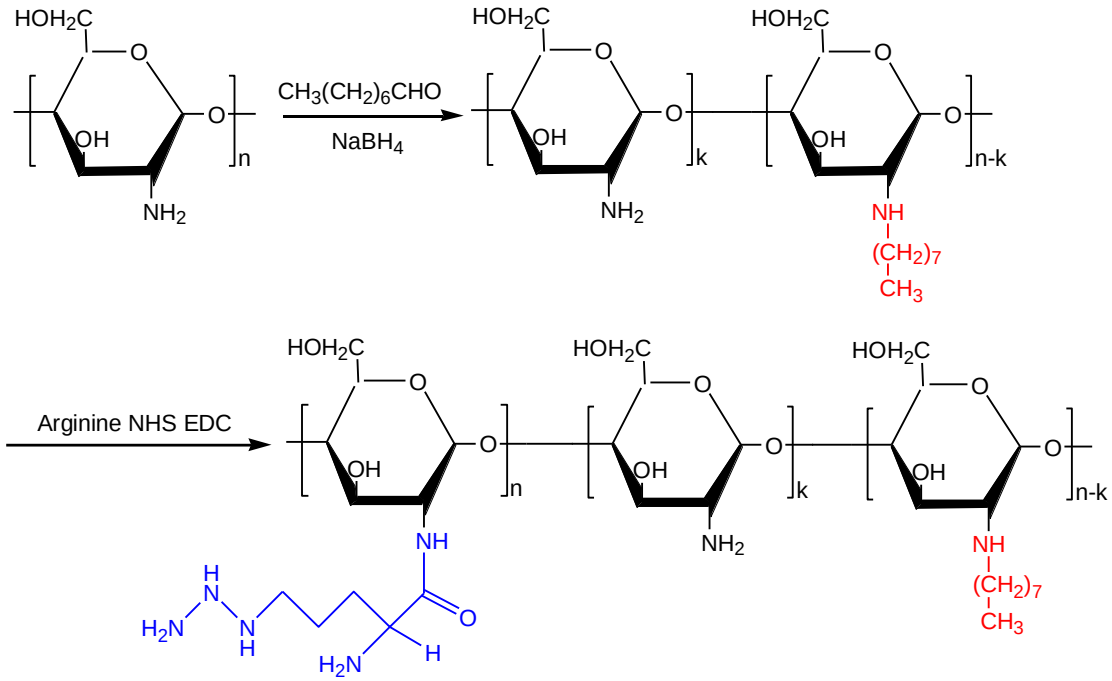

Scheme 1.24: Route to *N*-octyl-*N*-arginine functionalized CS (OACS).

In 2016, M. Mironov and coworkers synthesized chitosan derivatives bearing highly hydrophobic groups (DS 7%) from chitosan (Mw 190 kDa, 5% GlcNAc) by Ugi multicomponent condensation of chitosan amino groups in the presence of pelargonic acid, 2-methoxyethyl isocyanide and formaldehyde (**Figure 1.28**).[114] Triazavirin-loaded lipsomes (R_h=184±3 nm) were first prepared from phosphatidylcholine, methyl palmitate and tocopheryl acetate by the extrusion method (Triazavirin entrapment efficiency 77.9±1.8%). Capsules (R_h=147±3 nm) were then obtained by coating modified chitosan onto the liposomes surface (chitosan/lipid 1:8) via hydrophobic interactions (**Table 1.5**, **entry 12**). The drug release rate of uncoated and coated liposomes was 85 and 50% after 6 h.

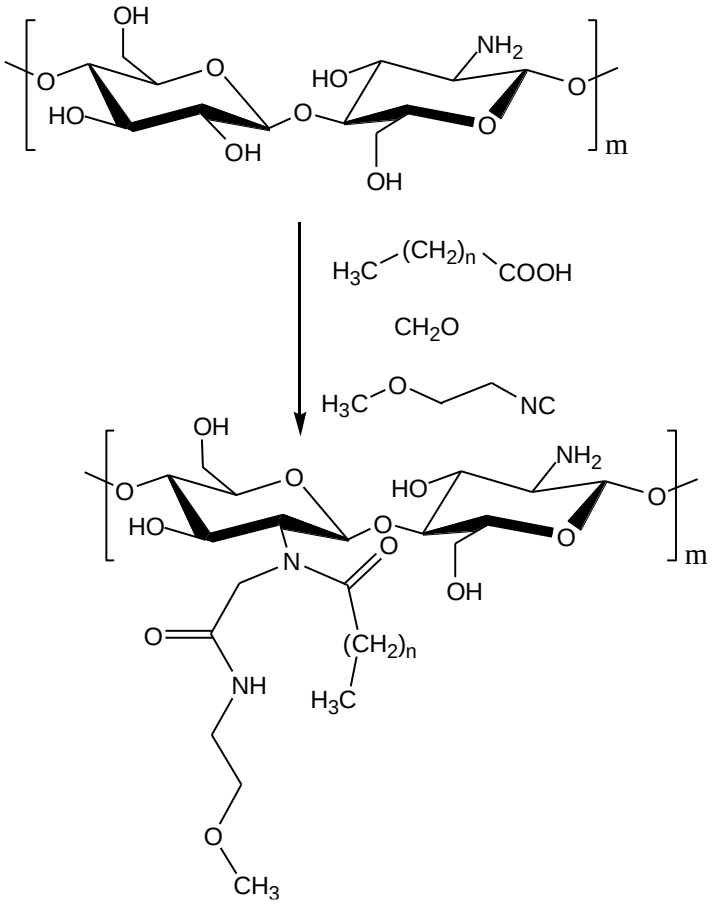

Figure 1.28: Molecular structure of modified chitosan.

In 2017, a series of thiol derivatized chitosans (CSSH) were synthesized via reaction of chitosan (15-25% of GlcNAc) with L-cysteine hydrochloride monohydrate. The degree of substitution of chitosan derivative ranged from 5.0,

6.5 and 6.0% as the chitosan/cysteine molar ratios varied from 3:1 to 1:3. After the preparation of curcumin-loaded liposome (Cur-Lip) using PC and cholesterol by thin-film hydration method, CSSH coated-Cur-Lip (Cur-Lip-CSSH) was fabricated by addition of a CSSH aqueous solution (1% wt) into a suspension of Cur-Lip (2 mg/mL) under stirring. The mean sizes of Cur-Lip and Cur-Lip-CSSH were 276 ± 4 nm and 406 ±12 nm, respectively (**Table 1.5**, **entry 13**)[115]. The curcumin loading efficiency (EE) and drug loading efficiency (DL) were enhanced for Cur-Lip-CSSH reaching 94±4% and 8±0.4% respectively and the release of actives in phosphate buffer was delayed in comparison with Cur-Lip liposomes thanks to the presence of the polymer outer layer (release of curcumin around 40% at pH 5.5 and 25% at pH 7.4 *vs* 64% and 74% for liposomes). Treatment of MCF-7 with curcumin and Cur-Lip-CSSH showed dose and time dependent cytotoxicity, with growth suppression at 200 μM after 72 h.

In 2018, the group of Kenji prepared pH-sensitive capsules by modification of egg yolk phosphatidylcholine liposomes (EYPC or Pyranine-loaded EYPC) with hyaluronic acid (HA, 8-50 kDa) derivatives, which were synthesized by introducing different contents of 3-methyl glutarylated (MGlu) or 2-carboxycyclohexane-1-carboxylated (CHex) units and subsequent decyl groups by reaction of decylamine with carboxyl groups.[116] The obtained HA derivatives $MGlu_{20}$-HA-C_{10}, $CHex_{27}$-HA-C_{10}, $MGlu_{57}$-HA-C_{10} and $CHex_{50}$-HA-C_{10} were coated onto EYPC lipsomes using the film hydration method, resulting in narrow distributed capsules with an average size of 191.5 ± 3.8, 128.6 ± 6.1, 144.8 ± 8.5 and 140.8 ± 8.5 nm, respectively. At pH 7.4, all liposomes retained their pyranine content. At pH 4.5, $MGlu_{20}$-HA-C_{10} and $CHex_{27}$-HA-C_{10} (pKa 5.4-6.4) modified liposomes showed a slight release (<10% in 1500 sec), whereas $MGlu_{57}$-HA-C_{10} and $CHex_{50}$-HA-C_{10} (pKa 6.1-6.7) modified liposomes induced significant release within 10 min (60-80%). Regarding interactions HeLa cells or Colon26 cells (expressing CD44 glycoproteins, a HA receptor), CHex-HA-

C_{10} lipsomes showed higher cellular association than HA-C_{10} modified and unmodified liposomes. Note that MGlu-HA-C_{10} liposomes inhibited cellular association. The authors concluded that the prepared liposomes are promising candidates as CD44-positive cell-specific intracellular drug delivery systems (**Figure 1.29**, **Table 1.5**, **entry 14**).

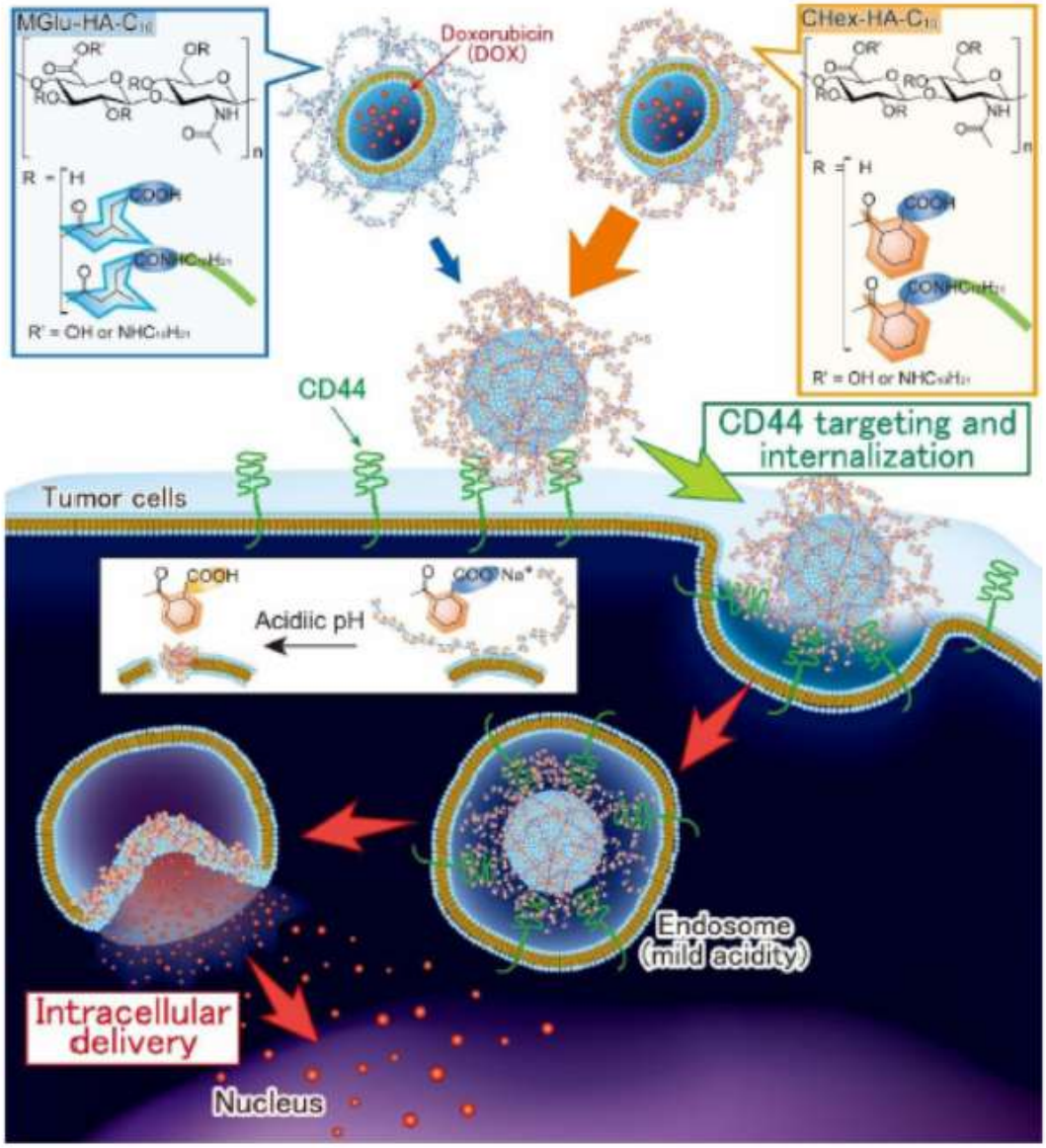

Figure 1.29: Design of hyaluronic acid derivative-modified liposomes for CD44-expressing cell-specific intracellular drug delivery.

1.2.2.3 Modification of preset capsules

In addition to the various methods described above, glyconanocapsules can

also be prepared by modification of preset polymer nanocapsules through chemical coupling reaction.

For instance, azide-decorated vesicles with a diameter of around 140 nm and a PDI of 0.11 were prepared by the group of E. R. Gillies via self- assembly of poly(ethylene oxide)-*b*-polycaprolactone (PEO_{44}-*b*-PCL_{82} containing 5, 7, 10, 20, 40, 70 or 100 wt% of N_3-PEO_{44}-*b*-PCL_{82}, **8**).[117] Sialic acid *N*-acetylneuraminic acid (**6**, Neu5Ac) terminated glycodendrimers were then conjugated to the surface of the polymersomes by CuAAC using 4 equivalents of (**8**) (**Figure 1.30** and **Table 1.5**, **entry 15**). At loadings ≤40 wt% of azide-terminated copolymer **8** in polymersomes, the conjugation yields for the CuAAC coupling with dendrons **4** (or rhodamine-tagged derivatives) were superior to 40% and no significant changes were witnessed for the resulting dendron-functionalized polymersomes. In contrast, coupling reactions involving azide-rich polymersomes (loading ≥ 40 wt%) resulted in the formation of aggregates. Lectin binding potencies of two dendritic sialopolymersomes (based on 20 wt% and 40 wt% copolymer **8**) were investigated using an Enzyme-Linked Lectin Inhibition Assay (ELLA). It was found that the incorporation of Neu5Ac motifs onto the polymersome surface leads to an almost 2000-fold enhancement in binding on a per-Neu5Ac basis in comparison to a small molecule analogue. As a comparison, a 17-fold enhancement was observed for the Neu5Ac-functionalized dendritic scaffold.

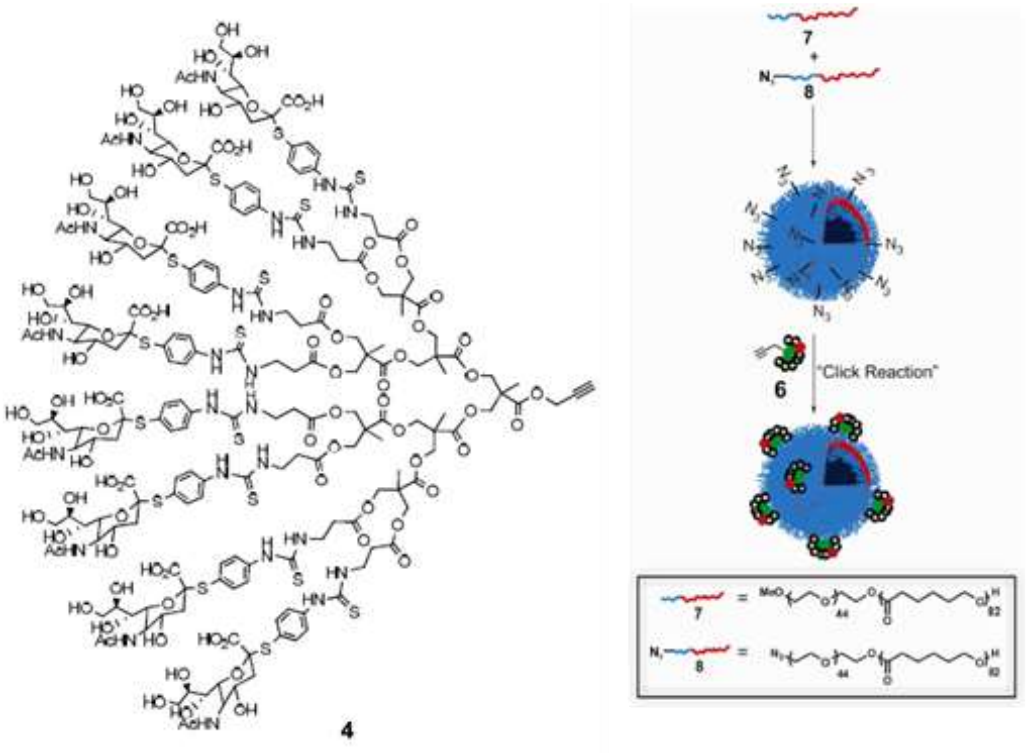

Figure 1.30: (Left) sialodendron 4 and (right) preparation of dendritic sialopolymersomes.

Recently, Gaitzsch and coworkers prepared a poly(ethylene glycol)-b-poly(diethyl amino ethyl methacrylate-stat-3,4-dimethyl maleic imidobutyl methacrylate) amphiphilic block copolymer, PEG_{45}-*b*-($PDEAEM_{73}$-*s*-$PDMIBM_{19}$) by ATRP (BCP1, Mn=29.3 $kg.mol^{-1}$, *Đ*=1.22). The pH-sensitive and photo-cross-linkable BCP1 self-assembled into stable polymersomes through pH switching followed by cross-linking of the PDMIBM block under UV irradiation. Upon addition of inulin (0.1% w/v), the polymersomes were lyophilized and redispersed in PBS buffer at pH 6.5 without aggregation or substantial increase of the dimensions (D_h = 67 nm at pH 8 and 127 nm at pH 5, PDI=0.15; after lyophilization or freezing, D_h = 145 nm PDI=0.22) (**Table 1.5**, **entry 16**). A HSA-βCD-FITC conjugate was synthesized through reaction of Albumin from human serum (HSA) with (1R, 8S, 9S)-bicyclo[6.1.0]non-4-yn-9-ylmethyl N-succinimidyl carbonate, subsequent click ligation with mono-(6-azido-6-desoxy)-*b*-cyclodextrin and coupling with fluorescein 5(6)-isothiocyanate in carbonate buffer pH 10. A diluted dispersion of polymersomes was further

mixed with HSA-βCD-FITC to decorate the colloids with HSA by PEG/β-CD host-guest complexation without significant modification of the dimensions (**Figure 1.31**)[118].

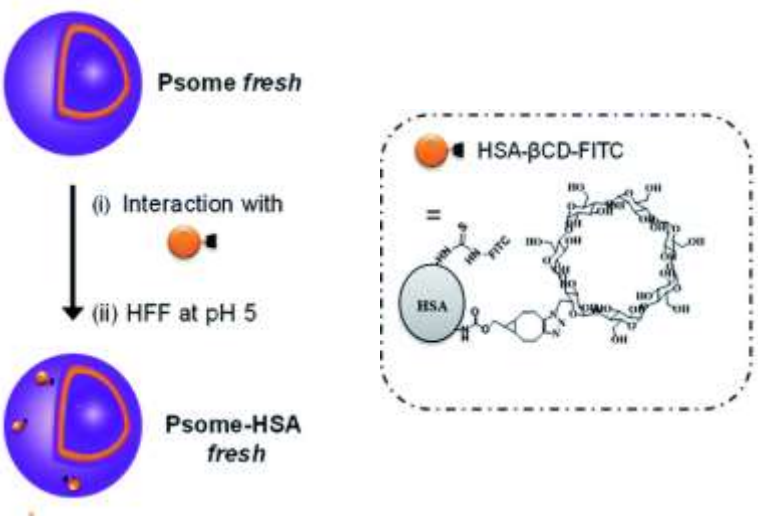

Figure 1.31: Fabrication of Psome-HAS *fresh*.

Table 1.5: Preparation of glyconanocapsules by template strategy.

Entries	Template	Template dimension (nm)	Polymer	Deposition Manner	Cross-linker	Core removal	Capsules dimension (nm)	Ref.
1	acyclovir		poly(vinyl raffinose-*co*-acrylic acid)/ poly(dimethyldiallyl ammonium chloride)	Electrostatic interaction		HCl		97
2	P(St-CPEM)	455	poly(N-2-4-(vinylbenzenesulfonamido) ethyl lactobionamide)	Surface polymerization		THF	640	98
3	siRNA-PEI complex	150-185	hyaluronan-*block*-poly(*γ*-benzyl L-glutamate)	Electrostatic interaction			90	99
4	SiO_2	110	chitosan-N-acetyl-L-cysteine/poly(dgluconamidoethyl methacrylate-*r*-3-acrylamidophenylboronic acid)	Electrostatic interaction	chloramine T	NH_4F/HF	254	100
5	SiO_2	195	chitosan/poly(γ-glutamic acid)-*g*-3-aminophenylboronic acid)	Electrostatic interaction		NH_4F/HF	240	101
6	Lipsomes	161	Folate-modified–chitosan	Incorporation			182	106
7	Lipsomes		Pectin	Electrostatic interaction			312-582	107
8	Liposomes	120-170	poly(ManEMA-*co*-CMA) poly(GalEMA-*co*-CMA)	Incorporation			120-170	108
9	Lipsomes	219	N-palmitoyl chitosan	Electrostatic interaction			231	109
10	Lipsomes	138.1±2.1	N-octyl-O-sulfate chitosan	Electrostatic interaction			147.6±1.9	111

11	Lipsomes	58.94	N-Octyl-N-Arginine-Chitosan	hydrophobic interaction	109.6	113
12	Lipsomes	184±3	Modified chitosan	hydrophobic interaction	147±3	114
13	Lipsomes	276.0±3.8	thiol derivatised chitosan	hydrophobic interaction	406.0 ±12.0	115
14	Lipsomes	193.5±26.7	$CHex_{50}$-HA-C_{10}	Electrostatic interaction	140.8± 8.5	116
15	Polymersome	140	sialodendron	Grafting		117
16	Polymersome		HSA-*β*CD-FITC	Grafting	127	118

1.2.3 Emulsification techniques

In the previous section, we have shown that a large range of solid nano-objects, *i.e.* silica particles, polymer particles or nanocrystals, can be used to design glyconanocapsules. In this section, we will describe synthetic routes to nanocapsules relying on emulsification techniques (miniemulsion, double emulsification, emulsion coacervation, emulsion diffusion and polymer coating) where liquid nanodroplets are exploited as templates for the generation of glyconanocapsules.

1.2.3.1 Mini-emulsion technique

Mini-emulsions are kinetically stable O/W dispersions prepared by high shear devices (using ultrasonication). The technique produces nanodroplets with dimensions in the 50 to 500 nm range and has been extensively exploited in combination with polymerization processes to design nanoparticles (polymerization in the dispersed phase) or nanocapsules (polymerization or polymer cross-linking at the O/W interface).[119] Examples of nanocapsules preparation can be found with ionic, radical, or metal-catalyzed polymerizations, enzymatic or chemical polycondensation and polyaddition reactions.

Breakthrough work has been reported by Landfester and coworkers on polymeric nanocapsules from polysaccharide such as chitosan[120], starch[121,122,123,124,125], cellulose[126] and dextran[127,128] and their derivatives[129]. The extensive developments regarding to emulsion process offer high potential in the construction of glyconanocapsules from derivatized polysaccharides. In 2014, Landfester's group prepared nanocapsules having a dextran-polyurethane shell through interfacial radical polymerization in inverse miniemulsion[130]. In brief, a 0.5 M NaCl aqueous solution containing $Zn(NO_2)_2$, an anti microbial agent, methacrylated dextran (dextran Mw~6, 40, 70 kDa,

DS=0.05-0.2) and acrylamide (AAm) with a 1:1 weight ratio was added dropwise into a solution of cyclohexane containing Lubrizol U (1 wt%) as surfactant. The medium was stirred and sonificated to form a water-in-oil emulsion. Radical polymerization of AAm was initiated by addition of V-59 and heating at 60°C, resulting the formation of a zinc-loaded polymer network in the aqueous droplets. Hydrophobic 2,4-toluene dissocyanate (TDI/OH 1:1 and 1:2) was then added dropwise in the dispersion to build a cross-linked DexMa-PAAm shell (**Scheme 1.25**). As determined by DLS, the size of the carriers was around 200 nm in cyclohexane whatever the DS of DexMa and significantly increased after redispersion in water especially when using DexMa with low DS (790±120, 610±90 and 390±65 nm with DS=0.05, 0.10 and 0.20 respectively) (**Table 1.6**, **entry 1**). The antimicrobial agent (2-2.5 wt% located in the aqueous core) was quantitatively released during the redispersion process.

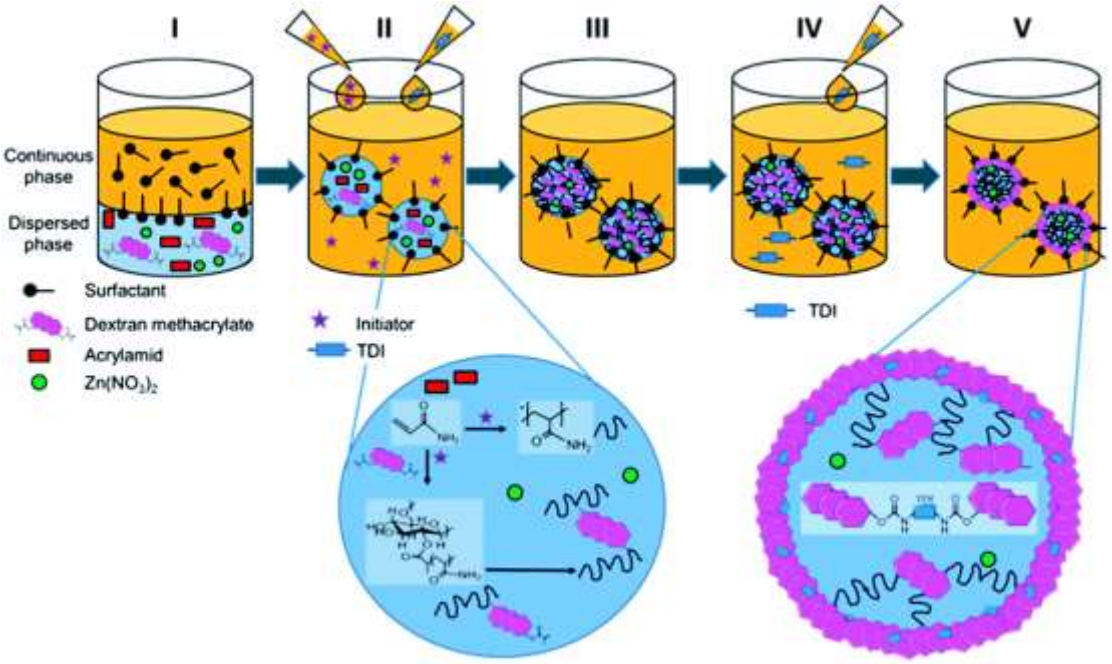

Scheme 1.25: Construction of dextran-based nanocapsules by miniemulsion process. The steps I–V depict the relevant steps to obtain nanogels with a TDI crosslinked dextran shell.

In 2006, J. Sheng and coworkers prepared dextrane-based nanocapsules by interfacial polymerization under emulsion conditions.[131] A chloroform-in-water

emulsion where methacrylated dextran (DdexMA, M_W~500 kg/mol, MMA grafting degree 7.7 wt%) or DdexMA together with chain-end methacrylated polylactide (PLAM, M_n=2100 g/mol) weight ratio 50/50 are respectively dissolved in water and chloroform, was initially formed under mechanical agitation in the presence of Triton X-100 (added in the aqueous phase at 2 mg/mL) as surfactant. The membrane was then formed by interfacial radical (co)polymerization of the macromonomer chains after addition of an initiator ($K_2S_2O_8$ /$NaHSO_3$), yielding DexMA or DdexMA/PLAM nanocapsules with diameters ~ 200 and 233 nm (**Table 1.6**, **entry 2**). Addition of ibuprofen in the organic phase before emulsification afforded the synthesis of ibuprofen-loaded nanocapsules (diameters ~ 200-250 nm, ibuprofen loading efficiency ~74%). The active was progressively released over time (13% and 83% of released molecules after 2h and 96h, respectively). In 2009, the same group prepared felodipine-loaded *N*-maleoylchitosan (NMCS)-based nanocapsules using a similar strategy (**Table 1.6**, **entry 3**)[132]. Felodipine and Triton X-100 in chloroform and *N*-maleoylchitosan macromonomer (NMCS) (Chitosan, 500 kg/mol, DS=0.23) in water were mixed to form O/W emulsion under mechanical agitation. After deoxygenating, the interfacial polymerization was initiated by addition of $K_2S_2O_8$ /$NaHSO_3$ aqueous solution at 40°C, generating NMCS nanocapsules. The size of the drug-free and drug-loaded nanocapsules (80% loading efficiency) were 159 nm and 251 nm, respectively. In order to investigate the effect of hydrophobicity on drug release behavior, drug-loaded NMCS with CS/MA weight ratio 1:0.5 (NMCS-1), 1:0.25 (NMCS-2) and 1:0.125 (NMCS-3) were prepared. A strong “burst effect” was observed for these systems. However, the amount of released drug eventually reached a plateau owing to the establishment of strong hydrophobic interactions of felodipine with the NMCS shell.

In 2010, W. Zhang et al. prepared Pluronic F127-chitosan nanocapsules using a modified emulsification/solvent evaporation method (**Figure 1.32**)[133]. *α, ω-*

carboxylic acid terminated Pluronic F127 (PEO_{100}-PPO_{65}-PEO_{100}, 12.6 kg/mol) and 1-ethyl-3-[3-dimethylaminopropyl]carbodiimide hydrochloride (EDC) were initially dissolved in dichloromethane. The resulting organic solution was added dropwise into a chitosan (2.5 $kg.mol^{-1}$) aqueous solution (pH 5) under sonication. Cross-linking of chitosan and Pluronic F127 through amidification was catalyzed by EDC. Note that nanocapsules were also formed without EDC (owing to the establishment physical cross-links through ionic interactions between the two polymers). Owing to the thermo-responsive of Pluronic F127, the size of resulting nanocapsules evolved from 37 nm at 37°C to 240 nm at 4°C. Consequently, nanocapsules were found to be highly permeable at low temperatures enabling their loading with molecules such as ethidium bromide and temperature-controlled release of the drug (triggered by heating). Loaded nanocapsules were found to be taken up by noncancerous and cancerous mammalian cells (C3H10T1/2 and MCF-7). Owing to their non-toxic nature and temperature-controlled wall-permeability, chitosan/Pluronic nanocapsules are promising candidates for drug delivery applications. (**Table 1.6**, **entry 4**).

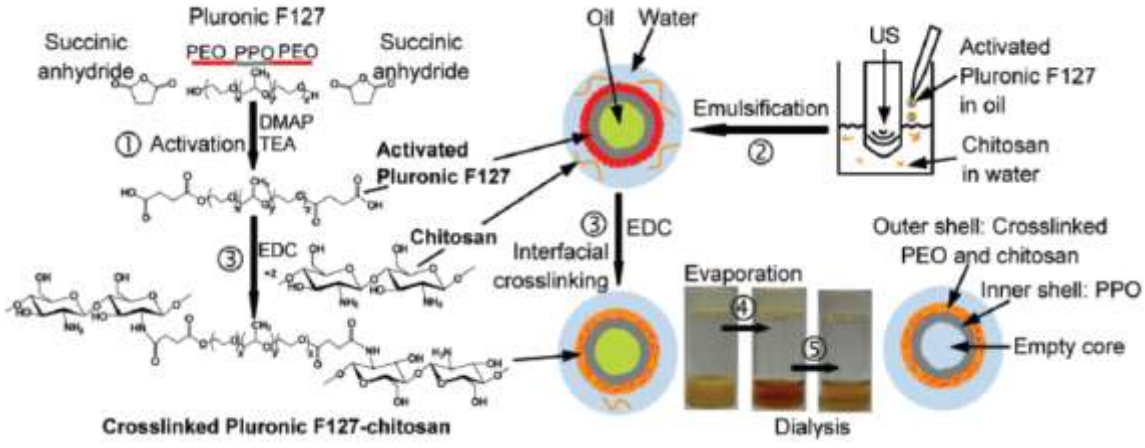

Figure 1.32: Route to Pluronic F127- chitosan nanocapsules.

In 2012, Roux *et al.* prepared glyconanocapsules through CuAAC interfacial polyaddition in mini-emulsion conditions (**Figure 1.33**, **table 1.6**, **entry 5**).[134] Typically, an oil-in-water mini-emulsion containing a water-soluble monomer, 6,6′-diazido-6,6′-dideoxysucrose (1), a miglyol soluble monomer,

bis(propargyloxy)butane (2), SDS as surfactant and water/miglyol (3/1, v/v) was formed by ultrasonication for 6 min at 25°C, presenting an average diameter of around 200 nm and PDI=0.107. The interfacial polyaddition was triggered upon addition of sodium ascorbate/$CuSO_4$ catalyst at 60°C, yielding 200 nm-glyconanocapsules with a miglyol core and a 20 nm thick glycopolytriazole shell (full conversion in 4h as monitored by ^{1}H NMR). The use of microwave irradiation spectacularly reduced the period of time required to attain full conversion of the monomers (98% in 30 min). The dispersions were colloidally stable for several months.

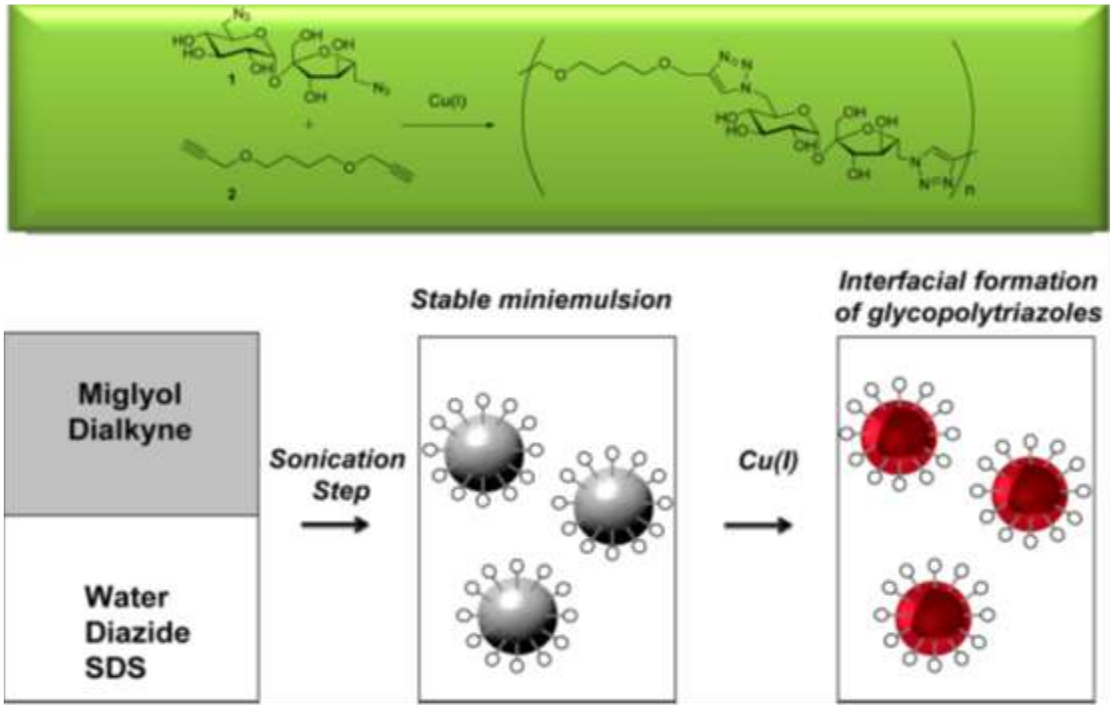

Figure 1.33: (Top) CuAAC Polyaddition of 1 and 2; (bottom) Glyconanocapsules generated from interfacial CuAAC polymerization.

Glyconanocapsules prepared by inverse mini-emulsion periphery RAFT polymerization method were reported by the group of Stenzel in 2015[135]. Poly(N-(2-hydroxypropyl methacrylamide) (PHPMA, Mn=5300 g/mol, *Đ*=1.12) macro-RAFT stabilizer was first synthesized by RAFT polymerization. A solution of PHPMA, pentafluorophenyl methacrylate (PFPMA, monomer), AIBN initiator and ethylene glycol dimethacrylate (EGDMA, permanent cross-linker)

or bis(2-methacryloyloxyethyl) disulfide (DSDMA, reducible cross-linker) in toluene, was mixed with water or a gemcitabine hydrochloride (GEM) solution and sonicated to form water-in-oil mini-emulsion. PFPMA RAFT polymerization was triggered by heating at 70°C, resulting in PHPMA-*b*-PPFPMA (M_n=16200 g/mol, *Đ*=1.18) shelled hollow nanocapsules (permanent shell SNP and reducible shell RNP, D_z=216 nm by DLS) or GEM-loaded nanocapsules (G-SNP and G-RNP, D_z =224 nm by DLS, encapsulation ~96% and loading ~12% efficiency). Further aminolysis of PFPMA group was performed by mixing of DMA and TEA dispersion of nanocapsules with Na_2CO_3 solution (pH 11) of D-(+)-glucosamine at 40°C under stirring, resulting in two series of glyconanocapsules (Glyco-SNP, 264 nm and Glyco-G-RNP, 290 nm) (**Figure 1.34**, **Table 1.6**, **entry 6**). In basic water (1 mg/mL, pH=11), the diffusion-controlled release of GEM was 17% within 48 h. Upon addition of glutathione, 84.5% of GEM was released in 2 h due to redox clivage of disulfide moieties between nods. Biologic tests with pancreatic cancer cell lines (AsPC-1) showed that the the hollow RNP and G-SNP capsules were not toxic. On the contrary, IC_{50} values were 270 and 136 nM for free GEM and G-RNP highlighting the higher toxicity of the loaded nanocapsules against the tumor cells.

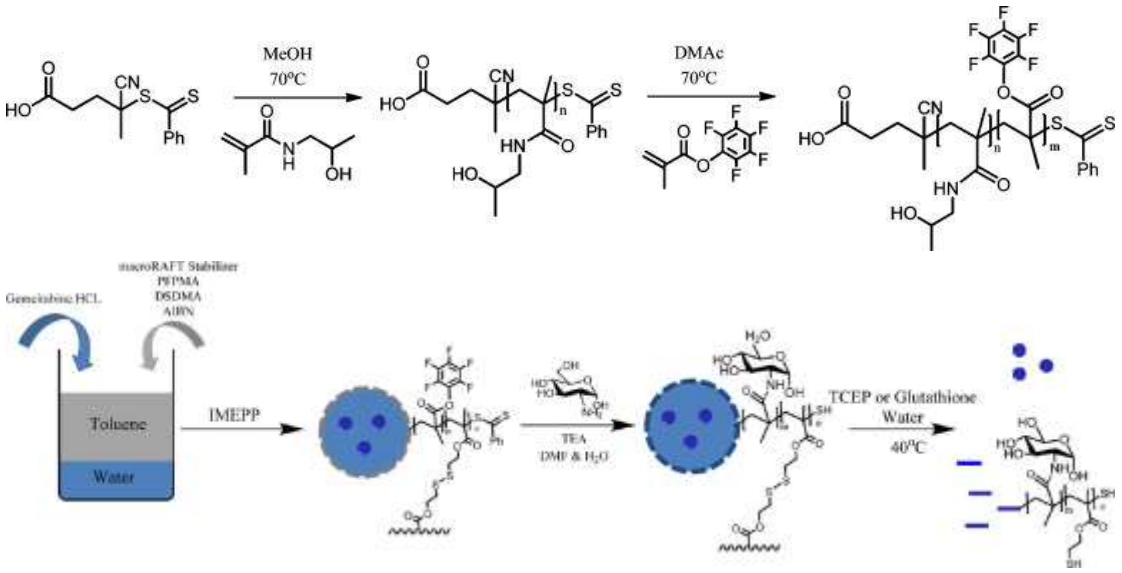

Figure 1.34: (Top) synthesis of PHPMA-b-PPFPMA by RAFT polymerization; (bottom) loaded glyconanocapsules having reducible shells.

Recently, Pitakchatwong and Chirachanchai prepared polysaccharide-based nanoparticles and nanocapsules with chitosan (CS, Mw=700 kDa, *pKa*~6.4) or alginate (AG, *pKa*~4) as constituents of the shell using pH shifting (**Figure 1.35**).[136] To build chitosan-based colloids, the authors initially prepared CS toluene/water miniemulsion by mixing toluene and an aqueous phase (pH 2-6 to ensure good solubility to CS) consisting of Tween 80 surfactant, hexadecane and glutaraldehyde (GA, cross-linker) and emulsification by ultrasonication for 4 min in an ice bath. Interestingly, different morphologies were generated depending on the pH of the initial aqueous phase. At pH=2 and 3, nanocapsules with a R_h ~35 nm were fabricated whereas nanoparticles with R_h of 40, 50 and 30-110 nm were obtained at pH=4, 5 and 6. Alginate-based sub-100nm nanocapsules were also prepared in a similar manner over a pH range of 5-9 (**Table 1.6**, **entry 7**).

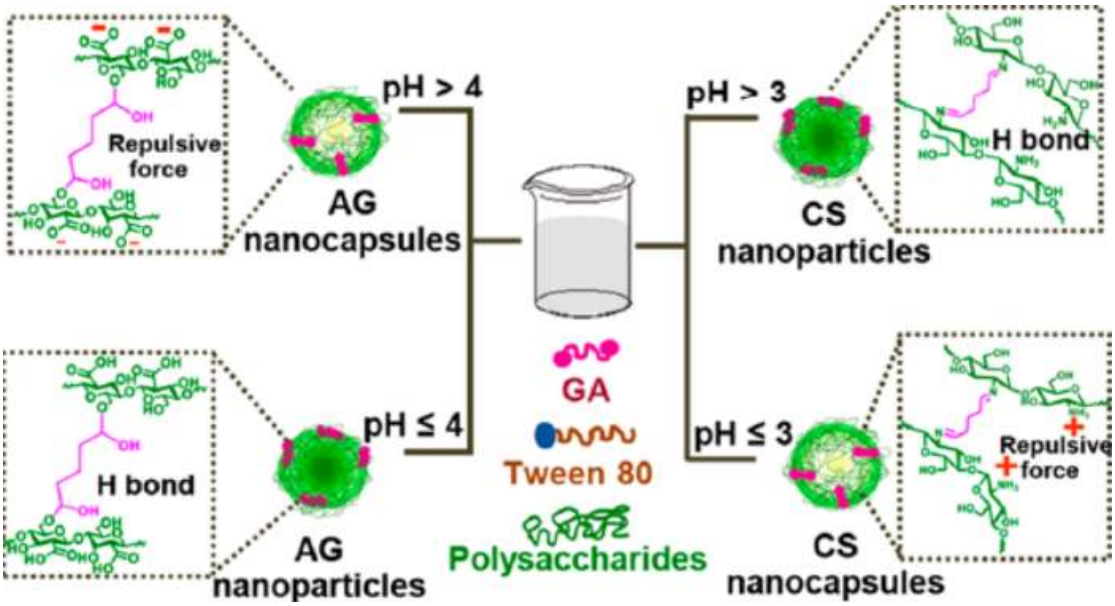

Figure 1.35: Pathway of pH variation for obtaining nanoparticle or nanocapsule polysaccharides.

1.2.3.2 Polymer coating technique

The generation of nanocapsules by the polymer-coating technique relies on the

deposition of polymer chains onto performed uncoated nanodroplets (at the oil/water interface) triggered by solvent evaporation.

In 2013, Li *et al.* prepared nanocapsules composed of bovine serum albumin-dextran (BSA-Dextran) conjugate shell and soybean oil core[137]. Typically, a BSA-Dextran conjugate was produced via a naturally occurring Maillard reaction between the *ε*-amino group in BSA and the reducing end (carbonyl group) of dextran chains (Mw~10 kDa). Toluene/soybean oil (1/1, v/v) containing sensitizor/annihilator (1:100 molar ratio) was added to the BSA-Dextran aqueous solution (10 % v) for emulsification and heating. After removal of toluene, nanocapsules were fabricated. The authors encapsulated different s/a couples in the nanocapsules, PtTPBP/BDP-G (D_h=116 nm, UCNC-G), PtTPBP/BDP-Y (D_h=95 nm, UCNC-Y) or PdOEP/DPA (D_h=93 nm, UCNC-B) to afford green, yellow or blue luminescent emissive nanocapsules. UCNC-G and UCNC-Y exhibited up conversion luminescence (UCL) emission (λ_{ex} = 635 nm) with quantum efficiencies of 1.7, 4.8 and 6.2%, respectively. The size of the nanocapsules displayed no significant change in pH range of 2-8 and pH 7.4 NaCl solution after 115 days of storage making these nano-objects promising for *in vivo* imaging applications (**Table 1.6**, **entry 8**).

Using a combination of emulsion-solvent evaporation process and interfacial CuAAC click reactions, Nouvel and co-workers prepared dextran-covered nanocapsules.[138] Practically, the organic phase containing dichloromethane (CH_2Cl_2), alkyne end-functionalized polylactide (*α*-alkyne PLA, Mn=4000 g/mol, *Đ*=1.1), and miglyol 810 (density=0.94 g/cm^3, viscosity=28 mPa·s, water content: 0.02 wt.%) was mixed with the aqueous phase containing derivatized dextran chains (precursor: Dextran T40, Mn=32 kg/mol, *Đ*=1.4) bearing 23 pendent azide groups per 100 glucose units (initial molar ratio Dex/PLA 0.334), acting both as stabilizer and reactant, to form an oil-in-water emulsion by

sonication. The addition of the copper salt ($CuSO_4$/ascorbic acid) catalyzed the interfacial CuAAC reaction between α-alkyne PLA and azide end-dextran under sonication. Optimization of the coupling reaction led to clicking yields around 70%. Finally, CH_2Cl_2 was evaporated at 37°C under stirring affording miglyol 810-loaded dextran-*graft*-PLA nanocapsules with a final Dex/PLA molar ratio ~ 0.240 (**Scheme 1.26**). The surface average diameter (D[3:2]) was 113，129，151 and 192 nm with initial Miglyol810 volume ratio 0, 5, 10 and 20%, respectively. Corresponding dextran surface coverage (Γexp) was 9.4±1.6, 5.7±0.2, 4.2±0.5 and 4.8±2.2. Thanks to covalent grafting of dextran on NPs surface, these values were much higher than the ones calculated for non clicked systems for which partial dextran desorption occurs during CH_2Cl_2 evaporation (**Table 1.6**, **entry 9**).

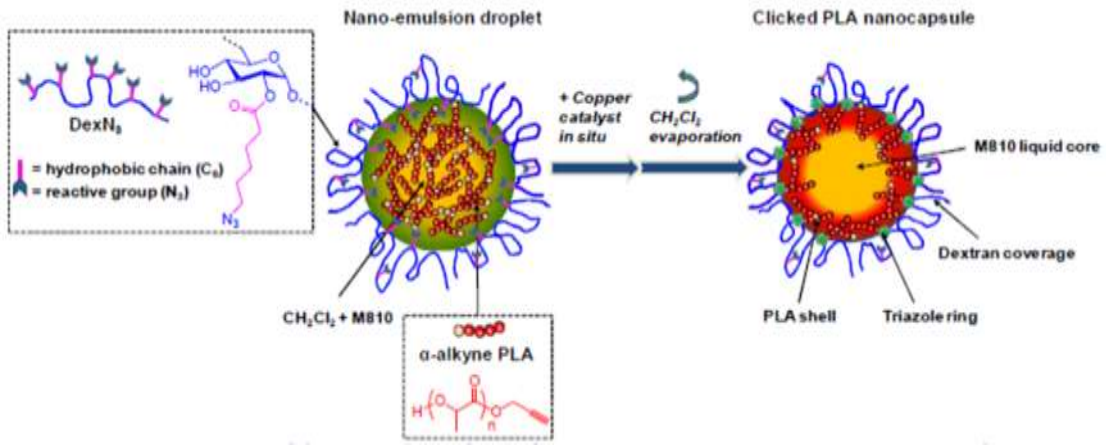

Scheme 1.26: preparation of miglyol-filled dex-*g*-PLA nanocapsules.

Table 1.6: Formation of glyconanocapsules using emulsification routes.

Entries	Interfacial reaction	Polymer	Monomer	Emulsion	Emulsion method	Cross-linker	Dimension (nm)	Ref.
1	Radical polymeriztion	DexMa-PAAm	acrylamide	water/cyclohexane	mechanical agitation	2,4-toluene dissocyanate	205±65	130
2	Reductive polymerization		PLAM	chloroform/water	mechanical agitation		233	131
3	Reductive polymerization		*N*-maleoylchitosan	chloroform/water	mechanical agitation		159	132
4	Cross-linking		Pluronic F127	dichloroform/water	mechanical agitation	chitosan	37/ 240	133
5	CuAAC polymerization		6,6′-diazido-6,6′-dideoxysucrose bis(propargyloxy)butane	water/miglyol	sonication		200	134
6	IMEPP Aminolysis	Poly(HPMA-*b*-Glucosamine)		water/toluene	sonification	PHPMA-*b*-PPFPMA	264	135
7	Cross-linking	Chitosan-glutaraldehyde		water/toluene	sonication	glutaraldehyde	35	136
8	Maillard reaction	Bovine serum albumin-dextran		water/soybean oil	sonication		116	137
9	CuAAC polymerization	Dextran-*g*-poly(lactide alkyne)		water/dichloromethane	sonication		150	138

1.2.3.3 Nanoprecipitation technique

The nanoprecipitation method, also called “solvent shifting process” or “ouzo effect” has recently emerged as a very simple and robust method to construct oil-filled nanocapsules in one step. This method primarily relies on the use of a hydrophobic solute (herein, an oil) dissolved into a polar organic solvent (usually ethanol, acetone, THF or DMSO) which is fully miscible with water. Upon addition of large amounts of water, the resulting solution abruptly becomes a non-solvent for hydrophobic molecules leading instantaneously to the supersaturation of the solute and the formation of nanometer-scale droplets with a narrow unimodal size distribution in the 50–300 nm range without using surfactant or any form of mechanical agitation. The resulting emulsions are metastable.[139] The establishment and overlapping of phase diagrams for acetone/water/oil and acetone/water/polymer ternary systems allow for identifying conditions of solvent shifting ensuring simultaneously the production of nanometer-scale droplets of oil in the Ouzo (or pre-Ouzo domain) and the adsorption of hydrophilic polymer chains at the interface (above the cloud point boundary of the polymer), see **Figure 1.36**.[140] Thus, starting from an aqueous phase containing a hydrophilic polymer and an organic phase incorporating a hydrophobic oil and proceeding to the solvent shifting in the green domain f given in Figure 1.36, it was anticipated that it would be possible to straightforwardly generate oil-filled nanocapsules.

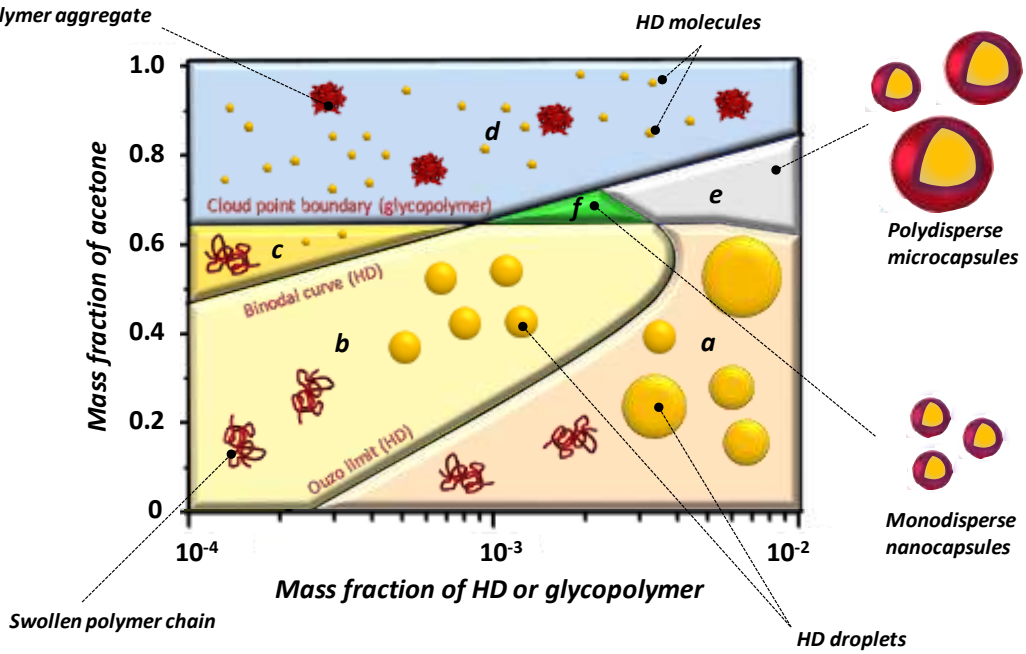

Figure 1.36: Overlapped phase diagrams of HD/water/acetone systerm and polymer/water/acetone system.

Based on these assumptions, our group investigated the preparation of a series of functional oil-filled glyconanocapsules using the nanoprecipitation technique. Poly(N-[7-(*α*-D-mannopyranosyloxy)-heptyl]methacrylamide) (PHMM, $M_{n,SEC}$ =24 kg/mol and 102 kg/mol, *Đ*<1.1) was first prepared by RAFT polymerization. A solution of acetone containing hexadecane (oil, 0.2 wt.%) and isophorone diisocyanate (IPDI, cross-linking agent) was mixed with a PHMM (0.1 wt.%) aqueous solution to work simultaneously in the Ouzo domain and above the cloud point boundary of PHMM (typically with acetone mass fraction ranging from 0.65 and 0.70). After brief shaking, glycopolymer coated hexadecane-filled nanocapsules were constructed in a simple and rapid one-pot procedure. By increasing the content of IPDI in the organic phase (1, 5, and 24 equivalents per polymer chain), the z-average diameter of the capsules gradually decreased from 248 nm, 200 nm to 150 nm with PDI 0.07, 0.12 and 0.07, respectively (**Table 1.7**, **entry 1**)[140]. To highlight the general character of this method, additional experiments were performed with another oil, Miglyol 812, a

non toxic and biocompatible triglyceride approved by the FDA, and another glycopolymer, poly(N-[7-(*α*-D-mannopyranosyloxy) ethyl] methacrylamide) (PEMM, $Mn,_{SEC}$=96 kg/mol, *Đ*=1.17). With these ingredients in hands, nanocapsules with a z-average diameter of 130 nm and a PDI ~ 0.04 were synthesized. Importantly, these nanocapsules could be loaded with fluorescent pyrene, and shell-decorated with biorelevant moieties or metallic nanoparticles such as AuNPs in one pot.

We subsequently adapted this methodology to generate nanocapsules loaded with Flumequine, a fluoroquinolone antibiotic agent, (z-average diameter of 117 nm in acetone/water mixture and 300 nm in water, **Table 1.7**, **entry 2**) using RAFT-made poly(N-[7-(*α*-D-mannopyranosyloxy) heptyl] methacrylamide)-co-poly(glycidyl methacrylate) random copolymer P(HMM_{206}-*stat*-GMA_{17}, $Mn,_{NMR}$=77.1 kg/mol, *Đ*=1.10).[141] The presence of pendant epoxy groups along the glycopolymer chains was exploited to decorate the membrane of the nanocapsules with fluorescent tags and magnetic nanoparticles through epoxy-amine reactions. Thanks to the very strong affinity of the pendent n-heptyl *α*-D-mannose residues for Fim H adhesin (located at the surface of *E. coli*), the glyconanocapsules efficiently agglutinated the bacteria and inhibited AIEC *E. coli.* bacterial adhesion to T84 cells.

In 2017, we reported that thermodynamically stable heterogeneities can be generated in the “monophasic” region of acetone/water/miglyol phase diagram (Surfactant-Free MicroEmulsion domain SFME, next to the Ouzo domain).[142] We showed that the dimensions of these aggregates (30 to 180 nm) can be precisely tuned by varying the acetone mass fraction (between 0.4 and 0.8). Finally, we transposed the Ouzo methodology *vide supra* to build size-controlled nanocapsules in the SFME region using poly(N-[2-(*α*-D-mannopyranosyloxy)ethyl]methacrylamide) (PEMM, $Mn,_{NMR}$=251 kg/mol, *Đ*=1.1, cloud point boundary: 0.40). Solvent shifting in the SFME domain at different acetone mass fraction (comprised of values between 0.40 and 0.80) afforded the preparation of nanocapsules with dimensions ranging from 47 nm

(at 0.40 acetone mass fraction) to 190 nm (at 0.8 acetone mass fraction) (**Table 1.7**, **entry 3**). Manipulation in the SFME domain offered the same attributes as in the Ouzo domain, that are shell functionalization and core loading with actives of interest. Incorporation of cystamine as a co-cross-linking agent (together with IPDI) conferred a redox-sensitivity to the resulting nanocapsules which degraded rapidly upon addition of dithiothreitol.

Finally, a series of of PHPMA-based nanocapsules were fabricated by nanoprecipitation in the Ouzo and SFME domain.[143] The cloud-point boundary (which can be depicted as a straight line at constant acetone/water ratio) were found at 0.85, 0.82, and 0.79 for $PHPMA_{259}$, $PHPMA_{322}$, and $PHPMA_{409,}$ respectively. Nanoprecipitation could only be performed in the SFME domain for PHPMA homoplymers producing HD filled nanocapsules with diameters of 195 nm, 187 nm, and 206 nm, respectively. The loading efficiency of camptothecin was 57%. To increase the "acetonophobic" character of the polymer chains, HPMA was RAFT copolymerized with a mannose-functionalized methacrylamide (EMM) resulting in P($HPMA_{302}$-*co*-EMM_{35}), P($HPMA_{258}$-*co*-EMM_{80}) and P($HPMA_{228}$-*co*-EMM_{109}). Incorporation of sugar residues within the chains induced a significant shift of the cloud point boundary (from 0.75 to 0.66 acetone mass fraction for P($HPMA_{302}$-*co*-EMM_{35}) and P($HPMA_{228}$-*co*-EMM_{109}) respectively) enabling the preparation of nanocapsules both in Ouzo and SFME domains for P($HPMA_{258}$-*co*-EMM_{80}) and P($HPMA_{228}$-*co*-EMM_{109}). In the SFME domain, nanocapsules with diameters around 150 nm and 91 nm were generated with P($HPMA_{258}$-*co*-EMM_{80}) ($W_{acetone}$=0.69) and P($HPMA_{228}$-*co*-EMM_{109}) ($W_{acetone}$=0.66) whereas nanocapsules of 350 nm in size were obtained in the Ouzo domain ($W_{acetone}$=0.66 or 0.69), see **Figure 1.37** and **Table1.7**, **entry 4**. Finally, the preparation of pH-responsive PHPMA-based nanocapsules was investigated. Using P($HPMA_{286}$-*co*-$DEMA_{32}$), P($HPMA_{261}$-*co*-$DEMA_{83}$), and P($HPMA_{223}$-*co*-$DEMA_{105}$) copolymers (cloud point boundary around 0.8), nanocapsules with a hydrodynamic diameter ~ 190 nm were

prepared in the SFME domain at pH 9 or 10. Meanwhile, P(HPMA$_{230}$-*co*-EMM$_{102}$-*co*-DEMA$_{44}$), a terpolymer exhibiting a cloud point boundary around 0.65, gave rise to the generation of nanocapsules at pH 10 both in SFME and OUZO domains (diameters ~ 70 nm and 320 nm, respectively).

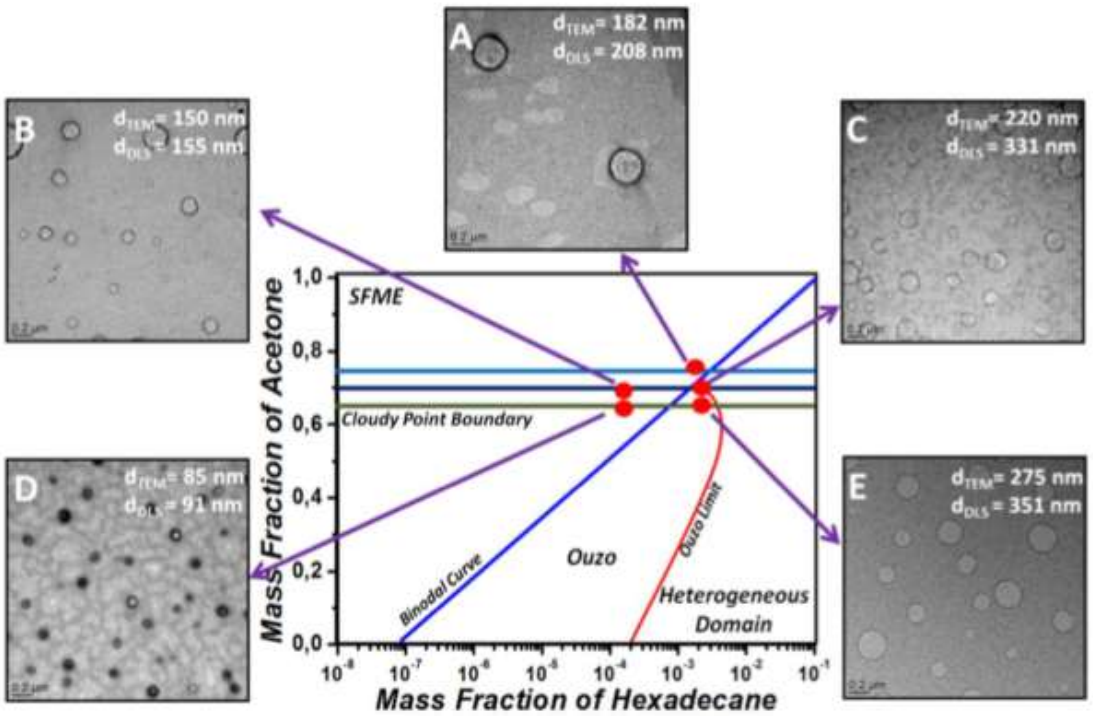

Figure 1.37: (Center) Overlapped phase diagrams of P(HPMA-*co*-EMM) copolymers and HD. TEM images of P(HPMA$_{302}$-*co*-EMM$_{35}$)-based naocapsules built in the SFME domain (A), of P(HPMA$_{258}$-*co*-EMM$_{80}$)-based naocapsules built in the SFME (B) and Ouzo (C) domains and of P(HMPA$_{228}$-*co*-EMM$_{109}$)-based naocapsules built in the SFME (D) and Ouzo (E) domains. Horizontal lines in the phase diagrams correspond to the cloud-point boundaries of P(HPMA$_{302}$-*co*-EMM$_{35}$) (light blue line), P(HPMA$_{258}$-*co*-EMM$_{80}$) (dark blue line) and P(HPMA$_{228}$-*co*-EMM$_{109}$) (dark green line).

Table 1.7: Glyconanocapsules generated by nanoprecipitation method.

Entries	Nanodroplet	Polymer	Emulsion	Emulsion method	Cross-linker	Dimension (nm)	Ref.
1	Hexadecane	poly(N-[7-(α-D-mannopyranosyloxy)-heptyl]methacrylamide)	Water/acetone	Shaking	isophorone diisocyanate	150	140
2	Miglyol 812	poly(N-[7-(α-D-mannopyranosyloxy) heptyl] methacrylamide)-*co*-poly(glycidyl methacrylate)	Water/acetone	Shaking	isophorone diisocyanate	117	141
3	Miglyol 812	poly(N-[2-(a-*D*-mannopyranosyloxy)ethyl] methacrylamide)	Water/acetone	Shaking	isophorone diisocyanate	190	142
4	Hexadecane	Poly(N-(2-hydroxypropyl) methacrylamide-co- N-[2-(a-*D*-mannopyranosyloxy)ethyl]methacrylamide)	Water/acetone	Shaking	isophorone diisocyanate	155	143

1.2.3.4 Other emulsification techniques

Polymeric nanocapsules can be generated by other emulsification techniques such as double emulsification, that is to say, Water-Oil-Water (W/O/W) and Oil-Water-Oil (O/W/O) emulsions. By combining a double emulsification process (O/W/O) with ionic and covalent crosslinking procedures, the group of Lionte prepared chitosan/gelatin based nanocapsules entrapping bioactive L-phenylalanine derivatives.[144] An O/W emulsion was first generated by mixing an acetic acid solution (containing 0.5% w/v of CS/Gel 1/1 w/w and 2% w/v of Tween 80) and toluene (containing 2% w/v of Span 80). Next, this O/W emulsion was added dropwise to a solution of toluene (containing 2% w/v of Span 80) to generate an $O_1/W/O_2$ double emulsion with a volume ratio of 1/3/17. A sodium sulphate aqueous solution and a glutaraldehyde-saturated solution of toluene were then sequentially added to the emulsion to ensure double cross-linking of the polymers. Entrapment of the L-phenylalanine derivatives was performed in the first emulsification by direct addition of a solution of DMSO containing the drugs (70 mg in 4mL) into the toluene phase. The resulting nanocapsules, whose diameters ranged from 100 to 700 nm as given by TEM analyses, were proven to exhibit enhanced antitumoral activity.

Using W/O/W emulsions, Wu et.al prepared insulin-loaded chitosan/alginate nanocapsules (488 nm from TEM) for oral delivery and observed good insulin intestinal absorption *in vivo*.[145]

Note that the preparation of nanocapsules has also been reported by emulsion coacervation technique using alginate[146,147] and chitosan-alginate mixtures.[148,149] To our knowledge, the generation of nanocapsules through emulsion coacervation technique from synthetic glycopolymers has not been explored yet.

1.3 Conclusion

In the quest for smart and sophisticated nano-objects, glycopolymers and glyconanocapsules are emerging as an important class of materials for a number of applications in life science. In this chapter, we have described the main chemical or physical routes towards the preparation of nanoscale encapsulation systems decorated with sugar residues. We showed that a myriad of nanocapsules can notably be prepared through block copolymer self-assembly, template strategies or emulsification techniques. However, as highlighted in this chapter, with the exception of few examples based on emulsification techniques, the preparation of glyconanocapsules is often tedious making the development of robust and straightforward methods to size-controlled glyconanocapsules remains particularly appealing. In this context, the objectives of this PhD work will consist in consolidating the foundations of the nanoprecipitation technique described by our group and extending it to new families of polymers, poly(vinyl esters)/poly(vinyl alcohols and poly(oxazoline)s.

1.4 Reference

1. D. Quintanar-Guerrero, E. Allemann, H. Fessi, and E. Doelker, *Drug Dev. Ind. Pharm.*, **1998**, 24, 1113-1128.
2. C. E. Mora-Huertas, H. Fessi, and A. Elaissari, *Int. J. Pharm.*, **2010**, 385, 113-142.
3. J. Rodriguez-Hernandez, F. Checot, Y. Gnanou, and S. Lecommandoux, *Prog. Polym. Sci.,* **2005**, 30, 691-724.
4. D. Yu, T. Fukuda, Tuoya , S. Kuroda, K. Tanizawa, A. Kondo, M. Ueda, T. Yamada, H. Tada and M. Seno, *IUBMB Life*, **2006**, 58, 1-6.
5. X. H. Dai, Z. M. Wang, W. Liu, C. M. Dong, J. M. Pan, S. S. Yuan, S. Yan, D. M. Liu, L. Sun, *Colloid Polym Sci*, **2014**, 292, 2111-2122.
6. A.Takasu, T. Houjyou, Y. Inai, and T. Hirabayashi, *Biomacromolecules*, **2002**, 3, 775-782.
7. A. Blanazs, S. P. Armes, and A. J. Ryan, *Macromol. Rapid Commun*., **2009**, 30, 267–277.
8. Z. C. Li, Y. Z. Liang and F. M. Li. *Chem. Commun.*, **1999**, 1557-1558.
9. Y. Z. Liang, Z. C. Li and F. M. Li. *New J. Chem.*, **2000**, 24, 323-328.
10. Z. C. Li, Y. Z. Liang, G. Q. Chen and F. M. Li. *Macromol. Rapid Commun*, **2000**, 21, 375-380.
11. C. M. Dong, X. L. Sun, K. M. Faucher, R. P. Apkarian, and E. L. Chaikof, *Biomacromolecules*, **2004**, 5, 224-231.
12. C. M. Dong, and E. L. Chaikof, *Colloid Polym Sci.*, **2005**, 283, 1366-1370.
13. W. Zhou, X. H. Dai, and C. M. Dong, *Macromol. Biosci.*, **2008**, 8, 268-278.
14. X. H. Dai, and C. M. Dong, *J. Polym. Sci., Part A: Polym.Chem.,* **2008**, 46, 817–829.
15. X. H. Dai, H. D. Zhang, C. M. Dong. *Polymer*, **2009**, 50, 4626-4634.
16. X. H. Dai, C. M. Dong, and D. Yan. *J. Phys. Chem. B,* **2008**, 112*,* 3644-3652.
17. G. Pasparakis and C. Alexander, *Angew. Chem.,* **2008**, 120, 4925 –4928.
18. K. Aissou, A. Pfaff, C. Giacomelli, C. Travelet, A. H. E. Muller, R. Borsali. *Macromol. Rapid Commun*., **2011**, 32, 912-916.
19. L. Albertin, A. Wolnik, A. Ghadban, F. Dubreuil. *Macromol. Chem. Phys.,* **2012**, 213,

1768-1782.

20. S. Menon and S. Das, *Polym. Chem.*, **2012**, 3, 2619-2624.
21. S. Menon, R. M. Ongungal and S. Das, *Polym. Chem.*, **2013**, 4, 623-628.
22. L. Su, Y. Zhao, G. Chen, and M. Jiang, *Polym. Chem.*, **2012**, 3, 1560-1566.
23. L, Su, C. Wang, F. Polzer, Y. Lu, G. Chen, and Ming Jiang, *ACS Macro Lett.,* **2014**, 3, 534−539.
24. X. Wu, L. Su, G. Chen, and M. Jiang. *Macromolecules*, **2015**, 48, 3705–3712.
25. W. Qi, Y. Zhang, J. Wang, G. Tao, L. Wu, Z. Kochovski, H. Gao, G. Chen, and M. Jiang, *J Am Chem Soc.,* **2018**,140, 8851-8857.
26. D. Pei, Y. Li, Q. Huang, Q. Ren, F. Li, T. Shi. *Colloids Surf., B: Biointerfaces,* **2015**, 127, 130–136.
27. Y. Xiao, H. Sun, and J. Du, *J. Am. Chem. Soc.,* **2017**, 139, 7640−7647.
28. J. Zhao and M. H. Stenzel, *ACS Symp. Ser.*, **2015**, 1188, 91-105.
29. J. Quan, F-W. Shen, H. Cai, Y-N. Zhang, and H. Wu, *Langmuir*, **2018**, 34, 10721-10731.
30. W. Wan, C. Hong, C. Pan, *Chem. Commun.,* **2009**, 39, 5883–5885.
31. G. Delaittre, C. Dire, J. Rieger, J-L. Putaux, B. Charleux, *Chem. Commun.,* **2009,** 20, 2887–2889.
32. V. Ladmiral, M. Semsarilar, I. Canton, and S. P. Armes, *J. Am. Chem. Soc.,* **2013**, 135, 13574−13581.
33. B. Charleux, G. Delaittre, J. Rieger F. D'Agosto, *Macromolecules*, **2012**, 45, 6753-6765.
34. K. Ferji, P. Venturini, F. Cleymand, C. Chassenieux and J-L. Six, *Polym. Chem.*, **2018**, 9, 2868–2872.
35. X. Yan, V. La Padula, S. Favre-Bonte, J. Bernard, *Eur. Polym. J.,* **2019**,112, 170–175.
36. L. You and H. Schlaad, *J. Am. Chem. Soc.,* **2006**, 128, 13336-13337.
37. Z. Hordyjewicz-Baran, L. You, B. Smarsly, R. Sigel, and H. Schlaad, *Macromolecules,* **2007**, 40, 3901-3903.
38. H. Schlaad, L. You, R. Sigel, B. Smarsly, M. Heydenreich, A. Mantion and A. Masic. *Chem. Commun.*, **2009**, 1478–1480.

39. A. Gress, B. Smarsly, and H. Schlaad. *Macromol. Rapid Commun*., **2008**, 29, 304-308.
40. I. Otsuka, K. Fuchise, S. Halila, S. Fort, K. Aissou, I. Pignot-Paintrand, Y. Chen, A. Narumi, T. Kakuchi, and R. Borsali, *Langmuir*, **2010**, 26, 2325–2332.
41. Y. Chen, P. Espeel, S. Reinicke, F. E. D. Prez, M. H. Stenzel. *Macromol. Rapid Commun.,* **2014***,* 35*,* 1128−1134.
42. R. Wang, N. Xu, F-S. Du and Z-C, Li, *Chem. Commun.,* **2010**, 46, 3902–3904.
43. J. Huang, C. Bonduelle, J. Thévenot, S. Lecommandoux, and A. Heise. *J. Am. Chem.Soc.,* **2012**, 134, 119−122.
44. J. R. Kramer, A. R. Rodriguez, U-J. Choe, D. T. Kamei and T. J. Deming. *Soft Matter*, **2013**, 9, 3389-3395.
45. Y-C. Huang, M. Arham, J-S. Jan. *Eur. Polym. J.*, **2013**, 49, 726–737.
46. D. Pati, A. Y. Shaikh, S. Das, P. K. Nareddy, M. J. Swamy, S. Hotha, and S. S. Gupta, *Biomacromolecules,* **2012**, 13, 1287–1295.
47. D. Pati, S. Das, N. G. Patil, N. A. Parekh, D. H. Anjum, V. Dhaware, A. V Ambade, and S. S. S. Gupta, *Biomacromolecules*, **2016**, 17, 466–475.
48. B. J. Ravoo and R. Darcy, *Angew. Chem. Int. Ed.,* **2000**, 39, 4324-4326.
49. P. Falvey, C. W. Lim, R. Darcy, T. Revermann, U. Karst, M. Giesbers, A. T. M. Marcelis, A. Lazar, A. W. Coleman, D. N. Reinhoudt, and B. J. Ravoo, *Chem. Eur. J.*, **2005**, 11, 1171-1180.
50. J. Voskuhl, M. C. A. Stuart, and B. J. Ravoo, *Chem. Eur. J.,* **2010**, 16, 2790–2796.
51. U. Kauscher and B. J. Ravoo, *Beilstein J. Org. Chem.,* **2012**, 8, 1543–1551.
52. S. K. M. Nalluri and B. J. Ravoo, *Angew. Chem. Int. Ed.,* **2010**, 49, 5371–5374.
53. S. K. M. Nalluri, J. Voskuhl, J. B. Bultema, E. J. Boekema and B. J. Ravoo, *Angew. Chem. Int. Ed*., **2011**, 50, 9747–9751.
54. A. Samanta, M. C. A. Stuart and B. J. Ravoo, *J. Am. Chem. Soc.*, **2012**, 134, 19909–19914.
55. L. Stricker, E-C. Fritz, M. Peterlechner, N. L. Doltsinis§ and B. J. Ravoo, *J. Am. Chem. Soc.*, **2016**, 138, 4547-4554.
56. A. Samanta, M. Tesch, U. Keller, J. Klingauf, A. Studer, and B. J. Ravoo, *J. Am. Chem. Soc.,* **2015**, 137, 1967-1971.

57. W. C. Vries, D. Grill, M. Tesch, A. Ricker, H. Nüsse, J. Klingauf, A. Studer, V. Gerke and B. J. Ravoo, *Angew. Chem. Int. Ed.,* **2017**, 56, 9603-9607.
58. D. A. Uhlenheuer, D. Wasserberg, C. Haase, H. D. Nguyen, J. H. Schenkel, J. Huskens, B. J. Ravoo, P. Jonkheijm, and L. Brunsveld, *Chem. Eur. J.*, **2012**, 18, 6788-6794.
59. B-S. Kim, W-Y. Yang, J-H. Ryu, Y-S. Yoo and M. Lee, *Chem. Commun.,* **2005**, 2035–2037.
60. B-S. Kim, D-J. Hong, J. Bae, and M. Lee, *JACS,* **2005**, 127, 16333-16337.
61. C. Houga, J-F. Le Meins, R. Borsali, D. Taton and Y. Gnanou, *Chem. Commun.,* **2007**, 3063–3065.
62. C. Houga, J. Giermanska, S. Lecommandoux, R. Borsali, D. Taton, Y. Gnanou and J-F. Le Meins, *Biomacromolecules,* **2009**, 10*,* 32–40.
63. C. Schatz, S. Louguet, J-F. Le Meins and S. Lecommandoux, Angew. *Chem. Int. Ed.,* **2009**, 48, 2572–2575.
64. Y. Tan, K. Xu, Y. Li, S. Sun and P. Wang, *Chem. Commun.,* **2010**, 46, 4523–4525.
65. L. Long, X. Yuan, J. Chang, Z. Zhang, M. Gu, T. Song, Y. Xing, X. Yuan, S. Jiang and J. Sheng, *Carbohydr. Polym.,* **2012**, 87, 2630– 2637.
66. R. Szilluweit, T. N. Hoheisel, M. Fritzsche, B. Ketterer, A. F. i Morral, D. Demurtas, V. Laporte, R. Verel, S. Bolisetty, R. Mezzenga, and H. Frauenrath, *Nano Lett.*, **2012**, 12, 2573−2578.
67. K. Ferji, C. Nouvel, J. Babin, M-H. Li, C. Gaillard, E. Nicol, C. Chassenieux and J-L. Six, *ACS Macro Lett.,* **2015**, 4, 1119−1122.
68. S. M. Brosnan, H. Schlaad and M. Antonietti, *Angew. Chem. Int. Ed.,* **2015**, 54, 9715 –9718.
69. J. Willersinn, A. Bogomolova, M. B. Cabre and B. V. K. J. Schmidt, *Polym. Chem.*, **2017**, 8, 1244-1254.
70. T. Nishimura, Y. Sasaki and K. Akiyoshi, *Adv. Mater.,* **2017**, 29, 1702406-1702413.
71. T. Nishimura, Y. Sasaki, and K. Akiyoshi, *Rapid Commun.,* **2018**, 1800384-1800389.
72. W. B. Turnbull and J. F. Stoddart, *Rev. Mol. Biotechnol*, **2002**, 90, 231-255.
73. Q. Xiao, S. Zhang, Z. Wang, S. E. Sherman, R-O. Moussodia, M. Peterca, A. Muncan,

D. R. Williams, D. A. Hammer, S. Vertesy, S. Andre, H-J. Gabius, M. L. Klein, and V. Percec, *PANS*, **2016**, 113,1162–1167.

74. V. Percec, P. Leowanawat, H-J. Sun, O. Kulikov, C. D. Nusbaum, T. M. Tran, A. Bertin, D. A. Wilson, M. Peterca, S. Zhang, N. P. Kamat, K. Vargo, D. Moock, E. D. Johnston, D. A. Hammer, D. J. Pochan, Y. Chen, Y. M. Chabre, T. C. Shiao, M. Bergeron-Brlek, S. Andre, R. Roy, H-J. Gabius, and P. A. Heiney, *J. Am. Chem. Soc.*, **2013**, 135, 9055−9077.
75. S. Zhang, R-O. Moussodia, H-J. Sun, P. Leowanawat, A. Muncan, C. D. Nusbaum, K. M. Chelling, P. A. Heiney, M. L. Klein, S. Andre, R. Roy, H-J. Gabius, and V. Percec, *Angew. Chem*. **2014**, 126, 1– 6.
76. S. Zhang, R-O. Moussodia, C. Murzeau, H-J. Sun, M. L. Klein, S. Vertesy, S. Andre, R. Roy, H-J. Gabius and V. Percec, *Angew. Chem.,* **2015**, 127, 4108 –4112.
77. S. Zhang, Q. Xiao, S. E. Sherman, A. Muncan, A. D. M. R. Vicente, Z. Wang, D. A. Hammer, D. Williams, Y. Chen, D. J. Pochan, S. Vertesy, S. Andre, M. L. Klein, H-J. Gabius and V. Percec, *J. Am. Chem. Soc.*, **2015**, 137, 13334–13344.
78. Q. Xiao, S. S. Yadavalli, S. Zhang, S. E. Shermana, E. Fiorina, L. da Silva, D. A. Wilson, D. A. Hammer, S. Andre, H-J. Gabius, M. L. Klein, M. Goulian and V. Percec, *PANS*, **2016**, 113, 1162–1167.
79. Q. Xiao, S. S. Yadavalli, S. Zhang, S. E. Sherman, E. Fiorin, L. da Silva, D. A. Wilson, D. A. Hammer, S. André, H-J. Gabius, M. L. Klein, M. Goulian, and V. Percec, *PANS*, **2016**, 113, 1134–1141.
80. J. F. Trant, N. Jain, D. M. Mazzuca, J. T. McIntosh, B. Fan, S. M. M. Haeryfar, S. Lecommandoux and E. R. Gillies, *Nanoscale*, **2016**, 8, 17694-17704.
81. F-Z. Lu, J-Q. Meng, F-S. Du, Z-C. Li, B-Y. Zhang, *Macromol. Chem. Phys.,* **2005**, 206, 513–520.
82. S. R. S. Ting, A. M. Gregory and M. H. Stenzel, *Biomacromolecules,* **2009**, 10, 342–352.
83. H. Yang, C. Zhang, C. Li, Y. Liu, Y. An, R. Ma and L. Shi, *Biomacromolecules,* **2015**, 16, 1372−1381.
84. K. M. Zepon, I. Otsuka, C. Bouilhac, E. C. Muniz, V. Soldi, R. Borsali, *Langmuir,* **2016**,

32, 4538-4545.

85. R. K. Iler, *J. Colloid Interface Sci.*, **1988**, 21, 569-594.
86. G. Decher, J. D. Hong and J. Schmitt, *Thin Solid Films*, **1992**, 210, 831-835.
87. G. Decher and J. Schmitt, *Trend in Colloid and Interface Science VI*, **2007**, 160-164.
88. L. Pastorino, E. Dellacasa, M. H. Dabiri, D. Fabiano and S. Erokhina, *BioNanoScience*, **2016**, 6, 496-501.
89. S. Chinnayelka and M. J. McShane, *Journal of Fluorescence*, **2004**, 14, 585-595.
90. Z. Poon, J. B. Lee, S. W. Morton and P. T. Hammond, *Nano Lett.,* **2011**, 11, 2096–2103.
91. S. W. Morton, Z. Poon and P. T. Hammond, *Biomaterials*, **2013**, 34, 5328-5335.
92. S. Correa, K. Y. Choi, E. C. Dreaden, K. Renggli, A. Shi, L. Gu, K. E. Shopsowitz, M. A. Quadir, E. Ben-Akiva and P. T. Hammond, *Adv. Funct. Mater.,* **2016**, 26, 991–1003.
93. S. Shu, X. Zhang, Z. Wu, Z. Wang and C. Li, *Biomaterials*, **2010**, 31, 6039-6049.
94. W. J. Liu, G. H. Chen, G. H. He, Z. C. He and Z. Qian, *J. Mater. Sci.*, **2011**, 46, 6758-6765.
95. T. Klemetsrud, H. Jonassen, M. Hiorth, A. L. Kjoniksen and G. Smistad, *Colloids Surf., B: Biointerfaces*, **2013**, 103, 158-165.
96. B. T. Kren, G.M. Unger, L. Sjeklocha, A. A. Trossen, V. Korman, B. M. Dietheim-Okita, M. T. Reding and C.J. Steer, *J. Clin. Investig.*, **2009**, 119, 2086-2099.
97. Q. Wu, Z. C. Chen, D. S. Lu, X. F. Lin, M*acromol. Biosci.,* **2006**, 6, 78-83.
98. T. Taniguchi, Y. Kunisada, M. Shinohara, M. Kasuya, T. Ogawa, M. Kohri, T. Nakahira, *Colloids Surf., A: Physicochem. Eng. Aspects*, **2010**, 369, 240–245.
99. L. Bui, S. Abbou, E. Ibarboure, N. Guidolin, C. Staedel, J-J. Toulme, S. Lecommandoux and C. Schatz, *J. Am. Chem. Soc.,* **2012**, 134, 20189−20196.
100. H. Guo, Q. Guo, T. Chu, X. Zhang, Z. Wu and D. Yu, *J Mater Sci: Mater Med*, **2014**, 25, 121–129.
101. D. Shi, M. Ran, L. Zhang, H. Huang, X. Li, M. Chen and M. Akashi, *ACS Appl. Mater. Interfaces*, **2016**, 8, 13688–13697.
102. M. X. Chen, B. K. Li, D. K. Yin, J. Liang, S. S. Li and D. Y. Peng, *carbohydr polym.*, **2014**, 111, 298-304.

103. S. Pistone, M. Rykke, G. Smistad, M. Hiorth, *Int. J. Pharm.,* **2017**, 516, 106-115.

104. T. Caon, L. C. Porto, A. Granada, M. P. Tagliari, M. A. S. Silva, C. M. O. Simoes, R. Borsali and V. Soldi, *Eur. J. Pharm. Sci.*, **2014**, 52, 165-172.

105. S. Alavi, A. Haeri and S. Dadashzadeh, *carbohydr. polym.*, **2017**, 157, 991-1012.

106. K. K. Yang, M. Kong, Y. N. Wei, Y. Liu, X. J. Cheng, J. Li, H. J. Park and X. G. Chen, *J. Mater. Sci.*, **2013**, 48, 1717–1728.

107. T. Klemetsrud, H. Jonassen, M. Hiorth, A-L. Kjøniksen and G. Smistad, *Colloids Surf. B.,* **2013,** 103, 158–165.

108. J. Chen, H-N. Son, J. Hill, S. Srinivasan, F-Y. Su, P. S. Stayton, A. J. Convertine and D. M. Ratner, *Nanomedicine*, **2016**, 12, 2031-2041.

109. L. Ge, J. Zhu, F. Xiong and B. Ni, *JPP*, **2007**, 59, 661–667.

110. C. Zhang, G. Qua, Y. Sun, T. Yang, Z. Yao, W. Shen, Z. Shen, Q. Ding., H. Zhoud and Q. Ping, *Eur J Pharm Sci.,* **2008**, 33, 415–423.

111. G. Qu, X. Wu, L. Yin and C. Zhang, *Biomed. Pharmacother.,* **2012**, 66, 46–51.

112. J. Deng, Z. Zhang, C. Liu, L. Yin, J. Zhou and H. Lv, *J. Pharm. Pharmacol.*, **2015**, 67, 1363–1370.

113. F. Yu, C. He, A. Y. Waddad, W. L. L. Munyendo, H. Lv, J. Zhou and Q. Zhang, *Drug Dev Ind Pharm*., **2014**, 40, 774–782.

114. K. Kozhikhova, M. Ivantsova, M. Tokareva, I. Shulepov, A. Tretiyakov, L. Shaidarov, V. Rusinov and M. Mironov, *Pharm. Dev. Technol.*, **2016**, 23, 334-342.

115. R. Li, L. Deng, Z. Cai, S. Zhang, K. Wang, L. Li, S. Ding and C. Zhou, *Mater. Sci. Eng. C.*, **2017**, 80, 156–164.

116. M. Miyazaki, E. Yuba, H. Hayashi, A. Harada and K. Kono, *Bioconjug Chem.*, **2018**, 29, 44–55.

117. A. Nazemi, S. M. M. Haeryfar and E. R. Gillies, *Langmuir*, **2013**, 29, 6420–6428.

118. R. Ccorahua, S. Moreno, H. Gumz, K. Sahre, B. Voit and D. Appelhans, *RSC Adv.*, **2018**, 8, 25436–25443.

119. F. Tiarks, K. Landfester and M. Antonietti, *Langmuir*, **2001**, 17, 908-918.

120. E. Marie, K. Landfester and M. Antonietti, *Biomacromolecules*, **2002**, 3, 475-481.

121. G. Baier, D. Baumann, J. M. Siebert, A. Musyanovych, V. Mailänder, and K.

Landfester, *Biomacromolecules,* **2012**, 13, 2704−2715.

122. G. Baier, A. Musyanovych, M. Dass, S. Theisinger and K. Landfester, B*iomacromolecules,* **2010**, 11, 960–968.
123. H. Freichels, M. Wagner, P. Okwieka, R. G. Meyer, V. Mailander, K. Landfester and A. Musyanovych, *J. Mater. Chem. B*, **2013**, 1, 4338–4348.
124. G. Baier, A. Cavallaro, K. Vasilev, V. Mailander, A. Musyanovych and K. Landfester, *Biomacromolecules*, **2013**, 14, 1103−1112.
125. S. U. Frick, M. P. Domogalla, G. Baier, F. R. Wurm, V. Mailander, K. Landfester and K. Steinbrink, *ACS Nano*., **2016**, 10, 9216−9226.
126. A. J. Svagan, A. Musyanovych, M. Kappl, M. Bernhardt, G. Glasser, C. Wohnhaas, L. A. Berglund, J. Risbo and K. Landfester, *Biomacromolecules,* **2014**, 15, 1852−1859.
127. K. Malzahn, F. Marsico, K. Koynov, K. Landfester, C. K. Weiss and F. R. Wurm, *ACS Macro Lett*., **2014**, 3, 40−43.
128. N. Jagielski, S. Sharma, V. Hombach, V. Mailander, V. Rasche and K. Landfester, *Macromol. Chem. Phys.,* **2007**, 208, 2229–2241.
129. C. Pitakchatwong, I. Schlegel, K. Landfester, D. Crespy and S. Chirachanchai, *Part. Part. Syst. Charact.,* **2018**, 35, 180086.
130. K. Malzahn, W. D. Jamieson, M. Droge, V. Mailander, A. T. A. Jenkins, C. K. Weiss and K. Landfester, *J. Mater. Chem. B,* **2014**, 2, 2175-2183.
131. B. Jiang, L. Hu, C. Gao and J. Shen, *Acta Biomater.,* **2006**, 2, 9–18.
132. A. Zhu, Y. Pan, S. Dai, F. Li, and J. Shen, *Biomacromolecules,* **2009**, 10, 1997–2002.
133. W. Zhang, K. Gilstrap, L. Wu, R. Bahadur K. C., M. A. Moss, Q. Wang, X. Lu and X. He, *ACS Nano.*, **2010**, 4, 6747-6759.
134. R. Roux, L. Sallet, P. Alcouffe, S. Chambert, N. Sintes-Zydowicz, E. Fleury, and J. Bernard, *ACS Macro Lett.*, **2012**, 1, 1074−1078.
135. R. H. Utama, Y. Jiang, P. B. Zetterlund and M. H. Stenzel, *Biomacromolecules,* **2015**, 16, 2144−2156.
136. C. Pitakchatwong and S. Chirachanchai, *Langmuir*, **2018**, 34, 15820−15826.
137. Q. Liu, B. Yin, T. Yang, Y. Yang, Z. Shen, P. Yao and F. Li, *J. Am. Chem. Soc.,* **2013**, 135, 5029−5037.

138. K. Poltorak, A. Durand, M. Léonard, J-L. Six and C. Nouvel, *Colloids Surf., A: Physicochem. Eng. Aspects,* **2015***,* 483, 8-17.

139. S. A. Vitale and J. L. Katz, *Langmuir,* **2003**, 19, 4105-4110.

140. X. Yan, M. Delgado, A. Fu, P. Alcouffe, S. G. Gouin, E. Fleury, J. L. Katz, F. Ganachaud and J. Bernard, *Angew. Chem. Int. Ed.,* **2014**, 53, 6910–6913.

141. X. Yan, A. Sivignon, P. Alcouffe, B. Burdin, S. Favre-Bonté, R. Bilyy, N. Barnich, E. Fleury, F. Ganachaud and J. Bernard, *Chem. Commun.,* **2015**, 00, 1-4.

142. X. Yan, P. Alcouffe, G. Sudre, L. David, J. Bernard and F. Ganachaud, *Chem. Commun.,* **2017**, 53, 1401-1404.

143. X. Yan, R. Ramos, E. Hoibian, C. Soulage, P. Alcouffe, F. Ganachaud, and J. Bernard, *ACS Macro Lett.,* **2017**, 6, 447−451.

144. M. Moise, V. Sunel, M. Holban, M. Popa, J. Desbrieres, C. Peptu and C. Lionte, *J Mater Sci.*, **2012**, 47, 8223–8233.

145. X. Li, J. Qi, Y. Xie, X. Zhang, S. Hu, Y. Xu, Y. L and W. Wu, *Int J Nanomedicine*., **2013**, 8, 23–32.

146. P. Lertsutthiwong, K. Noomun, N. Jongaroonngamsang, P. Rojsitthisak and U. Nimmannit, *carbohydr polym.*, **2008**, 74, 209–214.

147. S. Jana, A. Gangopadhaya, B. B. Bhowmik, A. K. Nayak and A. Mukherjee, *Int. J. Biol. Macromol.*, **2015**, 72, 28–30.

148. P. Lertsutthiwong, P. Rojsitthisak and U. Nimmannit, *Mater. Sci. Eng. C.,* **2009**, 29, 856–860.

149. D. Grebinisan, M. Holban, V. Sunel, M. Popa, J. Desbrieres and C. Lionte, *Cellulose Chem*. *Technol*., **2011**, 45, 571-577.

Chapter 2

Preparation of PVA-based Glycopolymers

Chapter 2 Preparation of PVA-based Glycopolymers

2.1 Introduction

Poly(vinyl alcohol) (PVA) stands out as a non toxic water-soluble polymer which can be degraded under certain microbial environmments.[1,2] Thanks to its emulsifying, adhesive and film forming abilities, PVA finds numerous applications in food packaging, textile, paper, pharmaceutics or biomaterials markets. PVA is typically obtained by free radical suspension polymerization of vinyl acetate followed by saponification of the resulting poly(vinyl acetate). PVA is commercially available but broad in molar mass distribution and generally limited to high hydroxyl contents (88-100%) to ensure water-solubility to the polymers.

As illustrated in the Chapter 1, vinyl-based glycopolymers and glycoparticles are powerful tools for the promotion of carbohydrate-directed targeting of receptors located on cells surfaces (lectins) and are widely used in drug delivery applications.[3, 4] However, this class of materials suffers from an inherent lack of degradability which may cause undesired immune responses or toxicity and limit their scope for in vivo applications. Although infrequently described, sugar-containing poly(vinyl ester) polymers constitute valuable alternatives to the styrenic or acrylic-based glycopolymers as the susceptibility of the pendant ester groups to cleavage[5] promotes the conversion of poly(vinyl ester)-based glycopolymers into non toxic and FDA-approved PVA.

In the present chapter, we will first describe the preparation of a series of precisely-defined poly(vinyl ester) glycopolymers with tunable compositions by xanthate-mediated homopolymerization of a glucose-functionalized vinyl ester or copolymerization with vinyl chloroacetate. In view of building a library of functional water-soluble PVA building blocks suitable for the conception of nanocapsules through nanoprecipitation, we will further investigate in details the alcoholysis of the copolymers in order to selectively cleave the chloroacetate esters and generate water-soluble PVA-based glycopolymers. To the best of our knowledge, the preparation of carbohydrate-functionalized

poly(vinyl alcohol) chains (through copolymerization of functional vinyl esters and selective alcoholysis) has not been reported yet.

2.2 Synthesis of sugar vinyl ester monomer (VAG)

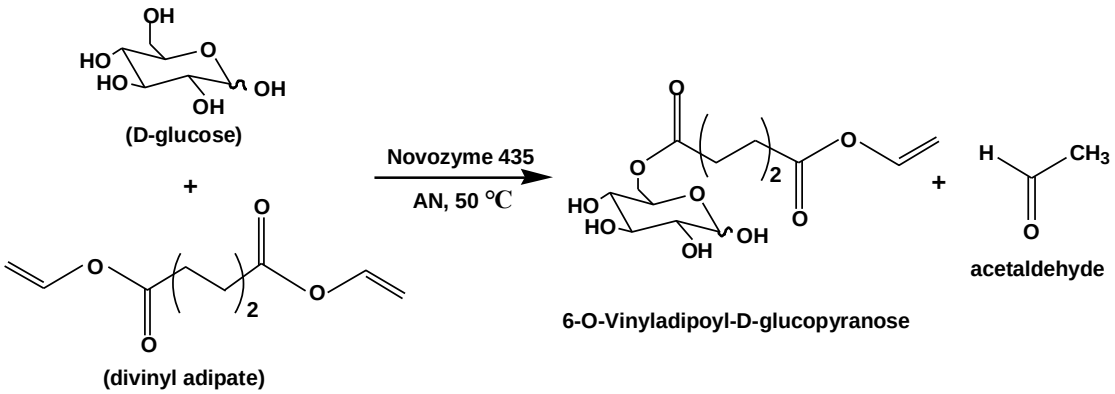

Scheme 2.1: Preparation of 6-*O*-Vinyladipoyl-D-glucopyranose (VAG) via lipase catalyzed transesterification of divinyl adipate with D-glucose (dry acetonitrile solvent, 50°C, 24h).

In the last decades, enzymes have been exploited as catalysts in the selective acylation of carbohydrates affording the preparation of vinyl-based glycomonomers. Novozyme® 435,[6] a lipase B Candida Antartica immobilized on acrylic beads, has, for instance, been used by two groups from Japan and another one from Australia to generate carbohydrate-functionalized vinyl esters.[7,8,9,10,11] In our study, we decided to focus on 6-*O*-vinyladipoyl-D-glucopyranose (VAG) whose synthesis through lipase-catalyzed acylation of D-glucose with divinyl adipate (in acetonitrile at 50°C for 24h) has previously been reported by Stenzel and co-workers (**Scheme 2.1**)[11]. Following a similar protocol, we obtained the vinyl ester glycomonomer as a white powder (yield ~ 34% with respect to D-Glucose). The synthesis of the desired glycomonomer was certificated by ^{1}H and ^{13}C NMR analyses (see **Figures 2.1** and **2.2**).

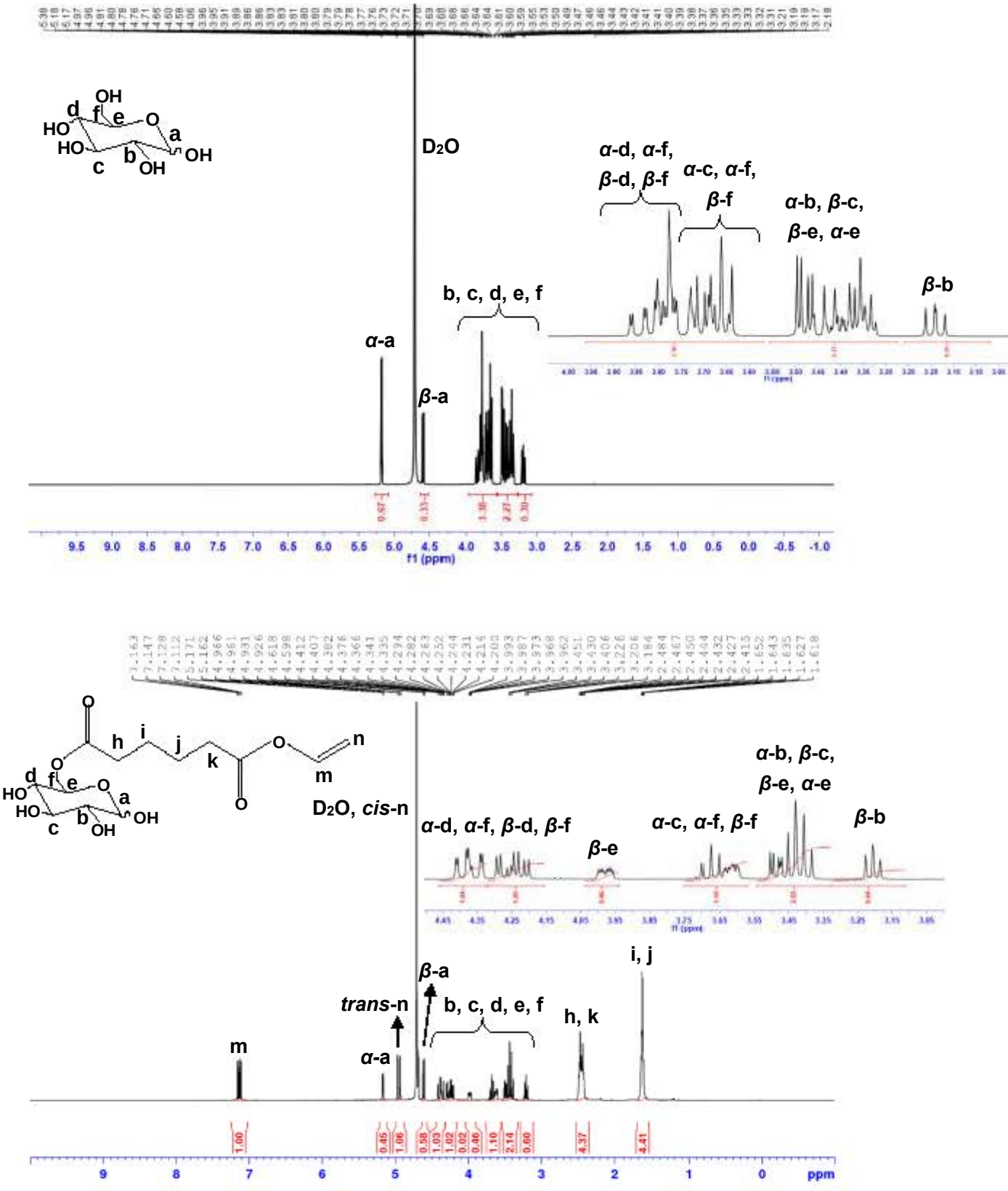

Figure 2.1: ^{1}H NMR spectra of D-glucose (top) and VAG (bottom, D_2O, r. t.).

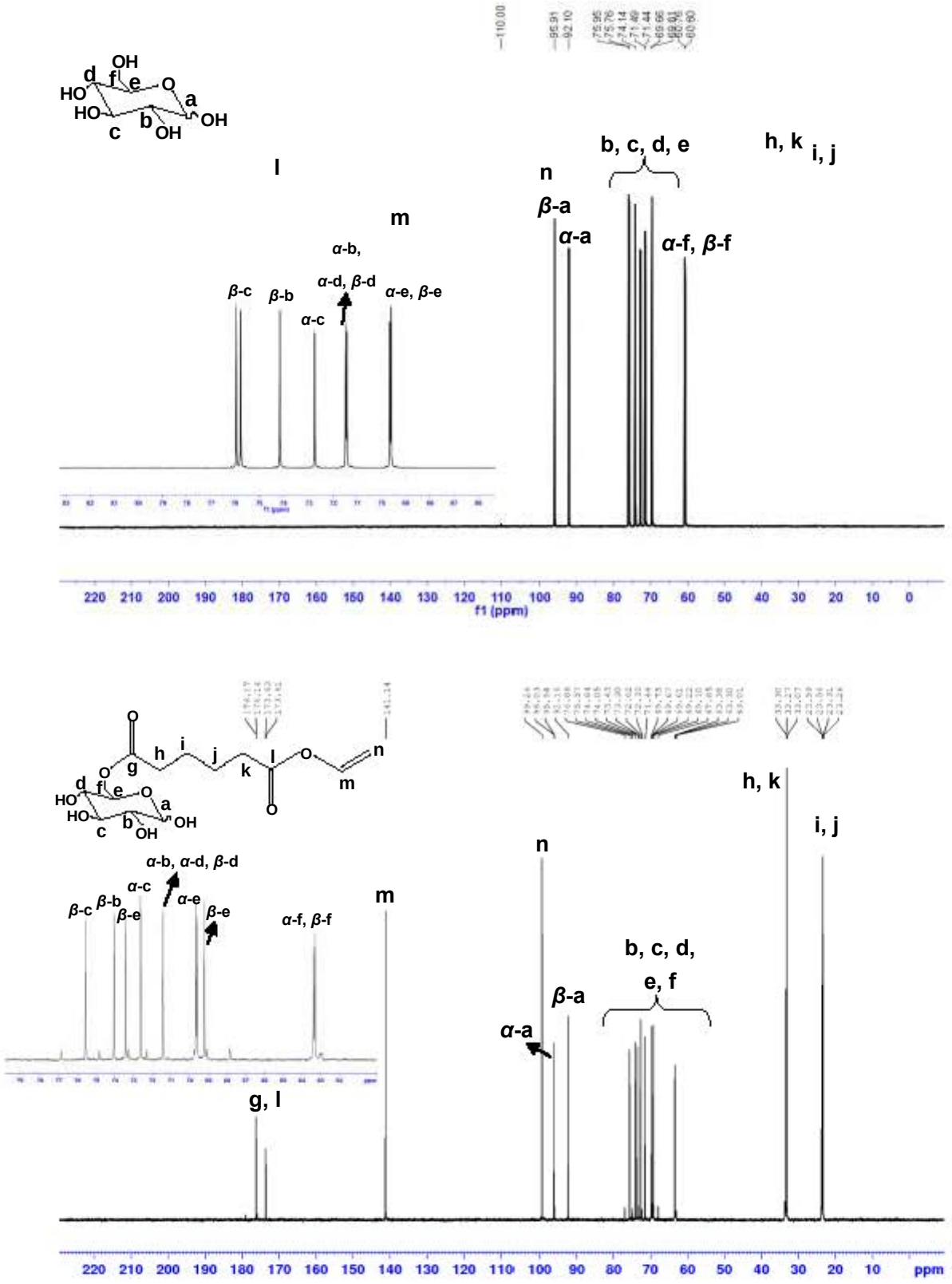

Figure 2.2: ^{13}C NMR spectra of D-glucose (top) and VAG (bottom, D_2O, r. t.).

On the ^{1}H NMR spectrum, the formation of VAG was assessed by the presence of peaks at 1.62 and 2.44 ppm corresponding to methylene groups, the

characteristic vinylic peaks at 4.96 and 7.15 ppm as well as the multiple peaks between 3.1 and 4.6 ppm ascribed to the glucose residues. On the ^{13}C NMR spectrum, peaks at 22.3, 33.3, 99.7, 141.1, 172.4 and 174.1 ppm belong to vinyl adipate groups whereas peaks between 60 and 100 ppm correspond to the glucose motif. Comparison between the ^{13}C spectrum of VAG with that of the starting D-glucose reveals that the greatest change in chemical shift has occurred for **e** (+4 ppm for the β form) and **f** (+2 ppm for both *α* and *β* forms), confirming that the acylation took indeed place in position f (C-6). The structure of VAG was further confirmed by ESI-MS analysis (**Figure 2.3**). The detection of a main population at 357.1149 m/z was in excellent agreement with the theoretical mass of $(M+Na)^+$ ($[C_{14}H_{22}NaO_9]^+$ at 357.1156 m/z). The population at 691.2416 m/z corresponds to $(2M+Na)^+$ species.

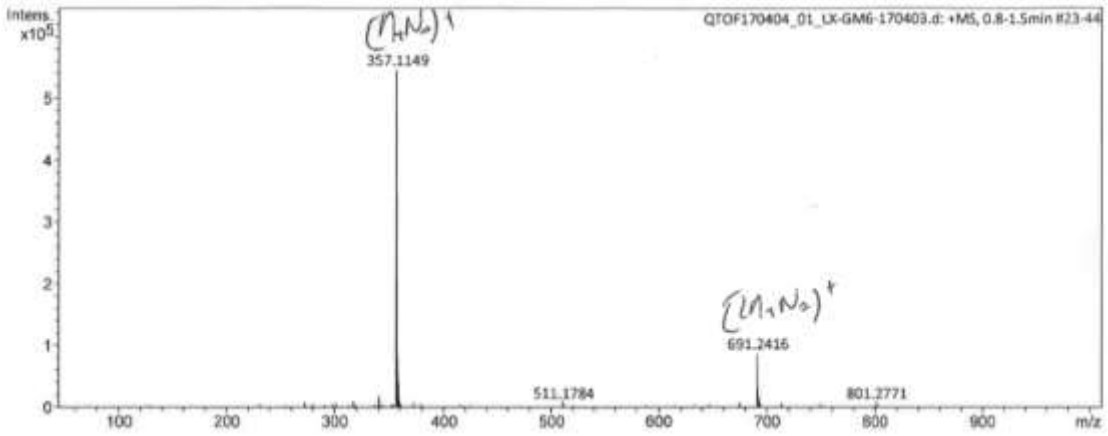

Figure 2.3: ESI-MS spectrum of VAG.

2.3 Synthesis of the chain transfer agent (CTA)

Reversible addition-fragmentation chain transfer (RAFT) polymerization is one of the rare polymerization techniques allowing for controlling the polymerization of vinyl esters. Since the early reports of Charmot et al. on the synthesis of poly(vinyl ester)s using xanthates as chain transfer agents,[12] the RAFT polymerization of vinyl esters, mediated by xanthates has been the subject of numerous theoretical[13,14] and experimental studies[15,16,17,18,19]. Based on

literature data[20] we selected methyl[(ethoxycarbonothioyl)sulfanyl acetate as a suitable chain transfer agent (CTA) for our experiments. As shown in **Scheme 2.2**, this CTA was prepared on the gram scale with good yield (around 88%) from *O*-ethylxanthic acid potassium salt (1g, 6.24 mmol, dissolved in 4 mL of dry acetone) and methyl bromoacetate (1g, 6.24 mmol)[21]. The structure and the purity of the CTA was confirmed by ^{1}H and ^{13}C NMR, see **Figures 2.4** and **2.5**.

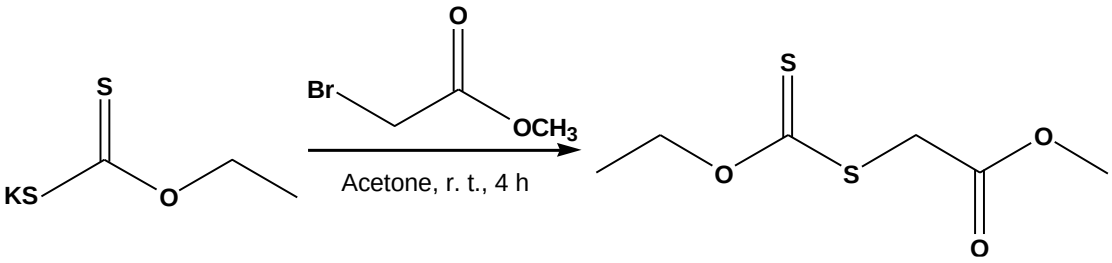

Scheme 2.2: Synthesis of methyl[(ethoxycarbonothioyl)sulfanyl] acetate.

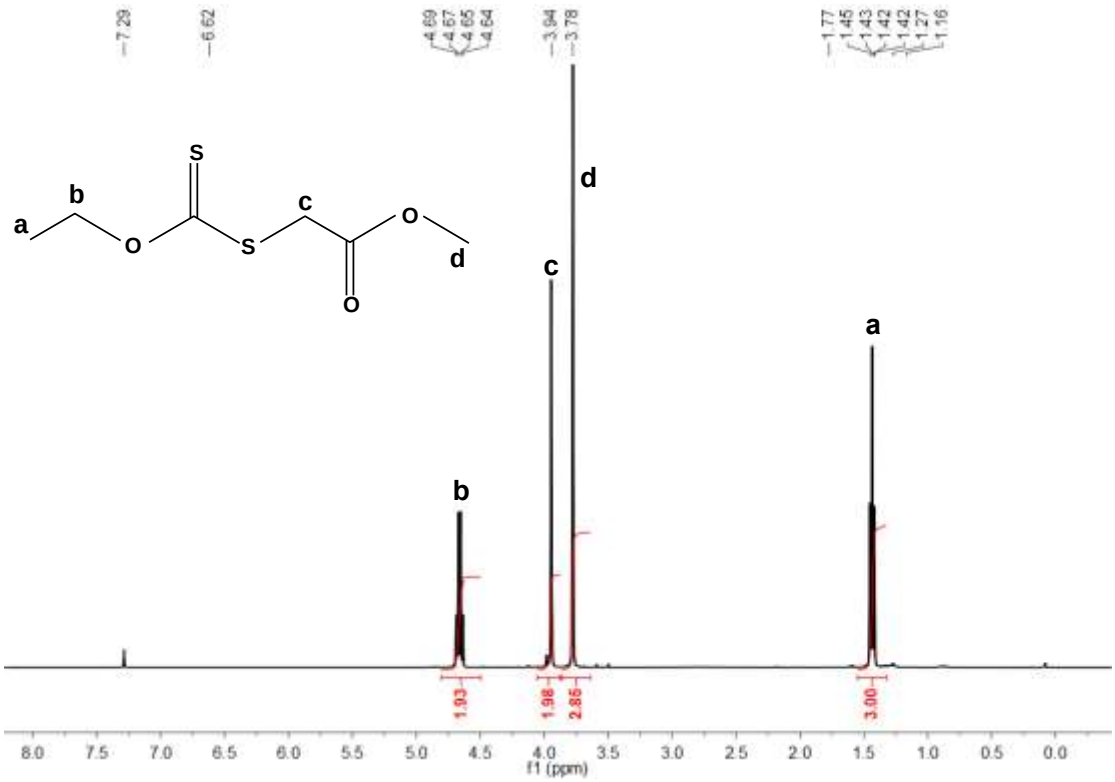

Figure 2.4: ^{1}H NMR spectrum of RAFT agent methyl (ethoxycarbonothioyl)sulfanyl] acetate ($CDCl_3$, r. t.).

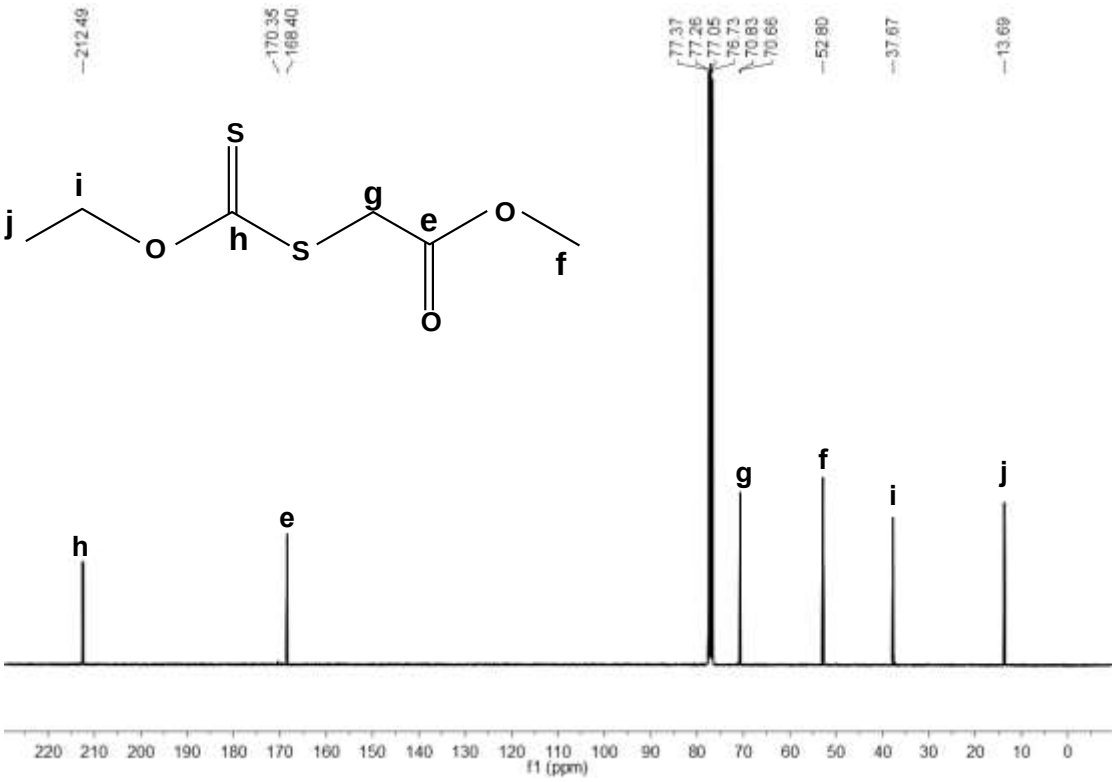

Figure 2.5: ^{13}C NMR spectrum of RAFT agent methyl [(ethoxycarbonothioyl)]sulfanyl acetate ($CDCl_3$, r. t.).

2.4 RAFT polymerization of vinyl chloroacetate (VClAc) and generation of PVA by methanolysis

The preparation of PVA from poly(vinyl ester)s under basic conditions has been established for decades.[22, 23] Recently, a study of Mahanthappa dealing with the preparation of well-defined poly(vinyl acetate-*b*-vinyl alcohol) block copolymers from RAFT-made poly(vinyl acetate-*co*-vinyl chloroacetate) underlined that chloroacetate esters can be selectively cleaved under specific conditions of alcoholysis.[24] In view of generating PVA with pendant glucose moieties randomly distributed along the chains, we first investigated the polymerization of vinyl chloroacetate (VClAc) and conditions of alcoholysis promoting the formation of PVA.

2.4.1 Preparation of PVClAc

In order to identify optimal conditions for the preparation of PVClAc with control over the degree of polymerization, VClAc was polymerized at different temperatures (at 60, 70 or 80 °C) in the presence of AIBN as initiator and methyl[(ethoxycarbonothioyl)sulfanyl]acetate as chain transfer agent. In a typical experiment, vinyl chloroacetate (VClAc, 264 mg, 2.2 mmol) was polymerized in 1.1 mL of ethyl acetate at the desired temperature in the following conditions: $[VClAc]_0/[CTA]_0/[AIBN]_0=200/1/0.2$. The resulting solution was precipitated in cyclohexane three times and dried under vacuum to obtain pure PVClAc (**Scheme 2.3**, **Figure 2.6**).

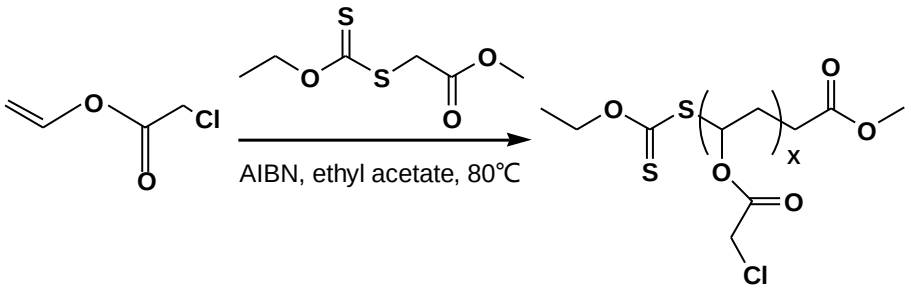

Scheme 2.3: RAFT preparation of PVClAc.

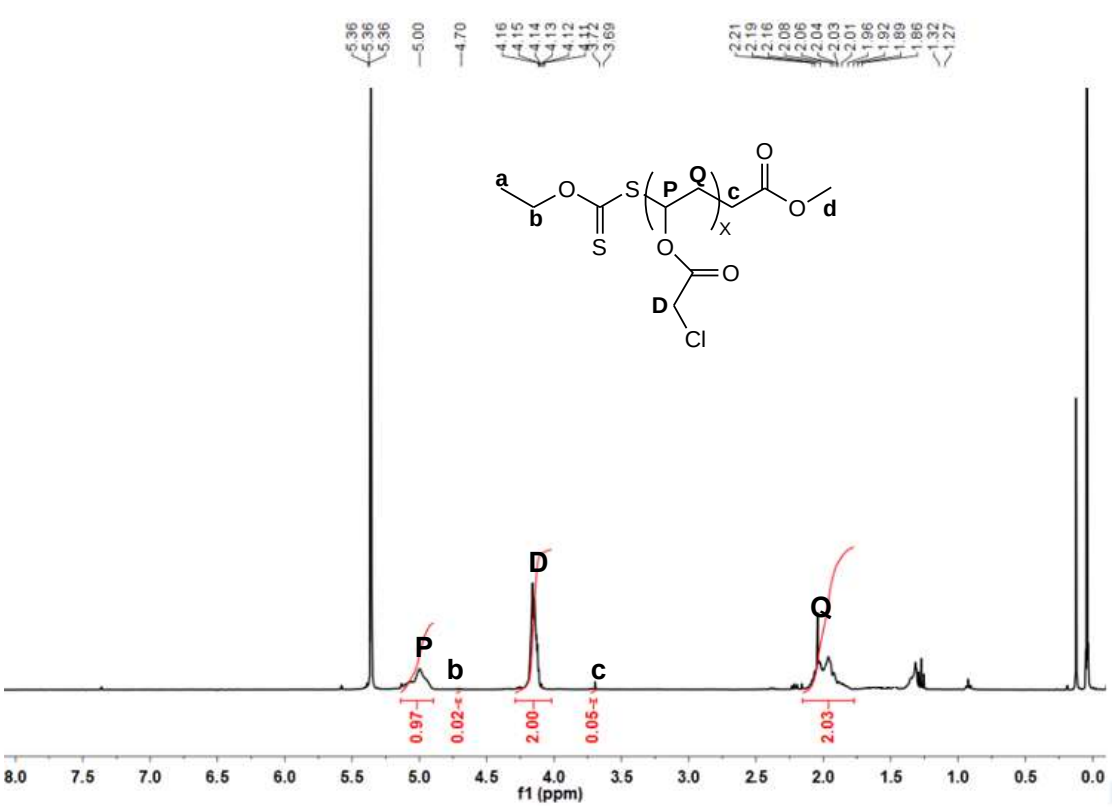

Figure 2.6: ^{1}H NMR of PVClAc after purification of the crude product obtained at 80°C RAFT polymerization (CD_2Cl_2, r. t.).

The conditions of RAFT polymerization and the characteristics of the resulting poly(vinyl ester)s are summarized in **Table 2.1**. SEC traces of the polymers are given in **Figure 2.7**. Polymerization of VClAc for 4 hours at 80°C ($[VClAc]_0$=2 mol·L^{-1}, $[M]_0/[CTA]_0/[I]_0$=200/1/0.2, entry 3) yielded PVClAc with relatively low dispersity ($Đ$ = 1.37) and conversion ~ 70% whereas polymers with broad molar mass distribution were grown when polymerizations proceeded at lower temperatures.

Table 2.1: Experimental data of PVClAc polymers produced at different temperatures by RAFT polymerization ($[VClAc]_0$=2 mol·L^{-1}, $[VClAc]_0/[CTA]_0/[I]_0$=200/1/0.2).

Entries	Temperature (℃)	Time (h)	Conv. [a] (%)	$[DP]_{th}$ [b]	$M_{n,th}$ [c] (g/mol)	$M_{n,SEC}$ [d] (g/mol)	$Đ$ [d]
1	60	7	29	58	7200	6800	1.62
2	70	4	49	98	12000	9300	1.57
3	80	4	73	146	17700	13600	1.37

[a)]: Calculated from the integrals of vinyl and methylene groups at 4.7 and 5.0 ppm; [b)]: Calculated from VClAc conversion and $[VClAc]_0/[CTA]_0$; [c)]: Calculated from molar mass of VClAc and $[DP]_{th}$; [d)]: Determined by SEC analysis in THF (PS calibration) after polymer purification.

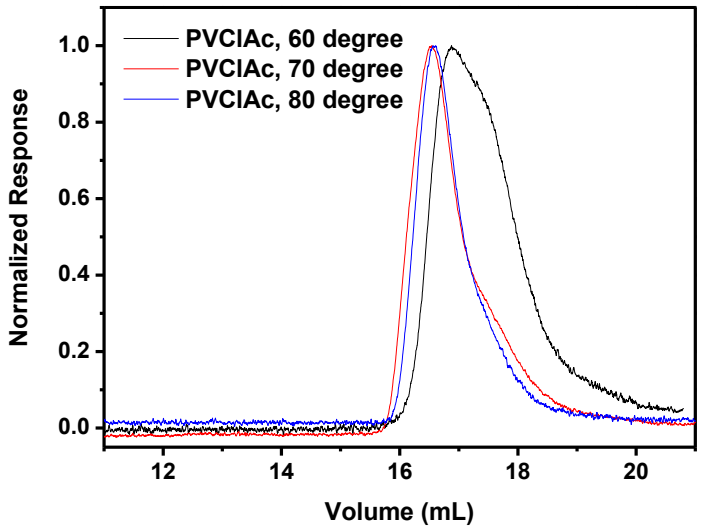

Figure 2.7: SEC traces of PVClAc produced at different temperature (THF eluent, PS calibration).

2.4.2 Alcoholysis of PVClAc

In view of identifying conditions that could afford a selective cleavage of chloroacetate esters in VAG/VClAc copolymers, we first investigated the alcoholysis of PVClAc homopolymers in DMF/methanol (1/3, v/v) mixtures in the presence of K_2CO_3 (2.7 mmol·L^{-1}) (**Scheme 2.4**) at different temperatures (0 or 25°C) and different reaction times (from 20 minutes to one hour), see **Table 2.2**. ^{1}H NMR spectra of the polymers after alcoholysis and purification through dialysis against water and freeze-drying measurements are given in **Figure 2.8**.

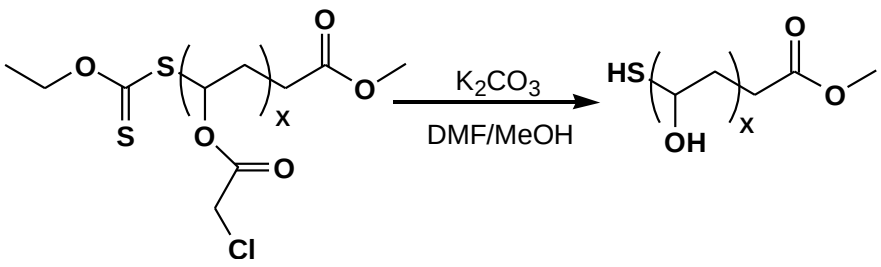

Scheme 2.4: Schematic alcoholysis of PVClAc under basic condition.

Table 2.2: Alcoholysis of PVClAc under varying reaction time and temperature (purified PVClAc obtained from PVClAc-80 °C, $[PVClAc]_0$=18.5 mmol·L^{-1}, $[K_2CO_3]$=2.7 mmol·L^{-1}).

Entries	Temperature (℃)	Time (h)	Alcoholysis (%)
1	25	60	100
2	25	20	100
3	0	20	100

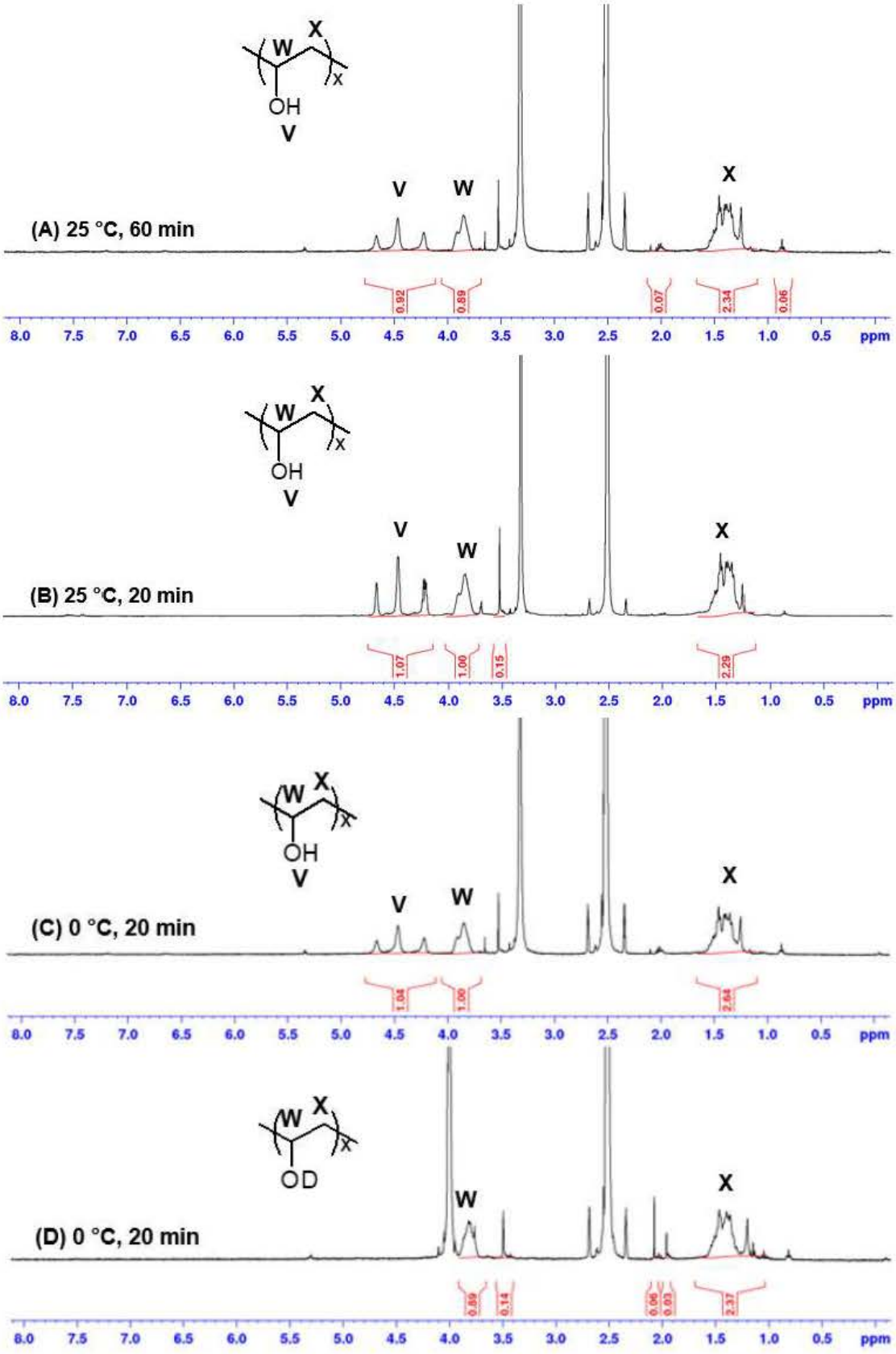

Figure 2.8: ^{1}H NMR spectra of (A) (B) (C) PVA obtained under conditions 1, 2 and 3 respectively (DMSO-d_6, r. t.); (D) was obtained from (C) after addition of D_2O (D_2O/DMSO-d_6, r. t.).

Analyses were performed in DMSO-d_6 or in D_2O/DMSO-d_6 mixtures at 298K to exchange the hydrogen of the alcohol groups with deuterium. The addition of heavy water indeed facilitates the estimation of the degree of alcoholysis as the peaks corresponding to the OH groups suddenly disappear in a region (between 4 and 5 ppm) where chloroacetate protons of the precursor could also be found in case of incomplete reaction. As shown in **Figure 2.8** (spectra A-D), the reaction of alcoholysis proceed smoothly and remains quantitative under very mild conditions (0°C, 20 min). Conversion of PVClAc to PVA was clearly assessed by the appearance of characteristic peaks of the OH groups between 4.1 and 4.7 ppm (see **Figure 2.8 C**). As mentioned earlier, these new peaks disappeared after addition of D_2O and no residual peaks relative to chloroacetate protons was observed (**Figure 2.8 D**) in agreement with a quantitative cleavage of these ester groups.

2.5 Investigation of VAG RAFT polymerization and alcoholysis of the resulting glycopolymer

2.5.1 RAFT polymerization for PVAG

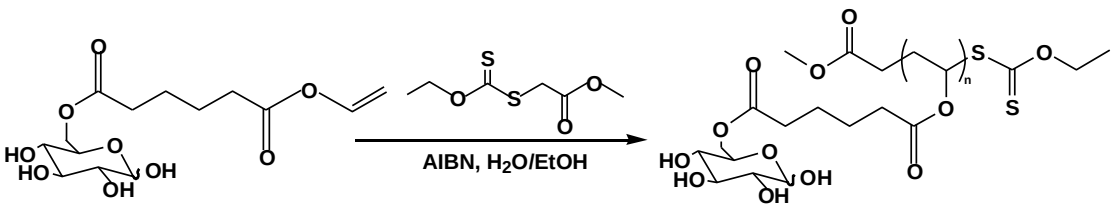

Scheme 2.5: RAFT preparation of PVAG.

As a further step towards the preparation of sugar-decorated PVA, we further examined the preparation of poly(6-*O*-vinyladipoyl-D-glucopyranose) (PVAG). The RAFT polymerization was carried out in water/ethanol mixture (1/1, v/v) at 60, 70 or 80 °C for 24 h using methyl [(ethoxycarbonothioyl)]sulfanyl acetate as CTA and AIBN as initiator ($[VAG]_0/[CTA]_0/[Initiator]_0$=160/1/0.2, $[VAG]_0$=0.75

mol·L^{-1}) (**Scheme 2.5**). After polymerization, 100 µl of solution was taken from the polymerization medium and redissolve in D_2O to determine the conversion by ^{1}H NMR analysis from the integrals of the peaks from vinyl and methylene (adipoyl) protons (at 7.2 and 2.6 ppm, respectively). RAFT polymerization of VAG was surprisingly slow with only 5% of conversion after 24h at 60°C. The conversion jumped to 35% and 39% upon increase of the polymerization temperature to 70 and 80°C respectively. The glycopolymers were purified by precipitation in diethyl ether/ethanol mixture (8/2, v/v) and finally characterized by ^{1}H and ^{13}C NMR (see **Figure 2.9**). Number-average molecular weights were estimated from relative integration of the peak at 1.31 ppm corresponding the CH3 group of the xanthate chain end (protons q), and the peaks (protons h, k at 2.3 ppm) corresponding to the adipoyl methylene pendant groups of the repeating units (see **Table 2.3**). Consistent with a controlled process, the experimental $DP_{n\ NMR}$ and $M_{n\ NMR}$ were in a good agreement with the theoretical values calculated from monomer conversion (see **Table 2.3**).

Table 2.3: Conditions of VAG RAFT polymerizations and characteristics of the resulting glycopolymers ($[VAG]_0$=0.75 mol·L^{-1}, $[VAG]_0/[CTA]_0/[I]_0$=160/1/0.2).

Sample	Temperature (°C)	Conv. [a] (%)	$[DP]_{th}$ [b]	$M_{n,\ th}$ [c] (kg/mol)	$[DP]_{NMR}$ [d]	$M_{n,\ NMR}$ [e] (kg/mol)
$PVAG_x$	60	5	8	2.9		
$PVAG_{60}$	70	35	56	18.9	60	20.2
$PVAG_{75}$	80	39	62	20.9	75	25.2

[a)]: Calculated from the integrals of the peaks from vinyl and methylene (adipoyl) protons at 7.2 and 2.6 ppm respectively; [b)]: Calculated from VAG conversion and $[VAG]_0/[CTA]_0$; [c)]: Calculated from molar mass of VAG and $[DP]_{th}$; [d)]: Determined from relative integration of the protons q at 1.31 ppm and the protons h, k at 2.3 ppm; [e)]: Calculated from molar mass of VAG and $[DP]_{NMR}$.

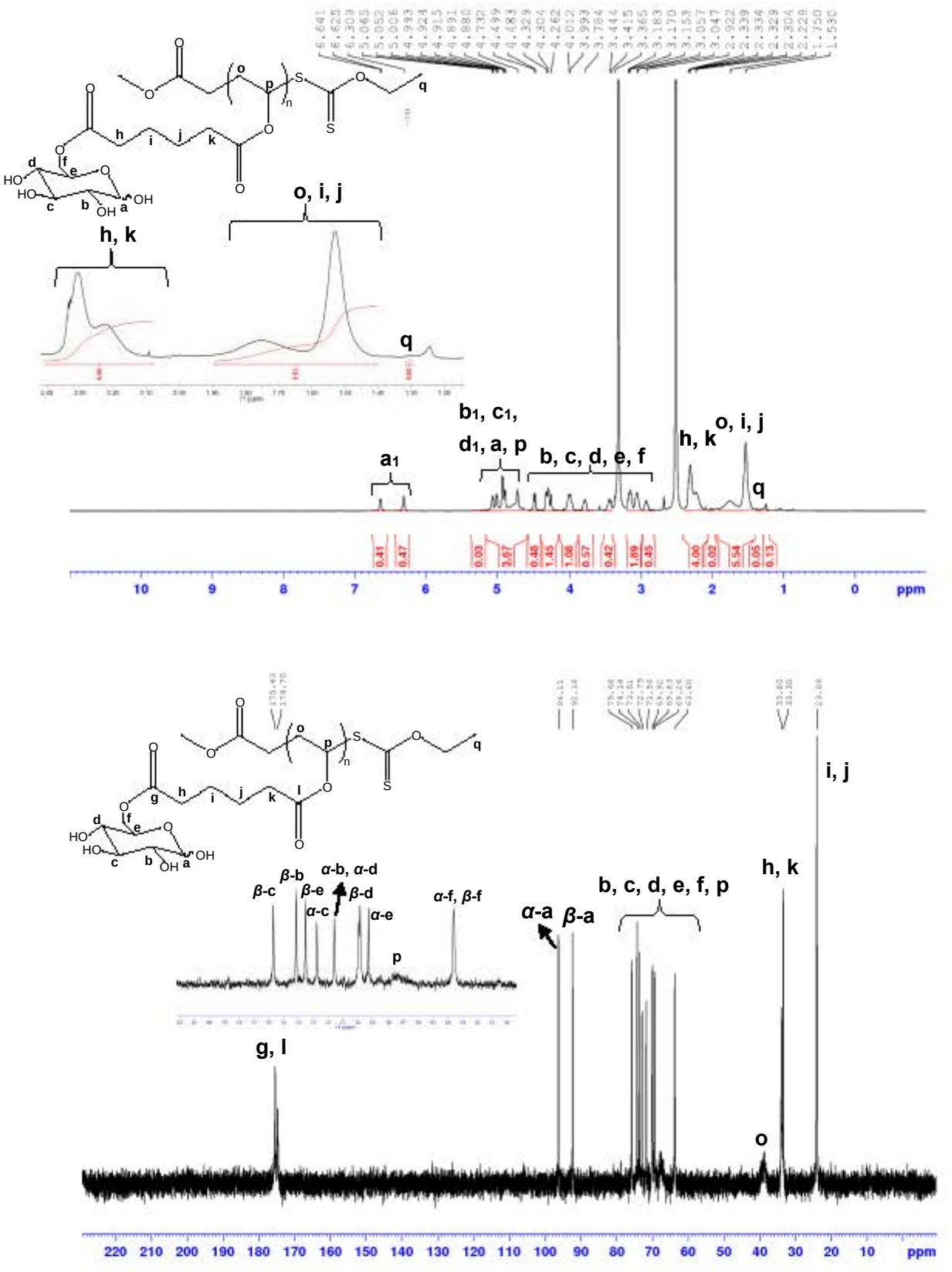

Figure 2.9: ^{1}H NMR and ^{13}C NMR spectra of PVAG obtained at 70°C polymerization (DMSO-d_6, r. t.). a_1, b_1, c_1, d_1 represent the corresponding hydroxyl peaks.

Characterization of the (unprotected) glycopolymers was proven very challenging by SEC and no reliable data could be obtained by using THF or DMF/LiBr as eluents possibly due to interactions of the polymers with the columns. In addition, the traditional acetylation process led to partially loss of sugar moieties (RT, overnight, stirring in the presence of 5 equivalents of acetic anhydride and 2 equivalents of pyridine *vs* hydroxyl group respectively). To overcome this issue, we decided to post-modify the glycopolymers by engaging the hydroxyl groups of the sugar residues in a reaction with phenyl isocyanate following a method reported in the literature.[25, 26] After derivatization of the glycopolymer chains, SEC experiments were performed in THF. Even though SEC data should be taken with caution owing to the use of PS calibration, comparison of the SEC traces for $PVAG_{60}$ and $PVAG_{75}$ confirmed that the molecular weight of the glycopolymer chains slightly increases with conversion of VAG ($M_{n,\,SEC}$ =17.1 and 25.5 kg/mol at 35 and 39% of conversion. However, the molecular weight distributions were quite high (*Đ* >1.50) (**Figure 2.10**). This could reflect a poor control of the RAFT/MADIX polymerization or could be due to the presence of numerous urethane groups onto the carbohydrate causing multiple H-bonding interactions and translating in ill-defined peaks.

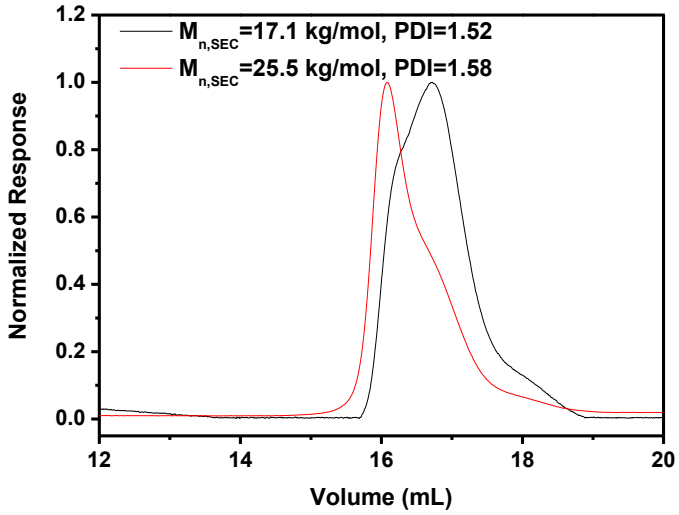

Figure 2.10: SEC traces of PVAG glycopolymers after derivatization with phenyl isocyanate (THF eluent, PS calibration).

2.5.2 Stability of PVAG

Next, we investigated the stability of PVAG under the conditions of alcoholysis developed for PVClAc (**Table 2.4**) to identify conditions that could possibly ensure selective cleavage of chloroacetate groups without removing the pendant sugar motifs. ^{1}H NMR spectra of PVAG before and after alcoholysis (at 0 and 25°C for 20 or 60 minutes in DMF/methanol in the presence of potassium carbonate) are given in **Figure 2.11**. **Figure 2.12** provides a zoom in of these spectra in a specific region of interest ranging from 3.0-4.5 ppm. Close comparison of spectra A and B gave clear evidence that the “strongest” conditions of alcoholysis (set for PVClAc, 1h@25°C, see entry 1 in Table 2.4) resulted in a partial detachment of the sugar groups. Accordingly, the integration values for glucose protons (typically between 3 and 5.5 ppm) decreased drastically and a peak attributed to the CH groups in PVA appeared at 3.66 ppm (marked as **r**). Note though that the integrations of the peaks relative to adipate spacer remain more or less constant suggesting that the ester group close to the main chain is not impacted. Decreasing the time of reaction to 20 minutes while maintaining the same temperature significantly limited the alcoholysis but the peak r was still visible (see spectrum C). Finally, when alcoholysis was undertaken at 0 °C for 20 min, conditions which are suitable for converting PVClAc into PVA, no degradation of PVAG was observed.

Table 2.4: Stability of PVAG under three different conditions of alcoholysis validated for PVClAc ($[PVAG]_0$=7.0 mmol·L^{-1}, $[K_2CO_3]_0$=2.7 mmol·L^{-1}).

Entries	Temperature (°C)	Time (min)	Alcoholysis (%)
1	25	60	partial
2	25	20	partial
3	0	20	no degradation

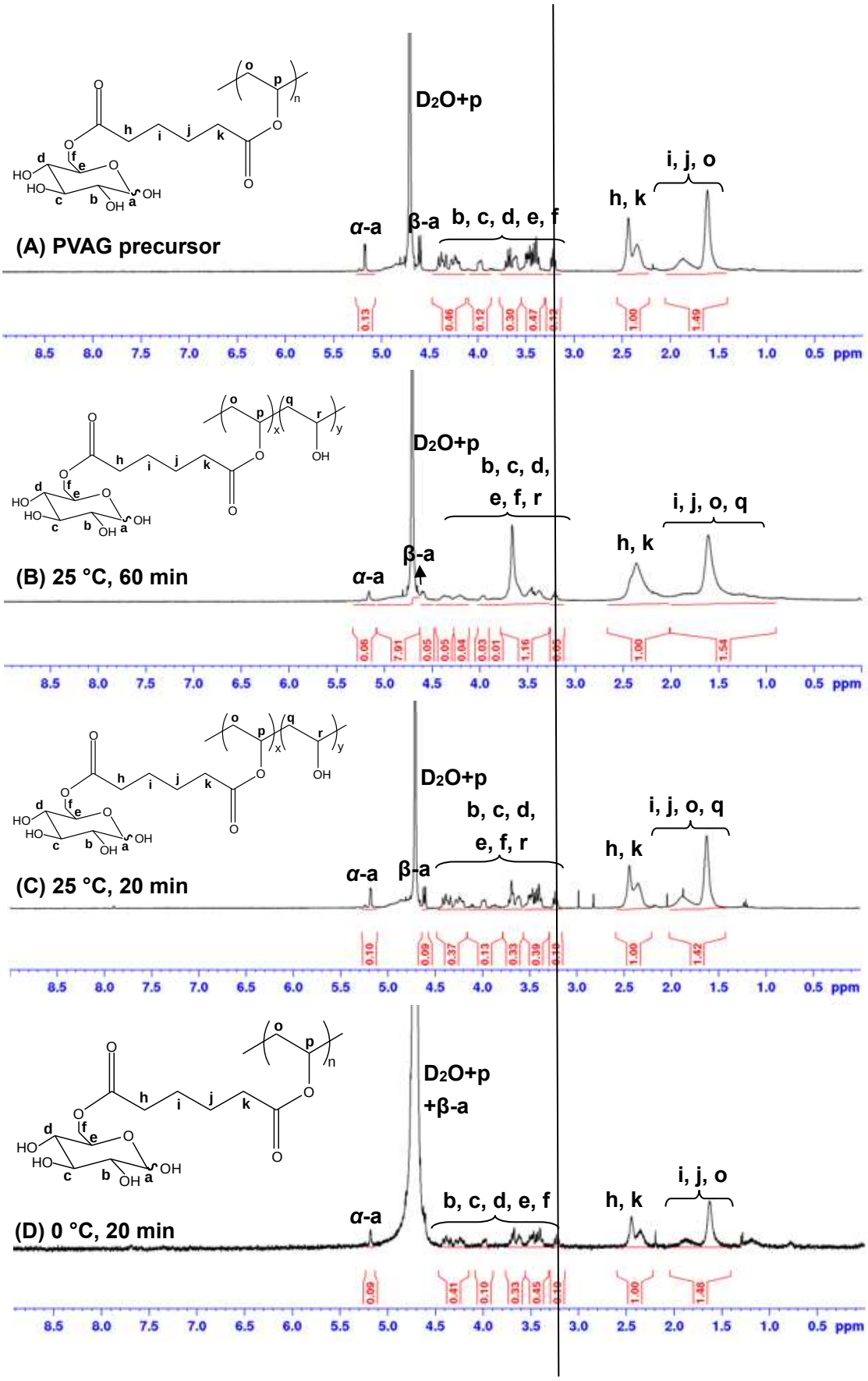

Figure 2.11: ^{1}H NMR spectra of PVAG before alcoholysis (A), partially degradation (B, C) and no degradation (D) (D_2O r. t.).

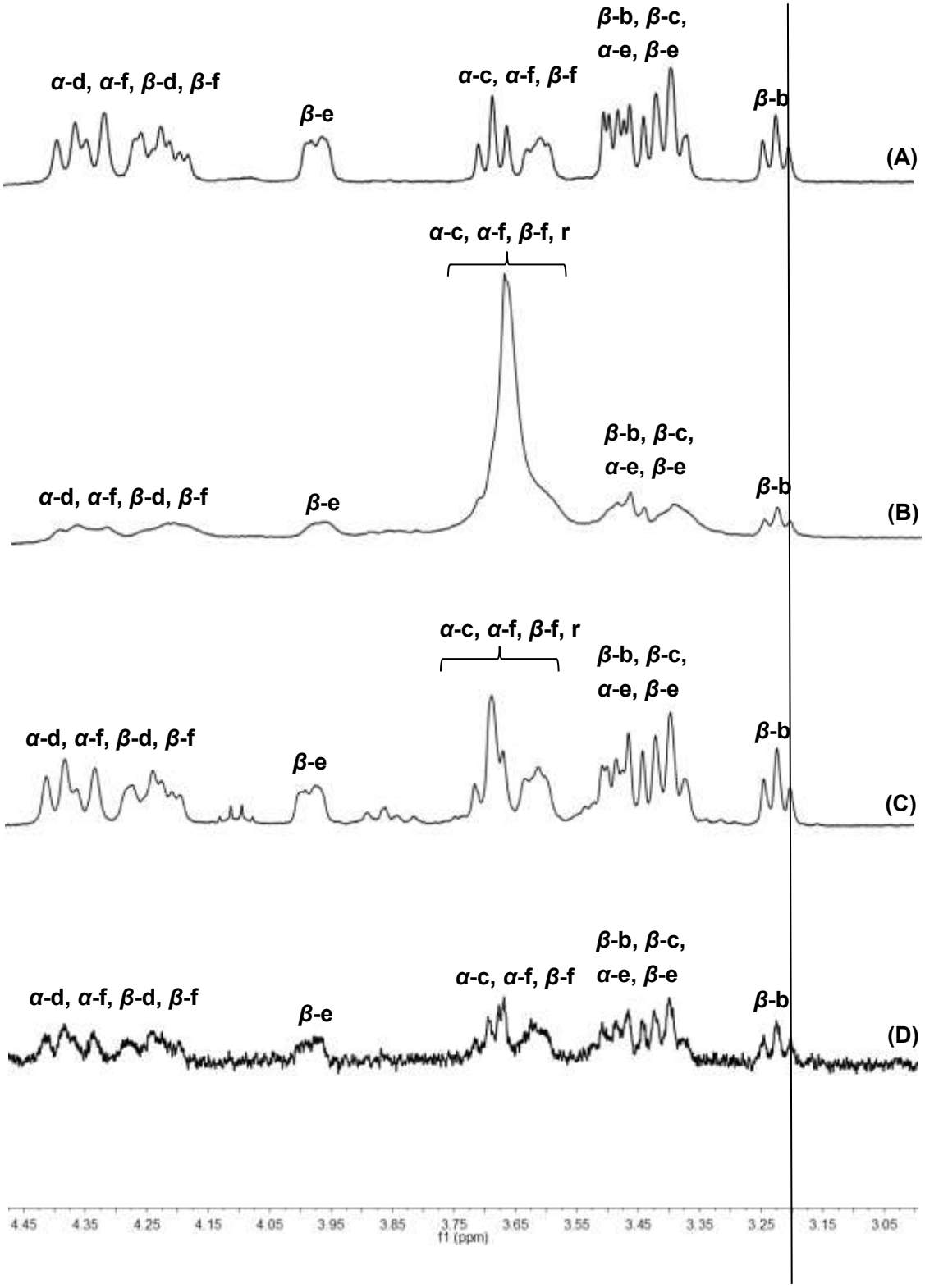

Figure 2.12: Zoom in of ^{1}H NMR spectra (D_2O r.t.) (3.0-4.5 ppm) of PVAG before alcoholysis (A), after treatment detailed in Table 2.4, entry 1 (B), after treatment detailed in Table 2.4, entry 2 (C) and after treatment detailed in Table 2.4, entry 3 (D).

2.6 Preparation of PVA-based glycopolymers

In the previous part, we have shown that PVClAc and PVAG can be polymerized using the MADIX/RAFT process and we identified conditions of alcoholysis promoting the selective cleavage of chloroacetate esters. In the following, we will examine the RAFT copolymerization of VClAc and VAG and alcoholysis of the resulting polymers in order to prepare a series of glucose-functionalized PVA.

2.6.1 RAFT polymerization for PVClAc-based glycopolymers

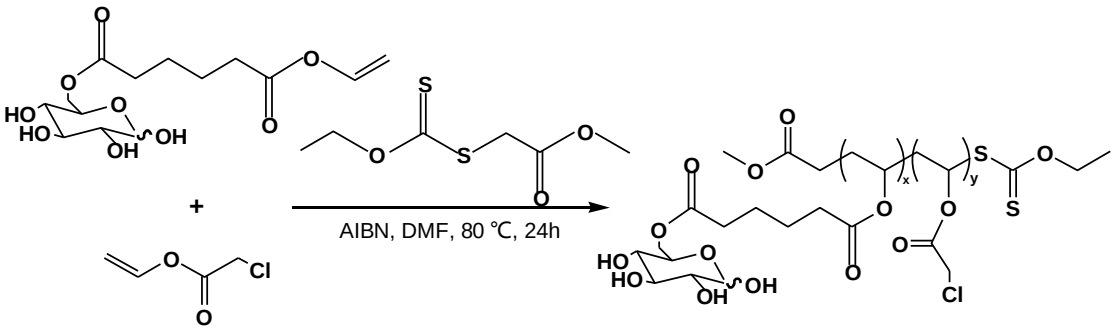

Scheme 2.6: RAFT preparation of Poly(VClAc-*co*-VAG).

PVClAc-based glycopolymers were prepared through RAFT copolymerization of VClAc and VAG with three different molar compositions (70/30, 90/9, 103/5) in order to prepare PVA-based glycopolymers with tunable compositions (**Scheme 2.6**). Copolymerizations were performed in DMF, a good solvent for both monomers. For clarity's sake, the preparation of of the copolymers will be exemplified with P(VClAc$_{59}$-*co*-VAG$_9$). The copolymerization was performed using methyl[(ethoxycarbonothioyl)sulfanyl] acetate as CTA and AIBN as initiator using the following conditions: $[VClAc+VAG]_0/[CTA]_0/[AIBN]_0$= (90+9)/1/0.2, $[CTA]_0$=0.26 M. After 24h of polymerization at 80°C, 71% of VClAc and 61% of VAG were consumed as determined by ^{1}H NMR as previously described for homopolymerizations of VClAc and VAG. It was observed that

both conversions of two monomers decreased with increasing VAG concentration. The overall degree of polymerization and corresponding molecular weight were estimated from the integration of chain end groups (peak q at 1.31 ppm) and repeating units protons (peaks h/k, r at 2.3 and 1.9 ppm for VAG and VClAc respectively). $DP_{NMR,VClAc}=3I_r/2I_q$, $DP_{NMR,VAG}=3(I_h+I_k)/4I_q$, where I_h, I_k, I_r and I_q represent the corresponding integral value (equation for calculation $I_r=I_{o+r+i+j}-I_o-I_{i+j}$) (see **Figure 2.13** and **Table 2.5**). SEC experiments were performed in THF eluent after functionalization of the hydroxyl groups with phenyl isocyanate. SEC traces of the resulting PVClAc-*co*-PVAG(Ph) performed in THF (PS calibration) are gathered in **Figure 2.15**. Similar to the results obtained for post-modified PVAG, dispersity of the copolymers was relatively high, with values comprised between 1.29 for P($VClAc_{34}$-*co*-VAG_{19}) to 1.62 for P($VClAc_{117}$-*co*-VAG_{10}) and apparent molecular weights were ranging between 6 and 10 kg/mol, see **Table 2. 5**.

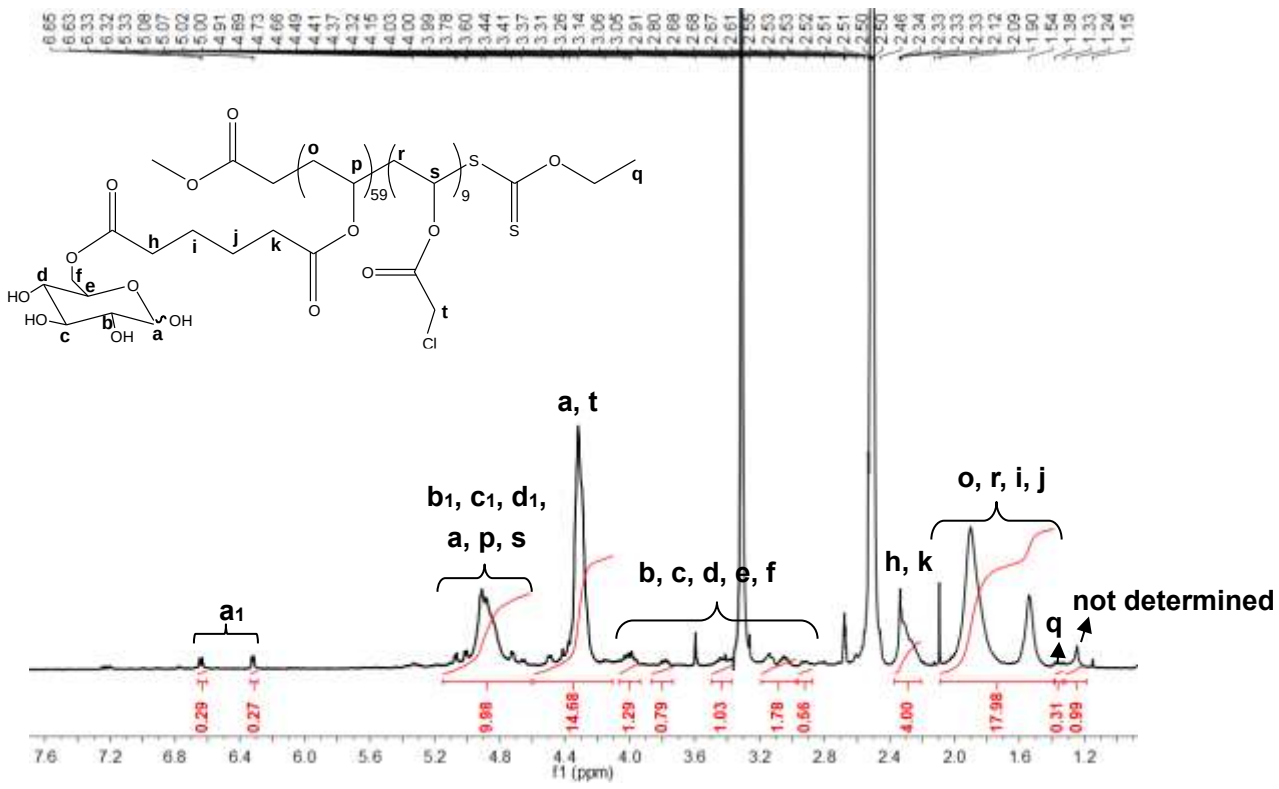

Figure 2.13: ^{1}H NMR spectrum of P($VClAc_{59}$-*co*-VAG_9) in DMSO-d_6. a_1, b_1, c_1, d_1 represent the corresponding hydroxyl peaks.

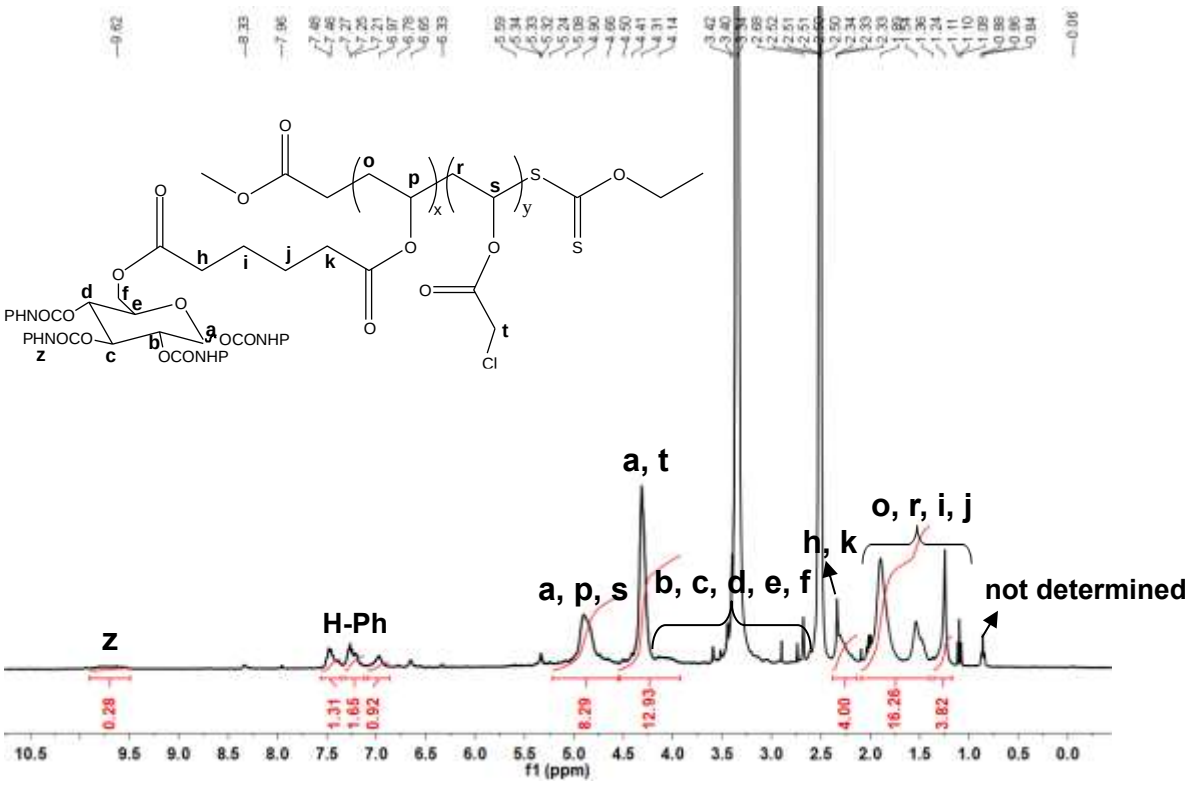

Figure 2.14: ^{1}H NMR spectrum of P(VClAc$_{59}$-*co*-VAG$_{9}$) derivative by phenyl isocyanate (DMSO-d$_6$, r. t.).

Table 2.5: Characteristics of P(VClAc-*co*-VAG) copolymers with varying compositions ([VClAc+VAG]$_0$/[CTA]$_0$/[AIBN]$_0$=X/1/0.2, [CTA]$_0$=0.26 mol·L^{-1}, 80°C, 24h).

Sample	[VClAc+GM]$_0$/[RAFT]$_0$/[I]$_0$	Conv. (%) [a] (VClAc)	Conv. (%) [a] (VAG)	$M_{n,\,th}$ [b] (kg/mol)	$M_{n,\,NMR}$ [c] (kg/mol)	$M_{n,\,SEC}$ [d] (kg/mol)	$Đ$ [d]
P(VClAc$_{117}$-*co*-VAG$_{10}$)	[103+5]/1/0.2	78	74	11.2	17.7	9.8	1.62
P(VClAc$_{59}$-*co*-VAG$_{9}$)	[90+9]/1/0.2	71	61	9.9	10.3	9.6	1.50
P(VClAc$_{34}$-*co*-VAG$_{19}$)	[70+30]/1/0.2	51	46	9.5	10.6	6.1	1.29

[a)]: Calculated from integration of the peaks from vinyl and methylene (adipoyl) protons at 7.2, 4.7 and 2.6 ppm respectively; [b)]: Calculated from monomer molar mass and corresponding [DP]$_{th}$ by conversion and [Monomer]$_0$/[CTA]$_0$; [c)]: Determined from monomer molar mass and [DP]$_{NMR}$; [d)]: Determined by SEC analysis of protected copolymers (THF eluent, PS calibration).

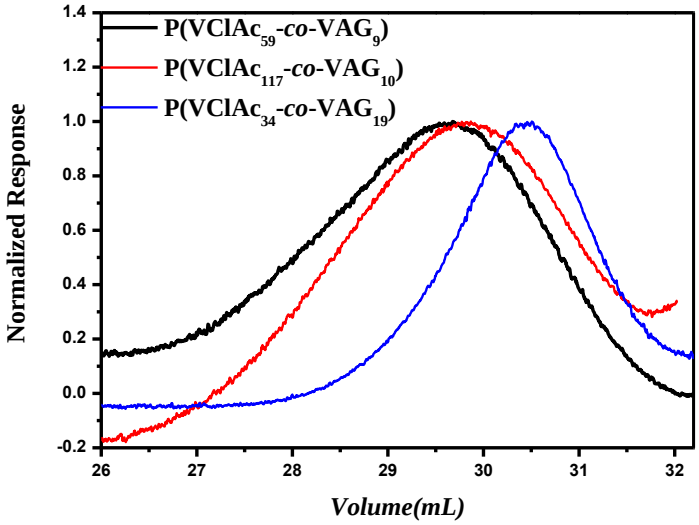

Figure 2.15: SEC analysis of P(VClAc-*co*-VAG) after modification with phenyl isocyanate (THF eluent, PS calibration).

2.6.2 Selective alcoholysis of the copolymers-Towards the generation of PVA-based glycopolymers

With respect to the study undertaken earlier on the stability of PVAG under K_2CO_3/MeOH conditions, the alcoholysis of poly(VClAc-*co*-VAG) copolymers was examined at 0°C and the reaction time was limited to 20 min. After reaction, the solution was dialyzed against distilled water for 2 days to remove reactants and solvents and the resulting copolymer was finally obtained by freeze-drying (**Scheme 2.7**).

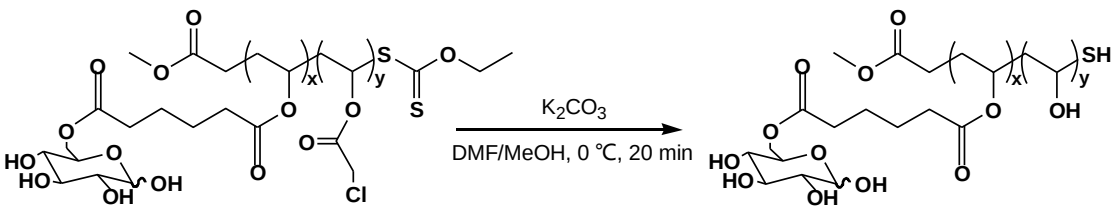

Scheme 2.7: Selective hydrolysis of Poly(VClAc-*co*-VAG) under mild basic condition.

The success of the selective removal of chloroacetate esters and the generation of PVA-based glycopolymers was confirmed by ^{1}H NMR (**Figures 2.16** and **2.17**) with the disappearance of the intense peak from the CH2 group of chloroacetate at 4.3 ppm (denoted **t**) and the presence of characteristic new peaks, at 4.7, 4.5 and 4.3 ppm (marked as **w**, which then vanish upon addition of heavy water, see spectrum C in Figure 2.16 and Figure 2.17) and at 3.8 ppm attributed to hydroxyl protons and CH groups of PVA respectively. In the meantime, peaks a_1, b-f remained visible confirming the attachment of sugar units. Comparison of the integrations for the peaks h and k relative to the adipate spacer, of peaks a_1 (due to OH groups of glucose between 6 to 7 ppm) and of those ranging from 1 and 2 ppm corresponding the CH2 groups in the backbone (peaks o and u) and in the adipate spacer (peaks i and j) highlighted that the two esters linking the glucose units to the main chain are not impacted by such conditions of alcoholysis.

The ^{13}C NMR spectrum of the resulting materials after alcoholysis gave further evidence of the successful generation of PVA-based glycopolymers. As illustrated by **Figure 2.18**, the peak **m** at 168 ppm attributed to the pendant C=O group of PVClAc is no more visible after treatment and the observation of multiple new peaks ("**v**", from 63 to 69 ppm "**u**" at 48 ppm) confirmed the efficient alcoholysis of PVClAc. Consistent with the conclusions drawn from ^{1}H NMR analyses, characteristic peaks of the glucose-based repeating units remained clearly visible. Therefore, we assumed that PVA-based glycopolymer $P(VA)_{59}$-*co*-$(VAG)_9$ was obtained after alcoholysis at 0°C. Similar results were obtained for the other copolymers.

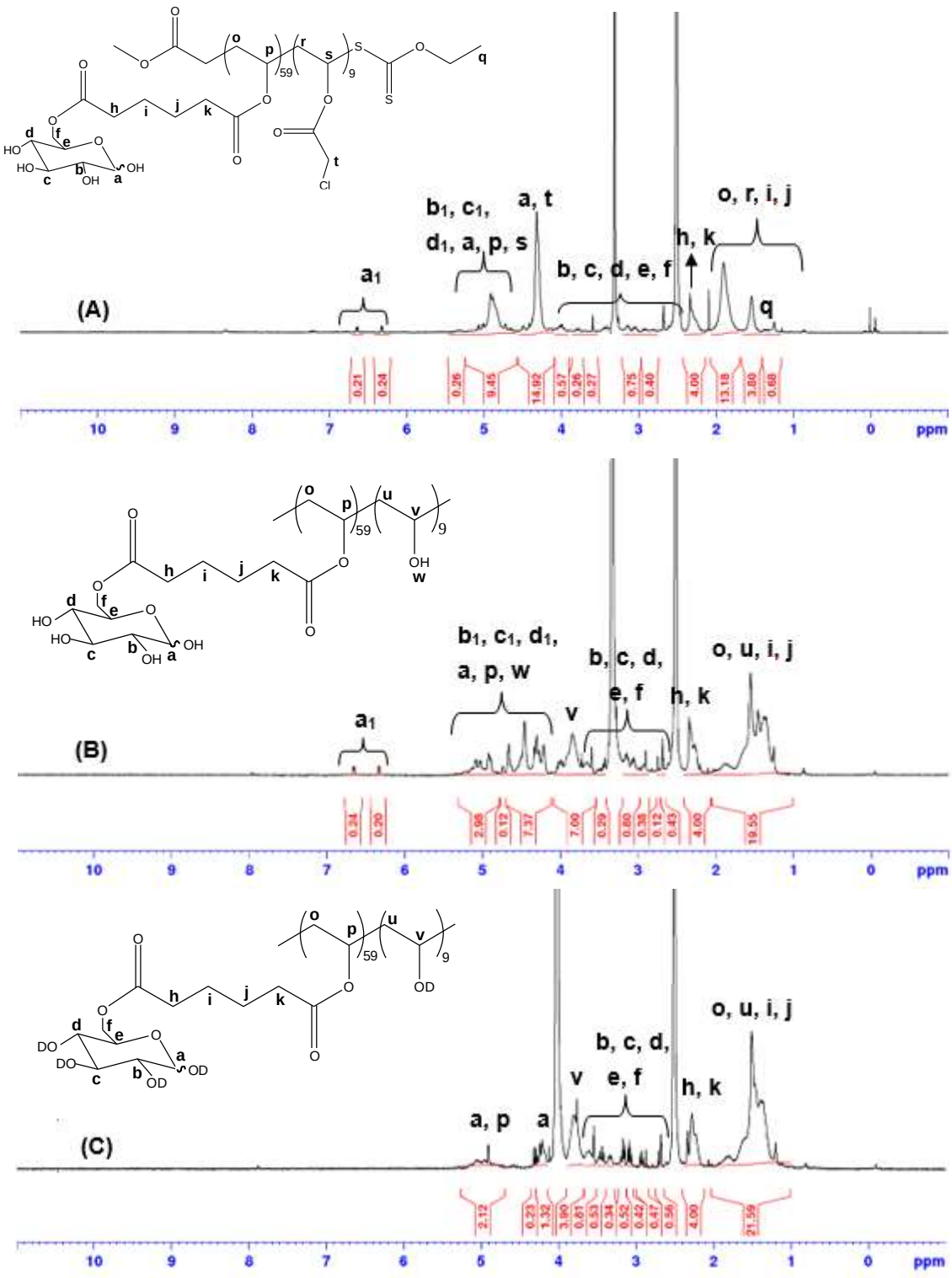

Figure 2.16: ^{1}H NMR spectra of (A) pure P(VClAc$_{59}$-*co*-VAG$_{9}$) in DMSO-d$_6$; (B) P(VA$_{59}$-*co*-VAG$_{9}$) in DMSO-d$_6$; (C) P(VA$_{59}$-*co*-VAG$_{9}$) in D$_2$O/DMSO-d$_6$. a$_1$, b$_1$, c$_1$, d$_1$ represent the corresponding hydroxyl peaks.

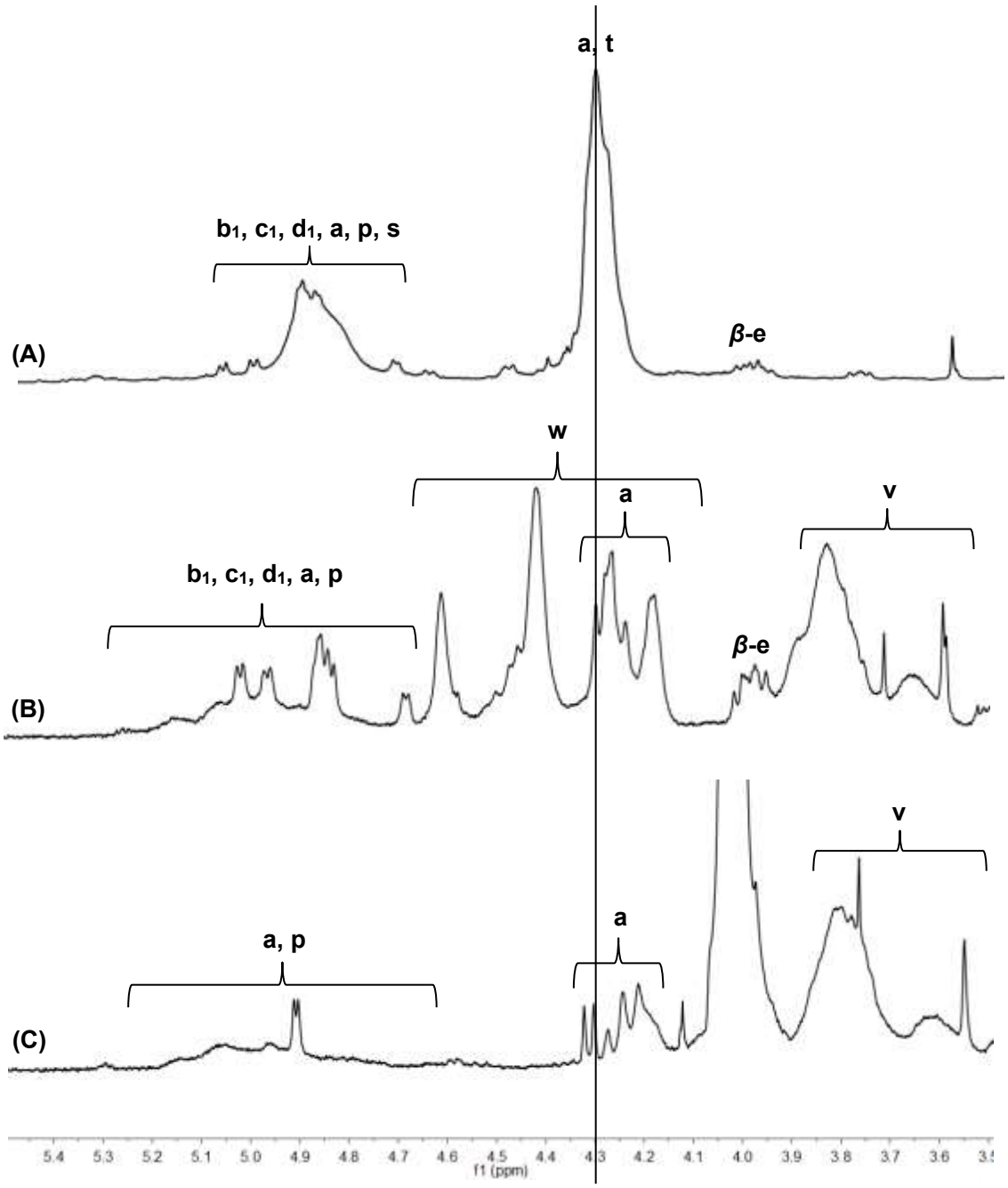

Figure 2.17: ^{1}H NMR spectra (3.5-5.5 ppm) of (A) P(VClAc$_{59}$-*co*-VAG$_9$) in DMSO-d$_6$, (B) P(VA$_{59}$-*co*-VAG$_9$) in DMSO-d$_6$ and (C) P(VA$_{59}$-*co*-VAG$_9$) in DMSO-d$_6$/D$_2$O (r. t.).

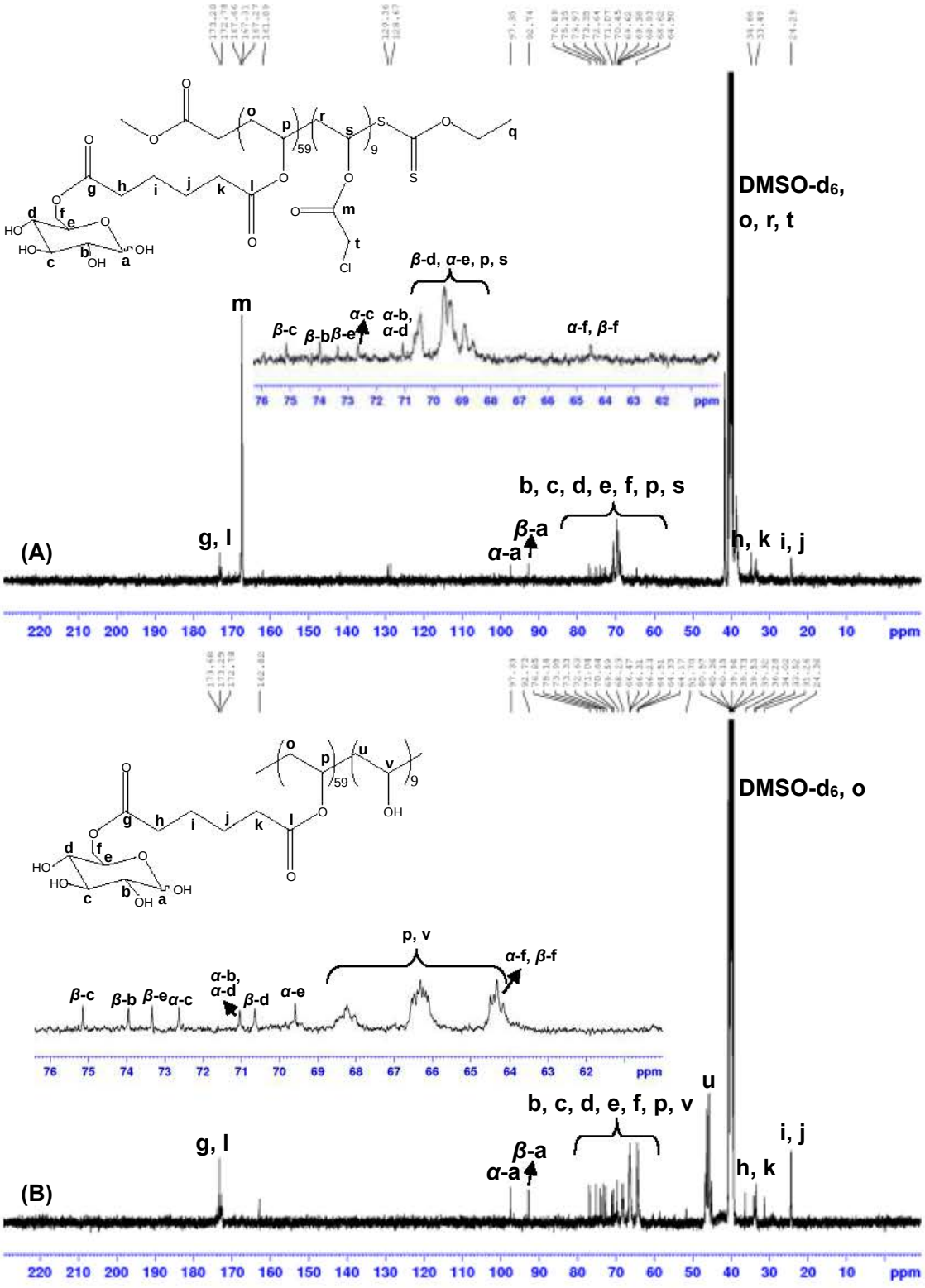

Figure 2.18: ^{13}C NMR of P(VClAc$_{59}$-*co*-VAG$_9$) (A) and P(VA$_{59}$-*co*-VAG$_9$) (B) (in DMSO-d$_6$, r. t.).

2.6.3 Water solubility of PVA-based glycopolymers

The solubility of the obtained homoglycopolymer and PVA-based glycopolymers in water was finally investigated by dynamic light scattering analysis (DLS) using aqueous solutions of copolymers at 1 mg/mL. The intensity-weighted and number-weighted size distributions for $PVAG_{60}$ and $P(VA_{117}$-*co*-$VAG_{10})$ solutions are given in **Figure 2.19**. These curves highlight a certain propensity of these two polymers to self-assemble in water (**Figure 2.19 A**, D_h= 321 nm and 284 nm). However, conversion into number-weighted size distribution clear shows that the number of free macromolecules (**Figure 2.19 B**, D_h=8 nm and 7 nm) is actually far bigger than that of the aggregates.

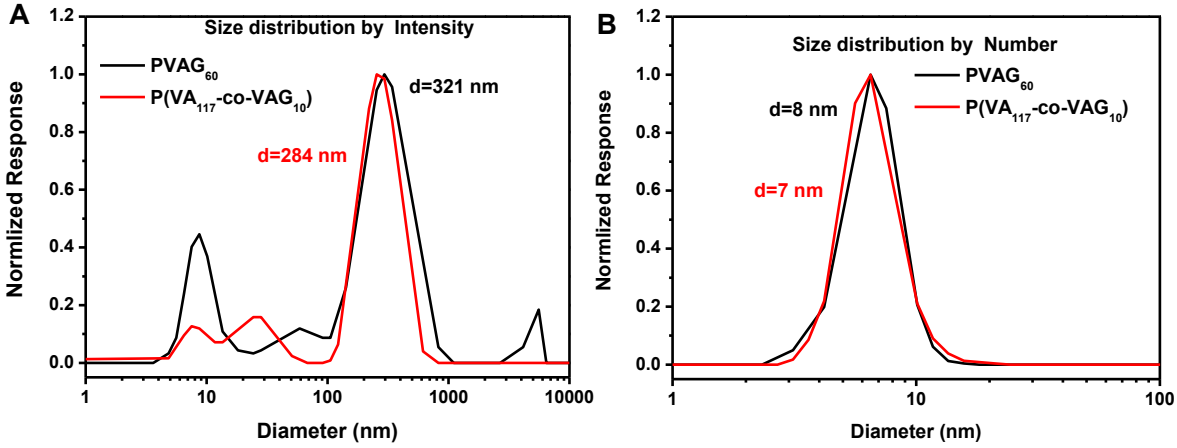

Figure 2.19: DLS of aqueous solution by (A) intensity size and (B) number size (1 mg/mL, 25 °C). Black solid: $PVAG_{60}$, red solid: $P(VA_{117}$-*co*-$VAG_{10})$.

DLS of aqueous solutions of $P(VA_{59}$-*co*-$VAG_9)$ and $P(VA_{34}$-*co*-$VAG_{19})$ underlined the presence of aggregates in **Figure 2.20 A**. However, contrary to $PVAG_{60}$ and $P(VA_{117}$-*co*-$VAG_{10})$, the presence of free macromolecules is no longer detected when converting into number-weighted size distribution. Instead, small aggregates (~15 nm) are then observed (**Figure 2.20 B**).

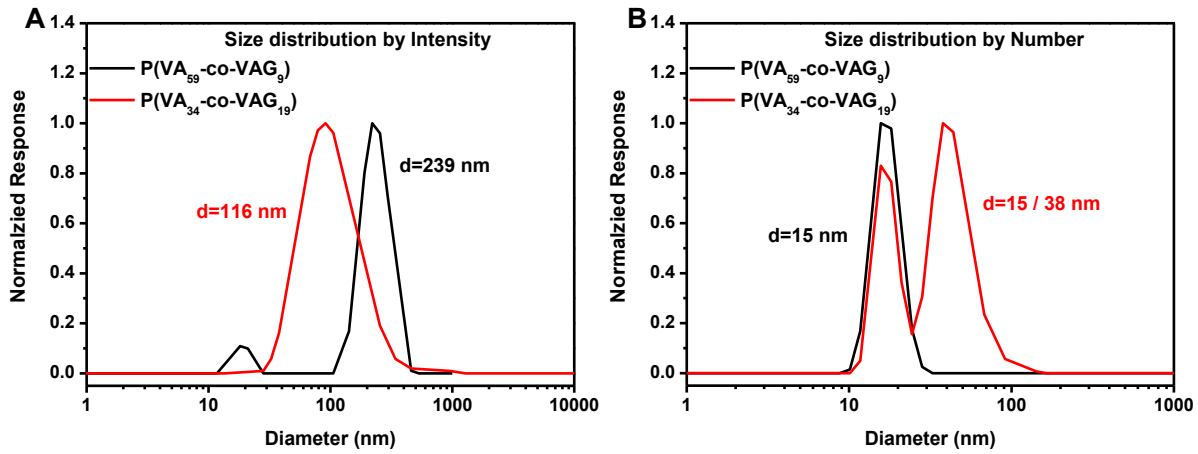

Figure 2.20: DLS of aqueous solution by (A) intensity size and (B) number size (1 mg/mL, 25 °C). Black solid: P(VA$_{59}$-*co*-VAG$_9$), red solid: P(VA$_{34}$-*co*-VAG$_{19}$).

2.7 Conclusions

In this chapter, we have prepared a series of PVClAc-based glycopolymers with tunable compositions by RAFT polymerization. After full characterization of these copolymers, we have sequentially explored the alcoholysis of PVClAc and PVAG homopolymers under mild conditions in order to convert PVClAc into PVA without impacting PVAG. Conditions enabling the selective removal of chloroacetate esters were found affording the synthesis of a series of water-soluble PVA-based glycopolymers from poly(VClAc-*co*-VAG) copolymers.

2.8 Reference

1. M. I. Baker, S. P. Walsh, Z. Schwartz and B. D. Boyan, *J. Biomed. Mater. Res. B: APPLIED BIOMATERIALS,* **2012,** 5, 1451-1457.
2. M. H. Christie and A. P. Nikolaos, *Polymers*, **2000**, 153, 37-65.
3. X. Yan, V. La Padula, S. Favre-Bonte, J. Bernard, *Eur. Polym. J.,* **2019**,112, 170–175.
4. R. H. Utama, Y. Jiang, P. B. Zetterlund and M. H. Stenzel, *Biomacromolecules,* **2015**, 16, 2144−2156.
5. H. Uyama and S. Kobayashi, *Chem. Lett.,* **1994**, 23*,* 1687-1690.
6. O. Kirk, F. Bjorkling, S. E. Godtredsen and T. O. Larsen, *Biocatalysis*, **1992**, 6, 127-134.
7. S. Shibatani and M. Kitagawa, Y. Tokiwa, *J. Pharm. Pharmacol*, **1995**, 47, 479-486.
8. M. Kitagawa, T. Tokiwa, H. Fan, T. Raku and Y. Tokiwa, *Biotechnol. Lett.,* **2000**, 22, 879-882.
9. M. Kitagawa, T. Raku, H. Shimakawa, H. Fan and Y. Tokiwa, *Macrom. Biosc.*, **2002**, 2, 233-237.
10. Y. Miura, T. Ikeda and K. Kobayashi, *Biomacromolecules*, **2003**, 4, 410-415.
11. L. Albertin; C. Kohlert, M. H. Stenzel, L. J. R. Foster and T. P. Davis, *Biomacromolecules,* **2004**, 5, 255-260.
12. Corpart et al., United States Patent, USOO6153705A, **2000**.
13. K. Matyjaszewski and R. Poli, *Macromolecules,* **2005**, 38, 8093.
14. M. L. Coote and D. J. Henry, *Macromolecules*, **2005**, 38, 1415.
15. M. H. Repollet-Pedrosa, R. L. Weber, A. L. Schmitt and M. K. Mahanthappa, *Macromolecules*, **2010**, 43, 7900-7902.
16. C. E. Lipscomb and M. K. Mahanthappa, *Macromolecules*, **2009**, 42, 4571–4579.
17. J. Bernard, A. Favier, L. Zhang, A. Nilasaroya, T. P. Davis, C. Barner-Kowollik and M. H. Stenzel, *Macromolecules,* **2005**, 38, 5475-5484.
18. A. Theis, T. P. Davis, M. H. Stenzel and C. Barner-Kowollik, *Polymer*, **2006**, 47, 999.
19. S. Harrisson, X. Liu, J-N. Ollagnier, O. Coutelier, J-D. Marty and M. Destarac, *Polymers*, **2014**, 6, 1437-1488.

20. M. H. Stenzel, L. Cummins, G. E. Roberts, T. P. Davis, P. Vana and C. Barner-Kowollik, *Macromol. Chem. Phys.*, **2003**, 204, 1160–1168.
21. J. Bernard, A. Favier, T. P. Davis, C. Barner-Kowollik, M. H. Stenzel, *Polymer*, **2006**, 47, 1073–1080.
22. L. S. Peixoto, P. A. Melo, M. Nele, J. C. Pinto, *Macromol. Mater. Eng.***, 2009**, 294, 463-471.
23. L. L. C. Olijve, M. M. R. M. Hendrix, I. K. Voets, *Macromol. Chem. Phys.*, **2016**, 217, 951−958.
24. M. H. Repollet-Pedrosa, R. L. Weber, A. L. Schmitt and M. K. Mahanthappa, *Macromolecules*, **2010**, 43, 7900–7902.
25. B. Bjorkqvist, *J. Chromatogr.,* **1981**, 218, 65-71.
26. D. Mondal, G. G. Zhanel and F. Schweizer, *Carbohydr. Res.*, **2011**, 346, 588-594.

Chapter 3

Rapid Access to Functional Oil-Filled Poly(vinyl alcohol)-based Glyconanocapsules through Nanoprecipitation

Chapter 3 Rapid Access to Functional Oil-Filled Poly(vinyl alcohol)-based Glyconanocapsules through Nanoprecipitation

3.1 Introduction

Establishment of water/acetone/oil and water/acetone/polymer phase diagrams enables to identify conditions of solvent shifting where oil-filled polymer nanocapsules can be straightforwardly built without recoursing to ultra-sonication or high shear force. As discussed in Chapter 1, this simple and rapid one-pot process has been lately exploited by our group to generate nanocapsules of tunable dimensions and functionality using a range of water-soluble polymers (methacrylamide-based glycopolymers, PHPMA, polysaccharides) and of oils (hexadecane, miglyol 812…). In this chapter, we will explore the nanoprecipitation technique with the aim of preparing oil-filled nanocapsules from commercial PVA and the RAFT-made PVA-based glycopolymers described in the Chapter 2. Functionalization of the PVA-based shell and loading of the core with actives will be investigated.

3.2 Preparation of PVA-based nanocapsules (PVA-NCs)

Commercial PVAs are typically obtained from poly(vinyl acetate) precursors through hydrolysis reactions which are not run to completion. By definition, these polymers are thus copolymers of PVA and PVAc. For a given molecular weight, the water-solubility of PVA is significantly influenced by the content in acetate. PVA grades exhibiting low acetate content (Degree of Hydrolysis DH ~ 90% or more) display relatively poor solubility in water at room temperature owing to multiple intra and inter-molecular H-bonding interactions promoted by the hydroxyl groups.[1] The dissolution of the polymers can however be greatly enhanced by increasing the temperature. In the present study, we will focus on two commercial PVA, Mowiol 4-88 (M_w~31 kDa, DP_n≈630, DH≈88%) and Mowiol 8-88 (M_w~67 kDa, DP_n≈1400, DH≈88%) from Aldrich, that can be readily dissolved in water at room temperature. PVA aqueous solutions were prepared at 1 mg/mL and stirred for one day at room temperature before analyses by

DLS (**Figure 3.1**). On the basis of these analyses, we drew the conclusion that most of the PVA chains exist as unimers in water (number-weighted hydrodynamic diameter around 10 nm for Mowiol 4-88 and Mowiol 8-88).

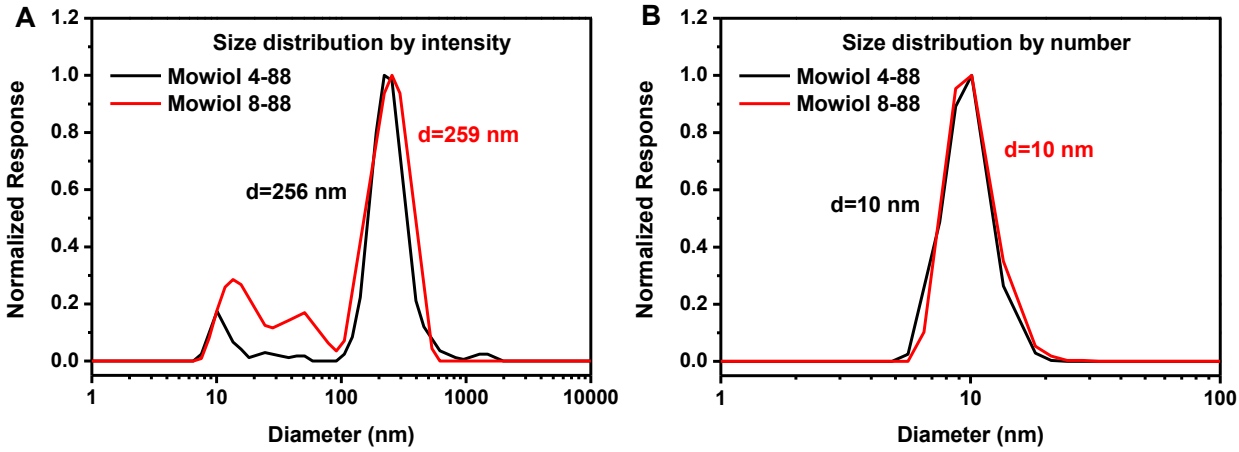

Figure 3.1: DLS of aqueous solution by (A) intensity size distribution and (B) number size distribution (1 mg/mL, 25 °C).

3.2.1 Cloud point boundary of PVAs

To find ideal conditions of solvent shifting for the construction of PVA-based nanocapsules, we first determined the cloud point boundary of PVA (Mowiol 4-88 and 8-88)/acetone/water ternary systems by titrating aqueous solutions of polymer (at different concentrations) with acetone (incorporated dropwise) until the solution turned milky owing to the precipitation of the PVA.

The results of the titration are plotted in **Figure 3.2**. Between 10^{-2} and 10^{-5} polymer mass fraction, Mowiol 8-88 chains started precipitating when the content of acetone was higher than 54 wt % whereas a further enrichment in acetone (61 wt% acetone) was required to initiate the precipitation of Mowiol 4-88 chains. Similar to previous studies on vinyl-based glycopolymers, poly(2-(N-hydroxypropyl) methacrylamide) or polysaccharides/acetone/water ternary systems,[2,3] the cloud point boundary for Mowiol 4-88 and 8-88 can be represented as a straight line at constant acetone mass fraction. Note though

that these boundaries should be manipulated with caution in the case of PVAs owing their large molecular weight distributions. The propensity of the chains to collapse upon addition of the non-solvent (here acetone) is indeed directly related to their molecular weights. Whereas highest molecular weight chains precipitate at the cloud point boundary, it is necessary to proceed to the solvent shifting well above the cloud point boundary to precipitate the whole PVA chains.

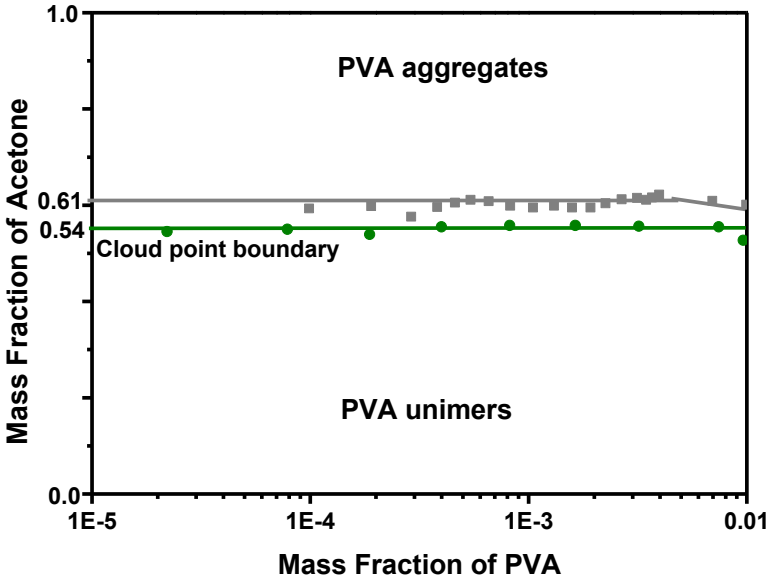

Figure 3.2: Phase diagrams of PVA/water/acetone ternary systems at room temperature. ■ Mowiol 4-88, ●Mowiol 8-88.

3.2.2 Phase diagrams for the preparation of PVA-based NCs

We recently established the phase diagram of hexadecane/water/acetone and miglyol/water/acetone ternary systems and identified the domains of composition, e.g. Ouzo and Surfactant-Free MicroEmulsion domains, where metastable or thermodynamically stable dispersions of oil nanodroplets with narrow size distribution can be produced by nanoprecipitation (**Figure 3.3**).[4,5] In these regions, dimensions of the droplets can be further modulated by varying acetone and/or oil mass fractions. Outside of these domains (see the

right part of the diagram), solvent displacement is expected to produce unstable dispersions where the oil rapidly demixes. Note that above 80 wt% acetone, no microstructuring was observed in hexadecane/water/acetone systems.

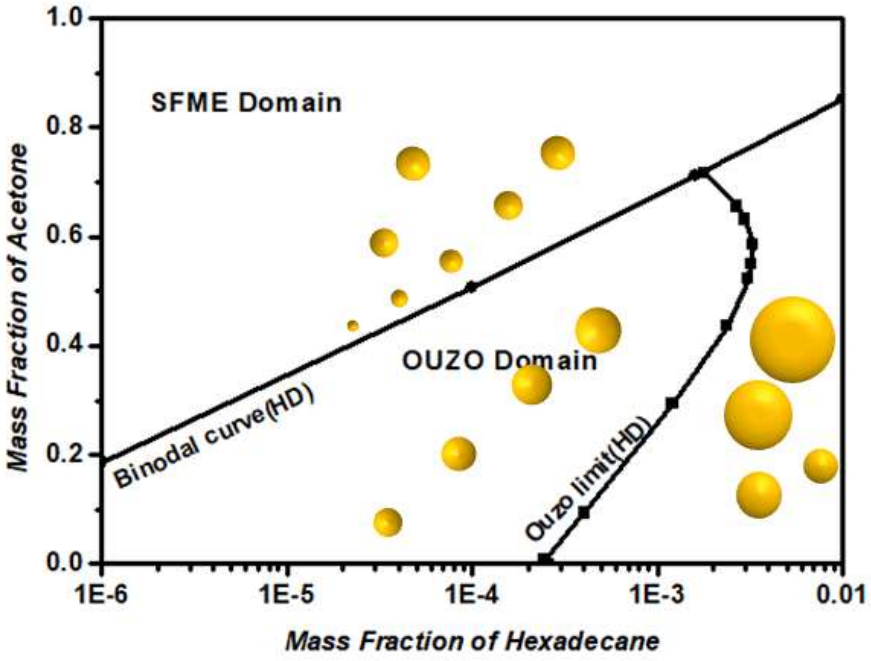

Figure 3.3: Phase diagram of HD in water/acetone ternary system.

After overlapping of PVA/water/acetone phase diagram and HD/water/acetone phase diagram, the conditions to possibly build nanocapsules were identified, see **Figure 3.4**. 6 regions can be clearly distinguished. Below the cloud point boundary of PVA (regions a-c, Figure 3.4), no nanocapsule can be theoretically formed as the conditions promoting the precipitation of the PVA chains and their adsorption at the interface are not attained. Above the cloud point boundary, we anticipated that monodisperse nanocapsules could be generated in the regions d and f corresponding to the SFME and Ouzo domains where concomitant generation of emulsion nanodroplets and adsorption of PVA chains are promoted. In the following, we initially focus on the construction of nanocapsules in the Ouzo domain (region f, Figure 3.4).

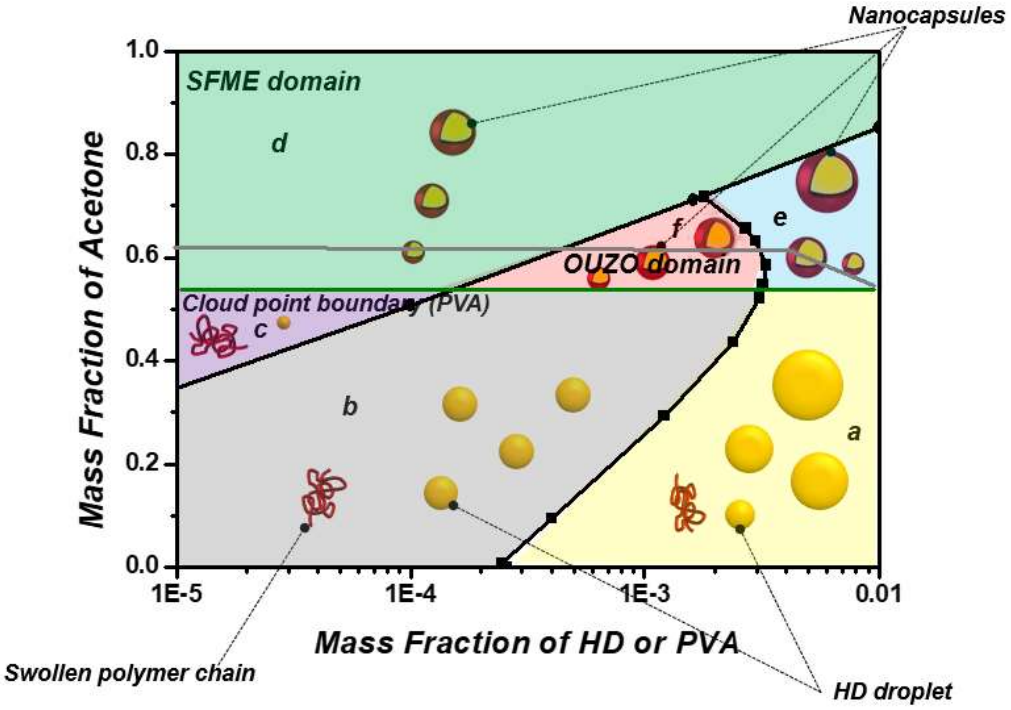

Figure 3.4: Polymer/HD/water/acetone phase diagram after overlapping of phase diagrams of polymer and HD in water/acetone mixture.

3.2.3 Preparation of nanocapsules with varying PVA/HD ratios

We primarily explored the nanoprecipitation in the Ouzo domain without having recourse to cross-linking agents to “stabilize” the adsorbed PVA shell. Practically, the oil (HD) was first dissolved in acetone (1.5 mg in 670 mg) and an aqueous solution of PVA (0.15, 0.75 or 1.5 mg Mowiol 4-88 in 330 mg of water) was next poured into the organic solution all at once. The solutions immediately turned milky after solvent shifting and were left overnight before analyses. The dispersions were further investigated by TEM and DLS (**Figure 3.5**). At polymer/oil weight ratios equal to 1:1 and 1:2, TEM analyses revealed the formation of ill-defined capsular systems with a diffuse polymer shell (**Figure 3.5 A**, **B**). The diameters of these nano-objects were around 270 and 210 nm, respectively. Importantly, such nanostructures co-existed with a myriad of nanoparticles of PVA (see dark dots on Figure 3.5 A, B) indicating that under such conditions, a non-negligible fraction of the PVA chains remain in solution

after solvent shifting and finally self-assemble upon casting on the TEM grids. DLS analyses also revealed the formation of one population with a *z*-average diameter above one micron (around 1400 nm) for both systems. In contrast, when the content of PVA was reduced to 0.15 mg (vs 1.5 mg HD), no nanoparticle of PVA was detected and smaller nanocapsules were observed. Accordingly, the *z*-average diameter dropped to 430 nm (Figure 3.5D). Unfortunately, the dialysis of the dispersion against water finally resulted in the destruction of the nanocapsules owing to the progressive redissolution of the non-crosslinked PVA shell (in the absence of acetone), see **Figure 3.6**.

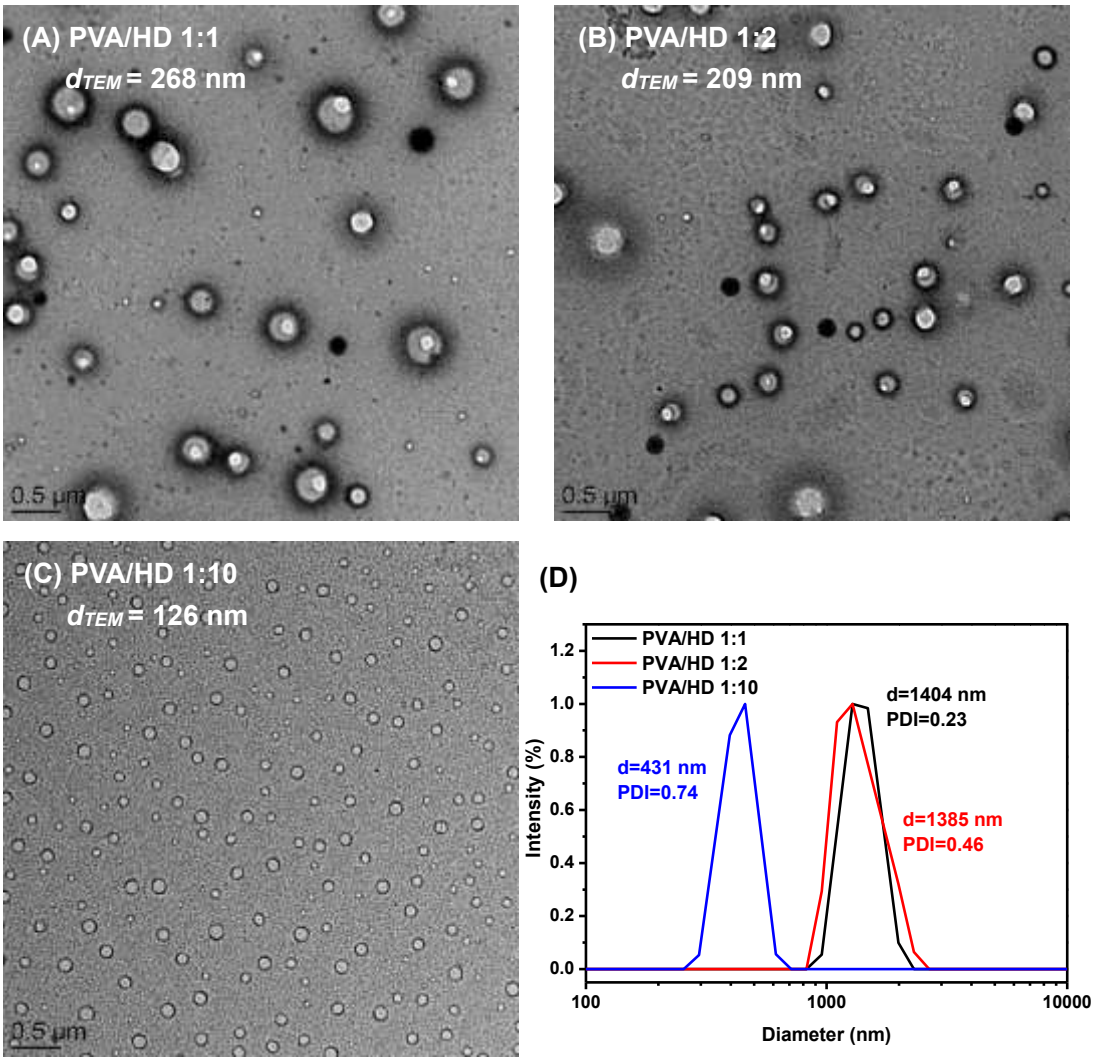

Figure 3.5: TEM images of Mowiol 4-88-based NCs prepared by nanoprecipitation at 0.67 acetone fraction using HD (1.5 mg). PVA/HD weight ratio (A) 1:1; (B) 1:2 and (C) 1:10. (D) DLS of the dispersions at different PVA/HD weight ratios.

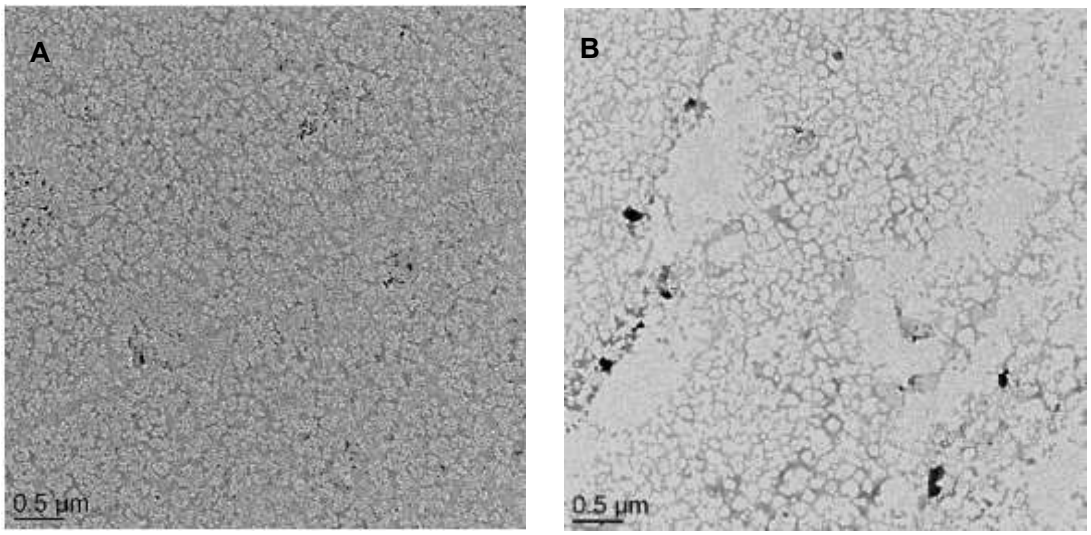

Figure 3.6: TEM images of (A) Mowiol 4-88 aqueous solution (1 mg/ml) and (B) PVA-NCs in pure water after removal of acetone (Mowiol 4-88: 0.15 mg, HD: 1.5 mg).

3.2.4 Preparation of shell cross-linked PVA-NCs

In order to build PVA-based nanocapsules exhibiting a good stability in water, we further developed a method allowing for constructing nanocapsules as previously described and concomitantly crosslinking the polymer chains adsorbed at the interface.

3.2.4.1 Preparation of shell cross-linked Mowiol 4-88-NCs

To do so, we implemented the nanoprecipitation process described above (0.15 mg of PVA, 1.5 mg of HD, 0.67 acetone mass fraction) in the presence of isophorone diisocyanate (IPDI), a cross-linking agent which is soluble in the oil but not in water and displays very low sensitivity towards water (**Scheme 3.1**).

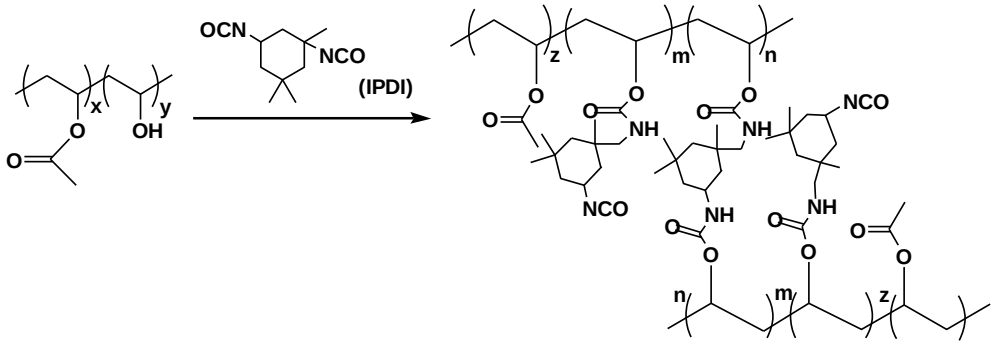

Scheme 3.1: Chemical reaction of IPDI with hydroxyl groups of PVA ensuring the stabilization of the polymer membrane.

In explorative experiments, tunable amounts of IPDI (ranging from 0.01 to 0.40 equivalent per PVA hydroxyl group) were incorporated in the initial organic phase to ensure the progressive cross-linking of the PVA shell (from the inner to the outer part of the shell). After solvent shifting, the dispersion was left overnight at room temperature before characterization by TEM and DLS.

As evidenced by the TEM pictures given in **Figure 3.7**, the morphology steadily evolved from core-shell structures having a very diffuse polymer corona mixed with small PVA nanoparticles (**Figures 3.7 A** and **B**) to clean robust spherical nanocapsules (**Figures 3.7 E**). Consistent with the increase of cross-linking agent content, the membrane of the nanocapsules progressively shrank to become relatively thin and dense owing to the formation of multiple cross-linkages between PVA chains.

These observations were also corroborated by DLS measurements (**Figure 3.8**), which confirmed that an enrichment of the organic phase in IPDI was accompanied by a reduction of the z-average diameter and a sharpening of the size distribution, D_z=562 nm and PDI=0.47 *vs* D_z=211 nm and PDI=0.17 using 0.01 and 0.4 equivalent of IPDI respectively.

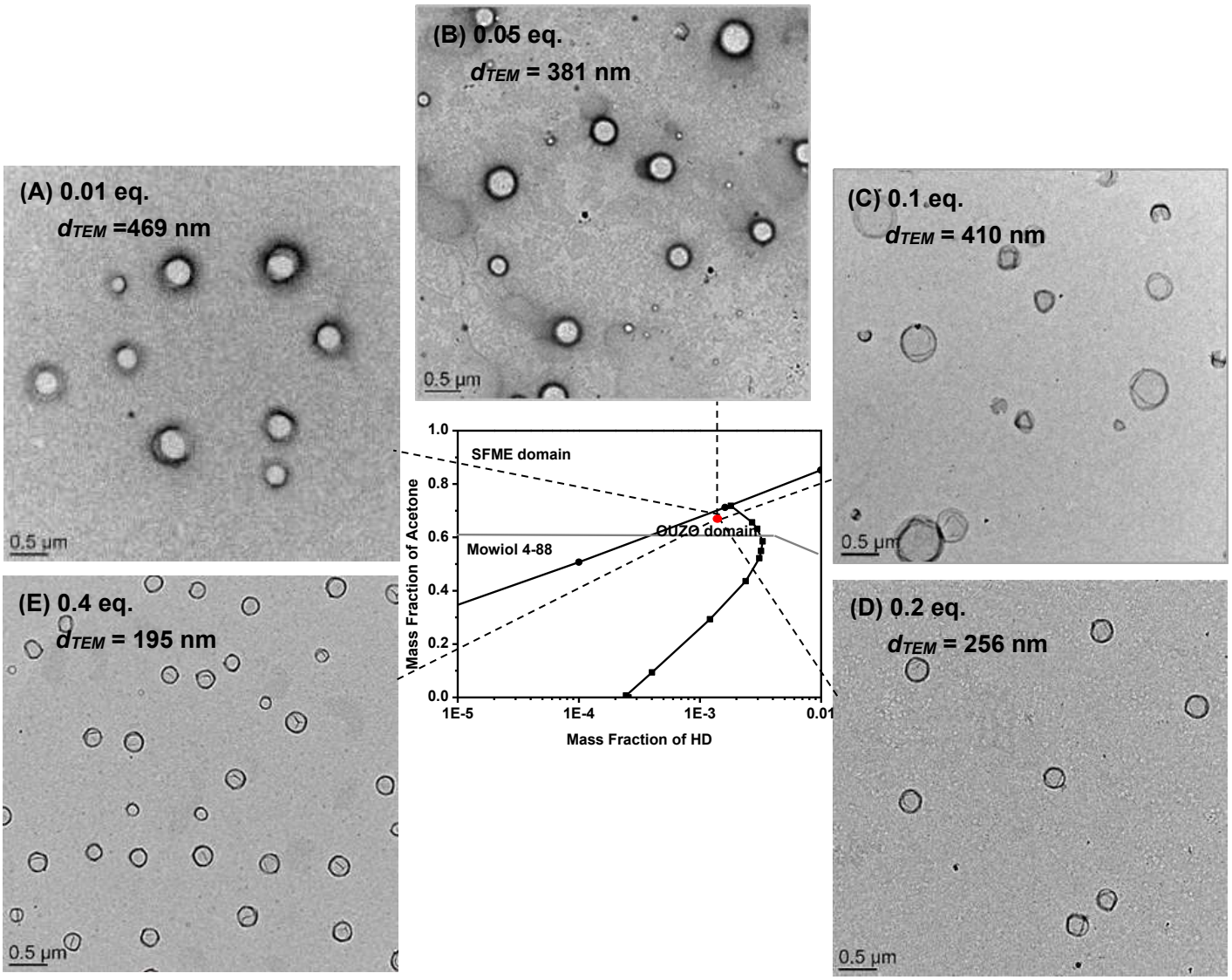

Figure 3.7: Mowiol 4-88-NCs prepared with tunable amounts of IPDI: 0.006 mg (0.01 eq, **A**), 0.03 mg, (0.05 eq, **B**), 0.06 mg, (0.1 eq, **C**), 0.12 mg (0.2 eq, **D**) and 0.24 mg (0.4 eq, **E**) of IPDI.

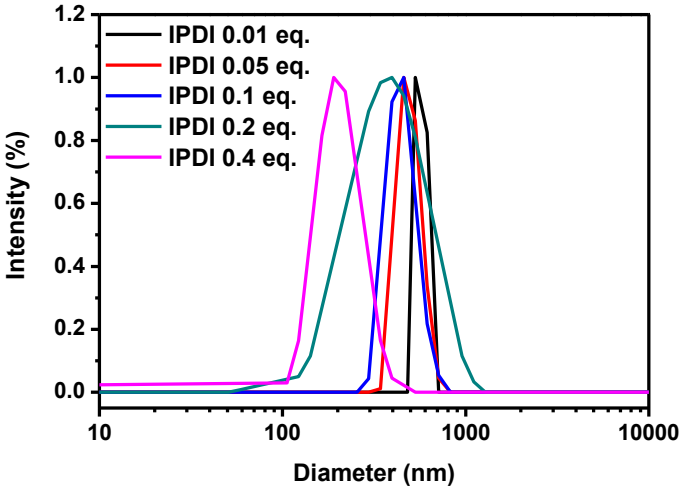

Figure 3.8: DLS traces of Mowiol 4-88-NCs (in acetone/water mixtures) prepared with varying contents of IPDI. 0.01 eq. IPDI: dz=562 nm, PDI=0.47; 0.05 eq. IPDI: dz=492 nm, PDI=0.39; 0.1 eq. IPDI: dz=452 nm, PDI=0.35; 0.2 eq. IPDI: dz=407 nm, PDI=0.21; 0.4 eq. IPDI: dz=211 nm, PDI=0.17.

Dispersions of the shell cross-linked nanocapsules were next dialyzed against water to remove acetone. Contrary to IPDI-free nano-objects which, as mentioned earlier, are rapidly degraded in aqueous medium, the elimination of acetone had no impact on the integrity of the cross-linked nanocapsules (see TEM picture in **Figure 3.9 B**). A slight increase of the hydrodynamic diameter was however observed (211 nm in acetone/water mixture *vs* 251 nm after dialysis) owing to the enhanced swelling of the PVA shell in pure water.

The dispersions were finally freeze-dried and subsequently re-dispersed in water at room temperature. As illustrated by TEM (see **Figure 3.9 C**), nanocapsules are still visible after the freeze-drying procedure but undefined domains, possibly HD domains and parts of broken membranes can also be distinguished. These results suggest that higher degrees of cross-linking or other post-treatments (as freeze-thaw cycles that promote crystallization of the PVA chains) are however required to further improve the robustness and make PVA-based nanocapsules suitable for freeze-drying.

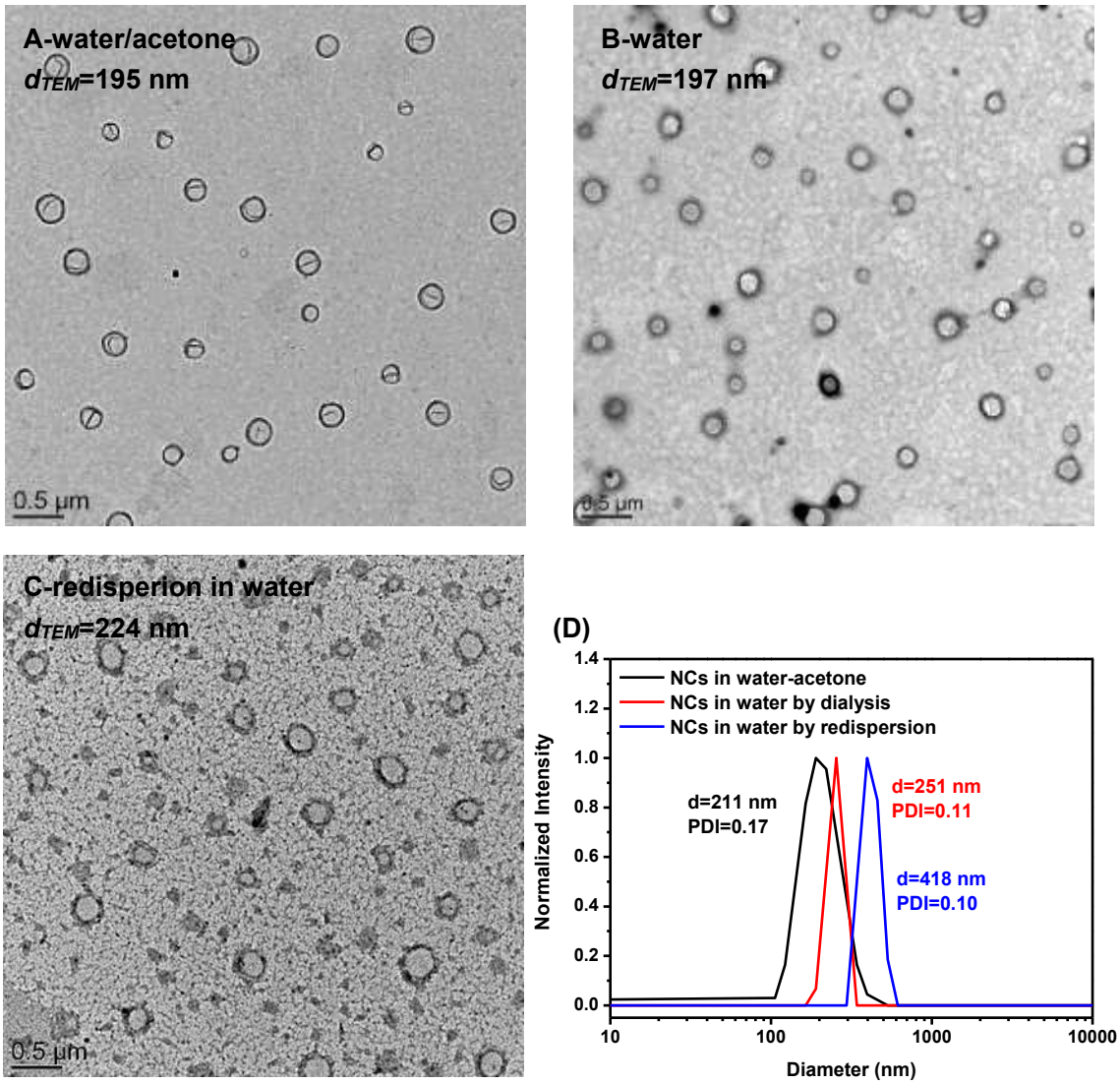

Figure 3.9: TEM images of HD-filled Mowiol 4-88-based nanocapsules cross-linked with 0.4 eq. of IPDI (nanoprecipitation undertaken with 0.15 mg of Mowiol 4-88 at 0.67 acetone mass fraction. (A) nanocapsules in water-acetone mixture; (B) nanocapsules in pure water after removal of acetone by dialysis; (C) nanocapsules after freeze-drying to remove water and redispersion in water; (D) DLS of the dispersions.

In order to investigate the versatility of this route to oil-filled PVA nanocapsules, solvent shifting experiments were subsequently performed in the domains d (SFME) and e by varying the concentration of oil (see **Figure 3.10 A** and **B**). As previously reported, solvent shifting in the SFME domain (0.70 acetone mass fraction, 0.15 mg of PVA, 0.1 mg HD and 0.4 eq. of IPDI) resulted in the

preparation of sub-200 nm spherical nanocapsules with narrow size distribution. To our great surprise, relatively well-defined nanocapsules (diameters below 300 nm and PDI =0.20!) were also obtained in the domain e where oil droplets are usually rapidly destabilized. Note though that under such conditions of solvent shifting, large domains of HD were also spotted (data not shown).

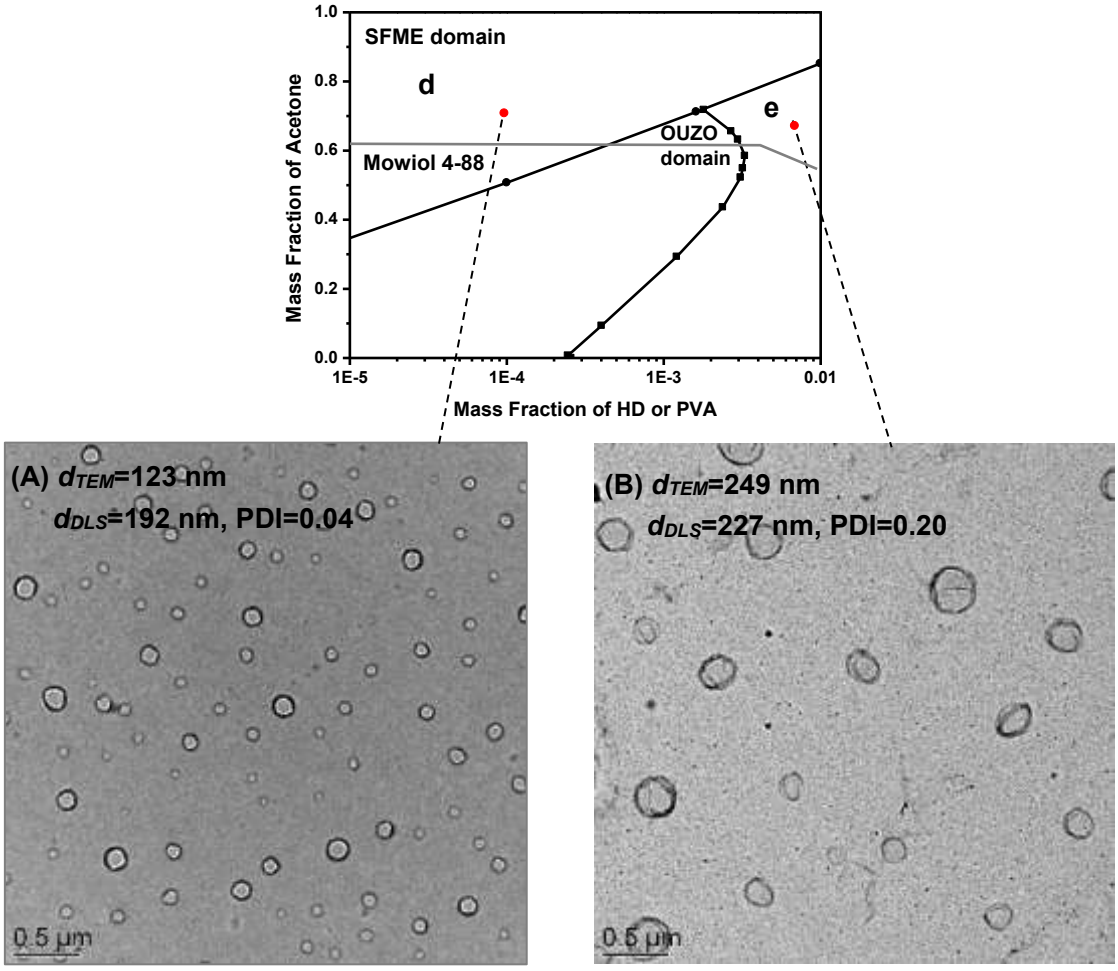

Figure 3.10: Morphologies observed for Mowiol 4-88-NCs in different domain with PVA 0.15 mg and 0.4 eq. of IPDI. (A) acetone mass fraction 0.7, HD 0.1 mg; (B) acetone mass fraction 0.67, HD 7 mg.

3.2.4.2 Preparation of shell cross-linked M8-88-NCs

The preparation of Mowiol 8-88 nanocapsules was initially studied in the Ouzo domain using the same conditions as the one established for Mowiol 4-88 (0.15 mg of PVA, 1.5 mg of HD, 0.4 eq/OH of IPDI and 0.67 acetone mass fraction). Unfortunately, we found out that at this polymer concentration, the PVA chains were not prone to adsorb quantitatively at the interface as evidenced by the concomitant presence of dark dots of pure PVA nanoparticles, see **Figure 3.11 A**. This issue was overcome by reducing the content in Mowiol 8-88 to 0.05 mg (PVA/HD 0.03:1) in the initial aqueous phase. By doing so, monodisperse spherical nanocapsules were prepared (D_z=279 nm, PDI=0.13) and the second population due to pure PVA nanoparticle was no longer observed (**Figure 3.11 B**). To explore other regions of the Ouzo domain, we examined nanoprecipitations at 0.55 and 0.60 acetone mass fraction in the presence of 0.7 or 1.5 mg of HD. Whereas nanocapsules were conveniently built at 0.60 acetone mass fraction, we failed at synthesizing PVA-based nanocapsules at lower acetone mass fraction (0.55) owing to the incomplete precipitation of the PVA chains close to the cloud point boundary.

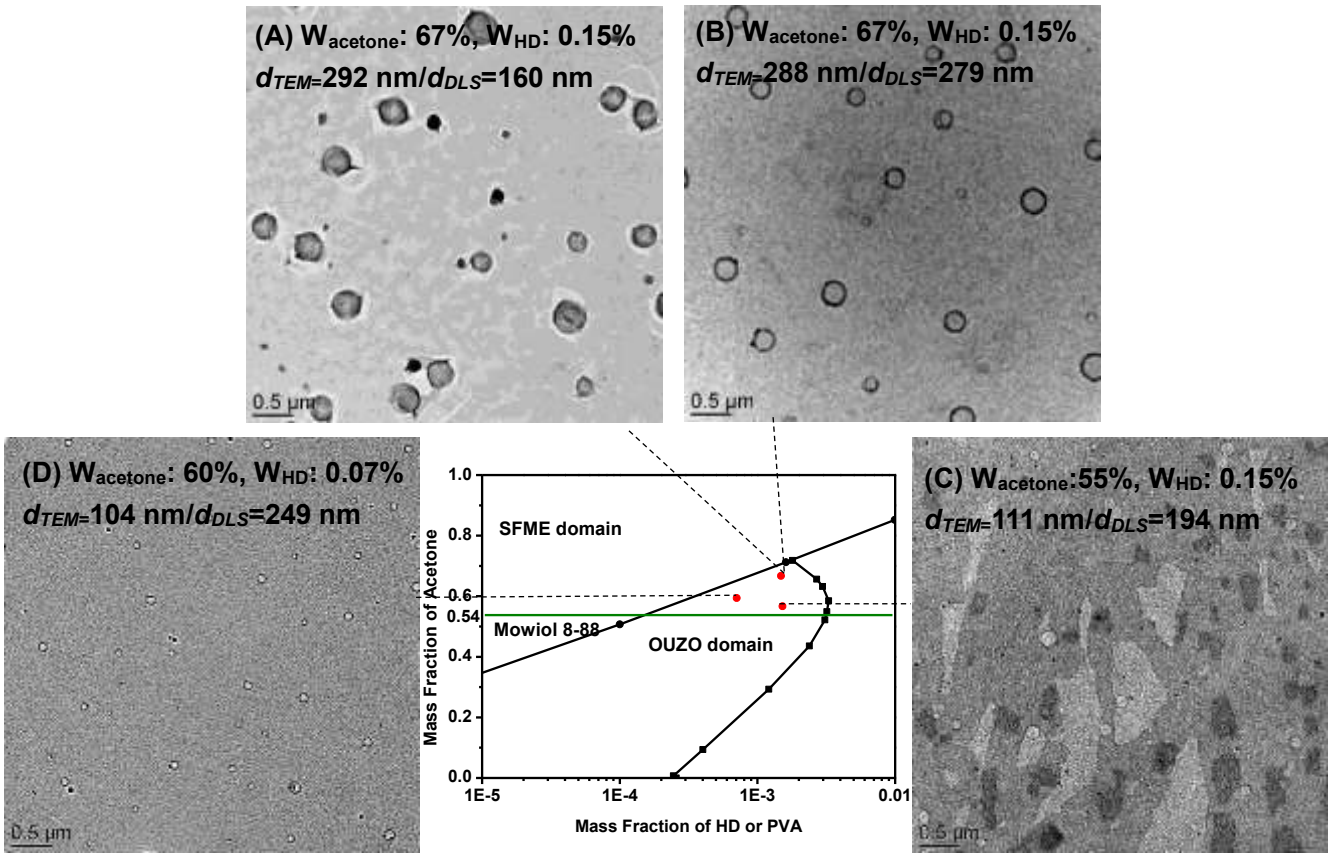

Figure 3.11: TEM images of nanocapsules prepared in the Ouzo domain with 0.4 eq. of IPDI and (A) Mowiol 8-88 0.15 mg; (B-D) Mowiol 8-88 0.05 mg.

Next, we investigated the preparation of Mowiol 8-88-based nanocapsules in the SFME domain with a particular emphasis on the influence of acetone mass fraction on the dimensions of the resulting nanocapsules (**Figure 3.12**). In a previous work dealing with water/oil/acetone ternary systems, we reported that, thermodynamically stable heterogeneities can be formed in the SFME domain (adjacent to the Ouzo domain) and that the dimensions of these aggregates can be precisely adjusted by tuning the acetone mass fraction. We also demonstrated that these heterogeneities can be used as templates for the generation of nanocapsules with controlled dimensions.

For a given oil content (established here at 0.01 wt%), the increase of the acetone mass fraction from 0.6 to 0.8 resulted in a gradual growth of nanocapsules dimensions (size ~ 236, 277 and 340 nm at 0.6, 0.7 and 0.8

acetone mass fraction respectively, see **Figure 3.12 A, B, C**). On the contrary, the dimensions of the nanocapsules remained more or less constant for a given acetone/water composition (size ~ 259, 277 and 289 nm at 0.001, 0.01 and 0.05 wt% HD and 0.6 acetone mass fraction, see **Figure 3.12 B, D** and **E**). This is in full agreement with the results obtained in the SFME domain with PHPMA and vinyl-based glycopolymers.[5,6]

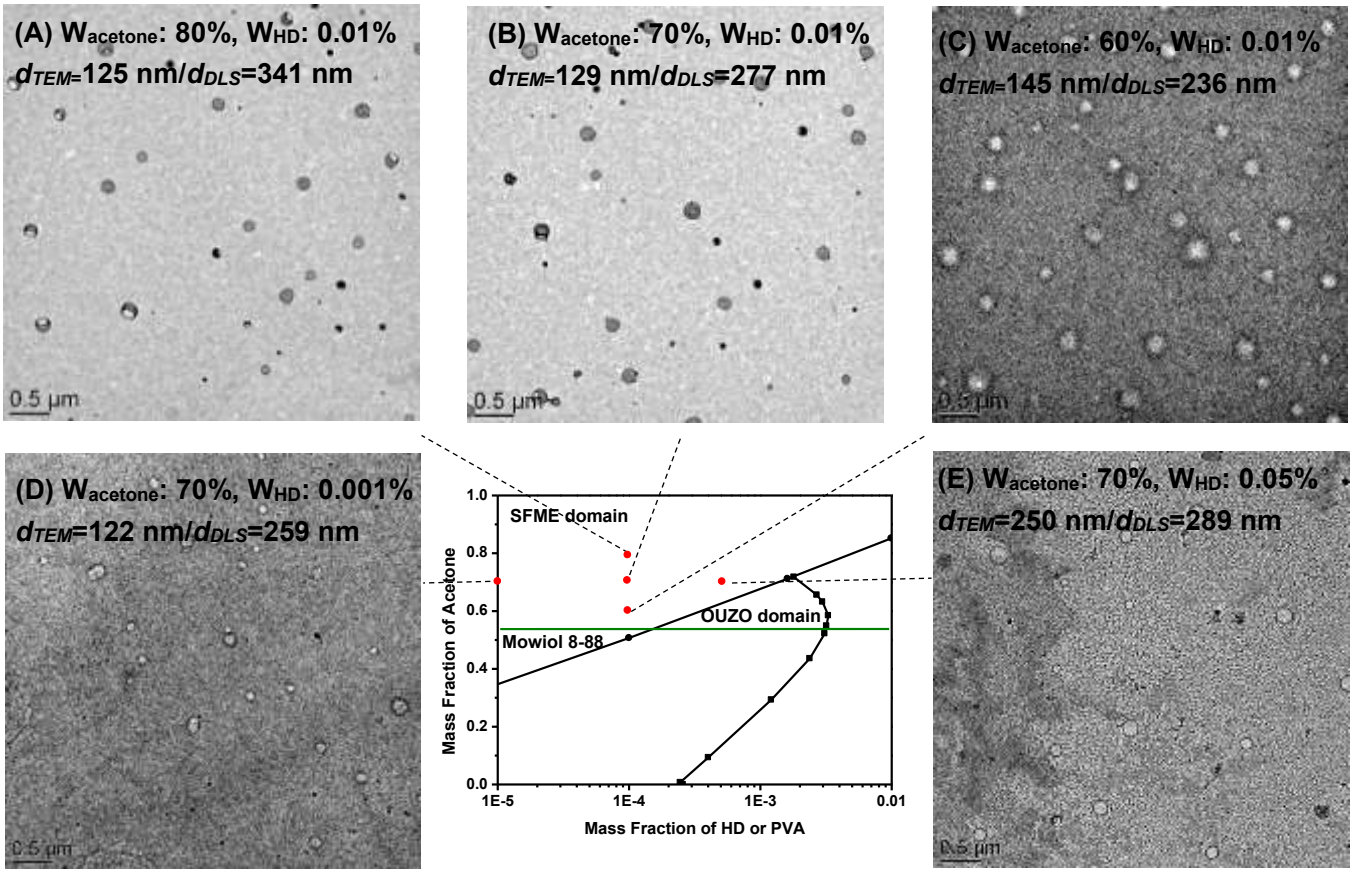

Figure 3.12: TEM images of nanocapsules prepared in the SFME domain with Mowiol 8-88 0.05 mg and IPDI 0.4 eq. Oil content and acetone mass fraction within the images. d_{DLS} and d_{TEM} were obtained from DLS measurements and image processing.

To improve the biocompatibility of the resulting nanocapsules, we further attempted to replace HD by miglyol, a FDA approved triglyceride used in numerous pharmaceutical formulations. After the overlap of PVA/water/acetone and miglyol/water/acetone phase diagrams, a very tiny OUZO region was

observed (acetone content from 0.54 to 0.6 vs 0.54 to 0.7 in HD/water/acetone phase diagram). As illustrated by Figure **3.13** (see TEM picture and DLS analyses of the dispersions), solvent shifting at 0.57 acetone mass fraction, using miglyol (at 0.05 wt%) as oil, Mowiol 8-88 as polymer (0.05 mg) and IPDI as cross-linking agent (0.4 eq per hydroxyl group) afforded the preparation of the miglyol-filled nanocapsules with a z-average diameter ~ 380 nm and a size distribution ~ 0.15.

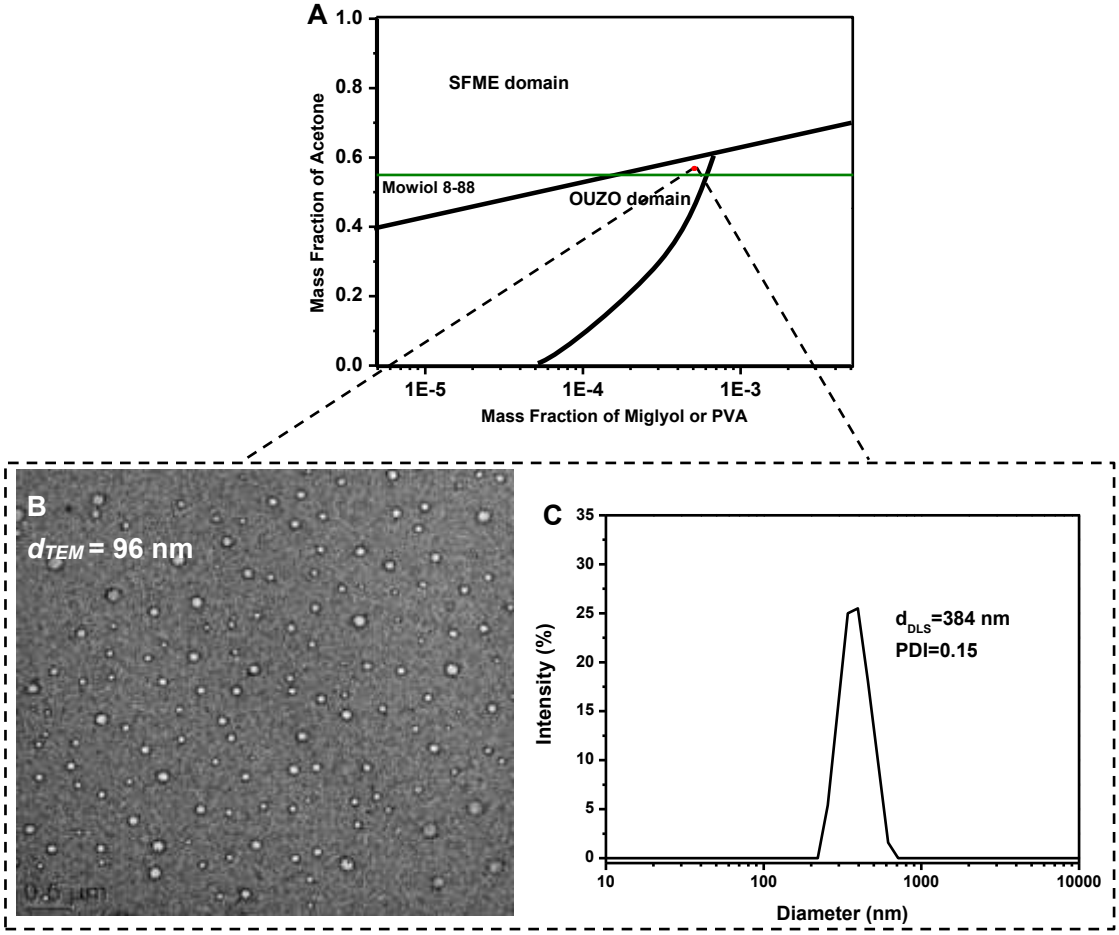

Figure 3.13: (A) Overlapped phase diagram of Mowiol 8-88 and miglyol; (B) TEM image of miglyol-filled Mowiol 8-88 NCs; (C) DLS plot of miglyol-filled Mowiol 8-88 NCs. Nanoprecipitation: Mowiol 8-88: 0.05 mg, Miglyol: 0.5 mg, IPDI: 0.4 eq./OH, acetone mass fraction: 0.57.

3.2.5 Salting out procedure for strengthening PVA membranes of NCs

Earlier in the chapter, we have shown that stable oil-filled nanocapsules can be built from PVA by nanoprecipitation provided that the solvent shifting is performed in the appropriate regions of the phase diagram (e.g. in Ouzo or SFME domains) and that a certain amount of cross-linking agent (at least 0.2 equivalent of IPDI per hydroxyl group) is initially incorporated in the organic phase. With respect to biomedical applications, it would be of great interest to minimize (or ideally to avoid) the use of potentially toxic diisocyanates. With that aim, we further examined the salting out procedure as a possible mean to promote the formation of additional physical cross-linkages between PVA chains (through dehydration of the PVA and establishment of intra and intermolecular interactions) and enhance the stability of the membranes in aqueous solutions. To do so, we relied on previous works of Zhu, Orhun and particularly Zelikin who reported the preparation of hydrogels from low molar mass PVA chains at low concentrations (2 wt%) by addition of a kosmotropic salt, i.e. Na_2SO_4 (at 0.5 or 1M) and a time of stabilization ~24 h.[7,8,9]

The “salting out” procedure was thus carried out as follows: after preparation of nanocapsules by solvent shifting as previously described (0.15 mg of Mowiol 4-88, 1.5 mg of HD, water/acetone 330 mg/670 mg and 0, 0.01 or 0.1 equivalent of IPDI), the dispersions were first dialyzed against Na_2SO_4 aqueous solution (0.5 M) for 24h and finally against water for 24h. As shown in **Figure 3.14**, PVA-based nanocapsules were visualized in all acetone/water dispersions whatever the content of IPDI. However, in the absence of IPDI, nanocapsules did not survive to dialysis against water or TEM analysis (**Figure 3.14 B**) suggesting that Na_2SO_4 alone is not capable to efficiently stabilize the PVA membranes in aqueous solutions. On the contrary, initial incorporation of IPDI within the organic phase afforded the preparation of nanocapsules capable to tolerate 100%

aqueous environments, see **Figures 3.14 D** and **F**. Note though that a minimal content of cross-linking agent, e.g. 0.10 equivalent per hydroxyl group, is required in order to get nanocapsules with a robust PVA shell (Figure 3.15 D vs F) after dialysis. The swelling behavior of the nanocapsules in water is also significantly impacted by the salting out procedure. As previously mentioned, the removal of acetone usually induces a large swelling of the PVA membrane at low cross-linking densities (typically below 0.40 eq. IPDI). In contrast, the diameters of the nanocapsules significantly shrank after the salting out procedure and subsequent dialysis against pure water. D_Z dropped from 533 and 553 nm in acetone/water mixture to 264 and 244 nm in water using 0.01 and 0.1 eq IPDI respectively. This drastic decrease of the dimensions clearly corroborates the formation of multiple physical cross-linking within the PVA shell and indicates that the resulting nanocapsules show no tendency to aggregate.

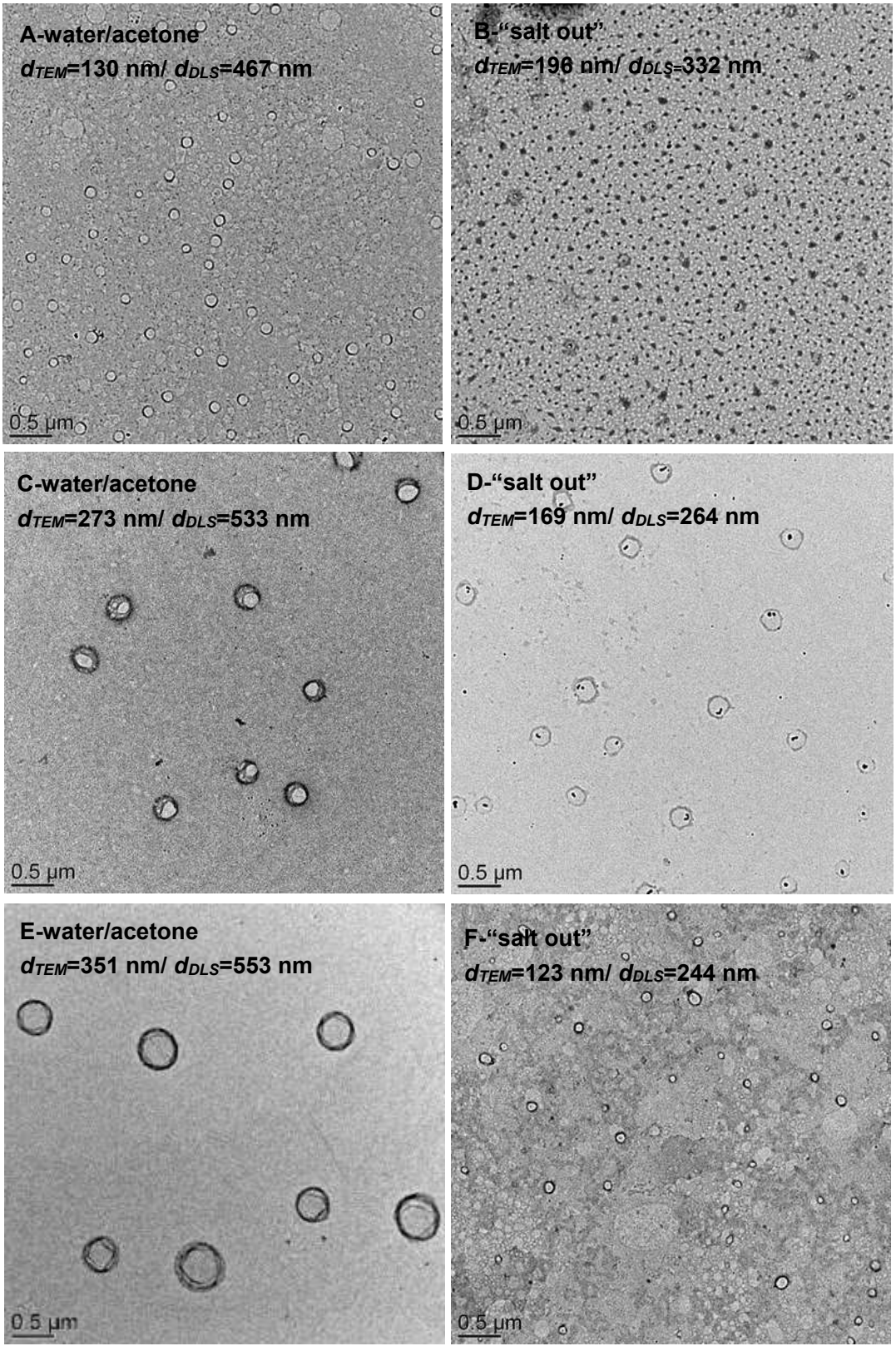

Figure 3.14: TEM images of Mowiol 4-88-NCs before and after "salting out" procedure. NC prepared in the OUZO domain at 0.67 acetone mass fraction with 0.15 mg PVA, 1.5 mg of HD and IPDI (A, B) 0 mg, (C, D) 0.006 mg, 0.01 eq., (E, F) 0.06 mg, 0.1 eq.

3.3 Preparation of PVA-based glyconanocapsules (PVA-glycoNCs)

3.3.1 Cloud point boundaries of PVA-based glycopolymers

In the previous chapter, we described the RAFT synthesis of a library of water-soluble poly(vinyl ester)-based glycopolymers, i.e. PVAG homopolymers and P(VA-*co*-VAG) random copolymers. In order to find suitable conditions for the generation of glyconanocapsules through nanoprecipitation, we next identified the cloud boundaries for $PVAG_{60}$ ($M_{n,th}$=18.9 kg.mol^{-1}) and three random copolymers with different VA/VAG compositions, P(VA_{34}-*co*-VAG_{19}) ($M_{n,th}$=7.8 kg.mol^{-1}), P(VA_{59}-*co*-VAG_{9}) ($M_{n,th}$=3.0 kg.mol^{-1}) and P(VA_{117}-*co*-VAG_{10}) ($M_{n,th}$ =4.9 kg.mol^{-1}), in acetone/water mixtures, see **Figure 3.15**. Depending on the molecular weights and the composition of the glycopolymers, the boundaries were comprised between 0.53 and 0.75 acetone mass fraction for P(VA_{117}-*co*-VAG_{10}) and P(VA_{34}-*co*-VAG_{19}) respectively. These values are consistent with the ones determined for Mowiol 4-88 (0.61) and 8-88 (0.54). Overlapping PVAG or P(VA-*co*-VAG) random copolymers/water/acetone and oil/water/acetone ternary systems revealed that the glycopolymers are suitable for the construction of glyconanocapsules in the Ouzo and SFME domains with the exception of P(VA_{34}-*co*-VAG_{19}), which can exclusively be handled in the SFME domain.

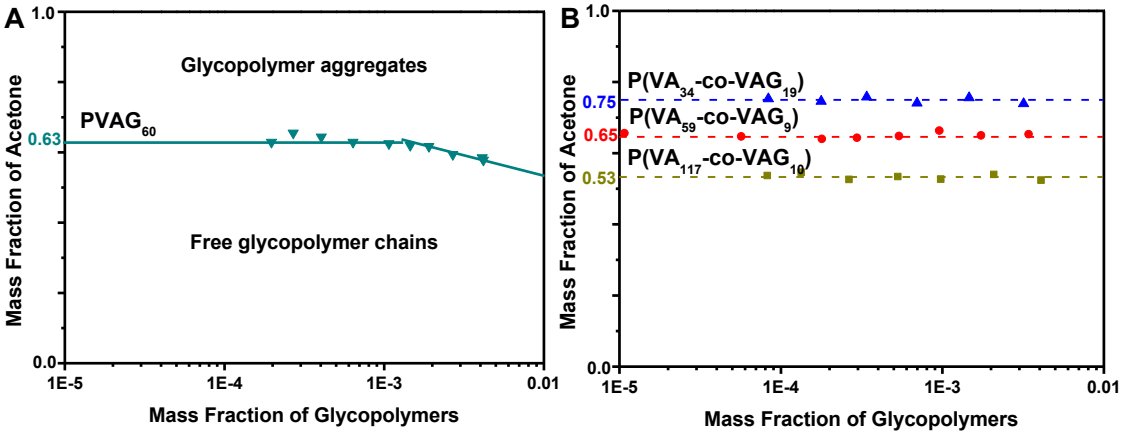

Figure 3.15: Cloud point boundary of (A) homoglycopolymer and (B) PVA-based glycopolymers in water/acetone mixtures.

3.3.2 Preparation of PVA-based glyconanocapsules

PVA-GlycoNCs were prepared using the same conditions as established with Mowiol 4-88 (0.15 mg of glycopolymer, 1.5 mg of HD, 0.4 eq IPDI and 0.67 acetone mass fraction). The morphologies and the diameters of the obtained dispersions were studied by TEM and DLS, respectively (**Figure 3.16**). As measured by DLS analysis (in water/acetone mixtures), the *z*-average diameter of PVA-GlycoNCs generated from P(VA_{117}-*co*-VAG_{10}), P(VA_{59}-*co*-VAG_9) and P(VA_{34}-*co*-VAG_{19}) were 270 (A), 312 (B) and 417 nm (C) whereas the smallest nanocapsules were built from $PVAG_{60}$ (dimeter around 230 nm). These disparities may stem from the solution behavior of the glycopolymer chains in water which exist mostly as unimers for $PVAG_{60}$ and P(VA_{117}-*co*-VAG_{10}) or as small aggregates for P(VA_{34}-*co*-VAG_{19}).

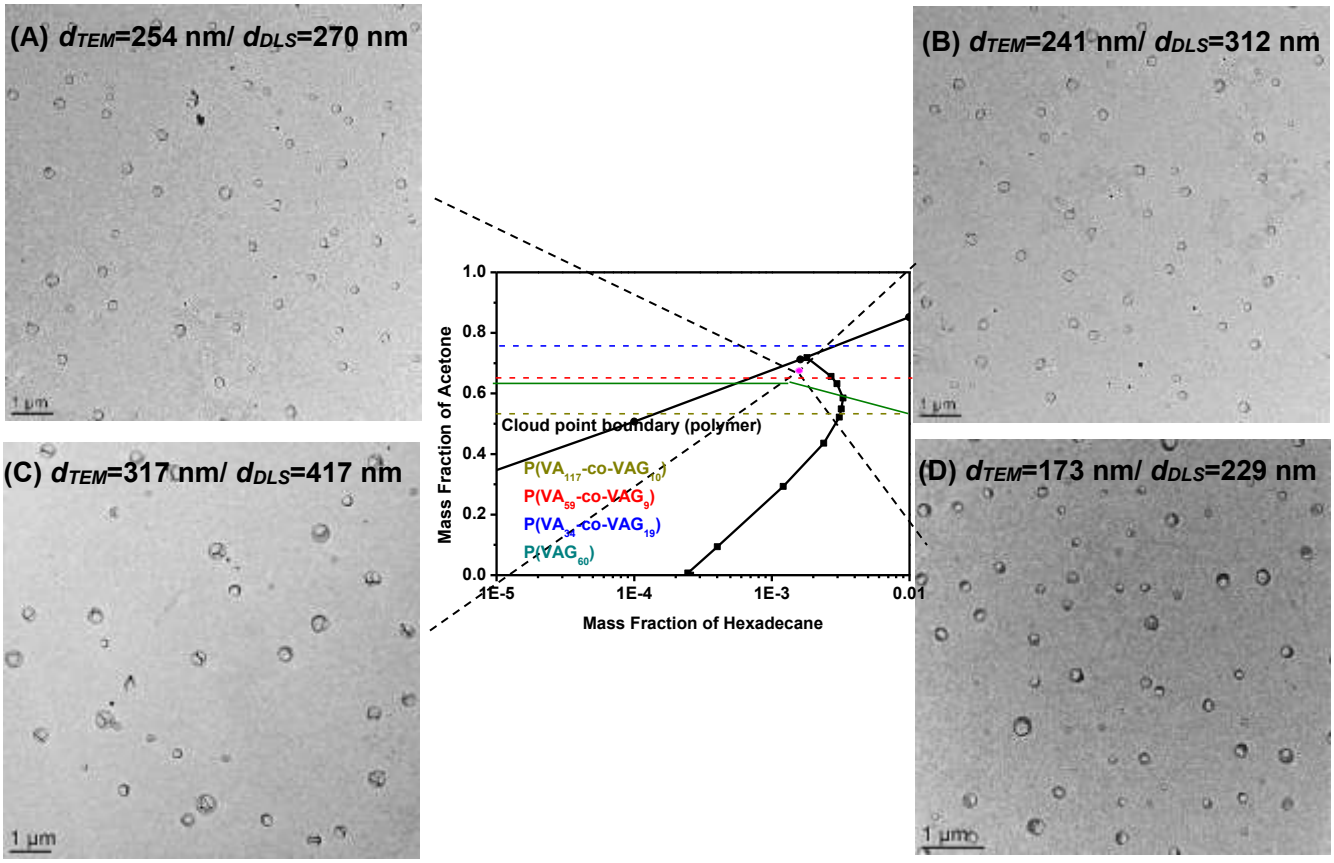

Figure 3.16: Phase diagram of glycopolymer/HD/water/acetone system and morphologies of NCs prepared with P(VA_{117}-*co*-VAG_{10}) (A), P(VA_{59}-*co*-VAG_9) (B), P(VA_{34}-*co*-VAG_{19}) (C) and $PVAG_{60}$ (D).

To extend the scope of PVA-based NCs, we pursued our work on the design of nanocapsules through nanoprecipitation with mixtures of PVA and PVA-based glycopolymers. Investigations were carried out in the Ouzo domain using HD as the oil and Mowiol 8-88/P(VA_{34}-*co*-V AG_{19}) as building blocks for the membrane. Practically, both Mowiol 8-88 (0.05 mg) and P(VA_{34}-*co*-VAG_{19}) (0.05 mg) were initially dissolved in 330 mg of water whereas HD and the cross-linking agent (0.2 equivalent IPDI per hydroxyl group) were dissolved in acetone. As illustrated by **Figure 3.17**, solvent shifting at 0.67 acetone mass fraction afforded the one-pot preparation of glyconanocapsules with a z-average diameter ~ 300 nm.

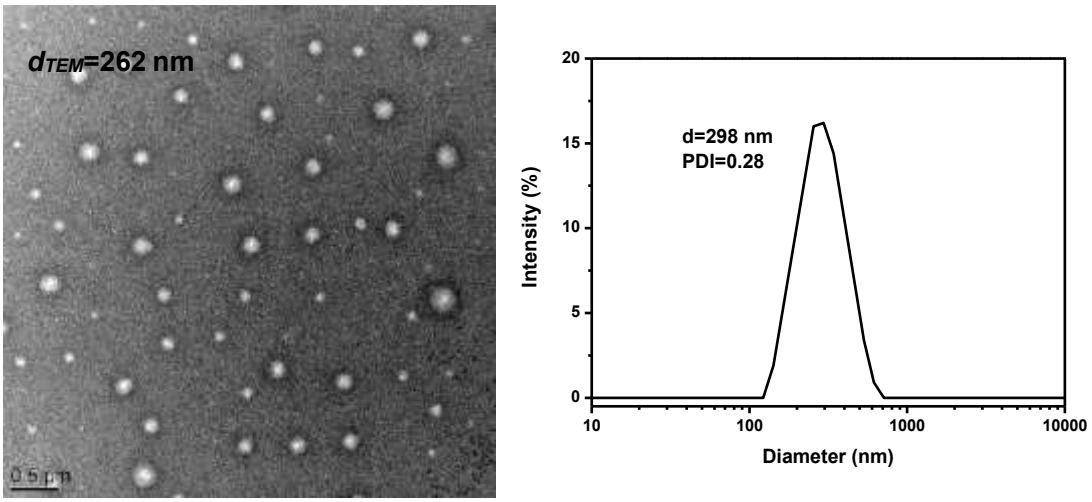

Figure 3.17: TEM picture and DLS of the glyconanocapsules prepared by nanoprecipitation at 0.67 acetone mass fraction (0.1 mg of polymer Mowiol 8-88/P(VA_{34}-*co*-VAG_{19}), 1.5 mg of HD, 0.2 eq. IPDI).

We subsequently investigated the preparation of IPDI-free PVA-GlycoNCs through solvent shifting procedure (0.33/0.67, w/w). When dispersions (z-average diameter ~135 nm in water-acetone mixtures by DLS) were casted onto TEM grids, uniform spherical nanocapsules with clear core-shell structures were observed (**Figure 3.18 A**). Contrary to pure PVA-based nanocapsules *vide supra*, the majority of the resulting glyconanocapsules survived to the removal of acetone by dialysis against water for 24h (**Figure 3.18 B**). It is however worth noting the presence of dark dots together with the nanocapsules suggesting that a fraction of the polymer chains is desorbed (in water) and that the glycopolymer membrane is weakened after such treatments (**Figure 3.18 B**). Accordingly, the hydrodynamic diameter of the nanocapsules considerably increases in water (z-average diameter over 500 nm) consistent with a drastic swelling of the polymer membrane (and the disruption of multiple physical cross-linkages). Lastly, freeze-drying/redispersion or basification of the aqueous dispersion (at pH=12) result in irreversible alteration of the nanocapsules (**Figure 3.18 C** and **D**).

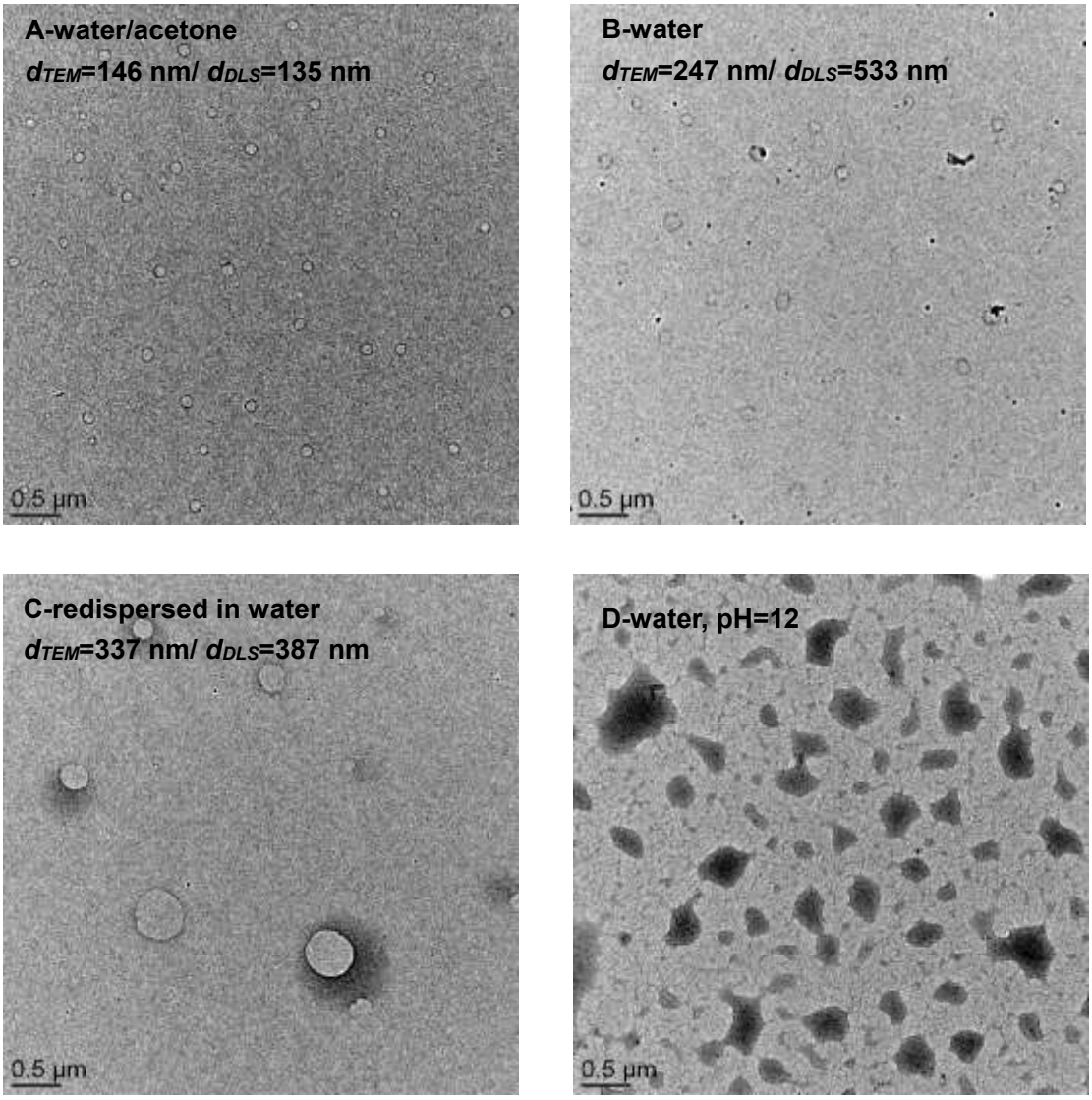

Figure 3.18: TEM images of P(VA_{59}-*co*-VAG_9) based glyconanocapsules built by nanoprecipitation at 0.67 acetone mass fraction, 0.15 mg of glycopolymer, 1.5 mg of HD in water-acetone mixture (A); after removal of acetone by dialysis (B); after dialysis, freeze-drying and re-dispersion in pure water (C); after dialysis, freeze-drying and re-dispersion in basic aqueous medium (NaOH, pH 12) (D).

As synthetic carbohydrate ligands are capable to undergo multiple recognition events with a range of lectins,[10] we next examined the ability of the numerous glucose residues anchored on the PVA-based nanocapsules to interact *in vitro* with lectins. Herein, we selected Concanavalin A (Con A), a popular and low-cost plant lectin with high binding affinity for mannose and glucose,[11] as a model

lectin to investigate the bioactivity of PVA-based glyconanocapsules (using P(VA_{59}-*co*-VAG_9) as building block for the shell). Nanocapsules (obtained at 0.67 acetone mass fraction, glycopolymer 0.15 mg, HD 1.5 mg and IPDI 0.4 eq./OH, Dz=396 nm) were obtained in water after removal of acetone by rotary evaporation and an aqueous solution of Con A (0.008 mg, 0.02 equivalent per chain) was added dropwise to the dispersion of glycoNCs. The establishment of sugar-lectin interactions was monitored by TEM and DLS. As illustrated by the **Figure 3.19**, the incorporation of Con A resulted in the formation of large ConA/NC aggregates (z-average diameter around 850 nm) owing to the presentation of multiple glucose units (on the shell the glyconanocapsules) promoting ConA-NCs interactions.

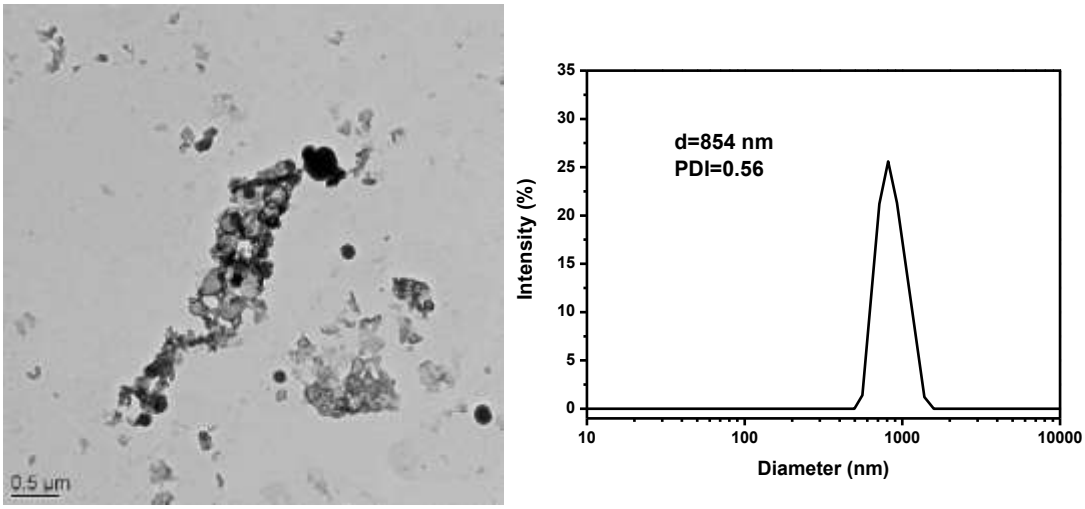

Figure 3.19: TEM image and DLS plot of PVA-GlycoNCs aggregations after removal of acetone and addition of Con A (glycopolymer 0.15 mg, HD 1.5 mg, IPDI 0.4 eq/OH, Con A 0.008 mg).

3.4 Functionalization and loading of nanocapsules

To extend the scope of this one-pot process, we subsequently aimed at decorating the shell of nanocapsules with biorelevant molecules and loading the core with hydrophobic actives (fluorescence tags, drugs…).

3.4.1 Shell functionalization of PVA-NCs

For biomedical purposes, it is crucial to develop one-pot nananoprecipitation procedures affording the incorporation of molecules or polymer chains of interest on the shell. To illustrate that point, we decided to study the grafting of amine-α-functionalized PEG chains (amino-PEG, Mw~2000 g/mol) which are useful to enhance colloidal stability in aqueous media and confer stealth properties to the NCs.[12,13] We anticipated that the strategy adopted to stabilize the shell of NCs, i.e through incorporation of IPDI in the organic phase, could be advantageously exploited to concomitantly cross-link the PVA corona and graft amino-PEG chains (**Scheme 3.2**). To design PEG-decorated PVA-based nanocapsules, amino-PEG (3 mg, 0.05 eq./OH) was then dissolved in the aqueous solution together with Mowiol 4-88 (1.5 mg) and subsequently mixed with the organic solution (containing both oil and IPDI). The resulting acetone mass fraction was 0.67. DLS revealed the presence of one population with a z-average diameter around 180 nm. TEM analysis confirmed the formation of PVA-based nanocapsules. Again, dark dots were spotted together with the NCs suggesting that a non-negligible part of the PEG chains are not grafted to the shell and form aggregates upon casting (**Figure 3.20**). To confirm the attachment of PEG chains, we further performed ^{1}H NMR analysis of the dispersion after dialysis against water, freeze-drying and redispersion in D_2O (**Figure 3.21**). In contrast with the dispersions generated through PEG-free solvent shifting procedure, the implementation of the nanoprecipitation with amino-PEG was accompanied by the appearance of an intense peak at 3.63 ppm on the NMR spectrum, the signature of PEG methylene protons.

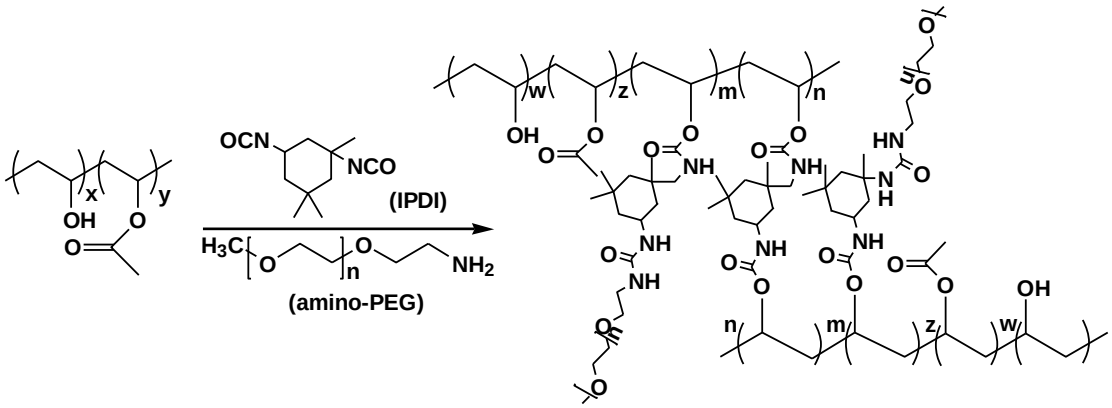

Scheme 3.2: IPDI cross-linking and amino-PEG functionalization of the PVA shell in one-pot procedure.

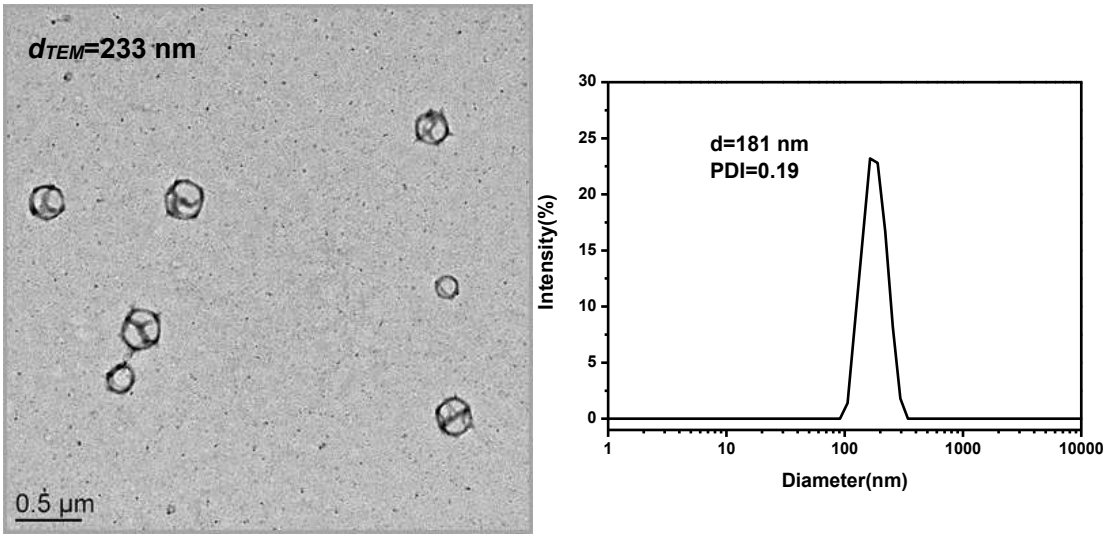

Figure 3.20: TEM image and DLS plot of PEG-functionalized PVA-NCs.

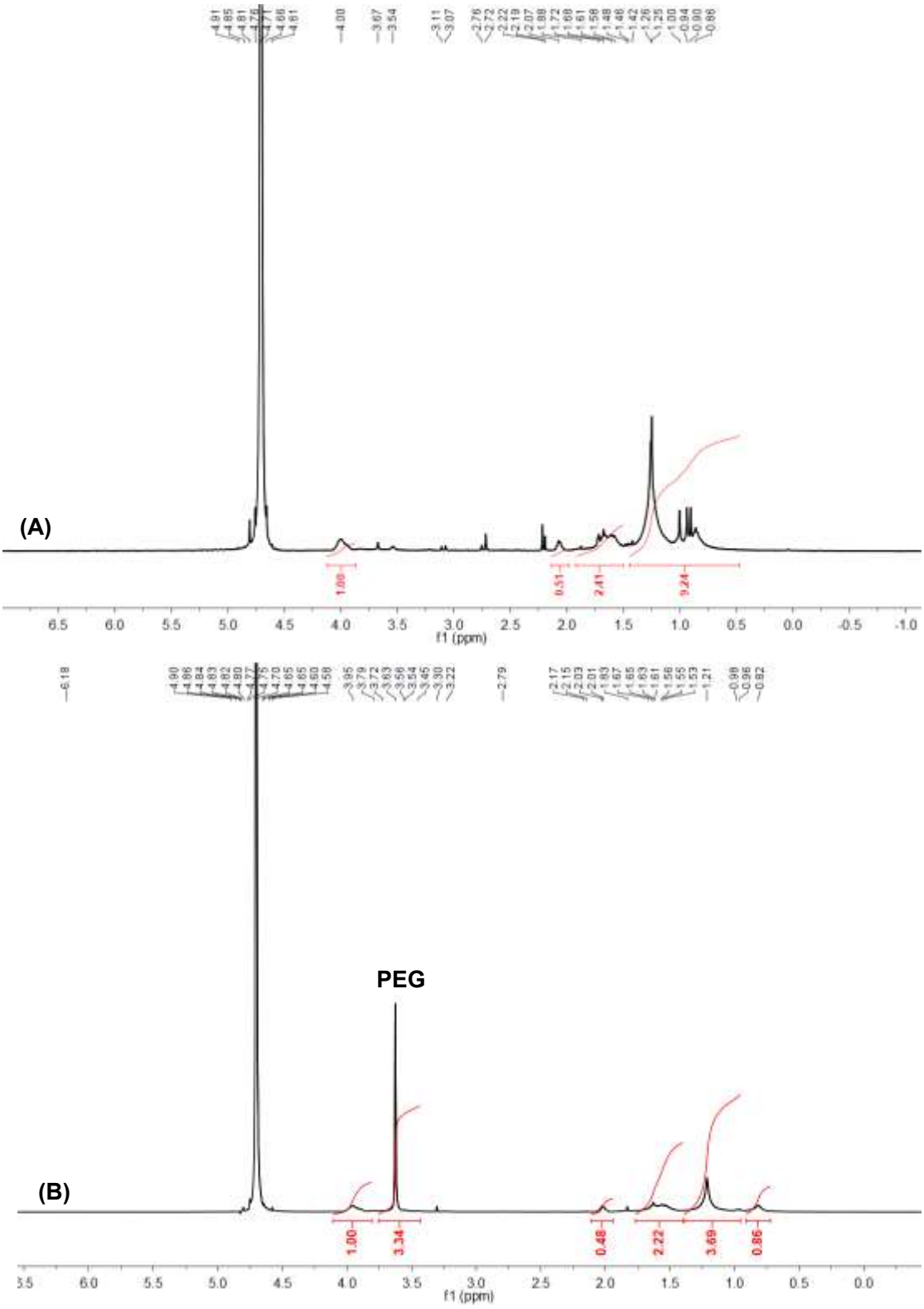

Figure 3.21: ^{1}H NMR spectra of naked nanocapsules (A) and PEG-functionalized nanocapsules (B) after dialysis against water (D_2O, r. t.).

3.4.2 Encapsulation of hydrophobic actives

3.4.2.1 Encapsulation of a fluorescent probe

We finally explored the loading of hydrophobic actives within the oily core of the PVA-based nanocapsules (using acetone mass fraction 0.67, Mowiol 4-88 0.3 mg, HD 3 mg, IPDI 0.4 eq./OH). Pyrene was chosen as a model compound to investigate the encapsulation properties of the nanocapsules owing to facile monitoring of the loading from pyrene fluorescence intensity. In that case, pyrene was first dissolved in the oil (HD with 2.5 wt.% pyrene inside) prior the nanoprecipitation procedure. Encapsulation of pyrene in the core of the NCs (see **Figure 3.22 A-D**) was confirmed by the presence of a vibronic band corresponding to the emission of excited-state dimers 470 nm (in addition to monomer emission between 375 to 470 nm) related to the close vicinity of the pyrene molecules in the cavity of the nanocapsules.

Relying on the calibration curve given in **Figure 3.22 A**, the encapsulation efficiency of pyrene in the HD-filled nanocapsules was estimated to be above 99% according to the following equation:

$$Encapsulation\ Efficiency\ (EE) = \frac{Total\ pyrene - Free\ pyrene}{Total\ pyrene} \times 100\%$$

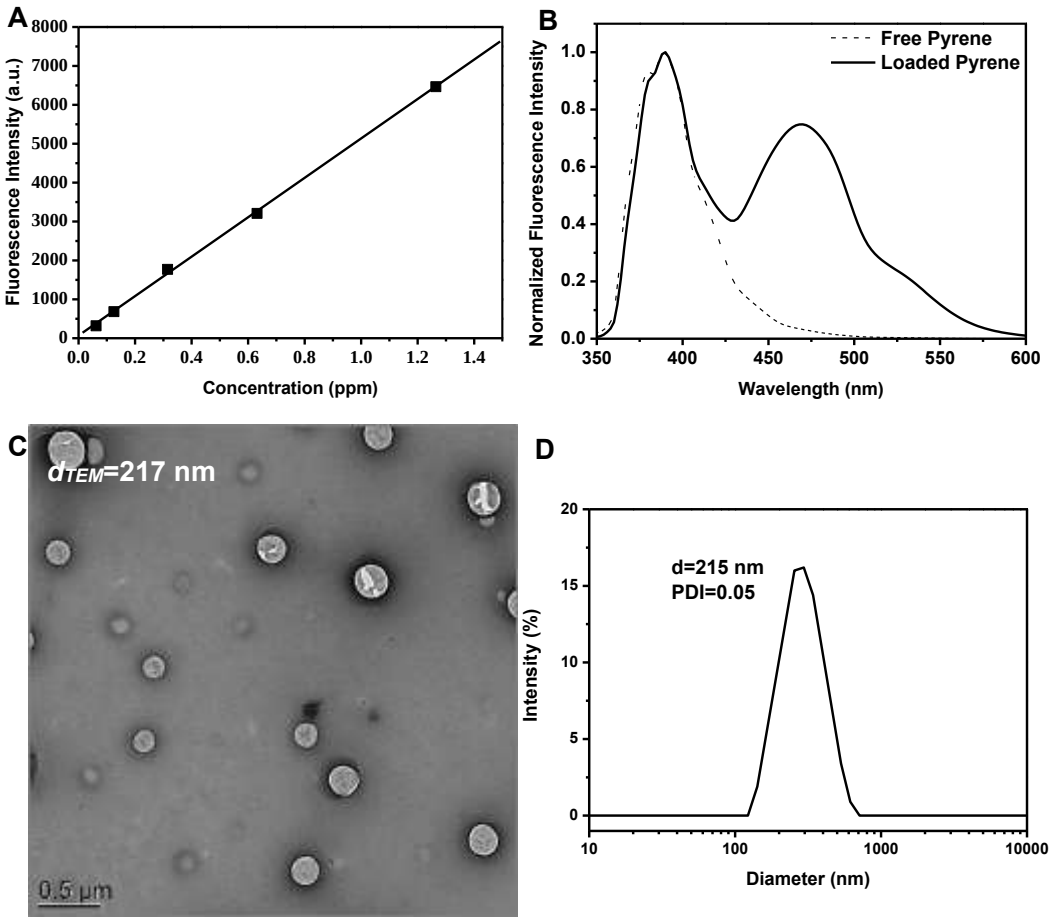

Figure 3.22: (A) Calibration curve of pyrene in acetone (λ_{ex}=335 nm); (B) Fluorescence emission spectra of pyrene-loaded PVA-NCs. The solid line corresponds to the loaded pyrene nanocapsules, the dash line corresponds to the free pyrene at same concentration in acetone (the reference); (C) TEM image of pyrene-loaded PVA-NCs; (D) DLS plot of pyrene-loaded PVA-NCs.

3.4.2.2 Encapsulation of drugs

CPT is a drug used for the treatment of numerous cancers such as colon, breast, ovarian, lung cancers.[14] Transposition of the solvent shifting procedure described for pyrene (dissolution of CPT in HD/acetone at 0.01 wt% and subsequent nanoprecipitation, see details in Experimental section Chapter 5). The hydrodynamic diameter of the nanocapsules was ~ 200 nm (**Figure 3.23 C, D**) and the EE was ~ 70%.

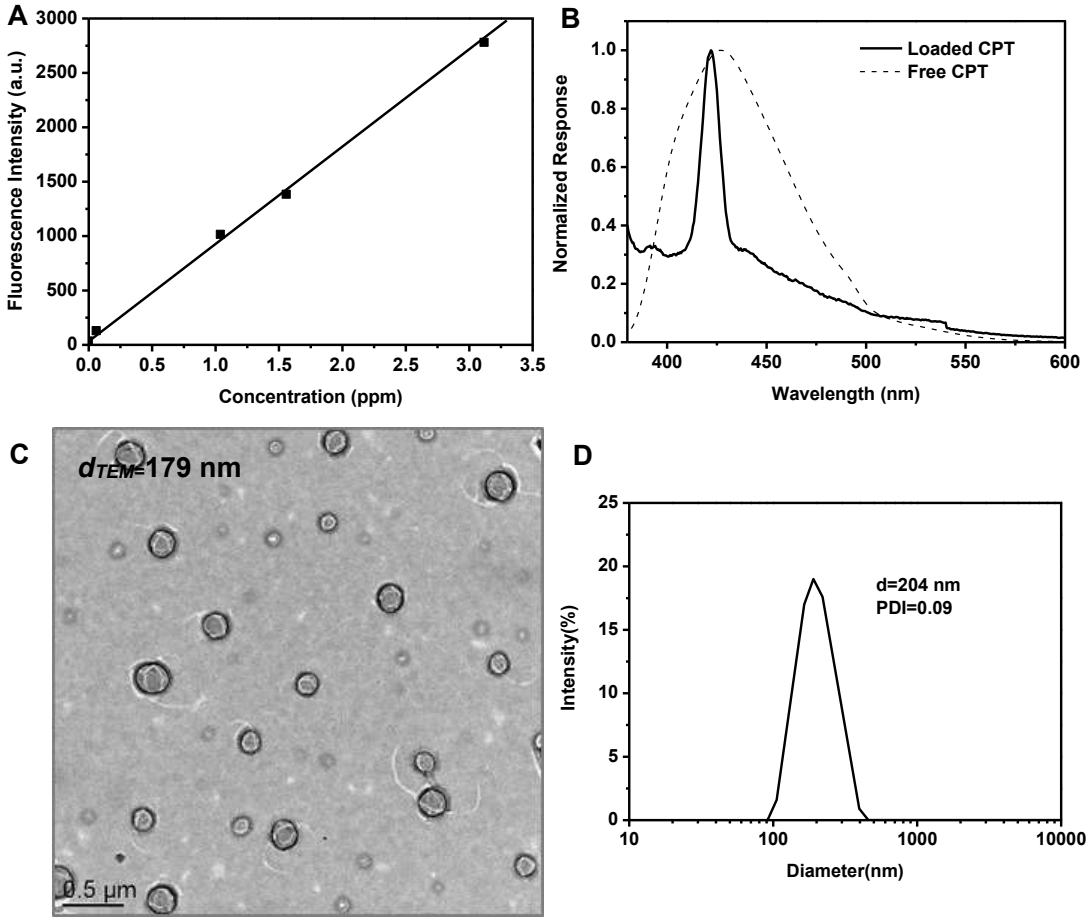

Figure 3.23: (A) Calibration curve of CPT in acetone (λ_{ex}=370 nm); (B) Fluorescence emission spectra of CPT-loading PVA-NCs. The solid line corresponds to the loaded CPT nanocapsules, the dash line corresponds to the free CPT at same concentration in acetone (the reference); (C) TEM image of CPT-loaded PVA-NCs; (D) DLS plot of CPT-loaded PVA-NCs.

Similarly, resveratrol, a naturally occurring polyphenolic derivative displaying a number of anti-aging health benefits including improved metabolism, carioprotection, and cancer prevention[15], was successfully encapsulated in 220 nm PVA-based NCs, see details in Chapter 5.

3.5 Preparation of degradable PVA-NCs

PVA-NCs prepared by solvent shifting procedure hold promise for diverse

applications, especially drug delivery. A key challenge for the capsules' application is to stabilize them in physiological conditions while also being able to trigger their disassembly and the release of a cargo under external stimulus. In this context, we decided to focus on the incorporation (within the shell) of disulfide bonds which can be rapidly cleaved in response to physiological reductive conditions, as typically observed in glutathione-rich intracellular environments.[16] With the aim of designing redox-sensitive systems, the route to PVA-based nanocapsules was then slightly modified (0.67 acetone mass fraction using 0.15 mg of Mowiol 4-88, 0.4 mg of HD and 0.4 eq IPDI eq./OH) by incorporating disulfide-containing cystamine in the aqueous phase (0.09 mg, 0.5 eq./IPDI) as co-cross-linking agent prior to solvent shifting.

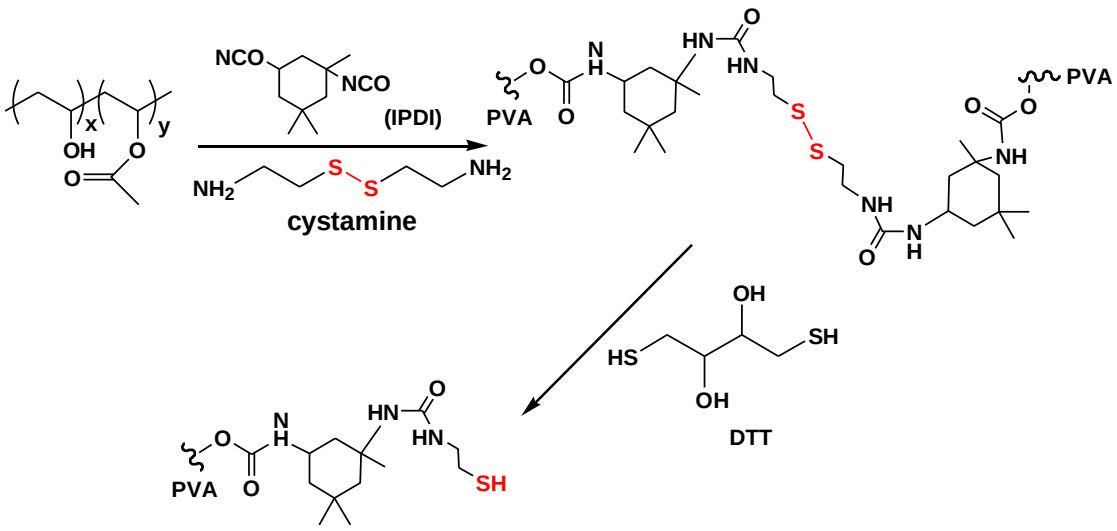

Scheme 3.3: Route to redox-sensitive PVA-based nanocapsules by nanoprecipitation.

Addition of cystamine had barely no impact on the nanoprecipitation process as nanocapsules with accurate dimensions and size distribution were effortlessly prepared under such conditions (see **Figure 3.24 A**). However, thanks to the presence of numerous disulfide bridges linking the PVA chains, the addition of dithiothreitol (DTT, 2 mg) efficiently triggered the destruction of the nanocapsules and the leakage of the oil confirming their susceptibility to reductive environments (see **Figure 3.24 B**).

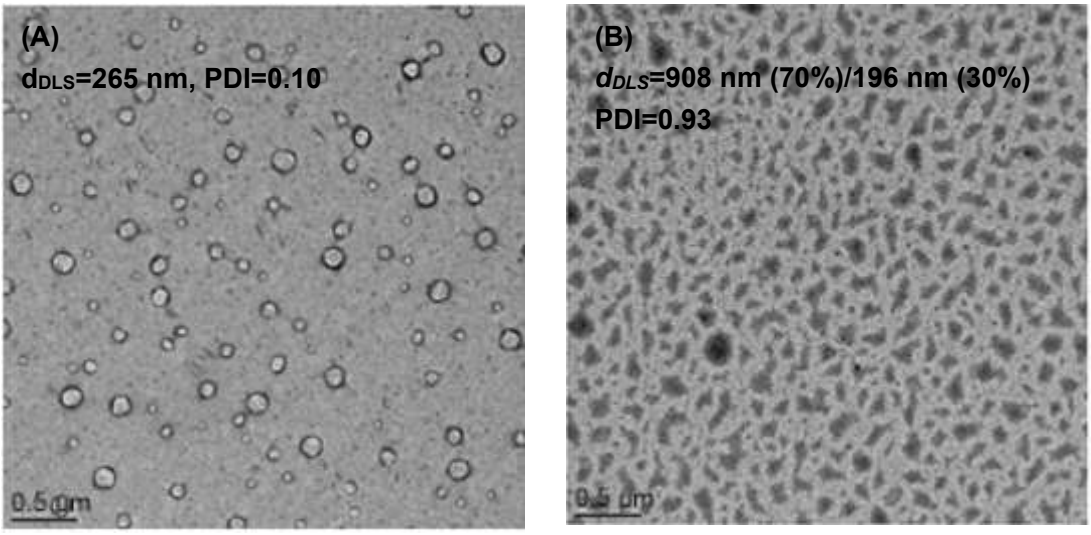

Figure 3.24: TEM images of gradient cross-linked nanocapsules as prepared (A) and after dialysis and addition of DTT (B).

3.6 Conclusion

In this chapter, we have demonstrated that PVA-based nanocapsules and glyconanocapsules can be straightforwardly generated by nanoprecipitation in both OUZO and SFME domains. Stabilization of the nanocapsules in water was ensured by covalent cross-linking of the shell (through incorporation of IPDI in the organic phase) and/or by addition of Na_2SO_4 (salting out procedure). Owing to its simplicity and robustness, the nanoprecipitation process was easily adapted to promote the decoration of the PVA shell with (macro)molecules of interest (here, PEG chains introduced initially in the aqueous phase), the encapsulation of hydrophobic actives in the oily core or the insertion of the redox-sensitive cross-linking bridges between PVA chains. The glucose moieties located at nanocapsules' surface were finally shown to interact with the corresponding lectin, *i.e* ConA, leading to the formation of large clusters. All together, these results are promising for future research on drug delivery systems or protocells.

3.7 Reference

1. C. M. Hassan and N. A. Peppas, *Advances in Polymer science*, **2000**, 153, 37-65.
2. X. Yan, R. Ramos, E. Hoibian, C. Soulage, P. Alcouffe, F. Ganachaud, and J. Bernard, *ACS Macro Lett.*, **2017**, 6, 447−451.
3. E. Aschenbrenner, K. Bley, K. Koynov, M. Makowski, M. Kappl, K. Landfester, and C. K. Weiss, *Langmuir*, **2013**, 29, 8845–8855.
4. X. Yan, M. Delgado, A. Fu, P. Alcouffe, S. G. Gouin, E. Fleury, J. L. Katz, F. Ganachaud, and J. Bernard, *Angew. Chem. Int. Ed.*, **2014**, 53, 6910–6913.
5. X. Yan, P. Alcouffe, G. Sudre, L. David, J. Bernard and F. Ganachaud, *Chem. Commun.*, **2017**, 53, 1401-1404.
6. X. Yan, R. Ramos, E. Hoibian, C. Soulage, P. Alcouffe, F. Ganachaud, and J. Bernard, *ACS Macro Lett.*, **2017**, 6, 447−451.
7. B. Briscoe, P. Luckham, S. Zhu, *Polymer*, **2000**, 41, 3851–3860.
8. C. Jeeyoung, B-S Hatice, J. K. Hsiang, S. M. Arnaz and K. M. Orhun, *Biomaterials*, **2007**, 28, 772–780.
9. B. E. B. Jensen, M.-H. Alves, B. Fejerskov, B. Stadler and A. N. Zelikin, *Soft Matter*, **2012**, 8, 4625-4634.
10. N. Sharon and H. Lis, *Science*, **1989**, 246, 227–234.
11. G. Yilmaz and C. R. Becer, *Polym. Chem.*, **2015**, 6, 5503-5514.
12. Y. Zhang, S. Zhu, L. Yin, F. Qian, C. Tang and C. Yin, *Eur. Polym. J.*, **2008**, 44, 1654–1661.
13. L. Zhang, F. Gu, J. Chan, A. Wang, R. S. Langer and O. C. Farokhzad, *Clin. Pharmacol. Ther.,* **2008**, 83, 761-769.
14. Y. Cirpanli, E. Bilensoy, A. L. Dogan and S. Calis, *Eur J Pharm Biopharm.*, **2009**, 73, 82–89.
15. L. G. Carter, J. A. D'Orazio and K. J. Pearson, *Endocr.-Relat. Cancer.,* **2014**, 21, 209–225.
16. S. Shu, X, Zhang, Z. Wu, Z. Wang, C. Li, *Biomaterials*, **2010**, 31, 6039-6049.

Chapter 4

Preparation of Poly(2-ethyl-2-oxazoline)-based Glyconanocapsules through Nanoprecipitation

Chapter 4 Preparation of Poly(2-ethyl-2-oxazoline)-based Glyconanocapsules through Nanoprecipitation

4.1 Introduction

First reported in the 1960s,[1] poly(2-oxazoline)s (POXs) are a class of biocompatible and biodegradable hydrophilic polymers synthesized by living cationic ring opening polymerization (CROP). Among POXs, poly(2-ethyl-2-oxazoline) (PEOX) has emerged as a suitable alternative to polyethylene glycol (PEG) due to its high solubility in water (and in some organic solvents), low toxicity, “stealth” behavior and its thermo-responsive character (LCST at approximatively 60°C).[2] Thanks to these appreciated features, PEOX has been recently used in a plethora of biomedical applications.[3, 4]

Another valuable characteristic of POXs relies on their suitability to post-polymerization modifications (note that new functionalities can also be incorporated through the design of original 2-oxazoline monomers provided that they are compatible with the CROP process). As previously reported,[5] PEOX can be effectively converted into poly(2-ethyl-2-oxazoline-*co*-ethyleneimine) (POEX-*co*-PEI) with tunable composition (through acidic hydrolysis). The secondary amine carried by POEX-*co*-PEI can further be used as handles to incorporate new functionalities onto POX backbones.[6, 7]

In this chapter, we will first focus on the synthesis and the characterization of lactose-functionalized poly(2-ethyl-2-oxazoline) glycopolymers exploiting a method described by Hoogenboom to attach sugar moieties onto POEX-PEI through reductive amination. In a second step, we will aim at constructing precisely-defined oil-filled glyconanocapsules from these glycopolymers based on the establishment of glycopolymer/acetone/water and oil/acetone/water phase diagrams. Finally, we will examine the pH-responsive behavior of these glyconanocapsules as well as their drug loading capacity.

4.2 Synthesis of poly(2-ethyl-2-oxazoline) glycopolymers

The synthesis of polyoxazoline-based glycopolymers was performed with two different commercial PEOX precursors, purchased to Aldrich. PEOX of M_w=50 kg/mol and *Đ*=3-4 was designated as $PEOX_{125}$ (assuming *Đ*=4, M_n=12.5 kg/mol and DP_n=125 by calculation). PEOX of M_n=50 kg/mol and *Đ*≤1.25 was designated as $PEOX_{500}$ (DP_n=500, courtesy of Aldrich). SEC characterization of the two polymers were performed in DMF as eluent, see **Figure 4.1**. Consistent with the data provided by Aldrich, large disparities in molar mass and dispersity were observed for $PEOX_{125}$ (M_n=5.4 kg/mol, *Đ*=3.8) and $PEOX_{500}$ (M_n=46.2 kg/mol, *Đ*=1.37).

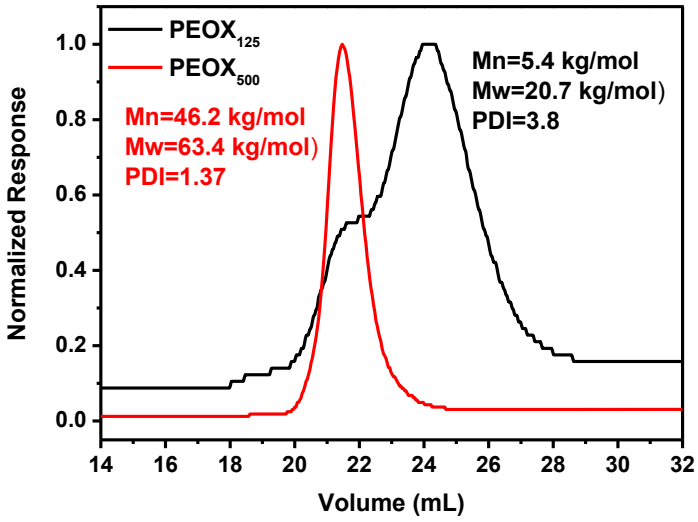

Figure 4.1: SEC traces of commercial PEOX precursors (DMF eluent, PS calibration, r. t.).

4.2.1 Acid hydrolysis of poly(2-ethyl-2-oxazoline) (PEOX)

As previously mentioned, the conversion of PEOX into POEX-PEI proceeds under strong acidic conditions and the rate and the extent of the hydrolysis can be precisely modulated by adjusting the temperature, the time of reaction and/or the concentration of hydrochloric acid (**Scheme 4.1**).[8,9] In a typical experiment, the PEOX precursor (500 mg) was first immersed in 5 mL of water

and stirred at 40°C for 20 min to ensure dissolution of the polymer. After addition of a concentrated solution of HCl (36.5 wt.%) to reach a final concentration of 6 M, the aqueous solution was heated to 100°C under stirring for a desired period. After cooling to room temperature in ice water, the polymer solution was immediately neutralized through addition of aqueous sodium hydroxide solution, followed by dialysis and freeze-drying. The resulting yellow sticky solid (yield > 95%) was analyzed by ^{1}H and ^{13}C NMR to determine the degree of hydrolysis. The ^{1}H NMR spectra of $PEOX_{500}$ and PEOX-PEI after purification by dialysis are given in **Figures 4.2 A** and **B**. The peaks observed on both spectra between 3.3 and 4.1 ppm (assigned as **a**) were attributed to the methylene protons of PEOX. The partial hydrolysis of PEOX was confirmed by the appearance of new peaks (peaks **b**) between 2.7 to 3.3 ppm assigned to CH_2 groups of ethylene imine units. The detection of an additional peak between 2.15 and 2.20 ppm highlighted the undesired presence of propionic acid (released during the hydrolysis). This was ascribed to hydrogen bonding interactions of propionic acid with PEI segments obstructing the removal of the acid.

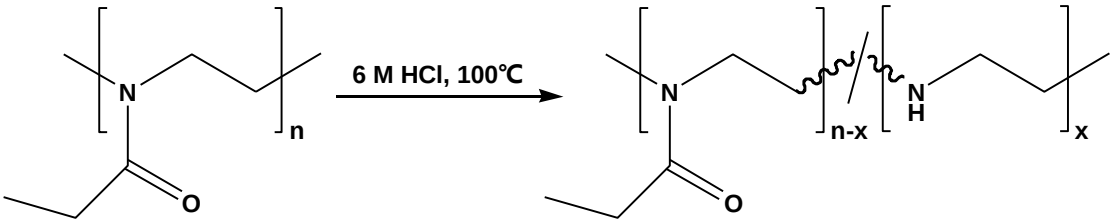

Scheme 4.1: Acid hydrolysis of PEOX to PEOX-PEI copolymers at 100°C and 6 M HCl.

The degree of acidic hydrolysis was further calculated from relative integrations of the peaks a and b using the following equation $I_b/(I_a+I_b)$ x 100 (see **Figure 4.2 B**, 42% for $PEOX_{500}$ after 2h of reaction). The overall composition and the molar mass (calculated theoretically from the molar mass of the PEOX precursor and the EOX/EI composition after hydrolysis) of the PEOX-PEI copolymer are gathered in **Table 4.1**. ^{13}C NMR spectra of PEOX and PEOX-

PEI in D_2O (see **Figure 4.3 B**) further corroborated the conclusions drawn from ^1H NMR spectra.

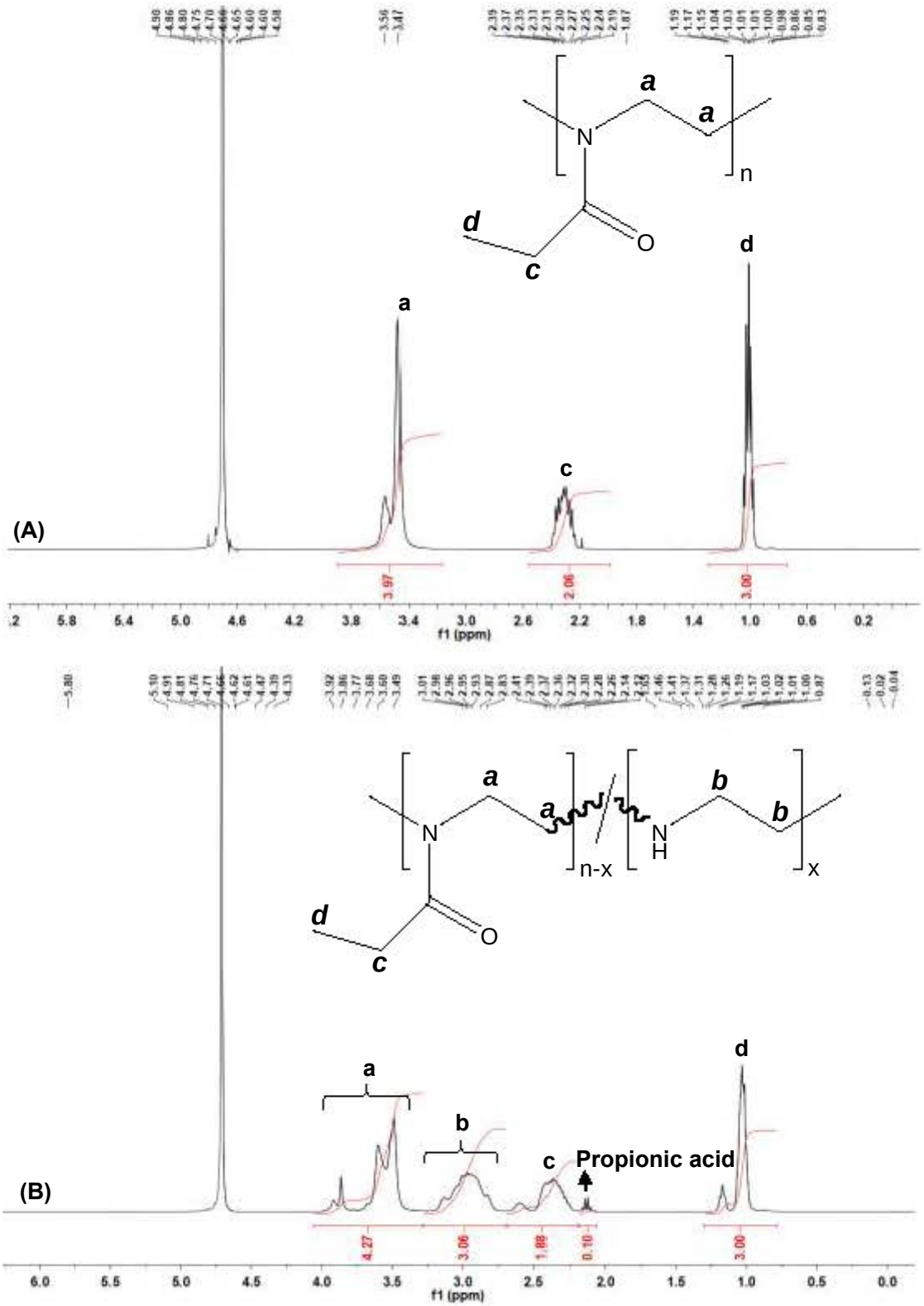

Figure 4.2: ^1H NMR of (A) $PEOX_{500}$ and (B) $PEOX_{290}$-PEI_{210} copolymer (in D_2O, r. t.).

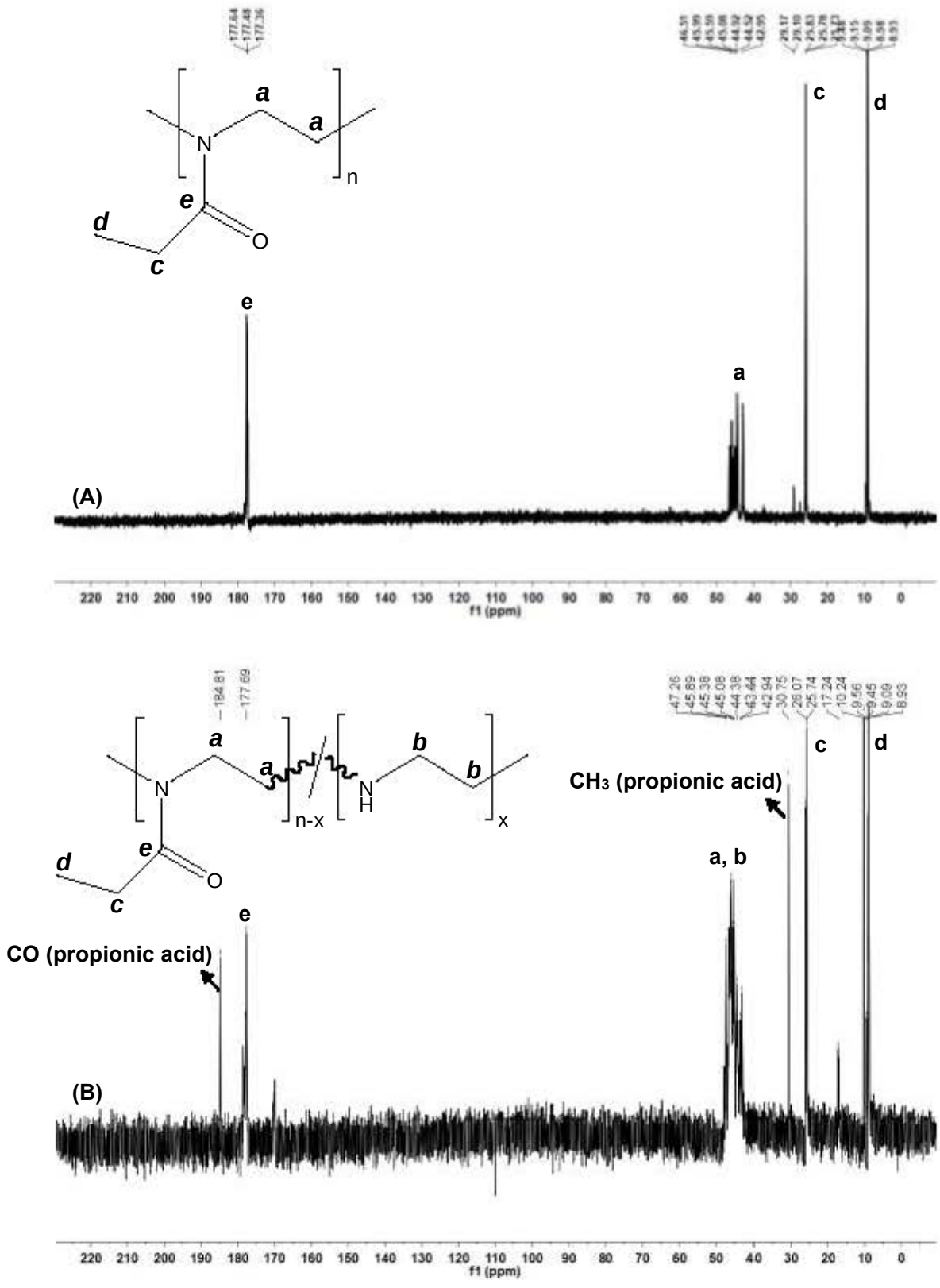

Figure 4.3: ^{13}C NMR of (A) $PEOX_{500}$ and (B) $PEOX_{290}$-PEI_{210} copolymer (in D_2O, r. t.).

The evolution of the degree of hydrolysis for $PEOX_{125}$ as a function of the reaction time is clearly illustrated in **Figure 4.4** and **Table 4.1**. PEOX-PEI copolymers with tunable compositions were synthesized by tuning the time of reaction and almost full hydrolysis of PEOX was observed after 4h of reaction (94% of hydrolysis). SEC characterization of the resulting PEOX-PEI copolymers was performed in DMF solution (see **Figure 4.5**).

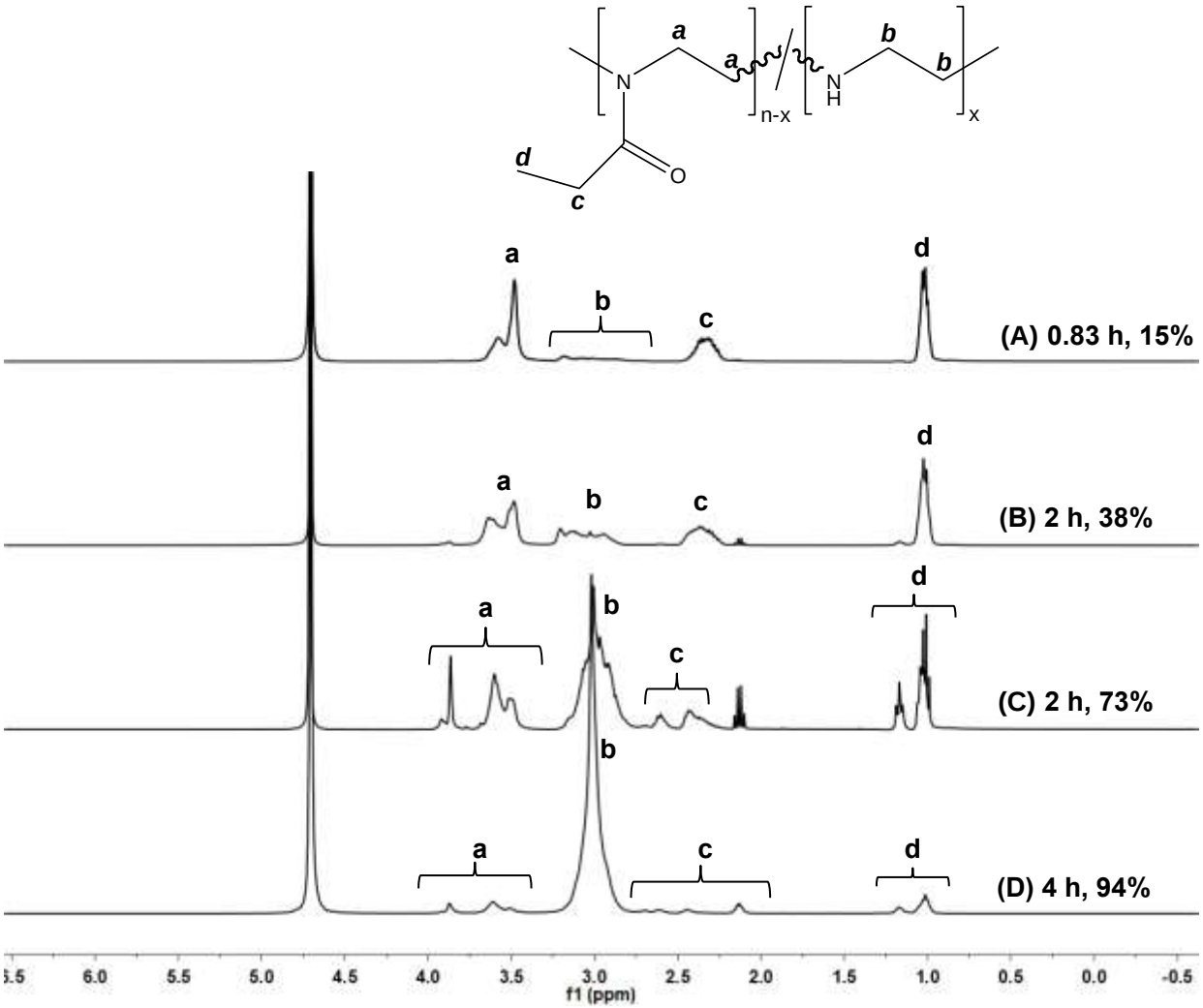

Figure 4.4: ^1H NMR spectra of PEOX-PEI copolymers obtained by tuning the time of acid hydrolysis of $PEOX_{125}$ precursor (in D_2O, r. t).

Table 4.1: PEOX-PEI copolymers obtained by acid hydrolysis as a function of the reaction time.

Copolymer	Precursor	Reaction time (h)	Degree of hydrolysis [a] (%)	$M_{n,SEC}$ [b] (kg/mol)	$Đ$ [b]
$PEOX_{106}$-PEI_{19} [c]	$PEOX_{125}$	0.83	15	13.6	3.1
$PEOX_{77}$-PEI_{48} [c]	$PEOX_{125}$	2	38	22.2	2.8
$PEOX_{290}$-PEI_{210} [c]	$PEOX_{500}$	2	42	68.9	1.5
$PEOX_{34}$-PEI_{91} [c]	$PEOX_{125}$	3	73	n.d [d]	
$PEOX_{7}$-PEI_{118} [c]	$PEOX_{125}$	4	94	n.d [d]	

[a)]: Calculated from the EOX/EI integration values by equation $I_b/(I_a+I_b)$ x 100; [b)]: determined from SEC analysis in DMF eluent with PS calibration; [c)]: the overall composition of PEOX-PEI determined from the composition of the PEOX precursor and the degree of hydrolysis; [d)]: not determined due to aggregation of polymer in DMF solution.

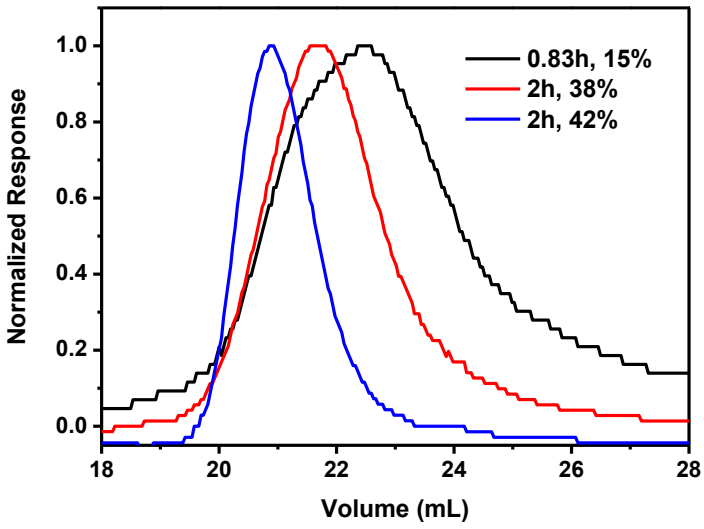

Figure 4.5: Evolution of the SEC traces of PEOX-PEI copolymers (DMF eluent, PS calibration).

Water solubility of the yielded PEOX-PEI copolymers was studied after dissolution of the copolymer in water (1 mg/mL) and stirring at room

temperature for 12h. DLS analysis certificated that chain aggregation takes place in all the transparent aqueous solutions of PEOX-PEI (**Figure 4.6**).

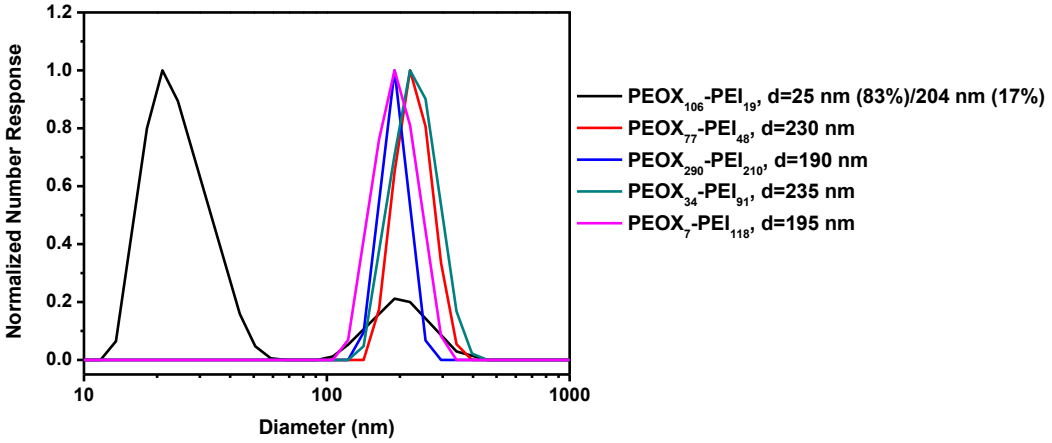

Figure 4.6: DLS of PEOX-PEI aqueous solutions (size distribution by number, r. t.).

4.2.2 Saccharide functionalization of PEOX-PEI copolymers

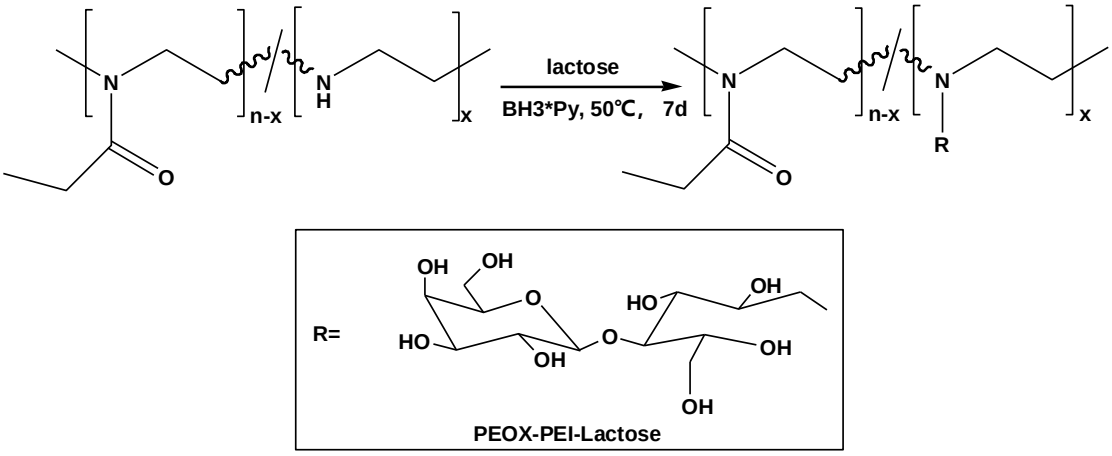

Scheme 4.2: Saccharide functionalization of PEOX-PEI copolymers.

For numerous biomedical applications, it is desirable to develop synthetic procedures allowing the incorporation of saccharidic moieties onto PEOX-PEI backbones. Herein, we decided to investigate the post-modification of PEOX-PEI with lactose through reductive amination of PEI secondary amines[10]. Lactose was selected owing to well-known interactions of *β*-galactoside residues with proteins mediating cancer cell activities such as Galectin-1[11]. The

coupling of lactose (added in large excess, 20 equivalents per secondary amine) was conducted in sodium borate buffer (0.1 M, pH=7.4) in the presence of borane-pyridine complex as a reducing agent (BH_3*Py, 8 M) at 50°C for 7 days to convert the formed imines into stable tertiary amines *in situ*. After dialysis against water to remove free lactose in excess, reducing agents and side-products, and freeze-drying, white fluffy powders were obtained. The detailed conditions for saccharide functionalization of PEOX-PEI copolymers are presented in **Table 4.2**.

Table 4.2: Reaction conditions for saccharide functionalization of PEOX-PEI copolymers.

Precursors	PEI [a] (mmol)	Lactose [b] (mmol)	BH_3*Py [c] (mmol)	Borate buffer [d] (mL)	Time (d)	Temperature (°C)
$PEOX_{106}$-PEI_{19}	0.16	3.20	3.20	10	7	50
$PEOX_{77}$-PEI_{48}	0.74	14.69	14.69	10	7	50
$PEOX_{290}$-PEI_{210}	0.57	11.48	11.48	10	7	50
$PEOX_{34}$-PEI_{91}	1.24	24.77	24.77	10	7	50
$PEOX_{7}$-PEI_{118}	2.03	40.60	40.60	10	7	50

[a)]: Calculated from the mass and the composition of PEOX-PEI copolymers; [b)]: 20 equivalent per EI unit; [c)]: Prepared by mixing 9.4 mL boric acid solution (0.2 mol/L) and 0.6 mL sodium boric acid solution (0.05 mol/L) and addition of 10 mL water.

The resulting lactose-containing polyoxazoline copolymers were subsequently analyzed by ^{1}H and ^{13}C NMR spectroscopy. The ^{1}H NMR spectrum of $PEOX_{290}$-PEI_{210}-Lactose is given in **Figure 4.7A**. As compared with the ^{1}H NMR spectrum of $PEOX_{290}$-PEI_{210} (Figure 4.2), the apparition of new peaks between 3.2 and 4.3 ppm (CH groups assigned as **2-6** and **2'-6'**) and around 4.40 ppm (anomeric proton **1**) clearly assessed the grafting of lactose units onto the secondary amine units of PEOX-PEI. On the basis of the integrals of the CH_3 groups of PEOX (peak d at ~ 1.04 ppm) and CH groups of lactose (between 3.2

and 4.3 ppm), we assumed that the coupling was 87%. The efficiency of lactose grafting obtained for other PEOX-PEI-Lactose copolymers by the same method was 80%, 89%, 84% and 80%, respectively (see Figures in Annex 6). The attachment of disaccharide moieties through reductive amination was further supported by ^{13}C NMR analyses (see **Figure 4.7 B**) with the observation of characteristic peaks for C1 and C1' (at 103 and 56 ppm respectively) together with a series of peaks between 60 and 80 ppm (peaks 2-6 and 2'-6', see inset Figure 4.7B). Additionally, a new peak assigned to the CH_2 group adjacent to the tertiary amine (marked as **b**) was found at 51 ppm consistent with the efficient reduction of the imines. Note that contrary to PEOX- PEI materials, the presence of propionic acid was no longer detected after purification of the resulting glycopolymer by dialysis.

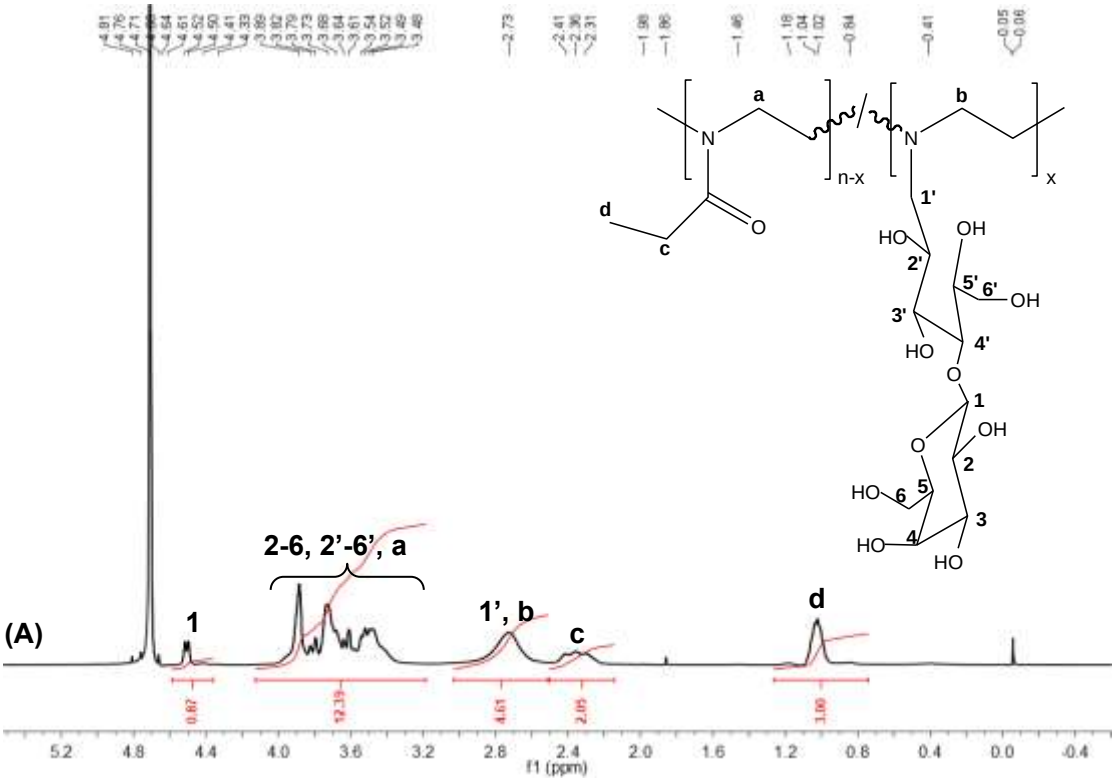

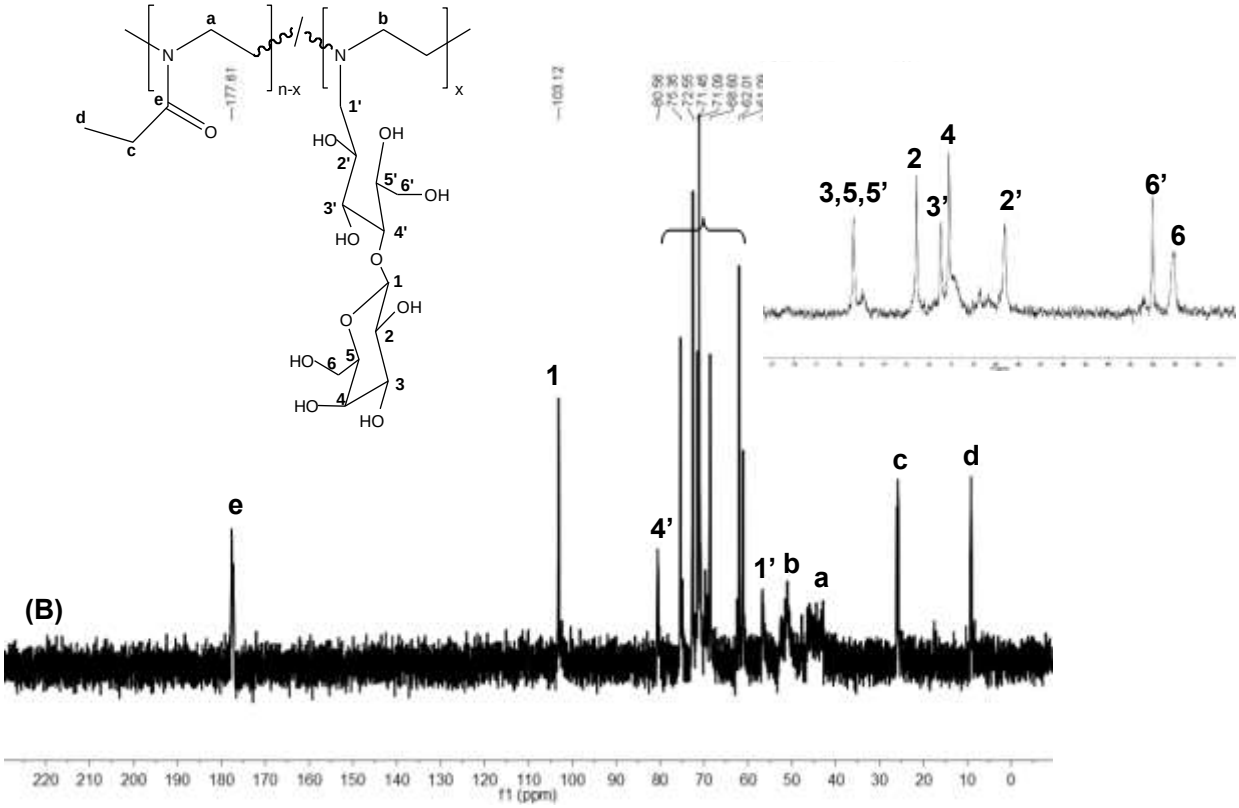

Figure 4.7: ^{1}H NMR and ^{13}C NMR of $PEOX_{290}$-PEI_{210}-Lac obtained from reductive amination of $PEtO_{290}$-PEI_{210} in the presence of excess lactose (Lac) (in D_2O, r. t.).

The polyoxazoline-based glycopolymers were subsequently analyzed by SEC in acetate buffer (pH=4.8) (**Table 4.3**, **Figure 4.8**). The molecular weights for PEOX-PEI-Lac copolymers were in relatively good agreement with theoretical values. In the case of the copolymers synthesized from $PEOX_{125}$, the SEC traces progressively shifted towards high molecular weight with increasing contents of lactose contents within the chains.

Table 4.3: Molecular weight and dispersity of PEOX-based glycopolymers.

Glycopolymers	$M_{n,th}$ [a] (kg/mol)	$M_{n,SEC}$ [b] (kg/mol)	$Đ$ [b]
$PEOX_{106}$-PEI_{19}-Lac	15.8	29.5	2.8
$PEOX_{77}$-PEI_{48}-Lac	22.5	34.5	3.5
$PEOX_{290}$-PEI_{210}-Lac	92.1	120.1	1.1
$PEOX_{34}$-PEI_{91}-Lac	29.7	47.4	2.2
$PEOX_{7}$-PEI_{118}-Lac	33.3	46.8	1.8

a): Calculated by equation $M_{w,th}=M_{EOX}\times N_{EOX}+ M_{Lac}\times N_{Lac}$, M_{EOX} and M_{Lac} are the molecular mass of EOX and Lactose, N_{EOX} and N_{Lac} are the number of repeat units in the copolymer;

b): Determined from the SEC analysis performed in acetate buffer (pH=4.8).

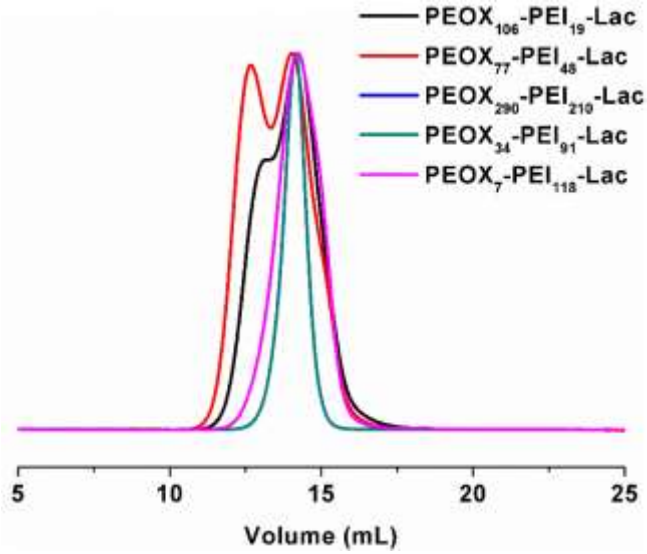

Figure 4.8: SEC traces of PEOX-PEI-Lactose copolymers using acetate buffer (pH=4.8).

The resulting glycopolymers were then dissolved in water at room temperature at a concentration of 1 mg/mL. After equilibration of the solution by stirring at room temperature overnight，DLS measurements were carried out in order to gain insight into their solution behavior in water (individual chains or self-assembled chains). The size distributions for PEOX-PEI-Lactose solutions are given in **Figure 4.9**. At room temperature, the intensity-weighted size

distribution clearly underlined a tendency to self-assemble of these glycopolymers in water (**Figure 4.9 A**, D_h>190 nm). However, the conversion into number-weighted size distribution emphasized the presence of a unique population between 8~12 nm (**Figure 4.9 B**), suggesting that individual glycopolymer chains are largely prominent over polymers aggregates. In contrast to the thermo-sensitive PEOX precursor (LCST around 60°C), increasing the temperature to 85°C during DLS measurements had barely no influence on solution behavior of the glycopolymers with the exception of $PEOX_7$-PEI_{118}-Lactose which generated large aggregates ~ 320 nm upon heating (**Figure 4.9 C**). This behavior was probably caused by an increase in the hydrogen bonding interactions between the sugar units and the polymer backbone as $PEOX_7$-PEI_{118}-Lactose retaining the highest lactose content.

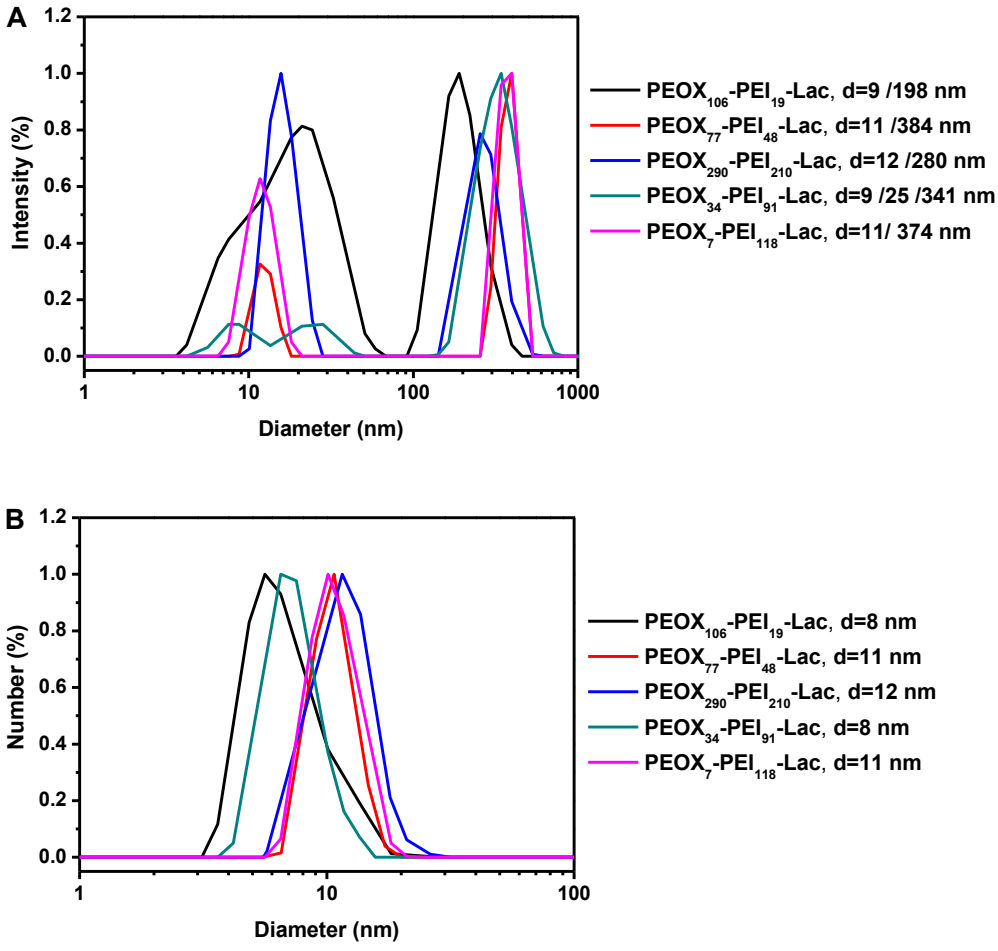

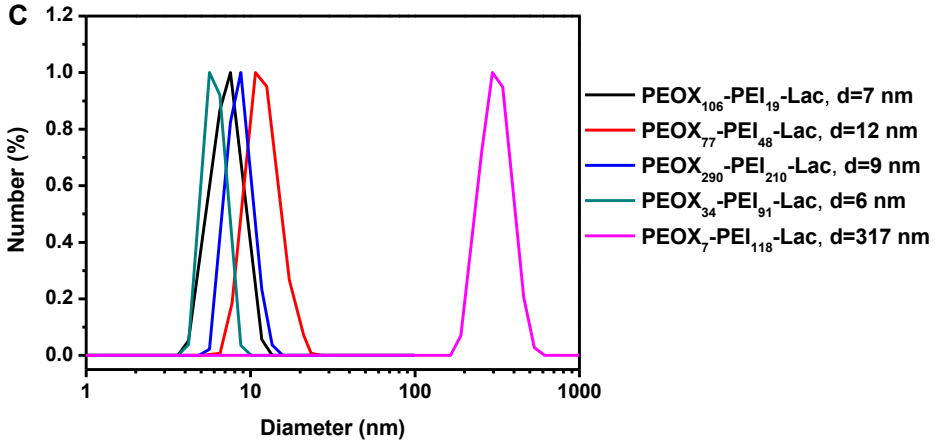

Figure 4.9: DLS traces of PEOX-PEI-Lac glycopolymers aqueous solution (1 mg/mL). (A) Intensity-weighted size distribution at 25°C; (B) Number-weighted size distribution at 25°C; (C) Number-weighted size distribution at 85°C.

4.3 Preparation of PEOX-based glyconanocapsules (PEOX-GlycoNCs) through nanoprecipitation

4.3.1 Phase diagram determination

The cloud point boundaries for water/PEOX-PEI-Lactose/acetone ternary systems were experimentally determined at room temperature using the titration method described in chapter 3. The results are plotted in the **Figure 4.10**. Basically, for each copolymer, the boundary is well described by a straight line (at a constant mass fraction of acetone). Increase of lactose content within the copolymer (*e.g.* $PEOX_{77}$-PEI_{48}-Lactose *vs* $PEOX_{7}$-PEI_{118}-Lactose) or increase of the glycopolymer molar mass (*e.g.* $PEOX_{77}$-PEI_{48}-Lactose *vs* $PEOX_{290}$-PEI_{210}-Lactose) is accompanied by a shift to a lower mass fraction of acetone. Therefore, cloud point boundaries can be tuned from 0.28 to 0.64 acetone mass fraction by simple modulation of the lactose content and molar masses. For clarity's sake, $PEOX_{77}$-PEI_{48}-Lactose, $PEOX_{290}$-PEI_{210}-Lactose

and $PEOX_7$-PEI_{118}-Lactose were selected for nanoprecipitation.

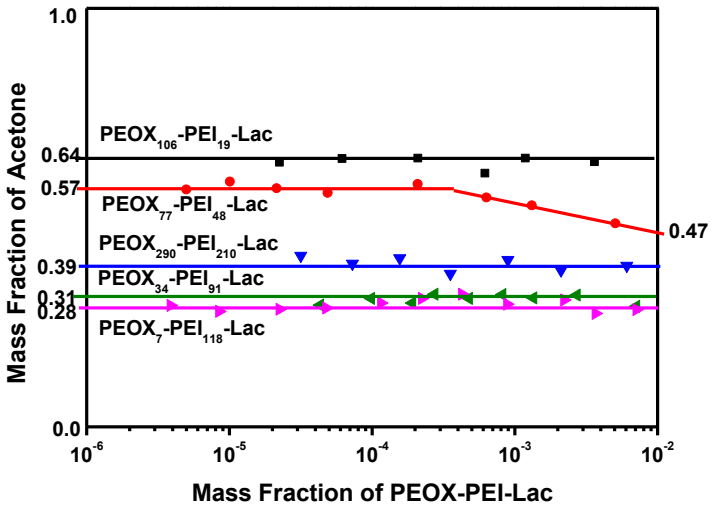

Figure 4.10: Phase diagram of water/PEOX-PEI-Lactose/acetone system.

Overlapping of water/glycopolymer/acetone and water/miglyol/acetone phase diagrams finally revealed the domain of composition where glyconanocapsules could be generated. Relying on the **Figure 4.11**, it was anticipated that well-defined glyconanocapsules could be easily constructed in the Ouzo domain in the case $PEOX_7$-PEI_{118}-Lactose and $PEOX_{290}$-PEI_{210}-Lactose whereas only a very tiny window of applicability was observed for $PEOX_{77}$-PEI_{48}-Lactose making manipulation in the Ouzo domain challenging. However, all the copolymers were found to be eligible for the preparation of glyconanocapsules in the SFME domain.

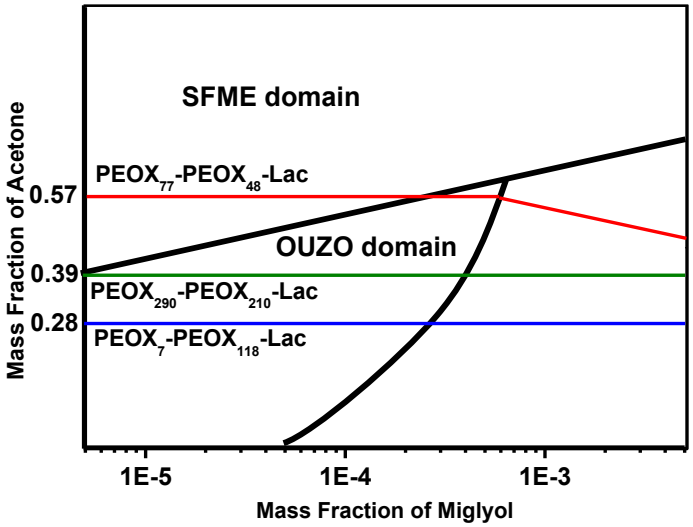

Figure 4.11: Overlapped phase diagrams of water/PEOX-PEI-Lactose/miglyol/acetone.

4.3.2 Construction of polyoxazoline-based glycoNCs by nanoprecipitation

With these phase diagrams in hands, we further examined the construction of the oil-filled polyoxazoline-based glyconanocapsules. (**Scheme 4.3**). In a preliminary step, conditions of solvent shifting were kept constant (0.2 mg of miglyol 812 in 500 mg acetone and 0.1 mg of $PEOX_7$-PEI_{118}-Lac in 500 mg of water) with the exception of IPDI initially incorporated in the organic phase to cross-link the lactose-functionalized polyoxazoline shell. As highlighted by the TEM picture given in **Figure 4.12 A**, addition of 0.01 equivalent of IPDI per hydroxyl group (0.005 mg) produced ill-defined nanocapsules with thin polymer membranes. Further increase of IPDI to 0.05 or 0.1 equivalent per hydroxyl group afforded glyconanocapsules with thick and robust shells, see **Figure 4.12 B** and **C**. Increase of IPDI content from 0.01 to 0.1 equivalent was accompanied by the progressive shrinkage of nanocapsules dimensions, with z-average diameters ranging from 338 nm with 0.01 eq of IPDI to 196 nm, with 0.1 equivalent of IPDI, see **Figure 4.12 D**.

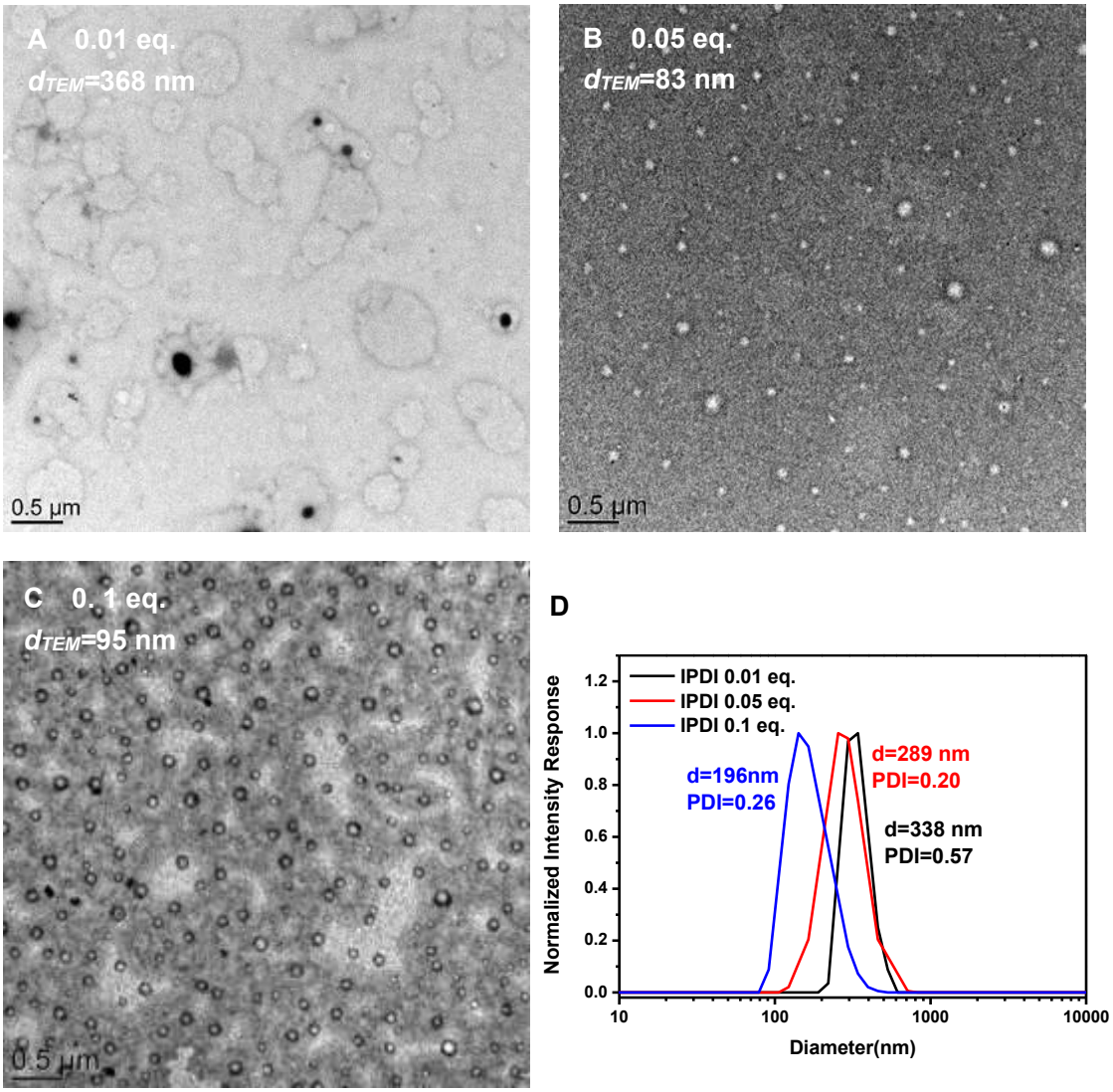

Figure 4.12: Selected TEM images and DLS plots of glyconanocapsules with $PEOX_7$-PEI_{118}-Lac 0.1 mg and IPDI 0.01, 0.05 and 0.1 equivalent per hydroxyl group (glycopolymer: 0.1 mg, miglyol: 0.2 mg, acetone mass fraction 0.5, IPDI 0.005, 0.025 and 0.05 mg respectively).

We further extended our study to $PEOX_{77}$-PEI_{48}-Lactose and $PEOX_{290}$-PEI_{210}-Lactose copolymers and explored different regions of the phase diagram (in the OUZO and SFME domain, see **Figure 4.13**). In this series of experiments, the quantity of glycopolymer and oil was maintained constant at 0.1 and 0.2 mg respectively and the amount of IPDI was fixed at 0.1 equivalent per hydroxyl group. The preparation of nanocapsules was explored at 0.50 (ouzo), 0.65 and

0.75 (SFME) acetone mass fraction. The diameter of the $PEOX_{290}$-PEI_{210}-Lac nanocapsules was 183 and 265 nm respectively in Ouzo and SFME. For $PEOX_{77}$-PEI_{48}-Lac in the SFME domain, the addition of acetone from 0.65 to 0.7 mass fraction resulted in an obvious increase of nanocapsules dimensions (from 216 to 362 nm by DLS), consistent with the previous results previously obtained in the SFME domain[12]. The hydrodynamic diameter of the nanocapsules (d_{DLS}) was obviously different from those calculated from TEM measurements in the dry state (d_{TEM}). This was attributed to the swelling capability of the nanocapsules in water resulting from the strong hydrophilicity of the PEOX-PEI-Lactose shell.

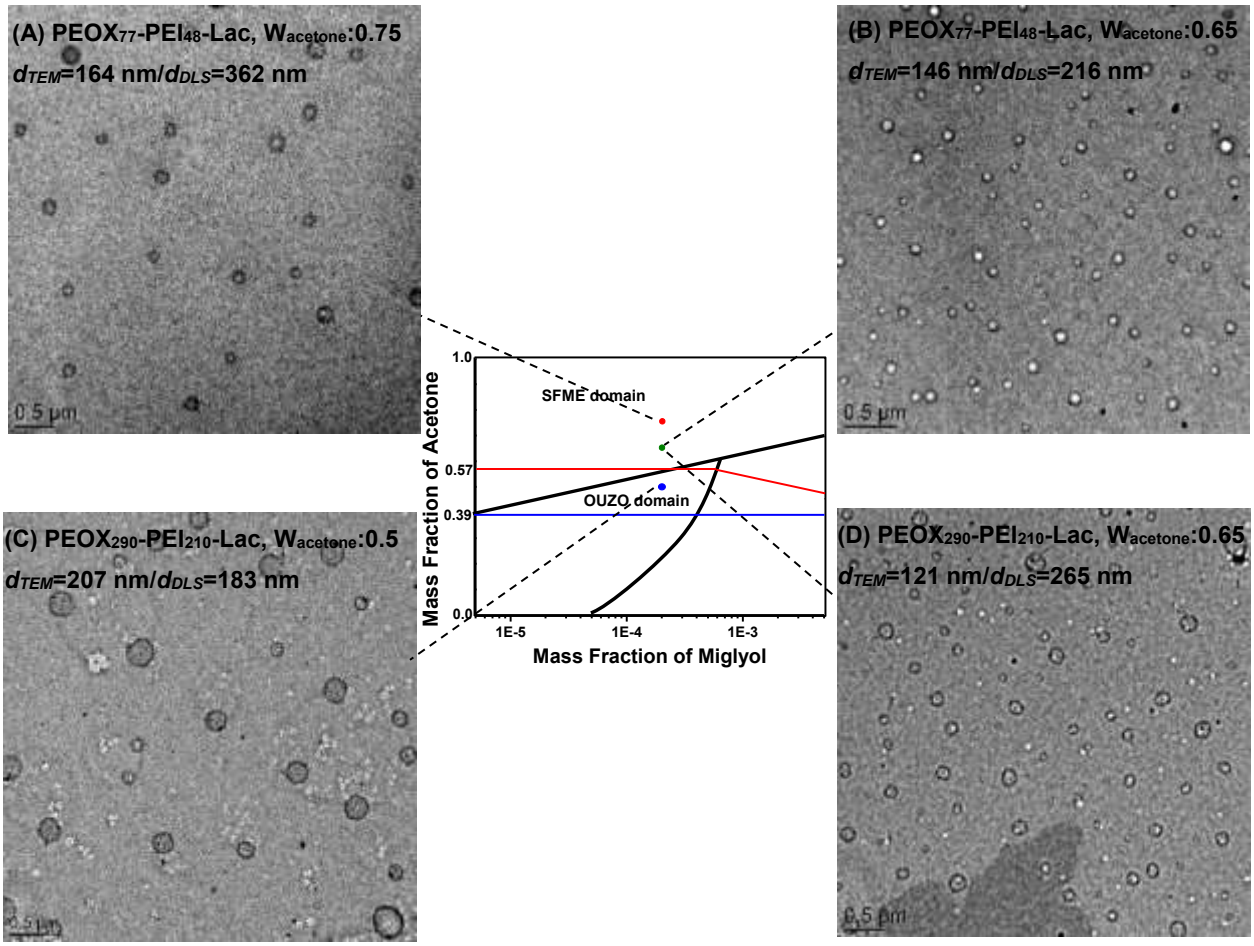

Figure 4.13: Morphologies of PEOX-PEI-Lac based nanocapsules in OUZO and SFME domain (glycopolymer: 0.1 mg, miglyol: 0.2 mg, IPDI: 0.1 eq., acetone mass fraction within images).

4.3.3 pH-Responsiveness of polyoxazoline-based glycoNCs

Owing to the presence of numerous tertiary amines within the backbone of lactose-functionalized polyoxazolines, pH-responsiveness of the resulting glyconanocapsules was subsequently explored. Capsules were first prepared from $PEOX_{290}$-PEI_{210}-Lac using solvent shifting conditions described in section 4.3.2 (glycopolymer 0.1 mg, miglyol 0.2 mg, IPDI 0.1 eq. and acetone mass fraction 0.5, resulting D_z=184 nm) (**Figure 4.14 A**). Addition of hydrochloric acid to the dispersion had a dramatic impact on the fate of nanocapsules. Exploded nanocapsules were observed by TEM after addition of 0.02 mL pH=4 HCl solution (10^{-4} N) whereas no apparent change could be stressed by DLS (**Figure 4.14 B**, D_z=166 nm). Upon addition of 0.02 mL pH=5 HCl solution (10^{-5} N), no alteration of nanocapsules morphology but a slight size increase was observed (**Figure 4.14 C**, D_z=226 nm). This acid responsive results highlighted the impact of tertiary amines protonation and the swelling of the membrane (electrostatic repulsion) on the integrity of the nanocapsules. The pH-triggered destruction of the nanocapsules (and the potential release of actives) could be of interest for drug delivery applications.

In contrast to the previous pH shifting (through addition of pH=4, 5 acid), an important swelling (D_z=736 nm) was observed upon addition of NaOH (pH=12, 0.02 mL) (**Figure 4.14 D**).

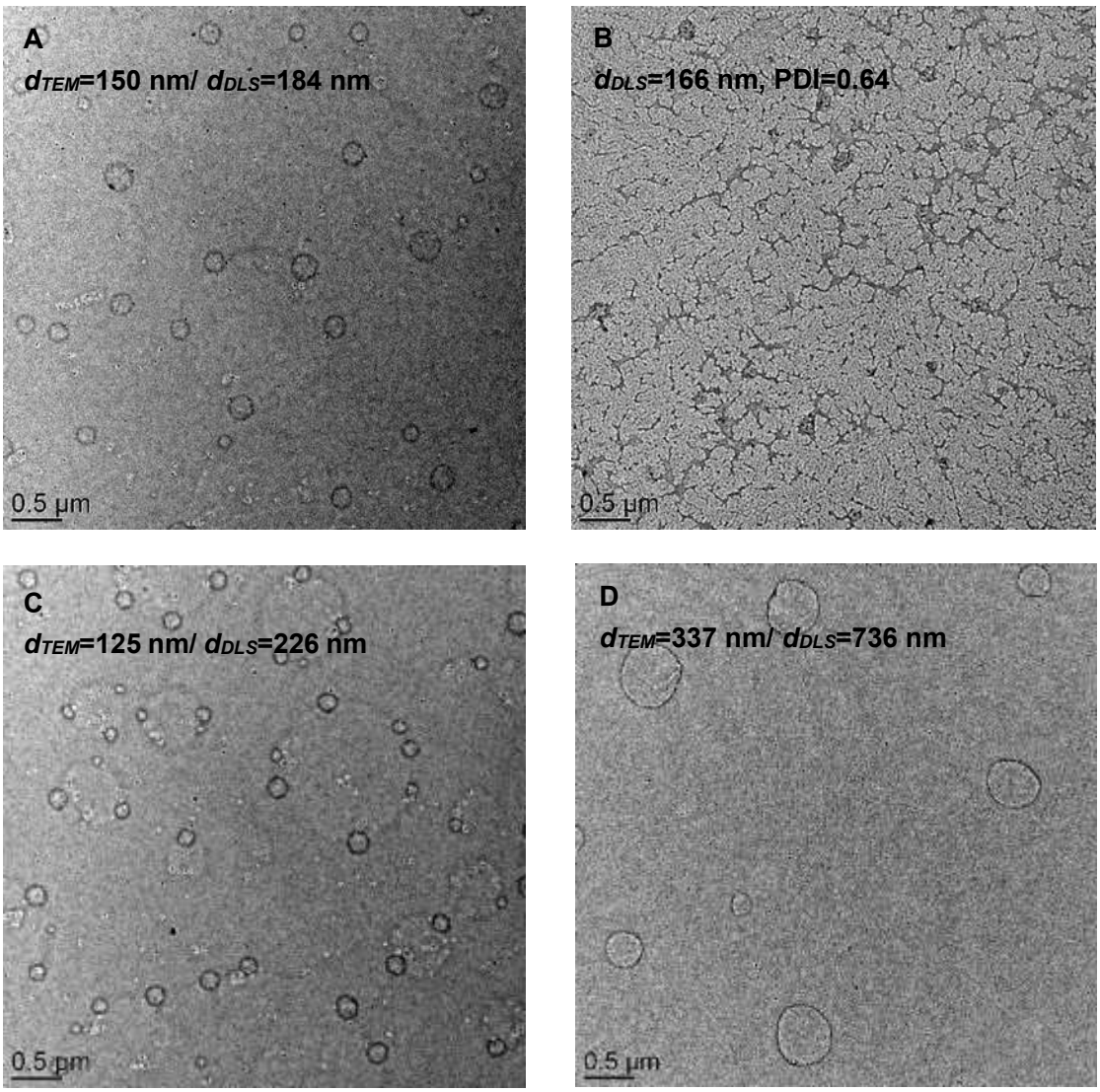

Figure 4.14: TEM images of the nanocapsules prepared from $PEOX_{290}$-PEI_{210}-Lac copolymer (A) before addition of HCl solution; (B) after addition of 0.02 mL pH=4 HCl solution; (C) after addition of 0.02 mL pH=5 HCl solution; (D) after addition of 0.02 mL pH=12 NaOH solution. (Nanoprecipitation condition: 0.1 mg polymer, 0.2 mg miglyol 812, 0.03 mg of IPDI and water/acetone mass ratio 500/500).

4.4 Functionalization of PEOX-based glyconanocapsules

4.4.1 PEG conjugated nanocapsules

Development of synthetic approaches to post-modify the shell of glyconanocapsules is highly desirable to confer additional features to the nanocarriers (enhanced colloidal stability, stealthiness, targeting…).

In this context, we decided to examine the PEGylation of the glyconanocapsules. In a preliminary test, PEG chains were incorporated in one phase before nanoprecipitation. In a typical experiment, a solution of acetone (500 mg) containing 0.2 mg of miglyol 812, 0.1 eq. of IPDI was poured into 500 mg of aqueous solution containing 0.1 mg of $PEOX_{290}$-Lac_{210}-Lac and amino-PEG (9×10^{-4} mg, 0.5 eq./polymer chain, 0.003 eq./IPDI). After overnight reaction, the formation of nanocapsules was examined by TEM (**Figure 4.15**). The hydrodynamic diameter of the resulting nanocapsules (322 nm as measured by DLS) was significantly higher than the one obtained for bare nanocapsules (normally around 180 nm by DLS).

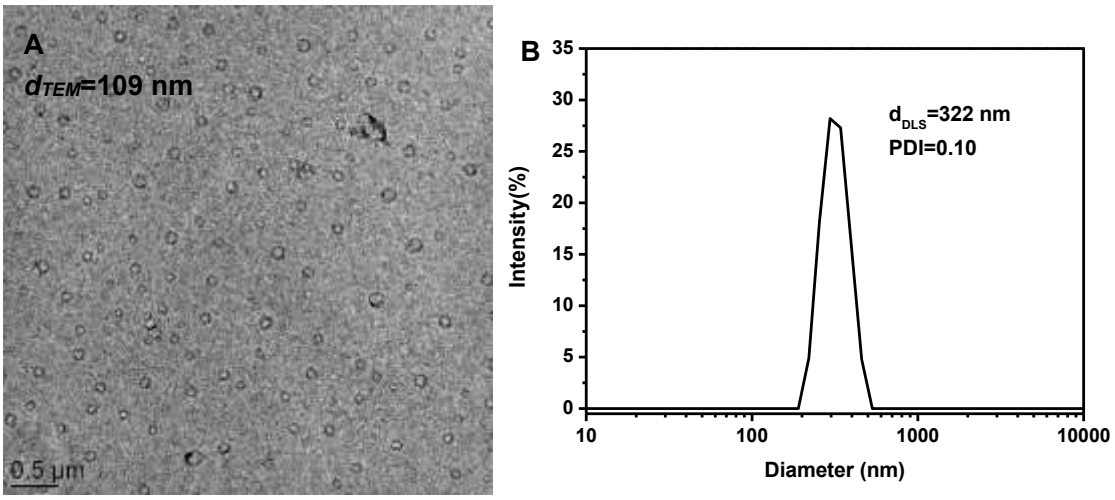

Figure 4.15: (A) TEM images of PEG-conjugated glyconanocapsules by addition of amino-PEG during nanoprecipitation procedure; (B) DLS plot of the corresponding PEG-conjugated glyconanocapsules.

In order to confirm the successful ligation of PEG segments onto the nanocapsules, we further proceeded to a scale up of the nanoprecipitation process (3 mg of polymer, 6 mg of oil, 0.9 mg of IPDI and 0.15 mg amino-PEG). After removal of acetone and free PEG chains by dialysis against water for 48 h and freeze-drying of the dispersion, the resulting material was redispersed in D_2O to perform ^1H NMR analysis. As shown in **Figure 4.16 B**, the attachment of amino-PEG on the surface of glyconaocapsules was clearly assessed by the appearance of an intense peak at 3.67 ppm corresponding to O-$\underline{CH_2CH_2}$-O groups (compared to the ^1H NMR spectrum of bare nanocapsules in **Figure 4.16 A**).

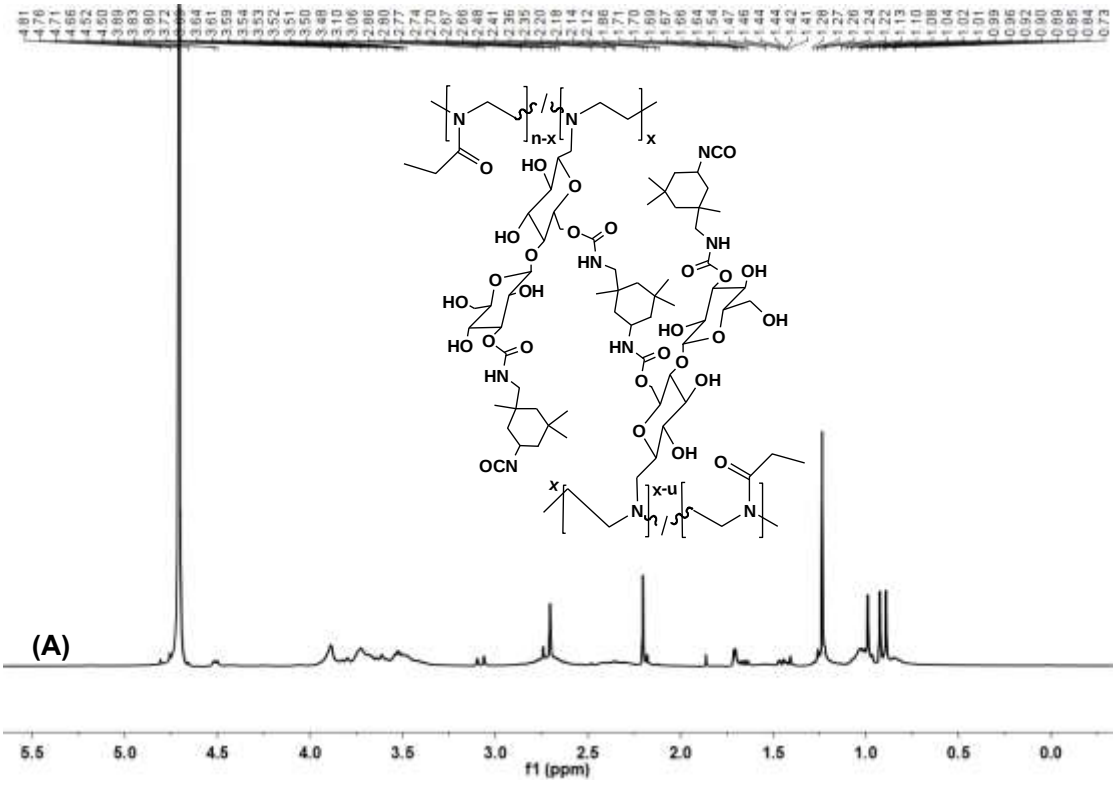

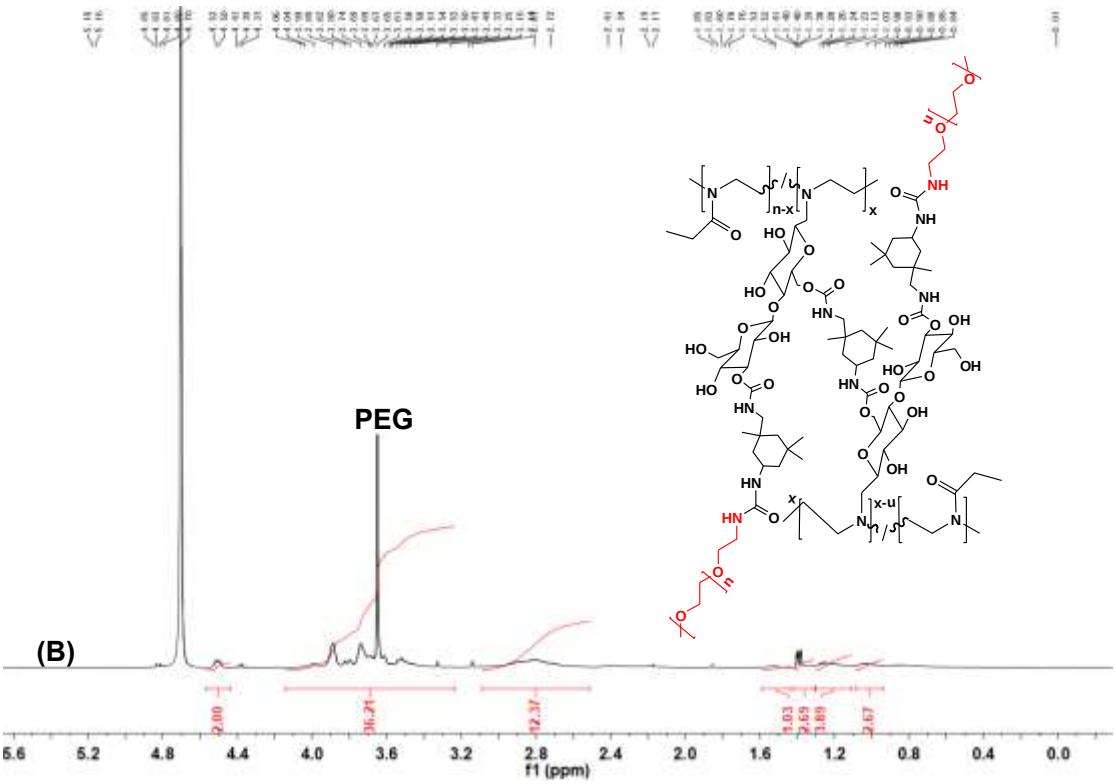

Figure 4.16: ^{1}H NMR spectra of (A) bare PEOX-based glyconanocapsules and (B) PEG conjugated PEOX-based glyconanocapsules after removal of free PEG by dialysis against water (D_2O, r. t.).

4.4.2 Conception of camptothecin-loaded glyconanocapsules

Next, we investigated the encapsulation of camptothecin (CPT), a hydrophobic anti-cancer drug within the oily core of the glyconanocapsules. To do so, CPT was initially incorporated within the organic phase using the CPT-contained miglyol (0.01 wt % of CPT *vs* miglyol) and solvent shifting was performed as previously described. 0.1 eq. of IPDI, 0.2 mg of oil and 0.2 mg of $PEOX_{290}$-PEI_{210}-Lac were used, generating glyconanocapsules of D_z=267 nm (see **Figure 4.17 A, B**). The loading of nanocapsules was directly calculated by using the intrinsic fluorescence of CPT (λ_{ex}=370 nm, λ_{em}=427 nm), see **Figure 4.17 C**. To evaluate the encapsulation efficiency in our system, the dispersion was then filtered twice through a 100 nm filter to remove the nanocapsules and the concentration of free CPT (in the filtrate) was determined from the calibration

curve given in **Figure 4.17 D**. Using the equation given below, we estimated that the encapsulation efficiency (EE) was around 70%.

$$EE\ (\%) = \frac{Total\ CPT - Free\ CPT}{Total\ CPT} \times 100\%$$

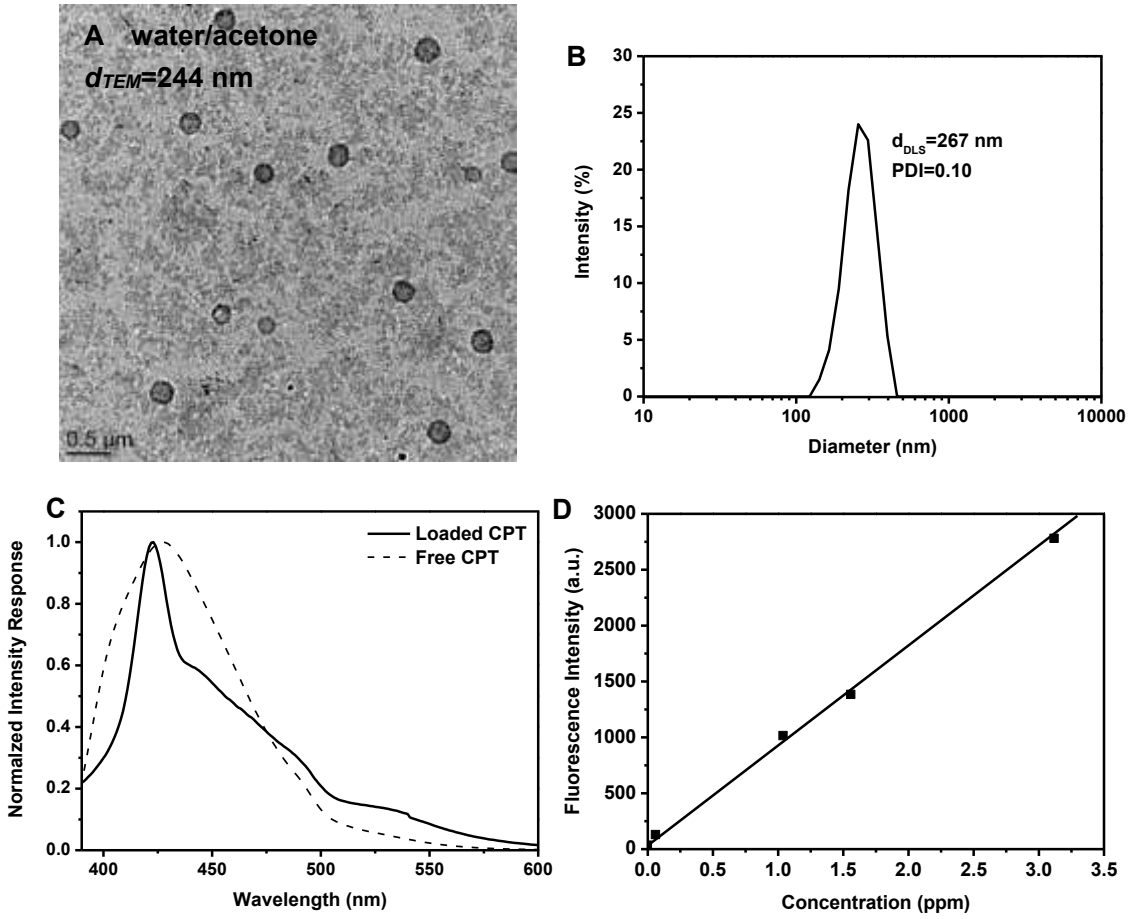

Figure 4.17: (A) TEM image of PEOX-based glyconanocapsules in water/acetone system obtained by nanoprecipitation (polymer: 0.2 mg, miglyol 0.2 mg, acetone mass fraction 0.5, IPDI 0.1 eq.; (B) DLS plot of PEOX-based glyconanocapsules in water/acetone system; (C) Fluorescence emission spectra of CPT-loaded glyconanocapsules from $PEOX_{290}$-PEI_{210}-Lactose. The solid line corresponds to the loaded CPT nanocapsules, the dash line corresponds to the free CPT at same concentration in water (the reference); (D) Calibration curve of CPT in acetone (λ_{ex}=370 nm).

After removal of acetone by dialysis against water, the pH of the aqueous phase was adjusted at 4.0 through addition of HCl and the dispersion was subsequently examined by TEM analysis. As illustrated by **Figure 4.18 B**, the CTP-loaded nanocapsules were rapidly destroyed at pH 4 affording the release of the drug contained in the core.

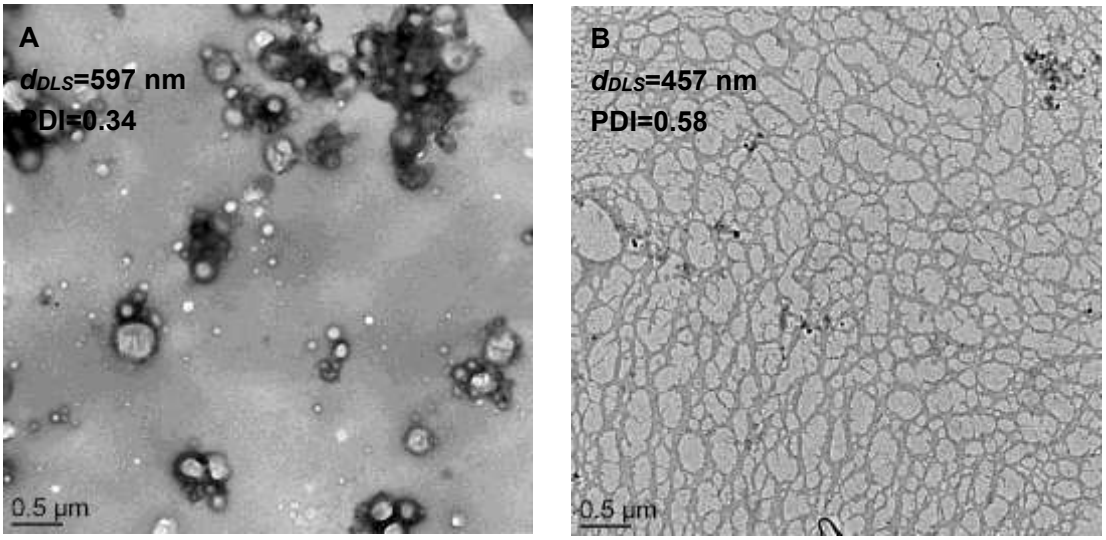

Figure 4.18: TEM image of (A) CPT-loaded PEOX-GlycoNCs in water and (B) nanocapsules degradation by addition of acid.

4.5 Conclusions

In this chapter, the successful synthesis of a series of lactose containing PEOX-based glycopolymers was described. The glycopolymers with tunable sugar contents were synthesized by varying the acidic hydrolysis time of the PEOX precursors. Nanoprecipitation process generated miglyol-filled glyconanocapsules in both OUZO and SFME domains. Besides, pH-responsive properties of the glyconanocapsules was investigated by the addition of HCl and NaOH, leading to nanocapsules' leakage or swelling. Thanks to the pH-responsiveness of the glycopolymer, the drug release could be achieved by degradation of the glyconanocapsules under acid conditions.

4.6 References

1. D. A. Tomalia, D. P. Sheetz, *J Polym Sci A.*, **1966**, 4, 2253–2265.
2. T. T. Chiu, B. P. Thill, W. J. Fairchok. In: Glass JE, editor. Advances in chemistry series 213, Washington: American Chemical Society, **1986**, 425–433.
3. S. Zalipsky, C. B. Hansen, J. M. Oaks and T. M. Allen, *J. Pharm. Sci.*, **1996**, 85, 133–137.
4. R. Hoogenboom, *Angew. Chem. Int. Ed.*, **2009**, 48, 7978–7994.
5. K. M. Kem, J. Polym. Sci., *Polym. Chem. Ed.*, **1979**,17, 1977-1990.
6. H. P. C. Van Kuringen, J. Lenoir, E. Adriaens, J. Bender, B. G. De Geest and R. Hoogenboom, *Macromol. Biosci.,* **2012**, 12, 1114-1123.
7. V. R. de la Rosa, E. Bauwens, B. D. Monnery, B. G. De Geest and R. Hoogenboom, *Polym. Chem.*, **2014**, 5, 4957-4964.
8. J. H. Jeong, S. H. Song, D. W. Lim, H. Lee and T. G. Park, *J. Controlled Release*, **2001**, 73, 391-399.
9. H. M. L. Lambermont-Thijs, F. S. Van der Woerdt, A. Baumgaertel, L. Bonami, F. E. Du Prez, U. S. Schubert and R. Hoogenboom, *Macromolecules*, **2010**, 43, 927-933.
10. M. A. Mees, C. Effenberg, D. Appelhans and R. Hoogenboom, *Biomacromolecules*, **2016**, 17, 4027−4036.
11. Q. A. Besford, M. Wojnilowicz, T. Suma, N. Bertleff-Zieschang, F. Caruso and F. Cavalieri, *ACS Appl. Mater. Interfaces*, **2017**, 9, 16869–16879.
12. X. Yan, P. Alcouffe, G. Sudre, L. David, J. Bernard and F. Ganachaud, *Chem. Commun.*, **2017**, 53, 1401-1404.

Chapter 5

Experimental Part

Chapter 5 Experimental Part

5.1 Material

Novozyme 435 (≥5,000 U/g), D-Glucose (anhydrous, 96%), sodium sulfate, O-ethylxanthic acid potassium salt, methyl bromoacetate (97%), 2,2′-Azobis(2-methylpropionitrile) (AIBN, 98%), vinyl chloroacetate (VClAc, 99+%), potassium carbonate (K_2CO_3), sodium hydroxide, BH_3*Py (8 M), boric acid, sodium boric acid, phenyl isocyanate (98+%), isophorone diisocyanate (IPDI, 98%), hexadecane (99%), methoxypolyethylene glycol amine (amino-PEG, Mw~2000 g/mol), Mowiol 4-88, Mowiol 8-88, and Mowiol 18-88, Poly(2-ethyl-2-oxazoline),) were purchased from Sigma-Aldrich and used as received. Divinyl adipate (99+%) was purchased from TCI Chemicals. Miglyol 812 was purchased from SASOL (Germany). N, N-Dimethylformamide (DMF, anhydrous), acetonitrile (anhydrous, 99.8%), methanol (HPLC, ≥99.9%), acetone (99.5%), hydrochloric acid (36-38.5%) and dialysis membranes (Mw cut-off 1000 Da, and 10,000 Da) were purchased from Carlo Erba and used as received. Water (HPLC), (S)-(+)-Camptothecin (CPT, 90%, HPLC), resveratrol (99%, HPLC), pyrene and dithiothreitol were purchased from Sigma-Aldrich and used without further purification. Cystamine was derived from the protonated cystamine dihydrochloride (Sigma Aldrich, 98%) by adding 3 eq. of triethylamine (Sigma Aldrich, 99%). Deuterium oxide (D_2O), Chloroform-d ($CDCl_3$, 99.96 atom % D), dichloromethane-d_2 (CD_2Cl_2, 99.9 atom % D) and dimethyl sulfoxide-d_6 (DMSO-d_6, 99.6%) were purchased from EURISO-TOP.

Hexadecane

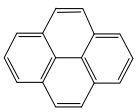

Pyrene

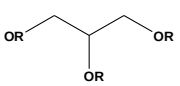

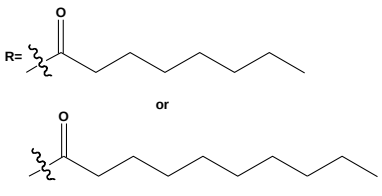

Miglyol 812

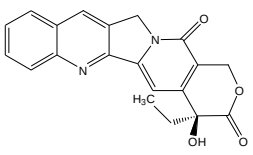

Camptothecin

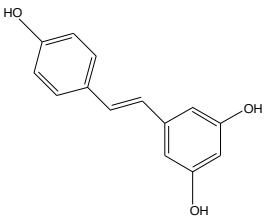

Resveratrol

226

5.2 General characterization methods

Proton nuclear magnetic resonance (^{1}H NMR) spectra and **Carbon nuclear magnetic resonance (^{13}C NMR)** were conducted on a Bruker Avance Ⅲ spectrometer (400 MHz) at 298K with $CDCl_3$, DMSO-d_6, D_2O or DMSO-d_6/D_2O as solvent.

Electrospray Ionization mass spectrometry (ESI-MS, m/z) of glycomonomer was performed on a MicrOTOFQ Ⅱ-Bruker equipped with 4 sources (ESI, APCI, DESI, CSI).

Flash chromatography was performed by loading 200 g of silica gel (60 Å, ≤63 μm, Fluka) on a 76 mm o.d. glass column. The fraction eluting was subjected to column chromatography and then used for TLC analysis, which was performed on glass-backed silica gel plates.

Size exclusion chromatography (SEC) of phenyl isocyanate protected glycopolymers were carried out on a Viscotek VE1121 System equipped with three columns (Waters HR2, HR1 and HR0.5) and a differential refractive index detector (Viscotek VE3580). THF was used as the eluent at a flow rate of 1 mL/min. The molecular weight and the distribution were calculated from polystyrene standard calibration curve. SEC analysis of polyoxazoline glycopolymers was performed in an acetate buffer (pH 4.8) at a flow rate of 0.5 mL/min at 25°C on a Waters 510 apparatus equipped with a refractive-index detector Water 410 and a laser light scattering (Wyatt Technology) dual detection and fitted with TSK6000 columns based on fused silica. The dn/dc coefficients were calculated at 664 nm detected with a laser source.

Dynamic light scattering (DLS) measurements were carried out on a

Zetasizer Nano device (Malvern Instrument, Malvern, U.K) and using the cumulant method. For each sample, at least five measurements were carried out. The mean size distribution of glycopolymers was approximated as the volume diameter and the mean particle size of capsules was approximated as intensity diameter. The width of distribution as the polydispersity index of the particles (PDI) obtained by the cumulant method.

Transmission electron microscopy (TEM) images were performed on a Philips CM120 electronic microscope. The capsules were observed at 80 kV electron beam accelerating voltage by loading a drop of sample solution on a Formvar-coated 200 mesh copper grid. The excess solution was carefully blotted off using filter paper and samples were dried for a few minutes before analysis.

Fluorescence spectroscopy measurements were obtained with a JASCO FP-8000 spectrofluorometer. For the construction of calibration curves, five different concentrations of fluorophores in acetone (pyrene, from 1.26 to 0.063 ppm; camptothecin, from 1.56 to 2.49E-5 ppm) or ethanol (resveratrol, from 0.1 to 7.5 ppm) were prepared. All experiments were carried out at room temperature.

5.3 Synthesis of 6-*O*-Vinyladipoyl-D-glucopyranose

D-Glucose (15.2 g, 0.084 mol), divinyl adipate (25 g, 0.13 mol), and novozyme 435 (8 g) were introduced into 140 mL of acetonitrile solvent in a round flask sealed with a rubber septum. The flask was stirred at 50°C for 24 h under 200 rpm. The reaction was stopped by filtering off the enzyme, and acetonitrile was then removed from the obtained bright yellow solution by rotary evaporation, yielding a yellow-brown syrup. After diluted with methanol, the crude product

was purified by flash chromatography, using ethyl acetate/cyclohexane/ethanol (11: 8: 1) as eluent. The collected fractions were checked by TLC with plates immersed in a 20% H_2SO_4/ethanol solution and heated at 80°C for the presence of the product (R_f 0.17). The title product was then extracted by rotary evaporation as white powder (9.5 g, yield 34% with respect to D-Glucose).

5.4 Synthesis of methyl [(ethoxycarbonothioyl)sulfanyl] acetate (CTA)

O-ethylxanthic acid potassium salt (1 g, 6.24 mmol) was dissolved in pre-prepared dry acetone (4 mL), methyl bromoacetate (1 g, 6.24 mmol) was added dropwise into the mixture under stirring at room temperature. After 4 h reaction, the KBr white precipitate was filtered off and acetone was evaporated off, yielding bright green liquid product. The fraction was purified by flash chromatography, using cyclohexane/ethyl acetate (4:1) as eluent. Finally, 1.1 g of liquid product was obtained (yield 88%).

5.5 Preparation and alcoholysis of PVClAc

Representative RAFT homopolymerization of VClAc. In a Schlenk tube, VClAc (264 mg, 2.2 mmol), AIBN (0.36 mg, 2.2×10^{-3} mmol) and CTA (2.13 mg. 0.011 mmol) were dissolved in ethyl acetate (1.1 mL) ([VClAc]:[CTA]:[I]=200:1:0.2). Then the tube was degassed by three freeze-pump-thaw cycles. The polymerization was carried out at 80°C and stopped at 4 h by cooling the solution in ice water. The resulting polymer solution was precipitated into stirring cyclohexane and dried in vacuum at room temperature to get pure PVClAc (185 mg, yield 96%).

Representative alcoholysis of PVClAc to PVA. PVClAc ((20 mg, 0.17 mmol VClAc groups) was dissolved in ice DMF/Methanol (9 mL, 1:3, v/v) for 20 min. K_2CO_3 (3.38 mg, 0.024 mmol) was added to the solution and allowed to react for 20 min in ice bath. The organic solvent was removed by dialysis against water. Freeze-dry to remove water and obtained white fluffy product.

5.6 Preparation and stabilization of PVAG

Representative RAFT homopolymerization of VAG. VAG (200 mg, 0.6 mmol), methyl [(ethoxycarbonothioyl)sulfanyl]acetate (0.7 mg, 3.8×10^{-3} mmol) and AIBN (0.1 mg, 7.6×10^{-4} mmol) were dissolved in 1 mL of ethanol/water mixture (1:1, v/v). The solution was subjected to a schlenk tube. After deoxygenated by three freeze-thaw cycles and filled with argon, the tube was placed in oil bath at 70°C for 24 h. The polymerization was quenched using liquid nitrogen (conversion 35%) and product was precipitate in diethyl ether/ethanol mixture (8:2, v/v) three times to remove excess of monomer and initiator and dried under vacuum to get PVAG as white solid (47 mg, yield 67%).

Derivatization of PVAG. In brief, PVAG (6 mg, 3.2×10^{-4} mmol) was dissolved in anhydrous DMF (0.5 mL) containing phenyl isocyanate (9 mg, 5 equivalent per hydroxyl group). The solution was stirred for 48 h at room temperature. After reaction, the crude product was washed with excess diethyl ether and dried under vacuum. The derived copolymer was obtained as a beige paste and used for SEC analysis.

Stabilization of PVAG. PVAG (20 mg, 0.06 mmol of VAG groups) was poured in 9 mL of DMF/Methanol solution (1:3, v/v) at 0°C. K_2CO_3 (3.38 mg, 0.024 mmol) was added into the system to react for 20 min in ice bath. The mixture was conducted into a membrane bag to dialysis against water for 24h at room

temperature. Polymers were extracted after water was freeze-dried.

5.7 Preparation of PVA-based glycopolymer

Representative preparation of P(VClAc-co-VAG). VAG (200 mg, 0.6 mmol) and vinyl chloroacetate (723 mg, 6 mmol) was dissolved in anhydrous DMF (0.25 mL), followed by the addition of CTA (13 mg, 0.067 mmol) and AIBN (2.2 mg, 0.013 mmol). The mixture was subjected to a schlenk tube. After deoxygenated by three freeze-thaw cycles and filled with argon, the tube was placed in oil bath at 80°C for 24 h (conversion: VClAc 71%, VAG 61%). The polymerization was quenched using liquid nitrogen and product was precipitate in diethyl ether/ethanol mixture (8:2, v/v) three times to remove excess of monomer and initiator and dried under vacuum to get 400 mg of P($VClAc_{59}$-*co*-VAG_9) as brown solid (yield: 63%). The copolymer was used for selective hydrolysis.

Derivatization of P(VClAc-*co*-VAG). Typically, P($VClAc_{59}$-*co*-VAG_9) (6 mg, 5.4×10^{-4} mmol) was dissolved in a solution of anhydrous DMF (0.5 mL) containing phenyl isocyanate (14 mg, 5 equivalent per hydroxyl group). The solution was stirred for 48h at room temperature. After reaction, the crude product was washed with excess diethyl ether and dried under vacuum. The derived copolymer was obtained as a beige paste and used for SEC analysis.

Selective hydrolysis of P(VClAc-*co*-VAG). P($VClAc_{59}$-*co*-VAG_9) (100 mg, 0.65 mmol of VClAc groups) was dissolved in 20 mL of DMF/methanol mixture (3:1, v/v) for 20 min stirring. Then the flask was placed in ice bath, followed by addition of K_2CO_3 (7.5 mg, 0.05 mmol). After 20 min reaction, the solution was put into a dialysis bag (Mw cut-off 1000 Da) and dialyzed against distilled water for 48h to remove the small molecules and organic solvents. The P(VA_{59}-*co*-VAG_9) was obtained after freeze-dry to remove excess of distilled

water as brown solid.

5.8 PVA-based nanocapsules (PVA-NCs)

Preparation of shell cross-linked PVA-NCs

(1) Preparation of HD-filled nanocapsules. In a typical experiment condition, PVA aqueous solution was prepared by dissolution of Mowiol 4-88 (0.15 mg) in 330 mg of water. The organic phase was composed of 1.5 mg of HD, 0.27 mg (0.4 eq./OH) of IPDI and 670 mg of acetone. This phase was poured all at once into the PVA aqueous solution at room temperature and stabilized overnight for DLS and TEM characterization. After that, the mixture was dialyzed against water foe 24h, followed by freeze-dry. The obtained solid was redispersed in water for further characterization.

(2) Preparation of miglyol-filled nanocapsules. Mowiol 8-88 (0.015 mg) was dissolved in 430 mg of water. 0.5 mg of miglyol dissolved in 570 mg of acetone, together with 0.027 mg of IPDI (0.4 eq./OH) as the shell cross-linker, was poured all at once into the PVA aqueous solution. After mixing by shaking immediately, the acetone aqueous solution was stabilized at room temperature for one night before characterization by DLS and TEM.

Stabilization of PVA-NCs by “salting out”

Mowiol 4-88 (0.15 mg) was dissolved in 330 mg of water. 1.5 mg of HD (and 0.006 mg of IPDI) was dissolved in 670 mg of acetone. After mixing water phase and acetone phase by briefly shaking at room temperature and saved overnight, the mixture was dialyzed against 0.5 M Na_2SO_4 aqueous solution for 24h. Consequently, the obtained solution was dialyzed against water for 24h.

5.9 PVA-based glyconanocapsules (PVA-GlycoNCs)

Preparation of shell cross-linked PVA-GlycoNCs

(1) Preparation of HD-filled PVA-GlycoNCs. In a typical run, glycopolymer (0.15 mg) was dissolved in 330 mg of water. 1.5 mg HD dissolved in 670 mg of acetone, together with a given amount of IPDI (0.4 eq./OH) was mixed with the glycopolymer aqueous solution at room temperature. The resulting mixture was left overnight and then characterized by DLS and TEM.

(2) Preparation of HD-filled glyco & PVA-based nanocapsules. Briefly, Mowiol 8-88 (0.05 mg) and P(VA_{34}-*co*-VAG_{19}) (0.05 mg) was dissolved in 330 mg of water. 670 mg of acetone was mixed with HD (1.5 mg) and IPDI (0.085 mg, 0.2 eq./OH). After the homogenization step by pouring acetone solution into water solution all at once, the produced mixture was stand overnight for later characterization.

(3) Carbohydrate-lectin binding. P(VA_{59}-*co*-VAG_{9}) (0.15 mg) was dissolved in 330 mg of water. 1.5 mg HD dissolved in 670 mg of acetone, together with IPDI (0.4 eq./OH) as the shell cross-linker, was poured all at once into the glycopolymer aqueous solution at room temperature for overnight. 670 mg of water was then added into the system, immediately followed by rotary evaporation to remove acetone. 40 ul of Con A aqueous solution (0.02 mg/mL) was added into the system and shaken 10 min for characterization.

Preparation of non-cross-linked PVA-GlycoNCs

Generally, 330 mg of water containing 0.15 mg of glycopolymer was poured all at once into 670 mg of acetone containing 1.5 mg of HD. After briefly shaking and stabilizing overnight, the system was dialyzed against water for 24h to remove acetone. Then, sodium hydroxide was added into the system to adjust aqueous solution pH=12 at room temperature. The yielded solution was characterized by TEM 1h later.

5.10 Functionalization and loading of PVA-NCs

PEG-functionalized nanocapsules. 3.3g of water containing 1.5 mg of Mowiol 4-88 and 3.0 mg of amino-PEG (0.05 equivalent with respect to hydroxy group) was added to 6.7g of acetone solution consisting of 15 mg of HD and 2.7 mg of IPDI cross-linker. After completely mixing by briefly shaking, the system was stand overnight at room temperature followed by dialysis against water for 48h. White powder was obtained after freeze-dry and then used to perform NMR analysis in D_2O.

Pyrene-loaded nanocapsules. The fluorescent pyrene was first dissolved in HD (2.5 wt.%). Experiment was performed with twice amount as the general condition. A total of 3 mg of HD and pyrene, together with 0.54 mg of IPDI (0.4 eq.), were dissolved in 1.34 g of acetone. 0.66 g of water containing Mowiol 4-88 (0.3 mg) was poured all at once into the acetone solution at room temperature. The resulting mixture was left overnight for stabilization. After that, the mixture was divided into two equal vials. The first vial was dialyzed against water for 48 h and then analyzed by DLS, TEM and fluorescence spectroscopy. The second vial was filtered 2-times through 100 nm filter to remove the nanocapsules. After evaporation to remove acetone and freeze-dry to remove water, the obtained product was redispersed in 2 mL of acetone for fluorescence analysis. The concentration of pyrene in the solution was determined from a calibration curve of pyrene in acetone. Thus, the encapsulation efficiency (EE) could be calculated by: $EE(\%) = \frac{Total\ pyrene - Free\ pyrene}{Total\ pyrene} \times 100\%$.

Encapsulation of camptothecin (CPT). Mowiol 4-88 (0.3 mg) was dissolved in 0.66 g of water. 3 mg of HD (0.01 wt. % CPT) dissolved 1.34 g of acetone, together with 0.54 mg of IPDI as the shell cross-linker, was poured all at once

into the aqueous solution at room temperature. After overnight, 1g of the mixture was taken out and dialyzed against water for fluorescence spectroscopy, DLS and TEM. Another vial of 1g mixture was filtered through 100 nm filter 2-times to remove nanocapsules. After removal of acetone by rotary evaporation and water by freeze-dry, the obtained product was redispersed in 2 mL of acetone for fluorescence analysis. Thanks to the calibration curve of CPT in acetone, the encapsulation efficiency could be calculated from: $EE(\%) = \frac{Total\ CPT - Free\ CPT}{Total\ CPT} \times 100\%$.

Encapsulation of resveratrol. Similarly, 0.66 g of water contained Mowiol 4-88 (0.3) was mixed with 1.34 g of acetone contained 3 mg of HD (0.1 wt. % resveratrol) and 0.54 mg of IPDI cross-linker. After left overnight, the resulting mixture was divided into two equal vials. One of the vials was dialyzed to remove free drugs and characterized by fluorescence spectroscopy, DLS and TEM. Another vial was filtered through 100 nm filter by 2-times. After evaporation to remove acetone and freeze-dry to remove water, the obtained product was redispersed in 2 mL of ethanol for fluorescence analysis. The concentration of resveratrol in the solution was determined thanks to a calibration curve of resveratrol in ethanol. The encapsulation efficiency (EE) induced from equation $EE(\%) = \frac{Total\ Resv - Free\ Resv}{Total\ Resv} \times 100\%$ was 37%.

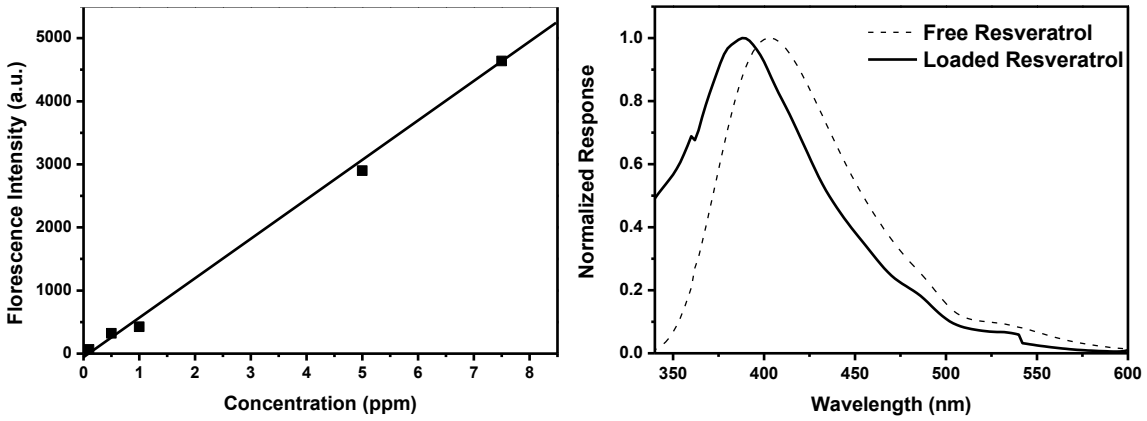

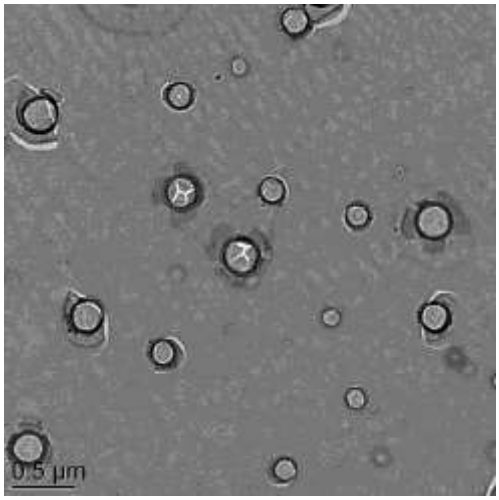

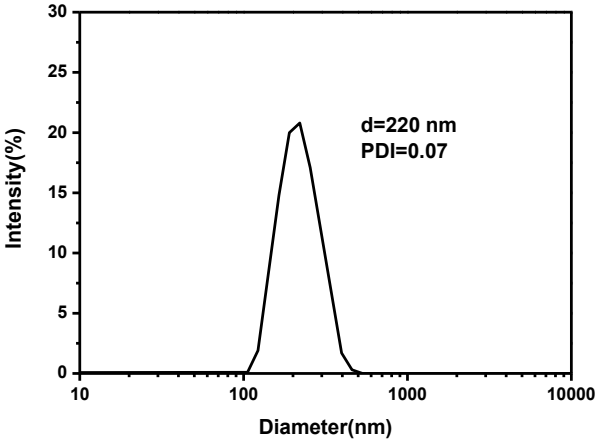

Degradation of PVA-NCs

Preparation: Mowiol 4-88 (0.15 mg) and cystamine (0.09 mg in triethylamine) were dissolved in 300 mg of water. In a second vial, HD (0.4 mg) and IPDI (0.27 mg) were dissolved in 700 mg of acetone. The acetone solution was then pure into the polymer aqueous solution all at once. The mixture was left over night.

Degradation: After removing of acetone by dialysis against water, dithiothreitol (DTT, 2 mg) was then added into the slightly cloudy dispersion. After 2 h reaction at room temperature and under stirring, the mixture became transparent and TEM was further performed for the degradation.

5.11 Synthesis of polyethyloxazoline glycopolymers

Representative acid hydrolysis of poly(2-ethyl-2-oxazoline) (PEOX)

$PEOX_{500}$ (500 mg) was fully dissolved in 5 mL of water in a glass flask by stirring and heating at 40°C for 20 min. 5 mL of concentrated HCl (36.5 wt.%) was added and the mixture was then heated to 100°C. The reaction was stopped after 2 h and cooled under running water. The acid solution was neutralized immediately by the addition of aqueous sodium hydroxide solution.

After dialysis and freeze-dry, 372 mg of white fluffy powder was obtained, with hydrolysis degree 42% and yield 98% calculated from ^{1}H NMR.

Synthesis of PEOX-based glycopolymers

$PEOX_{290}$-PEI_{210} precursor (100 mg, PEI 0.57 mmol), lactose (3.93 g, 11.48 mmol), and borane−pyridine complex (BH_3*Py, 8 M, 1.2 mL) was dissolved in a sodium borate buffer (0.1 M, pH=7.4, 10 mL). The solution was stirred at 50°C for 7 days. The crude product was purified by dialysis against deionized water for 2 days (1000 MWCO). A solid product was obtained by freeze-drying and for further characterization by NMR.

5.12 PEOX-based glyconanocapsules

Preparation of PEOX-based glyconanocapsules and pH-responsiveness. In one vial, $PEOX_{290}$-PEI_{210}-Lac (0.1 mg) was dissolved in 500 mg of water. In a second vial, 0.2 mg of miglyol 812 was dissolved in 500 mg of acetone, together with IPDI cross-linker 0.03 mg (0.1 equivalent per hydroxyl group). The organic phase was mixed with the aqueous phase and shaken under room temperature. The mixture was stand still overnight for TEM and DLS characterization. 0.02 mL of HCl solution (pH=4, 5) or NaOH solution (pH=12) was added into the mixture and homogenized by shaking. After 30 minutes, the mixture was analyzed by TEM and DLS.

PEG-functionalization. 500 mg of water solution contained $PEOX_{290}$-PEI_{210}-Lac (0.1 mg) and amino-PEG (9×10^{-4} mg, 0.5 equivalent of polymer chain) was mixed with 500 mg of acetone solution (miglyol 0.2 mg, IPDI 0.03 mg) by briefly shaking. The mixture was kept overnight and characterized by TEM and DLS. Nanoprecipitation of enlarged amount was

performed for investigation of successful attachment: water/acetone 15 g/15 g, $PEOX_{290}$-PEI_{210}-Lac 3 mg, miglyol 6 mg, amino-PEG 0.15 mg and IPDI 0.9 mg. After nanoprecipitation procedure, the mixture was evaporated and then dialyzed against water for 2d and then freeze-drying for NMR characterization.

Drug delivery and release. $PEOX_{290}$-PEI_{210}-Lac (1 mg) was dissolved in 2.5 g of water. 1 mg of miglyol (0.01 wt. % CPT) dissolved 2.5 g of acetone, together with 0.3 mg of IPDI as the shell cross-linker, was poured all at once into the aqueous solution at room temperature. After overnight, the mixture was separated to equal mass of solution into two vials. The first vial of solution was dialyzed against water for fluorescence spectroscopy, DLS and TEM. After that, the solution was adjusted to pH=4 for 2 h reaction for capsule degradation and drug release. Another vial of solution was filtered through 100 nm filter 2-times to remove nanocapsules. After removal of acetone by rotary evaporation and water by freeze-dry of the filtrate, the obtained product was redispersed in 2 mL of acetone for fluorescence analysis. Thanks to the calibration curve of CPT in acetone, the encapsulation efficiency could be calculated from: $EE(\%) = \frac{Total\ CPT - Free\ CPT}{Total\ CPT} \times 100\%$.

General Conclusion

General Conclusion

With the aim of preparing a new family of glyconanocarriers, this PhD research was dedicated to the fabrication of original biocompatible glycopolymers and multifunctional oil-filled glyconanocapsules thereof by nanoprecipitation.

In the literature review chapter, we reported on the main chemical and physical routes to glyconanocapsules and their applications. Whereas amphiphilic (glyco)copolymer self-assembly, template strategies and emulsification techniques are by far the most popular methods to generate glyconanocapsules from glycopolymers. It was shown that the nanoprecipitation process is emerging as a promising approach to build complex glyconanocarriers in a simple one-step procedure.

In the Chapter 2, we reported the synthesis of a series of PVA-based glycopolymers. Firstly, a sugar vinyl ester monomer was synthesized through a chemoenzymatic process. Secondly, three polyvinyl ester-based glycopolymers containing varying densities of sugar groups were obtained through copolymerization of vinyl chloroacetate and sugar vinyl ester using the MADIX/RAFT process. Finally, selective alcoholysis under mild conditions yielded the expected PVA-based glycopolymers. We confirmed the chemical structures and molecular weight distributions of these glycopolymers by NMR analyses and SEC and finally investigated the solution behaviour of the resulting glycopolymers in water.

In the chapter 3, we described the one-step construction of a series of nanocapsules from commercial PVA chains and PVA-based glycopolymers by a straightforward nanoprecipitation process in both OUZO and SFME domains. The evolution of capsule shell as a function of cross-linker content was

investigated. The dimensions of nanocapsules could be controlled precisely by varying the solvent ratio and oil contents. Stabilization of the nanocapsules in water was ensured by covalent cross-linking of the shell and/or by addition of salt. Owing to the simplicity of the process, the prepared PVA-based nanocapsules and glyconanocapsules could be conveniently decorated with biomolecules, loaded with hydrophobic actives and interacted with lectin (ConA). Through insertion of the redox-sensitive cross-linking bridges in the PVA shell, the nanocapsules were effectively degraded upon addition of DTT. These findings suggest that this simple route to oil-filled functional glyconanocapsules could be transposed to other oil and polymer systems.

In the chapter 4, we prepared a series of poly(2-ethyl-2-oxazoline-based glycopolymers with tunable lactose contents by modulating the acidic hydrolysis time for the polyethyloxazoline precursors. Miglyol-filled glyconanocapsules were built through nanoprecipitation process in OUZO and SFME domains. Due to the protonation of the tertiary amines present in the polymer chains , the nanocapsules were rapidly destroyed upon addition of an acidic solution (pH4) which was successfully exploited for the release of drug.

In terms of perspectives, the fascinating properties of glycopolymers offer multiple opportunities in the field of carbohydrate-based drug delivery systems. For instance, the construction of temperature responsive polyethyloxazoline-based glycopolymers would be of great interest to investigate the nanocapsules' morphologies and the related drug-loading efficiency and drug release speed at different temperatures.

Annex

Annex

Annex 1. Diameter of Mowiol 4-88-NCs with different PVA/HD

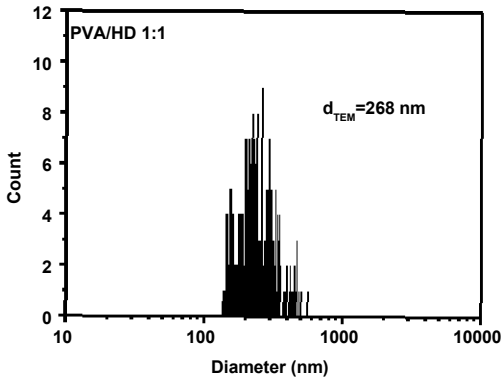

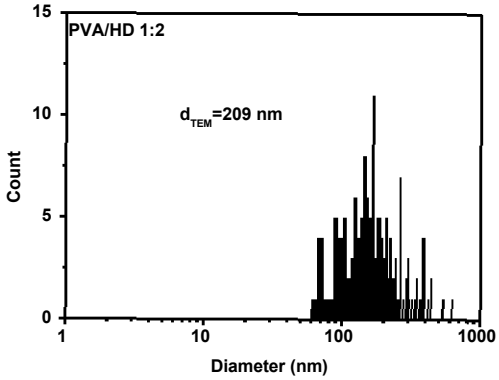

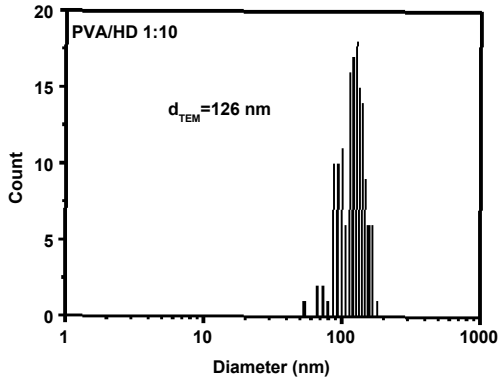

Annex 2. Diameter of shell cross-linked PVA-NCs

Figure A1. Diameter of Mowiol 4-88-NCs with varying contents of IPDI

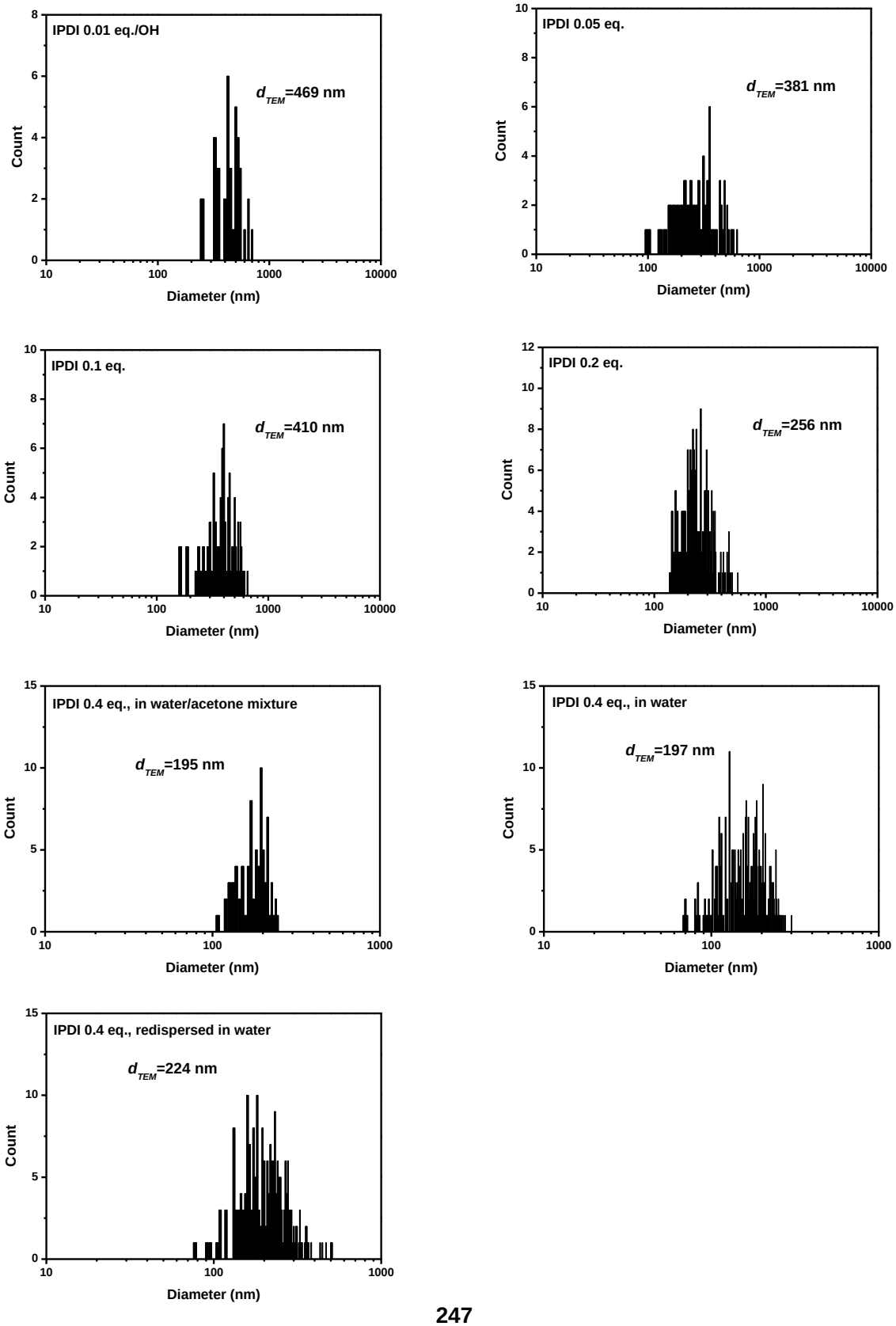

Figure A2. Diameter of Mowiol 4-88-NCs beyond OUZO domain (IPDI 0.4 e q)

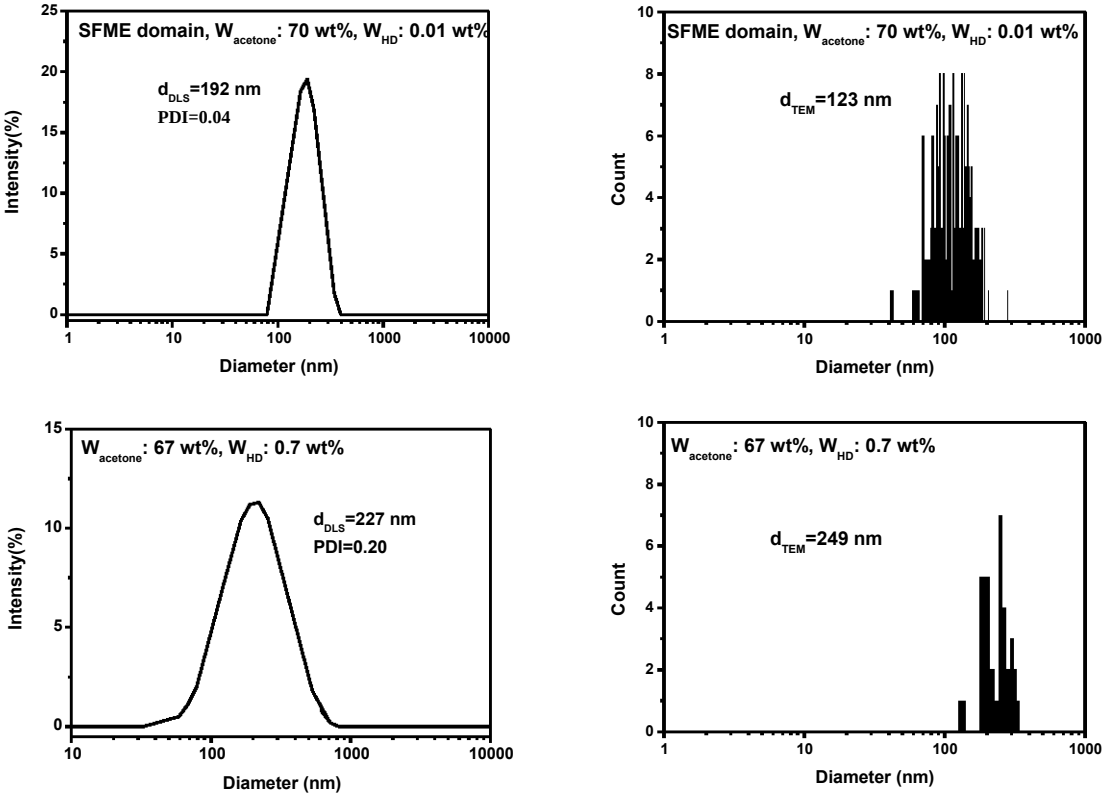

Figure A3. Diameter of Mowiol 8-88-NCs in OUZO domain (IPDI 0.4 eq)

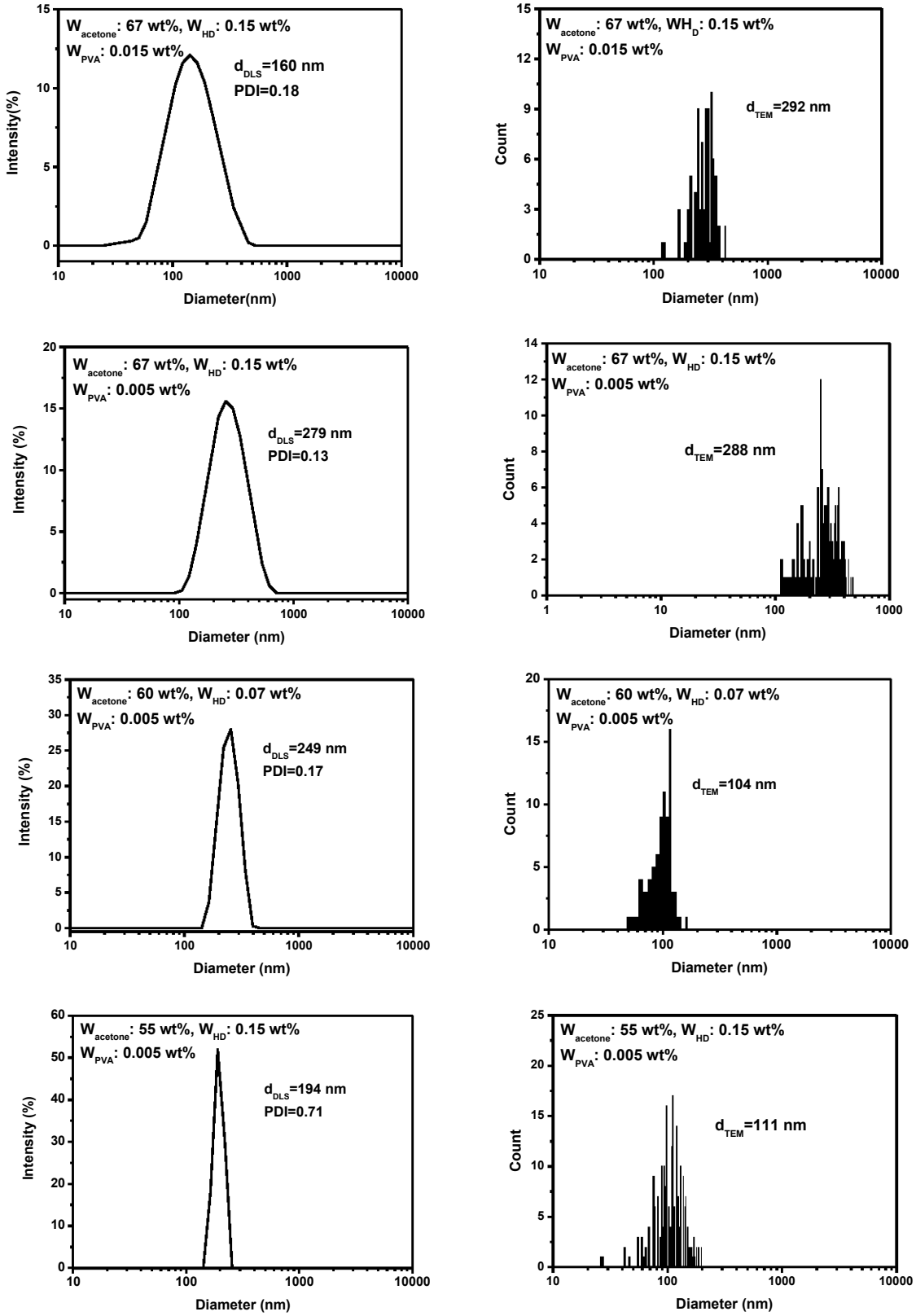

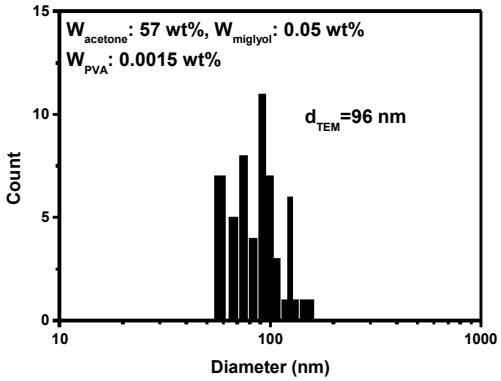

Figure A4. Diameter of Mowiol 8-88-NCs in SFME domain (IPDI 0.4 eq)

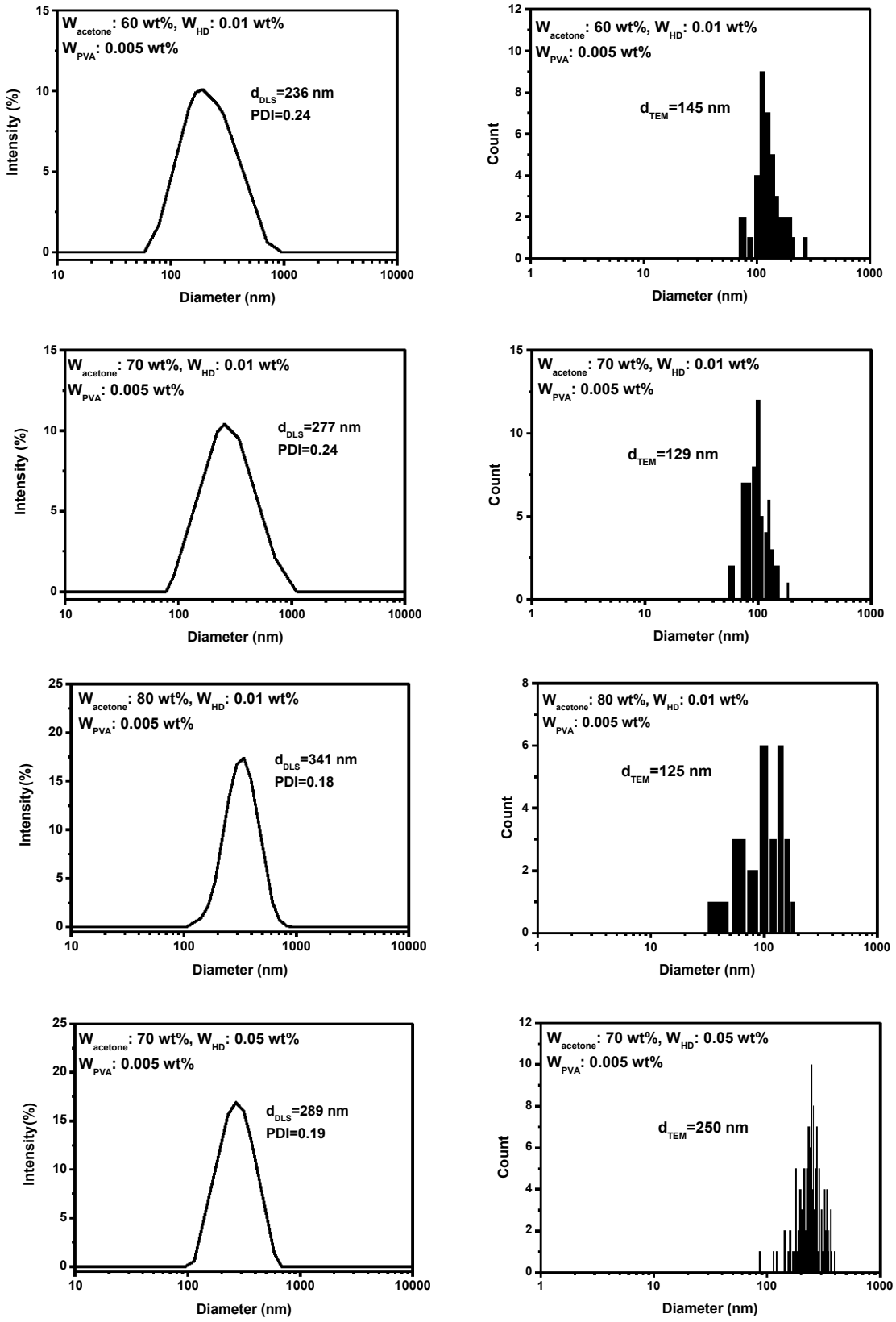

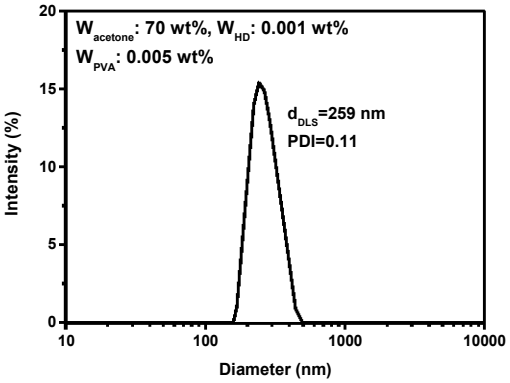

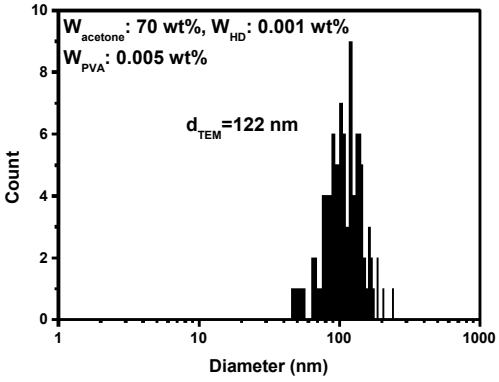

Annex 3. Diameter of Mowiol 4-88-NCs through “salting out”

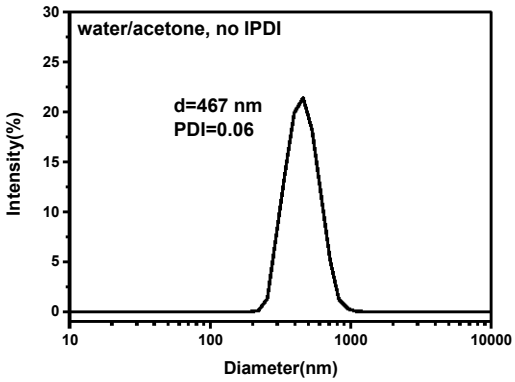

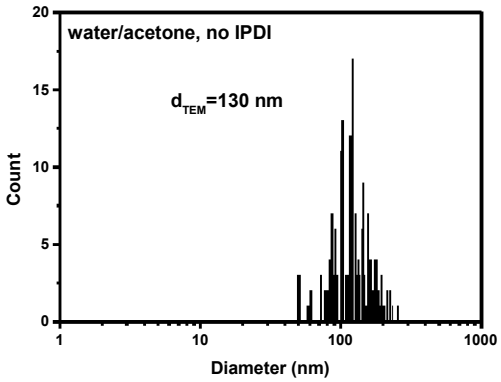

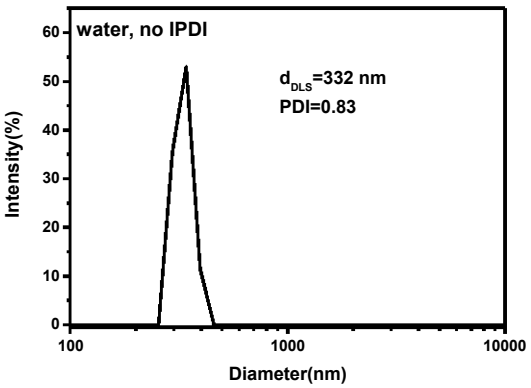

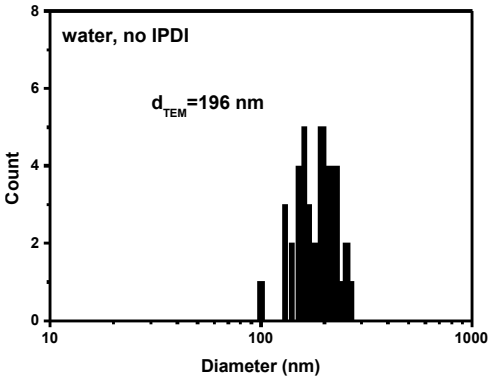

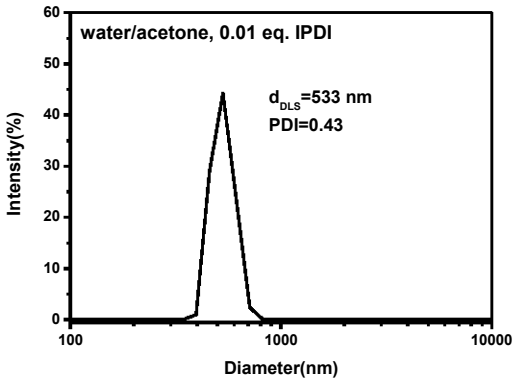

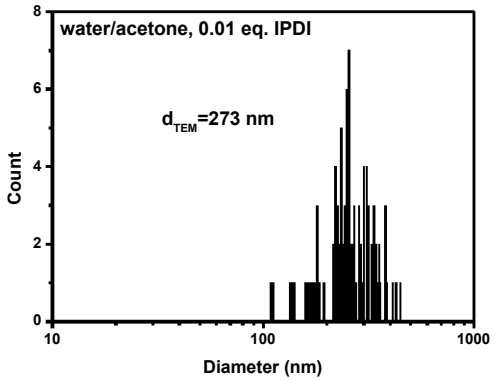

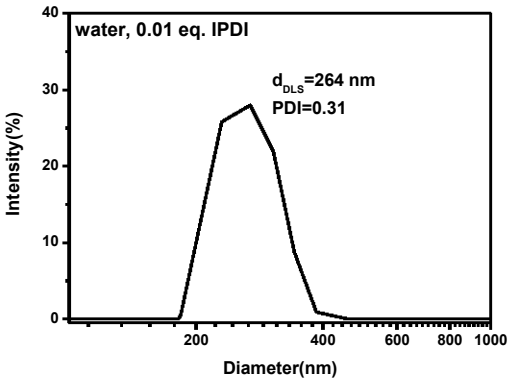

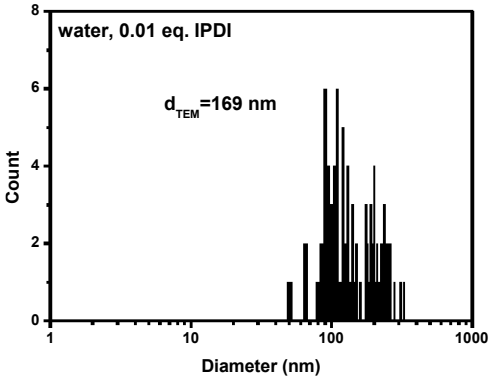

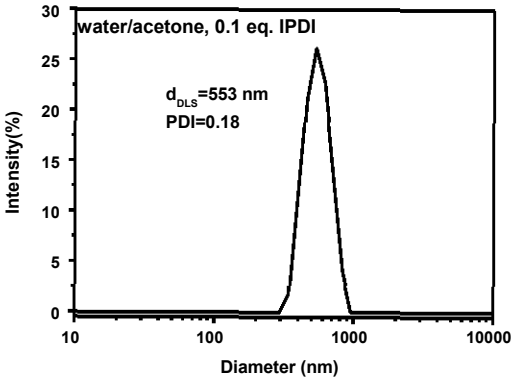

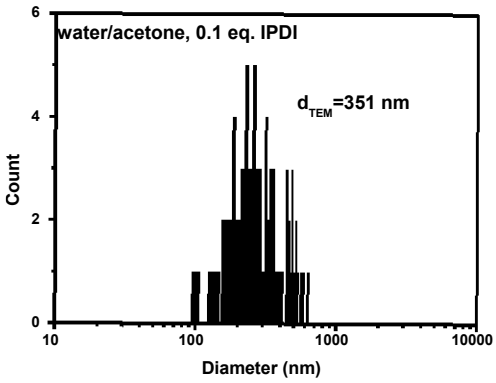

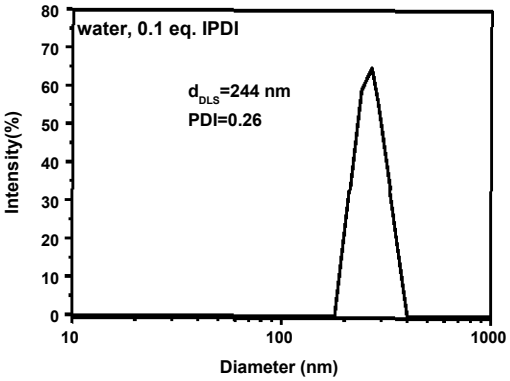

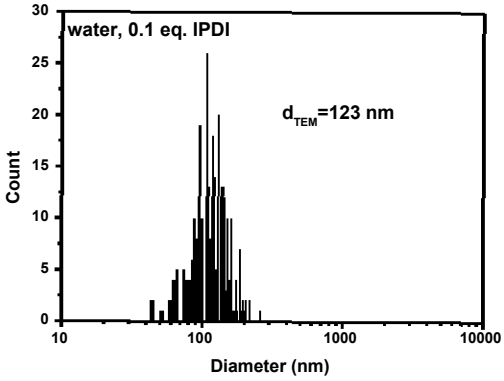

Annex 4. Diameter of PVA-GlycoNCs

Figure A1. Diameter of shell cross-linked PVA-GlycoNCs

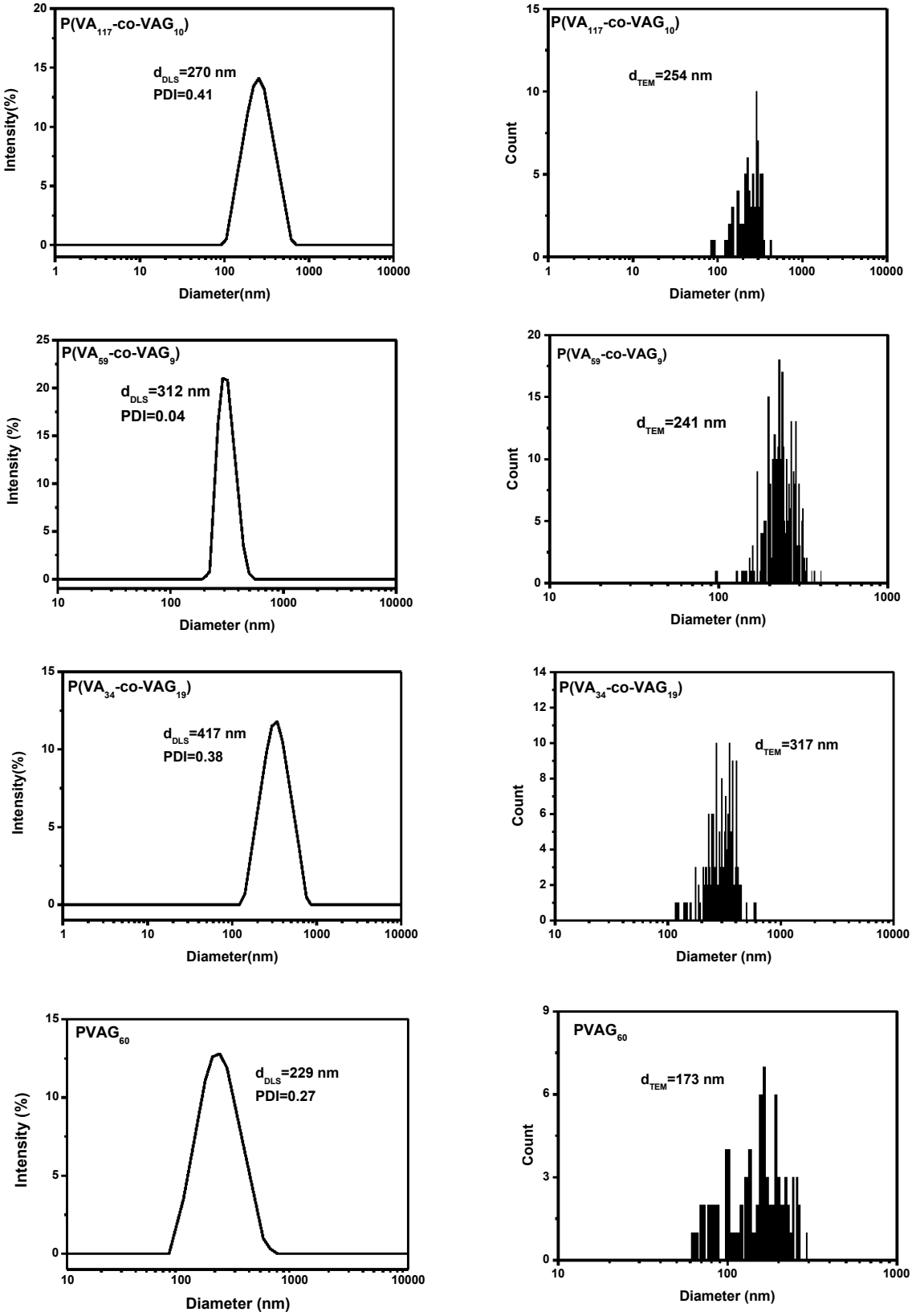

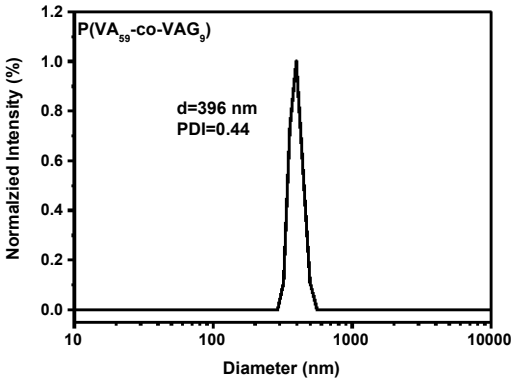

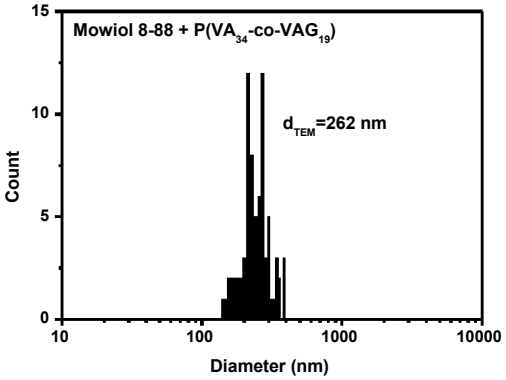

Figure A2. Diameter of non-cross-linked PVA-GlycoNCs

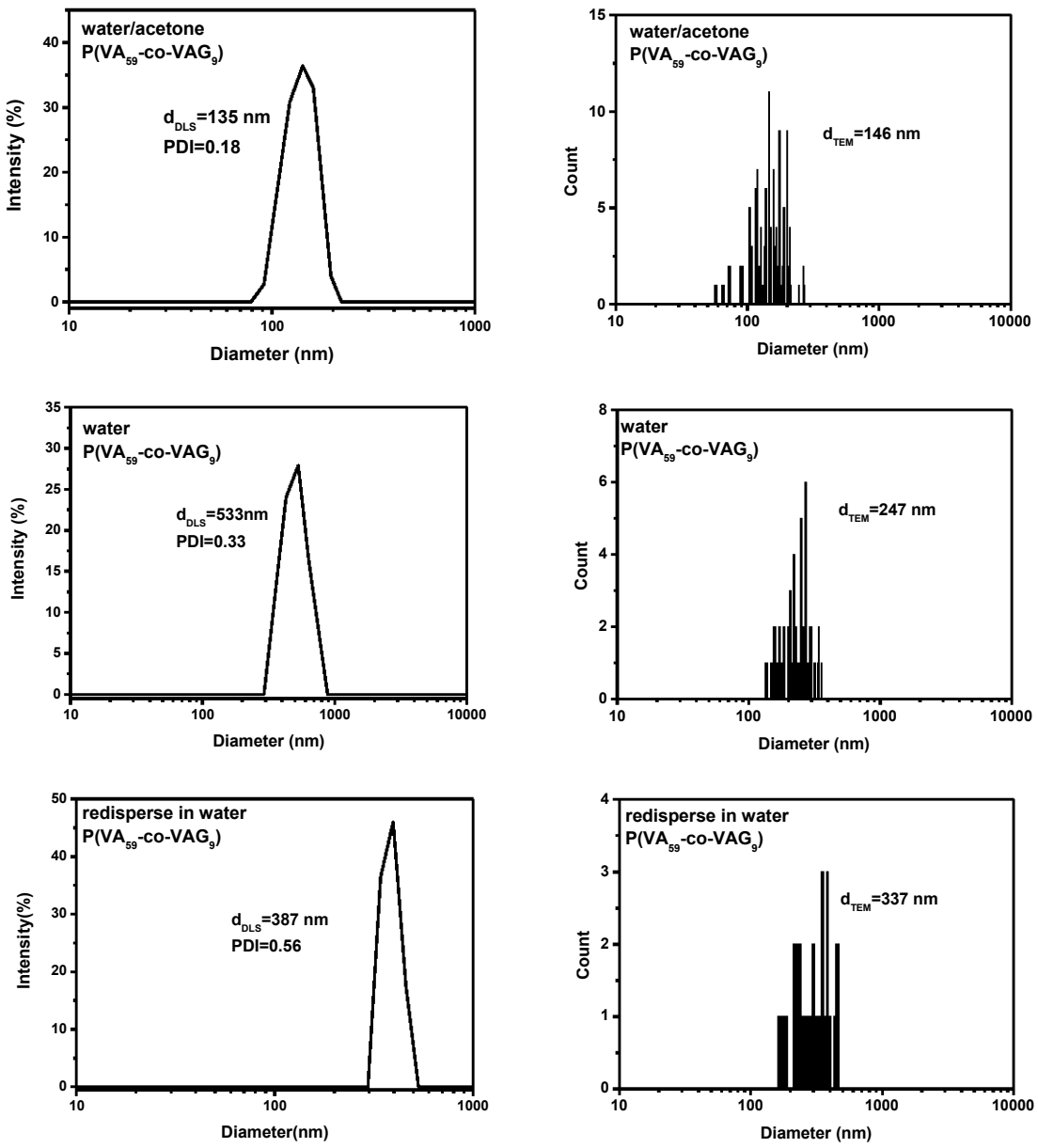

Annex 5. Diameter of functionalized PVA NCs and GlycoNCs

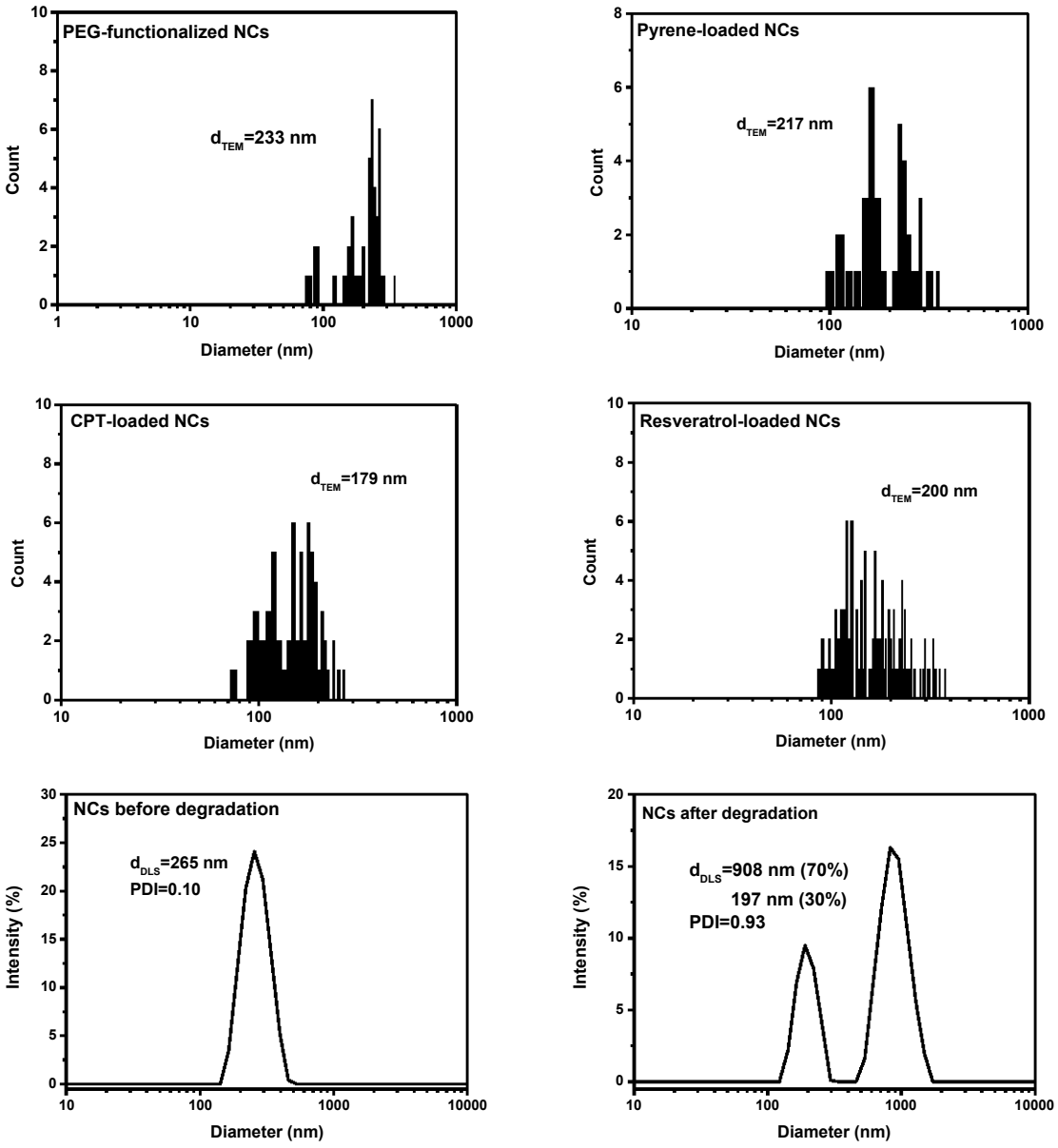

Annex 6. NMR spectra of PEOX-PEI-Lactose copolymers

Figure A1. ^{1}H NMR and ^{13}C NMR of $PEOX_{106}$-PEI_{19}-Lac copolymer (D_2O, r.t)

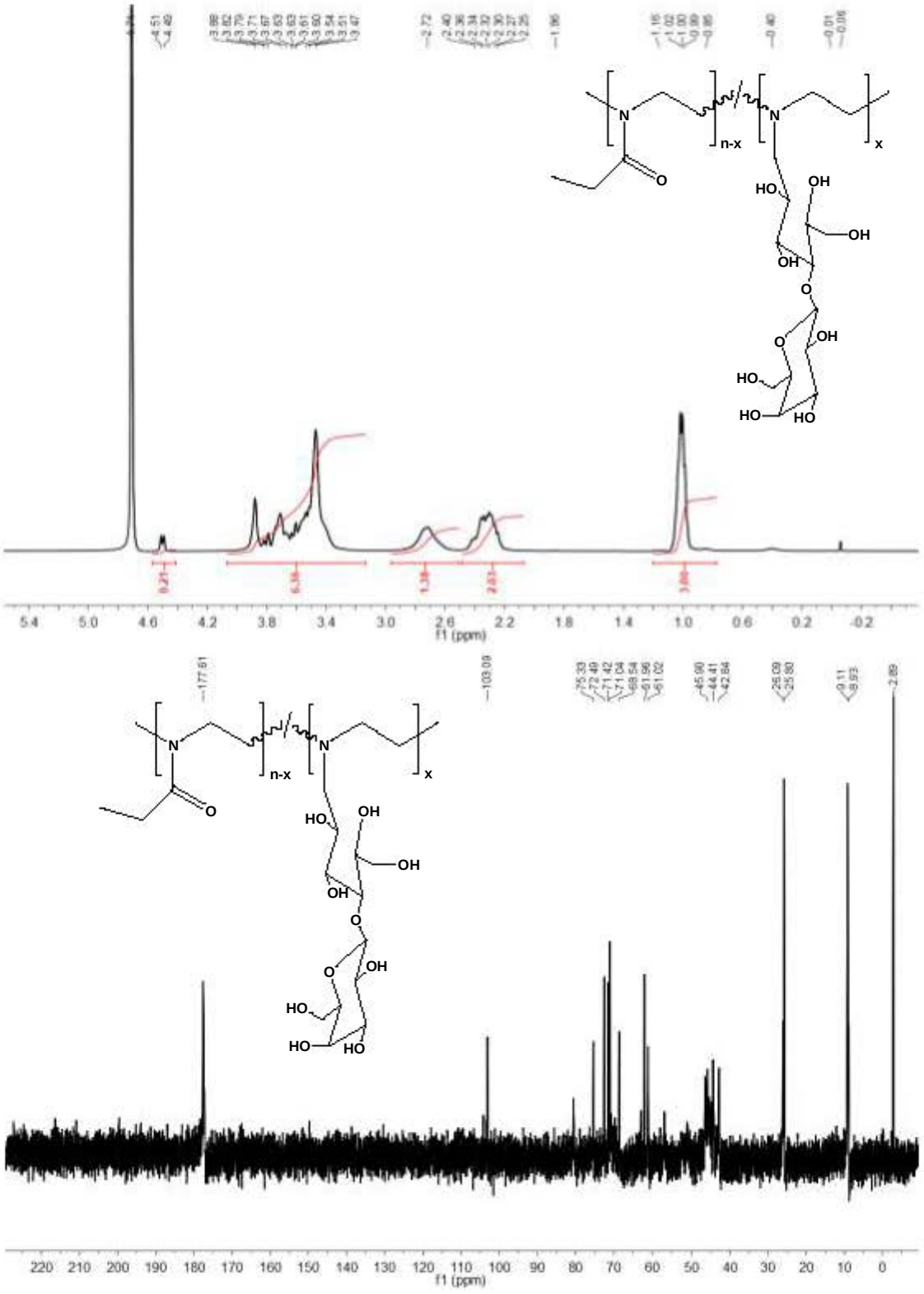

Figure A2. ^{1}H NMR and ^{13}C NMR of $PEOX_{77}$-Lac_{48}-Lac copolymer (D_2O, r. t.)

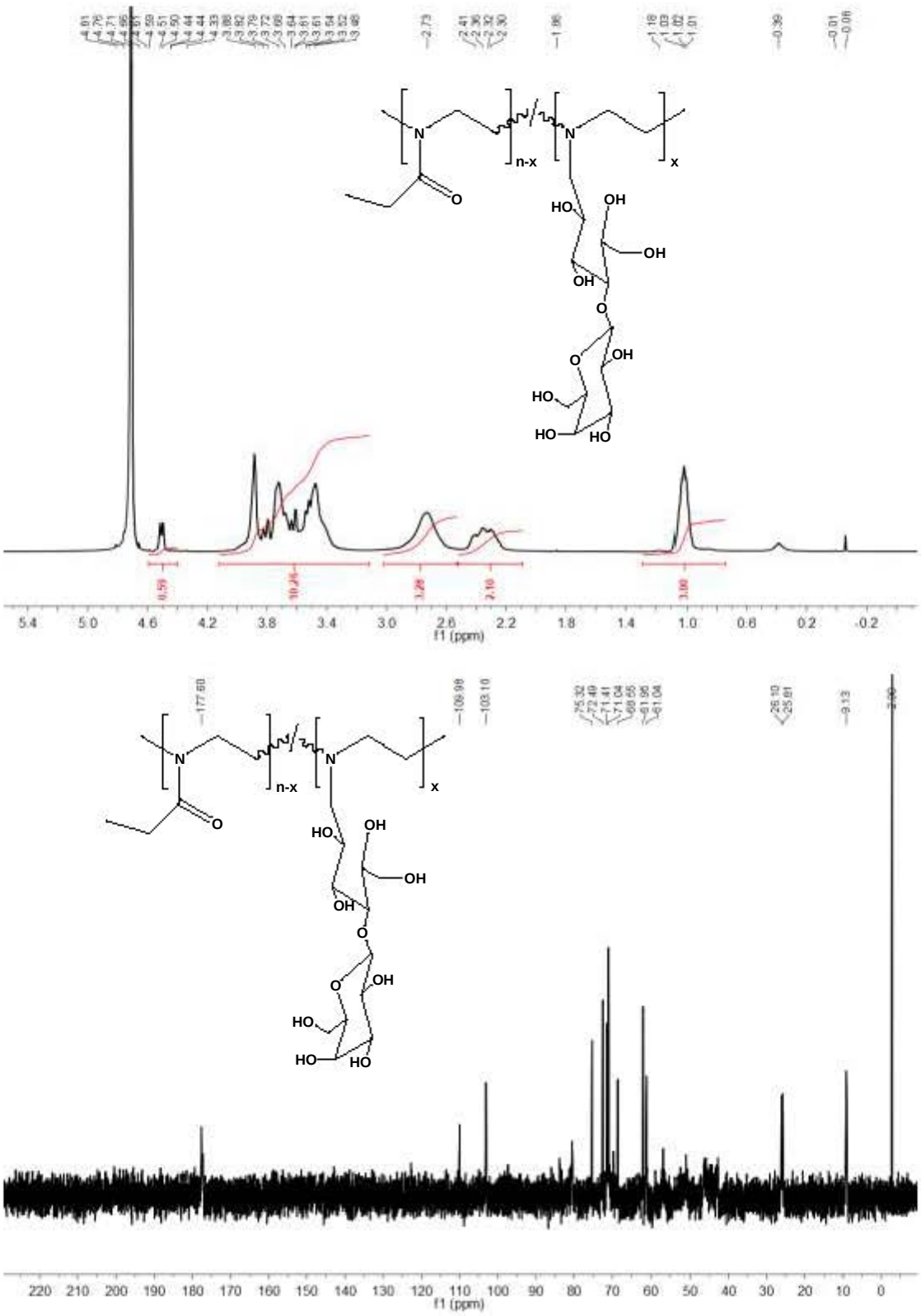

Figure A3. ^{1}H NMR and ^{13}C NMR of $PEOX_{34}$-PEI_{91}-Lac copolymer (D_2O, r. t.)

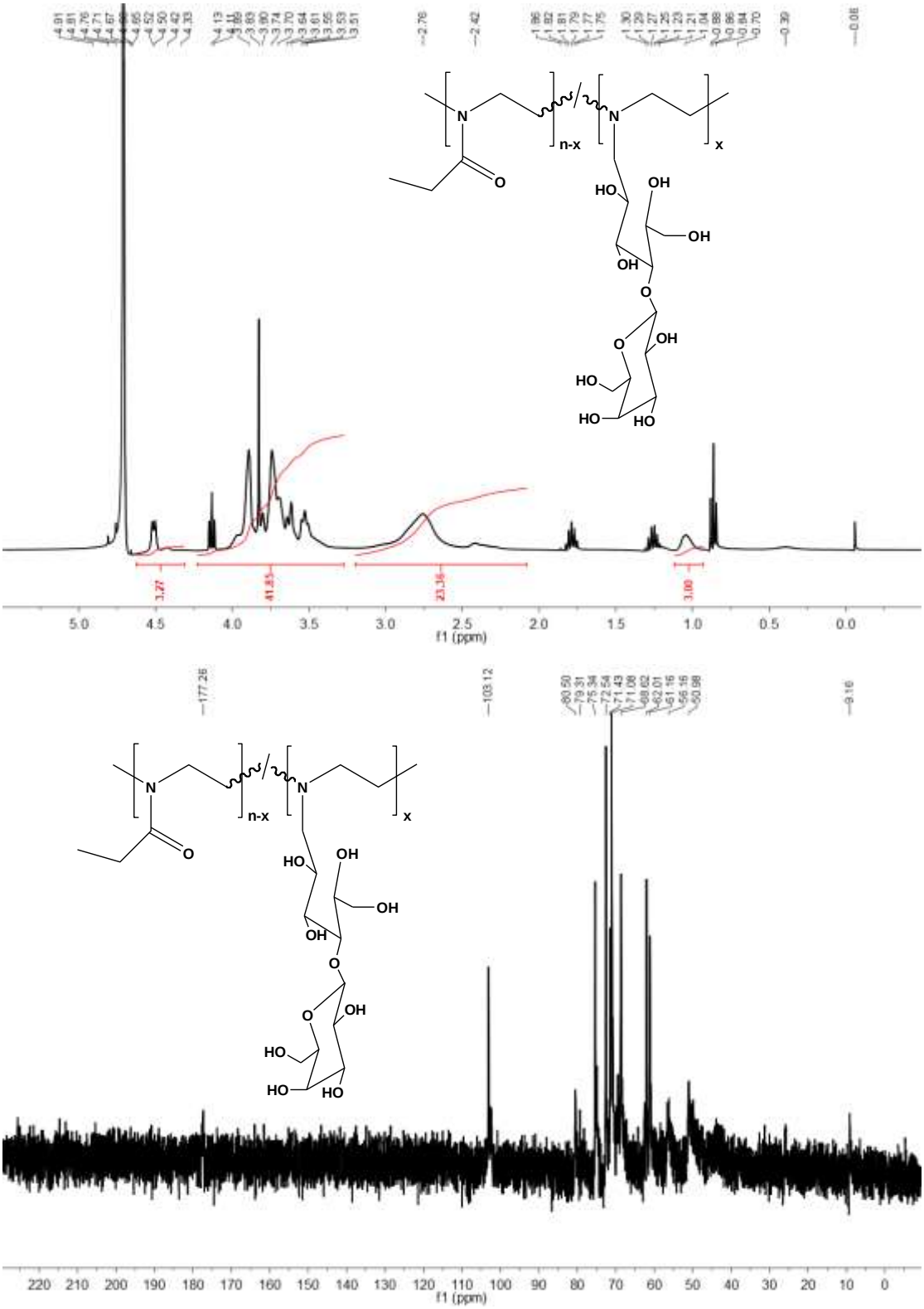

Figure A4. ^{1}H NMR and ^{13}C NMR of $PEOX_{7}$-PEI_{118}-Lac copolymer (D_2O, r. t.)

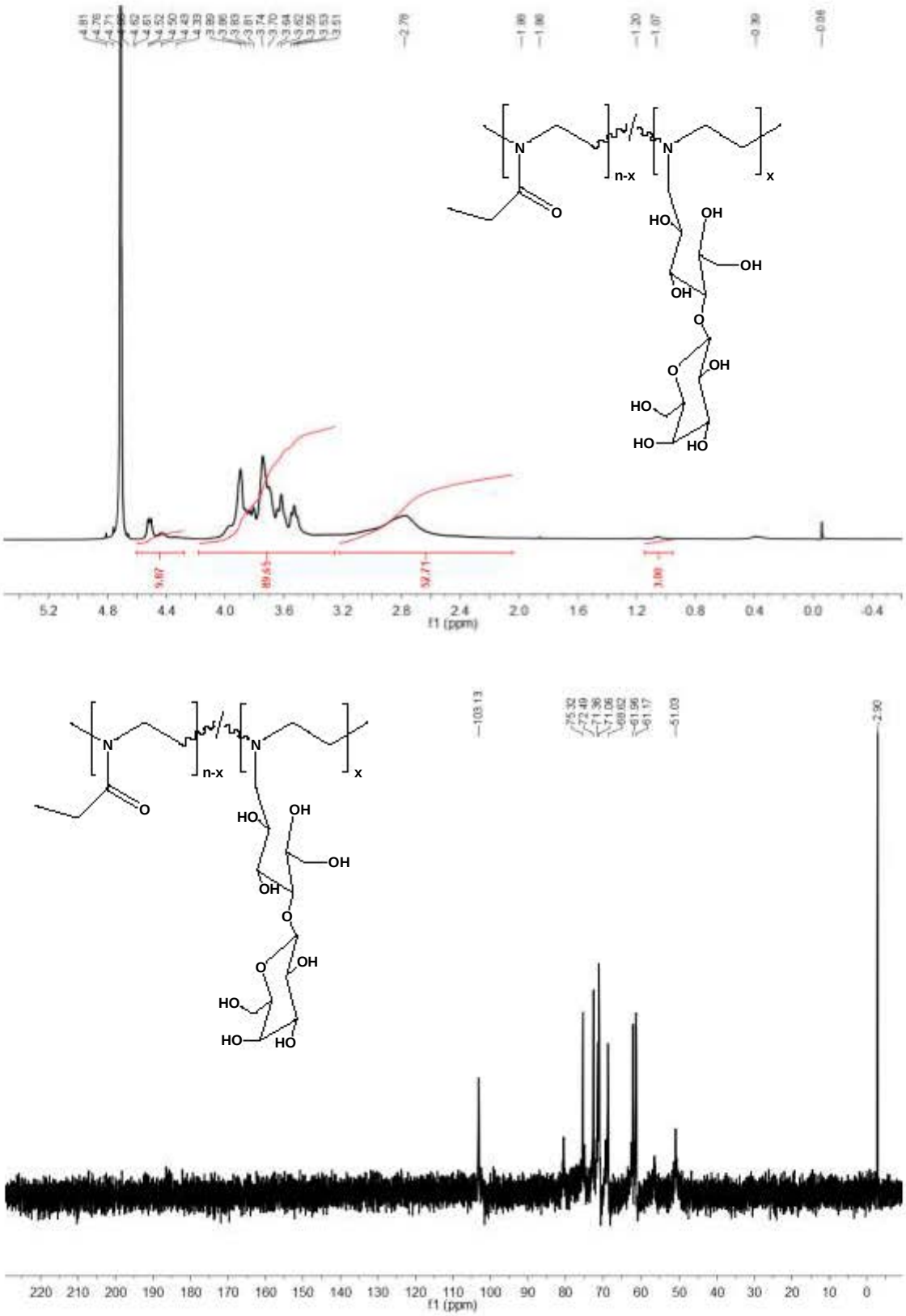

Annex 7. Diameter of PEOX-GlycoNCs with increasing IPDI content

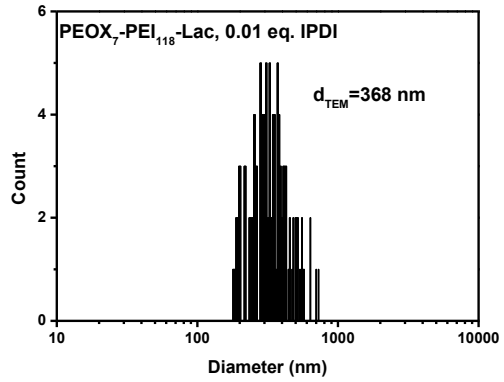

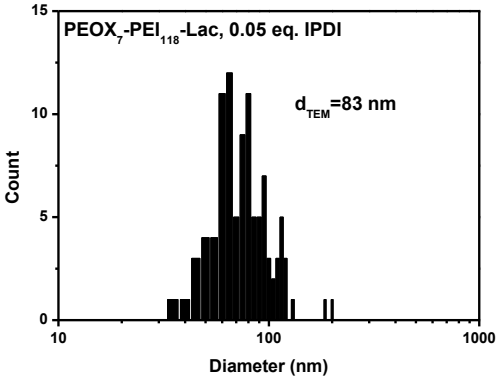

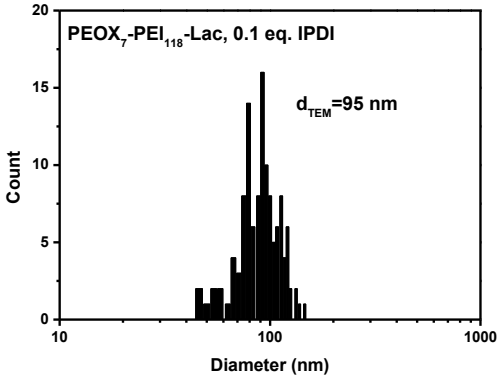

Annex 8. Diameter of PEOX-GlycoNCs

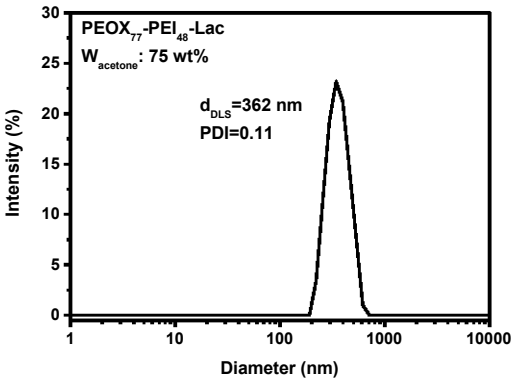

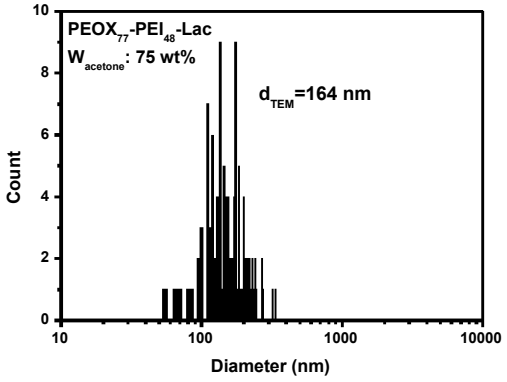

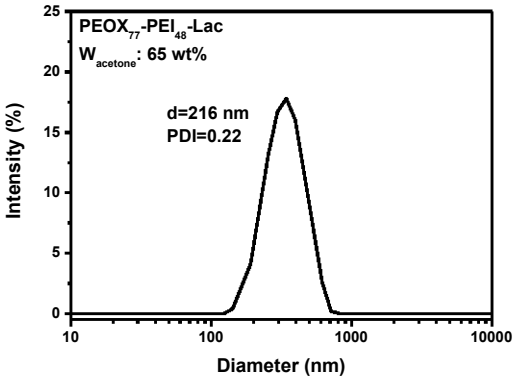

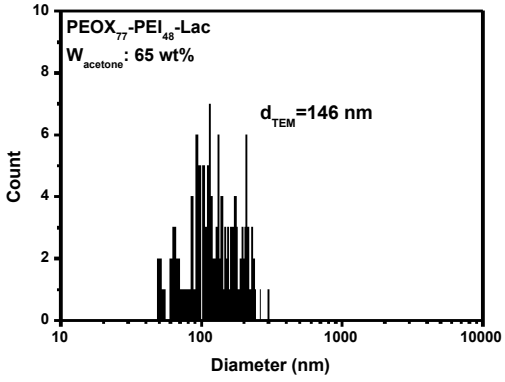

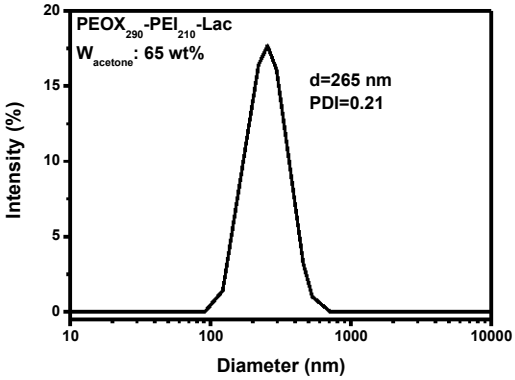

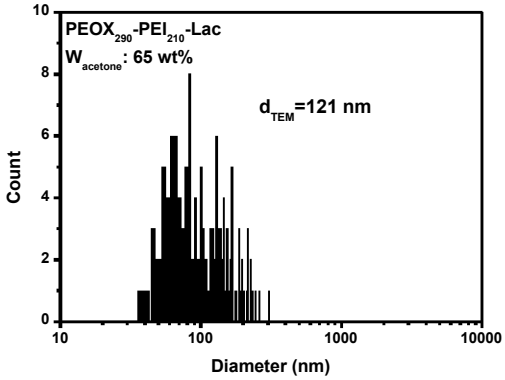

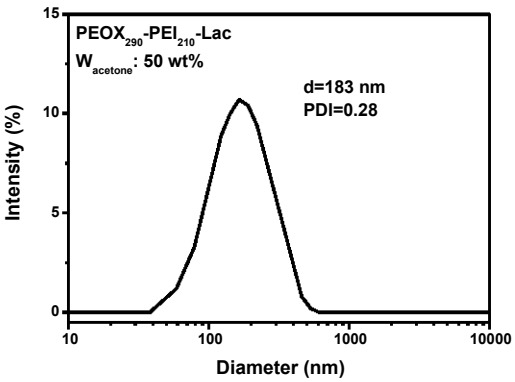

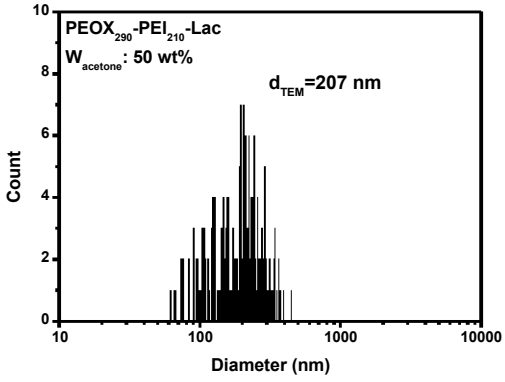

Annex 9. Diameter of pH-responsive PEOX-GlycoNCs

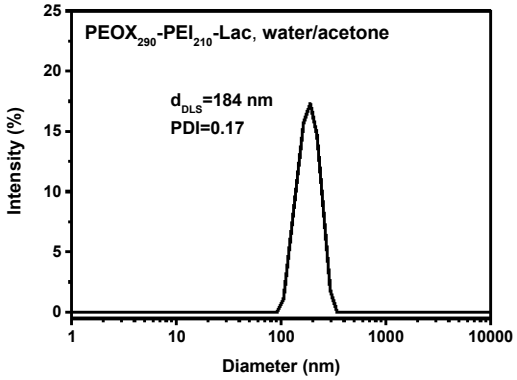

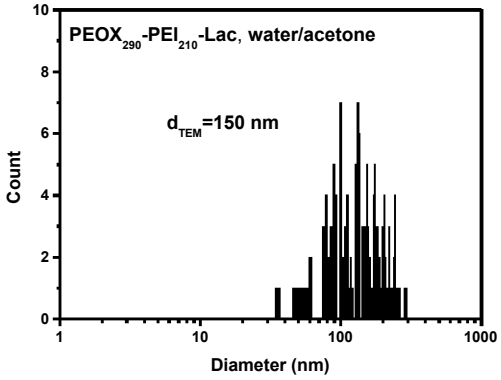

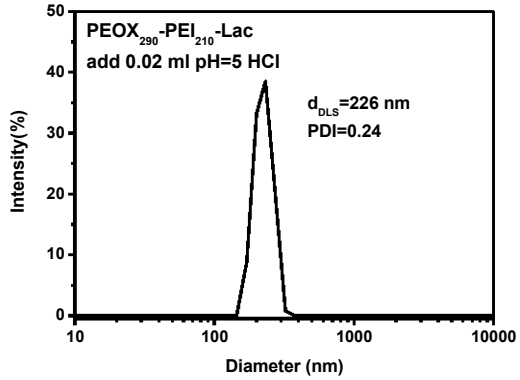

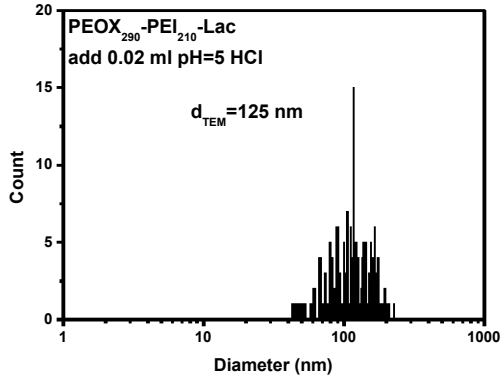

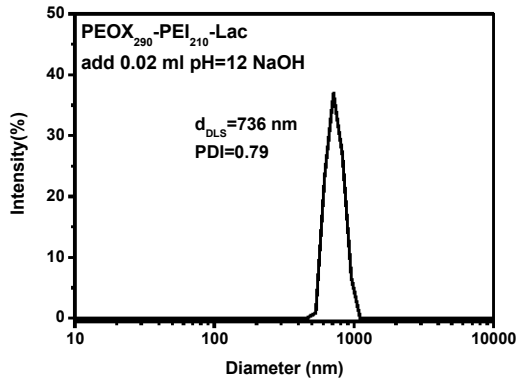

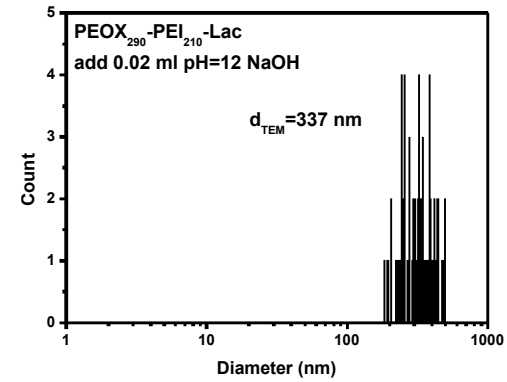

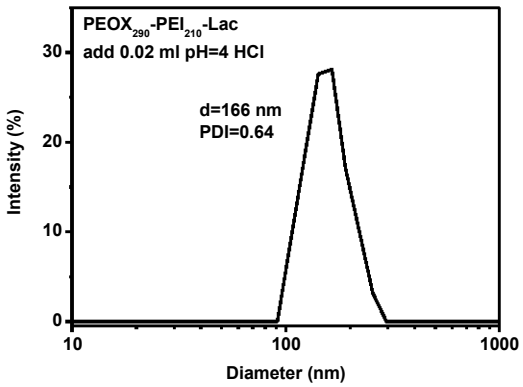

Annex 10. Diameter of functionalized PEOX-GlycoNCs

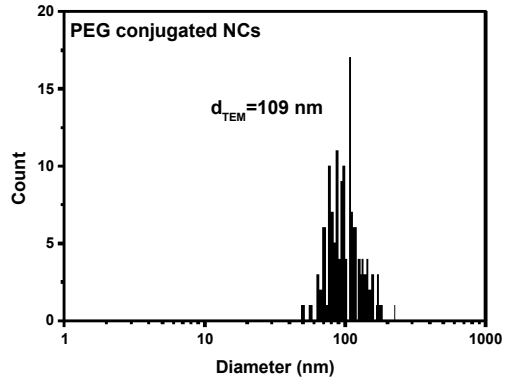

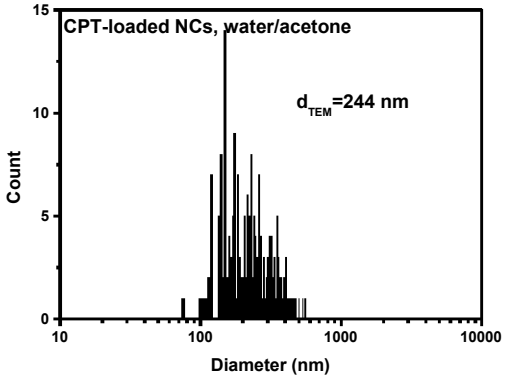

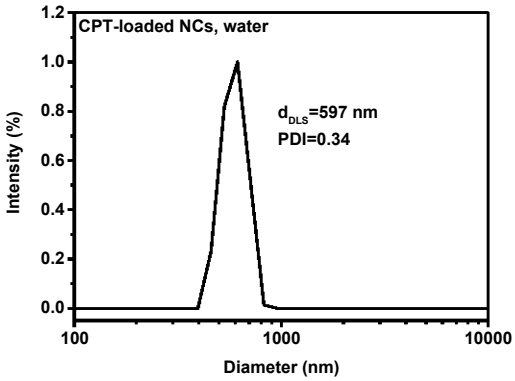

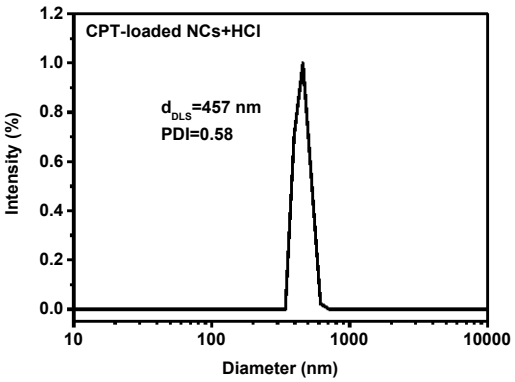

FOLIO ADMINISTRATIF

THESE DE L'UNIVERSITE DE LYON OPEREE AU SEIN DE L'INSA LYON

NOM : CHAI **DATE de SOUTENANCE** : 15/07/2019

Prénoms : Luxiao

TITRE : Rapid access to functional oil-filled nanocapsules through nanoprecipitation

NATURE : Doctorat **Numéro d'ordre** : 2019LYSEI047

Ecole doctorale : ED34 - Matériaux de Lyon

Spécialité : Matériaux polymère

RESUME : In this PhD work, we designed a series of precisely-defined water-soluble PVA-based glycopolymer chains with tunable compositions using RAFT copolymerization and selective alcoholysis reactions. In a second approach, we prepared a library of poly(2-ethyl-2-oxazoline)-based glycopolymers by partial acidic hydrolysis and reductive amination reactions with sugar residues.

Relying on the establishment of phase diagrams for water/acetone/oil and water/acetone/polymer ternary systems (commercial PVA, PVA or polyoxazoline-based glycopolymers), we identified the conditions of solvent shifting (in the Ouzo and /or the SFME domains) for which oil-filled nanocapsules can be constructed in one step thanks to spontaneous emulsification of the oil and concomitant adsorption of the polymer chains at the interface. Stabilization of the nanocapsules in water was typically achieved by covalent cross-linking of the shell or, in the case of PVA-based materials, by addition of Na_2SO_4 (salting out). This straightforward nanoprecipitation process was further effortlessly implemented to confer redox-sensitivity to the polymer shell (to trigger the release of actives), decorate the nanocapsules with diverse molecules of interest and to entrap hydrophobic actives within the oily core. Release of the drugs and bioactivity of the nanocapsules were demonstrated.

MOTS-CLÉS : poly(vinyl alcohol); poly(2-ethyl-2-oxazoline); glycopolymer; nanoprecipitation; glyconanocapsules; encapsulation.

Laboratoire (s) de recherche : Ingénierie des Matériaux Polymères (IMP) (UMR 5223)

Directeur de these :
FLEURY Etienne
BERNARD Julien

Président de jury :
MARGAILLAN André

Composition du jury :
NOUVEL Cécile
HALILA Sami